EXPERIMENTALLY DERIVED BETA (β) CORRECTIONS TO ACCURATELY

MODEL THE FATIGUE CRACK GROWTH BEHAVIOR AT COLD

EXPANDED HOLES IN 2024-T351 ALUMINUM ALLOYS

by

Scott Spencer Carlson

A thesis submitted to the faculty of
The University of Utah
in partial fulfillment of the requirements for the degree of

Master of Science

Department of Mechanical Engineering

The University of Utah

August 2008

		Form Approved OMB No. 0704-0188

Report Documentation Page

Form Approved
OMB No. 0704-0188

Public reporting burden for the collection of information is estimated to average 1 hour per response, including the time for reviewing instructions, searching existing data sources, gathering and maintaining the data needed, and completing and reviewing the collection of information. Send comments regarding this burden estimate or any other aspect of this collection of information, including suggestions for reducing this burden, to Washington Headquarters Services, Directorate for Information Operations and Reports, 1215 Jefferson Davis Highway, Suite 1204, Arlington VA 22202-4302. Respondents should be aware that notwithstanding any other provision of law, no person shall be subject to a penalty for failing to comply with a collection of information if it does not display a currently valid OMB control number.

1. REPORT DATE **03 JUN 2008**	2. REPORT TYPE **N/A**	3. DATES COVERED **-**

4. TITLE AND SUBTITLE **Experimentally Derived Beta(â)Corrections to Accurately Model the Fatigue Crack Growth Behavior at Cold Expanded Holes in 2024-T351 Aluminum Alloys**	5a. CONTRACT NUMBER
	5b. GRANT NUMBER
	5c. PROGRAM ELEMENT NUMBER
6. AUTHOR(S) **Scott Spencer Carlson**	5d. PROJECT NUMBER
	5e. TASK NUMBER
	5f. WORK UNIT NUMBER
7. PERFORMING ORGANIZATION NAME(S) AND ADDRESS(ES) **Department of Mechanical Engineering The University of Utah AND A-10 Systems Program Office (SPO) at Hill AFB, Utah**	8. PERFORMING ORGANIZATION REPORT NUMBER
9. SPONSORING/MONITORING AGENCY NAME(S) AND ADDRESS(ES)	10. SPONSOR/MONITOR'S ACRONYM(S)
	11. SPONSOR/MONITOR'S REPORT NUMBER(S)

12. DISTRIBUTION/AVAILABILITY STATEMENT
Approved for public release, distribution unlimited

13. SUPPLEMENTARY NOTES
The original document contains color images.

14. ABSTRACT

15. SUBJECT TERMS

16. SECURITY CLASSIFICATION OF:			17. LIMITATION OF ABSTRACT	18. NUMBER OF PAGES	19a. NAME OF RESPONSIBLE PERSON
a. REPORT **unclassified**	b. ABSTRACT **unclassified**	c. THIS PAGE **unclassified**	**UU**	**219**	

Standard Form 298 (Rev. 8-98)
Prescribed by ANSI Std Z39-18

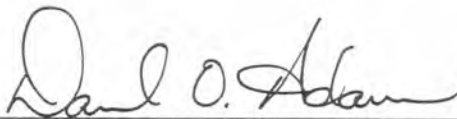THE UNIVERSITY OF UTAH GRADUATE SCHOOL

SUPERVISORY COMMITTEE APPROVAL

of a thesis submitted by

Scott Spencer Carlson

This thesis has been read by each member of the following supervisory committee and by majority vote has been found to be satisfactory.

6/3/08

_____
Chair: Daniel O. Adams

6/3/08

_____
Paul N. Clark

6-3-08

_____
Mark L. Thomsen

ABSTRACT

Fastener holes represent one of the most common fatigue details found in airframe structures. In order to minimize the impact fastener holes have on the fatigue behavior of critical aircraft components, many are processed by cold expansion. Cold expansion imposes a residual compressive stress field around a hole that retards fatigue crack growth from the volume of cold working and increases the fatigue life of the component. According to the current United States Air Force's guiding documents state that a damage tolerance analysis can take advantage of cold expansion by reducing the initial flaw size to a minimum of a 0.005 inch corner crack.

A more physically based approach was investigated to take analytical advantage of the cold expansion process. The author explored, through experimental fatigue testing, the development of an empirical correction factor β for the effects of cold expansion in 2024-T351 aluminum alloy. This method takes into account the interaction of the fatigue crack and the residual stress field found in the body. Many common current methods are unable to account for this critical interaction. The β correction factor can be used in fatigue crack growth and damage tolerance analysis and can be shown to provide a more accurate model of the crack growth behavior at cold expanded holes.

I would like to first and foremost thank my beautiful wife Catherine and our three wonderful children for all their support throughout this project. They are truly the light in my life. I would also like to thank Robert Pilarczyk without whom this project would never have been completed. Thank you for your friendship. Finally, I would like to thank my parents. You have truly made me who I am today and continue to inspire me and teach me every day. This thesis is dedicated to our three boys, A.J., Daniel, and Nathan. I hope that all of you will continue to love jets and strive to be the best that you can. I love you A.J., Daniel you are "Totally Wicked", and Nathan thank you for your smiles.

TABLE OF CONTENTS

LIST OF TABLES

ACKNOWLEDGMENTS

I would like to thank my graduate committee, Dr. Daniel Adams, Dr. Mark L. Thomsen, and Dr. Paul N. Clark, for their help in with this research project and making sure that would be a success.

I would like to thank Robert Pilarczyk for all his help with this research project. Without his help it would not have been possible. He oversaw the manufacturing of all the testing specimens. He helped with all the setup for the fatigue testing that was performed at the Hill AFB Materials Testing Laboratory. He produced all the basic models used for the finite element portion of this project as well as the outline of their specifics. Robert helped with all the fatigue testing that was performed during this research project. His assistance in the production of this report must also be acknowledged. We made a great team and were always able to bounce ideas off of each other. We helped to keep each other on task and focused on what needed to be done.

I would also like to especially thank Dr. David W. Hoeppner from the University of Utah's Mechanical Engineering Department for letting me take up some of his precious time to discuss the challenges and triumphs of this project. You will never know the impact that you have had on my life as a student and as an engineer. Thank you. Also, I would like to thank Amy Turner for her assistance in working on the SEM. Thank you for being so kind.

1 INTRODUCTION

1.1 Historical Perspective of Aircraft Structural Design Philosophies

With the advent of powered human flight in December of 1903 by Orville and Wilbur Wright the need to design aircraft structures that can withstand the damage sustained during flight has become an ever increasingly difficult field of expertise. From the original powered Wright Flyer I that flew for only 12 seconds at a maximum speed of almost 7 miles per hour to today's supersonic advanced fifth generation fighters the path that has led to where we are today has been fraught with danger and sprinkled with success.[1]

As the designs of aircraft have evolved over time, so have the philosophies used to build them. Each philosophy was limited in its time by the ability to test and understand the materials used in the building of aircraft structures. Viewed in a historical perspective one can see the great leaps that have been made in the design and maintenance of aircraft structures. This natural progression of design philosophy has made it possible to fly farther, faster and safer than ever before.

1.1.1 Early Design Philosophies

As aircraft evolved from its earliest forms to what is now considered to be the "jet age" the use of high strength materials was thought to be the most logical

design methodology. However, many failures occurred during this time due to component or even system failures. Even though the concept of fatigue was understood it had not been applied to aircraft structures. During this time in aviation history most aircraft did not last long enough in battle to see the effects of fatigue on structural components.

In order to reduce the number of structural failures seen in aircraft fail-safe and safe-life design approaches were introduced. The fail-safe design methodology required that redundant structures be built into the aircraft to allow for a back-up structure in the event that the primary structure failed. This design approach was also supplemented by the safe-life design approach. The safe-life design paradigm allowed the engineer to design and build a structure at would be immune to fatigue for a given number of cycles. This approach was based off of the fatigue work done by Milton Miner that is commonly known as "Miner's Rule".[2] The guidelines outlined in the Miner's Rule states that a component will not fail if the stresses are low enough even if the component is cycled an infinite number of times. The safe-life design approach, however, does not take into account in the calculation of fatigue life. the effects of material discontinuities or manufacturing induced discontinuities. These can all have a great impact on the fatigue life of a component as they can begin the nucleation of fatigue cracks in the material. Also, the safe-life design approach does not require that the component or structure be inspected throughout its life for damage accumulated during flight. These limitations have had dramatic and devastating consequences in the aerospace industry and have driven designers and

maintainers to more thorough design philosophy which allows the engineer to deal with fatigue as a process instead of an instantaneous event.

1.2 Current Aircraft Structural Design Philosophy

1.2.1 Damage Tolerance Design Philosophy

The United States Air Force (USAF) was one of the pioneers in the transition from the safe-life design approach to more real world based approach known as the damage tolerance design philosophy. This manufacturing and maintenance centered approach was implemented after it became obvious that the current design was not adequate in its ability to maintain aircraft safety by accurately predicting the fatigue life of loaded components. The most notable failure during this time was the 1969 crash of a nearly new F-111 Aardvark. This aircraft failed while in flight at one of the wing attachment lugs where a defect in the material had been induced during the manufacturing of the component.[3] That failure was one of the main catalysts in the transition of the USAF to the damage tolerance design philosophy in 1975. [4]

The damage tolerance design philosophy assumes a structure contains cracks or initial discontinuities in the material when manufactured and uses a fracture mechanics based lifing approach to determine the total life of a part along with the initial inspection requirements. Damage tolerance uses linear elastic fracture mechanics to determine the life of a component and its residual strength due to the presence of a flaw or crack. The objective of the damage tolerance approach is to detect cracks in critical parts before they propagate to failure. With the structure of the damage tolerance design philosophy there are

three key elements. These three elements as seen in Fig. 1, are the fatigue

crack growth behavior, residual strength, and nondestructive inspections.[5]

1.2.1.1 Residual Strength

      Residual strength is defined as the failure strength of a component as a

function of crack size. This value could be as high as the ultimate or yield of the

material if it were assumed that the material were perfectly homogeneous,

isotropic and without internal discontinuities or voids. This assumption however

is not valid as all materials have within their crystalline structure internal

discontinuities and voids. Therefore, the residual strength of a critical component

is at its highest when no cracks are present and continually decreases as cracks

nucleate and propagate through the material.
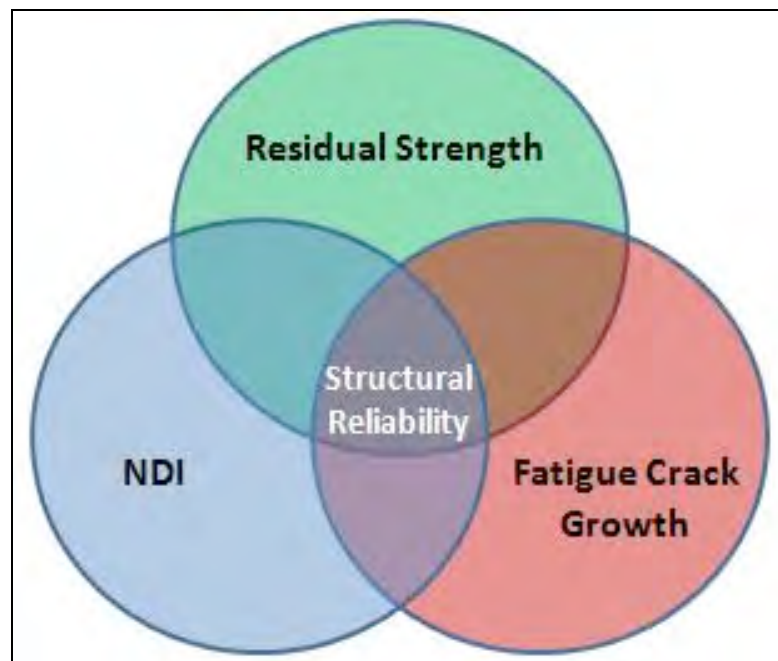
Fig. 1 Fundamental design elements for the damage tolerance design
philosophy.

1.2.1.2 Nondestructive Inspection (NDI)

Nondestructive inspection is the last of the three critical components that make up the damage tolerance design philosophy. NDI is used as a means to determine if a flaw or crack is present in the material at the time of inspection. These inspections are performed in a manner that does not interfere with the structural integrity of the critical component. Some of the techniques used in the USAF are bolt hole eddy current, x-ray, dye penetrant, and magnetic particle inspection. All of these methods have inherent process benefits and drawbacks. Each method also has a lower limit on its capability of detection. This lower limit is the smallest size "indication" or crack that can be detected with a minimum allowable degree of confidence. The lower limit and degree of confidence are used to define the technique's probability of detection (POD). The technique and its probability of detection are directly integrated into the damage tolerance design approach. These two critical NDI components are used to define the initial flaw size of a given component or structure. This allows for a starting point in the fracture mechanics based fatigue life prediction, known as a damage tolerance analysis.

1.2.1.3 Fatigue Crack Growth

With an initial flaw size determined using specific NDI techniques the next phase in the damage tolerance design philosophy is to predict the life of critical components using a fracture mechanics based fatigue crack growth model. This type of modeling approach requires the knowledge of loads and forces applied to the critical structure. These loads are determined during the initial design phase

of the component and can be recalculated during any fatigue testing performed on the component. These loads can be of constant stress and frequency, known as constant amplitude or they can vary over time. Loading sequences that vary over time are often called loading spectra. The loading spectrum characterizes and models the loads and stresses seen in a component during service. With the initial flaw size determined the loading spectrum is used to calculate the fatigue life of the critical component. This type of fatigue life calculation is able to predict the life of a component with greater accuracy because it models more accurately what the state of the material is and what loads are being seen by the material during its life.

1.2.1.4 Benefits of the Damage Tolerance Design Philosophy

The essential requirements of a damage tolerance design have a significant impact on the design and maintenance of a part/component/system. The designer and maintainer must:

1) Have knowledge of material fatigue characteristics such as crack growth behavior and residual strength and their associated variability
2) Understand the material processing and part manufacturing processes and the associated discontinuities that may be induced in the material/part
3) Understand the Initial Discontinuity State (IDS) and the modes of failure that will drive the NDI inspections used
4) Understand NDI techniques and their capabilities and detection thresholds
5) Specify the NDI techniques for critical areas
6) Statistically address the variability in detecting a given flaw size/the probability of detection

With the employment of a damage tolerant philosophy, all parties associated with the production and maintenance of critical structures and

components are forced to understand and address the three key aspects of damage tolerance as it applies to them. A trickledown effect occurs with the transition from the safe-life design paradigm to a damage tolerant philosophy where the critical issues that are not addressed with safe-life become an integral part of the design and maintenance of critical structures and components. Material fatigue characteristics as well as its behavior in application became a critical component of design.

<p style="text-align:center">1.3 Aircraft Structural Fatigue Issues</p>

<p style="text-align:center">1.3.1 Holes in Aircraft Structures</p>

As the use of the damage tolerance design philosophy has matured over time there has developed an increased awareness of the fatigue crack growth behavior of critical and noncritical structural components. With an increase in the testing and experimentation of structural materials, it became apparent that the majority of fatigue issues found in aircraft structures were located at specific component locations and geometries. These areas exhibited a dramatic decrease in fatigue life during testing due to an increased stress concentration in that region. This stress concentration was in most cases due to geometric notches in the material or component. These notches come in the form of holes, corners, geometric fillets, and structural cutouts and increase the local stress in the material in the vicinity of the notch.

In aerospace structures, one of the most common locations of fatigue cracking issues is fastener holes.[6] Manufacturing induced defects like gouges or elongations are common at fastener holes and during aircraft operation the

adverse effects of these defects are magnified by high stress concentrations associated with holes, which leads to the nucleation and propagation of fatigue cracks in these structures.

1.3.2 Process to Minimize the Effects of Structural Holes on Overall Durability

1.3.2.1 Split Sleeve Cold Expansion™

In an attempt to minimize the propagation of fatigue cracks that nucleate at holes a process known as cold expansion was developed.

1.3.2.1.1 Process History

A widely used technique for cold expanding fastener holes was developed by the Boeing Company in the early 1970s and is now marketed by Fatigue Technology Inc. (FTI).[7] The process was developed in an effort to increase the retardation of fatigue crack growth in critical holes on an aircraft's structural components. Holes in fatigue critical structures present a serious fatigue problem. This is because at the edge of a hole the material experiences an increase in the local stress due to the presence of the hole. The local stress increase due to the geometric notch is known as a stress concentration factor and is roughly equal to three for holes in structures.[8] Cracks can thus nucleate much faster and propagate through the material at a much more rapid rate. The Split Sleeve Cold Expansion™ process induces a residual compressive stress in the material surrounding the critical hole that can extend up to an additional diameter away from the edge of the hole. This residual stress is extremely effective at delaying crack nucleation and retarding fatigue crack propagation.

Like other cold working processes, the residual compressive stress induced by

Split Sleeve Cold Expansion™, reduces the net tensile stress seen at the tip of a

fatigue crack that has nucleated at the surface, bore or edge of the hole. Fig. 2

is a photoelastic image of what the residual stress field looks like after the Split

Sleeve Cold Expansion™ process has been performed on a material. This type

of Split Sleeve Cold Expansion™ process can cause a dramatic increase the

fatigue life of a component compared to a hole that has not had this process

performed on it.

1.3.2.1.2 Application Process

The Split Sleeve Cold Expansion™ process is the same regardless of

whether it is performed on holes in aluminum, steel or titanium. The process is

based on the fact that the tip of the mandrel is just smaller in diameter than the
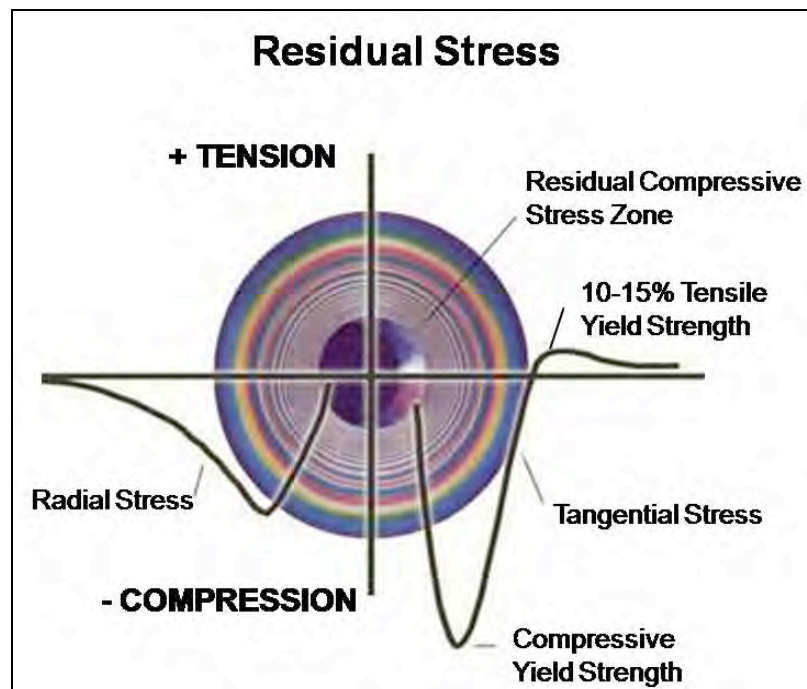
Fig. 2 Photoelastic image of the residual stress field around a cold expanded
hole.[9] Reprinted by permission of Fatigue Technology Inc.

hole but when the sleeve is slid on to the mandrel the combined diameter of the

mandrel and sleeve is larger than the diameter of the hole. With this difference in

diameter the mandrel has to be hydraulically pulled through the material. The

pulling of the mandrel through the material is what induces the residual

compressive stress field in the material. The setup for the cold expansion

process can be seen in Fig. 3.

The compressive zone can span from one radius to one diameter from the

edge of the hole, for hole diameters up to 0.50 inch for most materials.[10] Once

the hole has been coldworked the mandrel is removed and the sleeve is

discarded. The hole is then checked for proper expansion size and is final

reamed for surface integrity purposes.

The processing variables in the Split Sleeve Cold Expansion™ process

are very important and must be held within the bounds set by FTI. Material

properties such as hardness, modulus, grain size, orientation and structure will

all affect the outcome of the cold expansion process. These variables must be
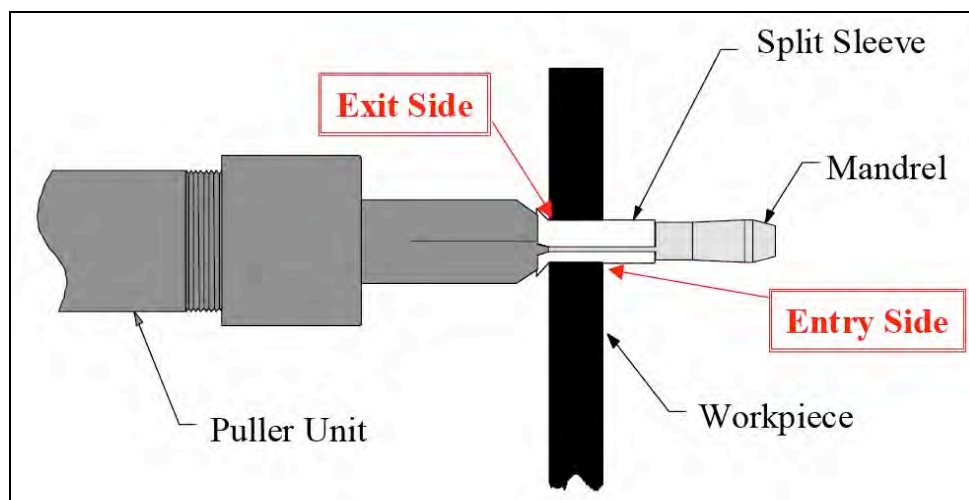
Fig. 3 FTI Split Sleeve Cold Expansion™ set-up with mandrel, sleeve and
material shown.

statically characterized and understood to apply this cold expansion process properly. Other variables that are specific to the split sleeve coldworking process are initial hole size, initial ream size, sleeve thickness, mandrel diameter and pulling force. These variables can have a dramatic impact on the residual stress field characteristics in the material that is being coldworked.

The application of the cold expansion process to holes is virtually unlimited. It can be applied to any application in which fatigue is a concern and the material that is undergoing this cyclic loading is made of steel, aluminum or titanium. With its origins in the aerospace industry it is understandable that it is one of the biggest industries to use this technology. Split Sleeve Cold Expansion™ is used in a wide range of aerospace application, particularly where a hole experiences fatigue loading. The Split Sleeve Cold Expansion™ process can be applied to component material stack-ups as well as individual layers of material with relatively similar fatigue life results.[11] This allows for multiple components such as a spar cap and web to be coldworked together and thus reduces the time and cost associated with these processes. With this application possibility the cold expansion process can be performed post manufacturing of the part and then performed on the component after it has been installed, this allows for greater flexibility for manufacturing and design. Cold expansion can be performed on holes as small as 0.125 inch to holes as large as 1 inch, using standard equipment.[9] This allows for flexibility and efficiency when working on fatigue-critical structures with holes.

<u>1.3.2.2 Analytical Methods to Take Advantage</u>
<u>of the Cold Expansion Process</u>

As the need to support aging aircraft has increased so has the research

that focuses on understanding of how materials behave when a residual stress

field is imposed on them and how to take analytical advantage of residual stress

inducing processes performed on materials.[12,13,14,15] As this research has

progressed one of the major challenges that has to be address is how to predict

the residual stress field with minimal testing.[16,17] Currently there is no

established method to predict the residual stress field that is imposed into a

material by cold expansion. With the limited current knowledge of the residual

stress field it is very difficult to accurately incorporate into a fatigue crack growth

analysis the benefits that are gained by cold expansion.

1.3.2.2.1 Superposition of Stress Intensities

The use of superposition in fracture mechanics allows for the addition of

multiple loading conditions and geometric configuration factors.[18] This process

can also be applied to the addition of stress intensities for residual stress fields

caused by residual stress inducing processes. In order to perform the addition of

residual stress intensities the residual stress profile must be known or assumed

and mapped through the surface.

There are several methods used to obtain the residual stress field stress

intensity which include weight functions, Green's function, boundary integration,

alternating methods, and finite element models.[19,20] Once the residual stress

profile has been mapped for the given component the residual stress field stress

intensity can be obtained by inserting a crack face at the desired location and loading with the residual stresses that exists normal to the plane of crack growth. The stress intensity is added to the applied component stress intensity using superposition. This addition of stress intensities allows one to determine the sum of the applied and residual stress intensities under Mode I conditions. Equation 1 below shows this principle mathematically and Fig. 4 illustrates both a compressive and tensile superposition example. This method allows one to simply add the residual stress intensity and the applied stress intensity to develop a total stress intensity seen in the component. The effective stress intensity can be used with an unmodified crack growth law to estimate the crack growth rate as a function of the total stress intensity.[21]

$$\Delta K_{combined\_total} = \Delta K_{applied} + \Delta K_{residual} \tag{1}$$
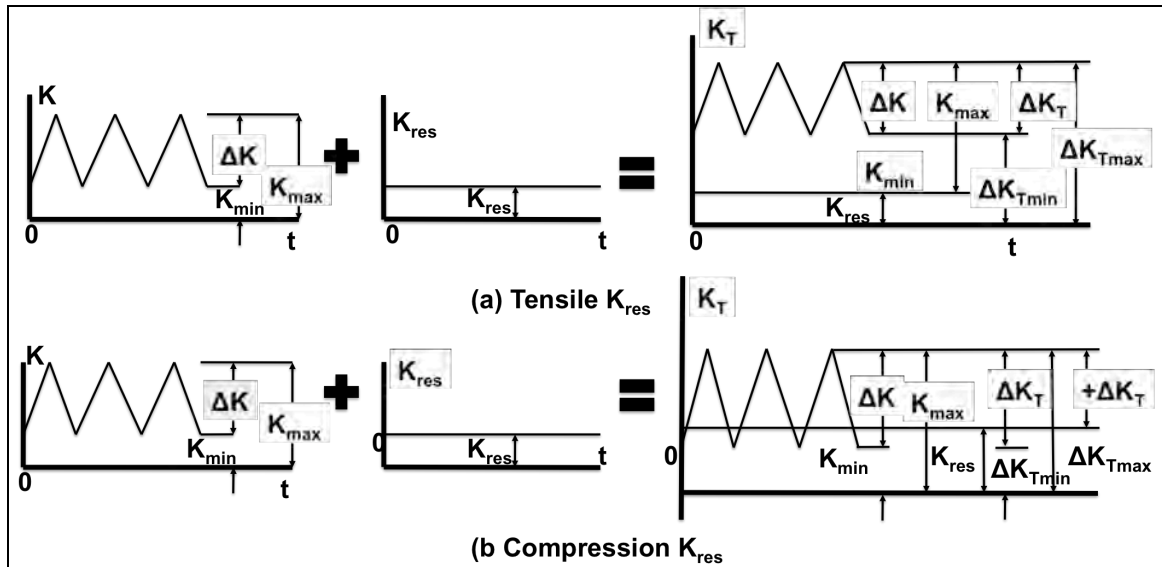
Fig. 4 Initial stress intensities for applied loading, residual stresses, and superposition. (a) tensile ΔK_{res}, (b) compression ΔK_{res}.

1.3.2.2.2 Application Based Limitations of Superposition

The specific application of superposition to model the residual stress field is limited in its application to situations where linear superposition of the stress intensities is valid. These situations include positive applied stress ratios, which means the crack tip is in constant tension and not compression and where the maximum net stresses are not above yield. Another limitation of this approach involves the accuracy of the integration of the superposition model, da/dN, as a function of the initial calculated stress intensity. This comes into question since the residual stress profile changes as a crack grows through the residual stress field, altering the original residual stress intensity. Residual stress relaxation due to cyclic plasticity, cyclic softening, and temperature stress relief is also a serious issue that is not addressed through the superposition approach. Also, the crack tip contains its own residual stress field within the plastic zone that will interact with the original residual stress. This interaction is also not addressed when using the superposition approach. Another issue that causes problems with this approach is that it allows for the possibility to have a negative stress intensity from the sum of the applied and residual. This, however, does not physically model what is occurring during fatigue testing. If the net stress intensity were negative it would be impossible to nucleate and propagate a crack through the residual stress field. It is known, however, that cracks do nucleate and propagate through the residual stress field imposed in a material by cold expansion.

The use of superposition to take advantage of the residual stress field caused by cold expansion has also demonstrated a lack of correlation between the predicted and actual fatigue crack growth testing data.[13,22,23,24] This method has also proven to be very sensitive to possible errors and is often very conservative in its prediction of the life of a component.[25]

1.3.2.2.3 Reduction of Initial Flaw Size (IFS)

The current approach used by the Department of Defense (DoD) and the USAF to take analytical advantage of the cold expansion process in a structural hole is to reduce the initial flaw size from 0.05 inch to 0.005 inch at the edge of the analyzed hole. The 0.005 inch initial flaw size was determined by a method of back extrapolating the fatigue crack growth curve to estimate the initial flaw size.[5] This practice is based on the DoDs Joint Service Specification Guide from 2006. This document states that:

> For durability fracture mechanics analysis, the limits of the beneficial effects to be used in design should be no greater than the benefit derived by assuming a .005 inch radius corner flaw at one side of an as manufactured, non-expanded hole containing a neat fit fastener in a non-clamped-up joint.[26]

This DoD approach is applied to all materials, loading conditions and geometric configurations that have been cold expanded. It does not allow for effects caused by these variables in fatigue crack growth. It is a "one size fits all" approach to this type of problem. In some instances this approach is very conservative and in others it is possibly very aggressive. It does not represent the material behavior in an accurate manner and therefore induces more risk into the analysis that is not necessary. The approach does give some analytical

16

benefit for cold expansion as seen in Fig. 5. When the initial flaw size is reduced

from 0.05 to 0.005 inch the fatigue life of a component is increased by almost five

times. This is because the fracture mechanics model is based on a ΔK

calculation which is directly related to the crack size and therefore with a smaller

initial crack size the ΔK stays smaller for a much larger time and give a greater

life calculation.

1.4 Application Based Testing Approach for (β) Correction

1.4.1 Background of Linear Elastic Fracture Mechanics (LEFM)

In linear elastic fracture mechanics (LEFM) a β correction is used to adjust

the basic analytical model to match the real-life situation that is being analyzed.
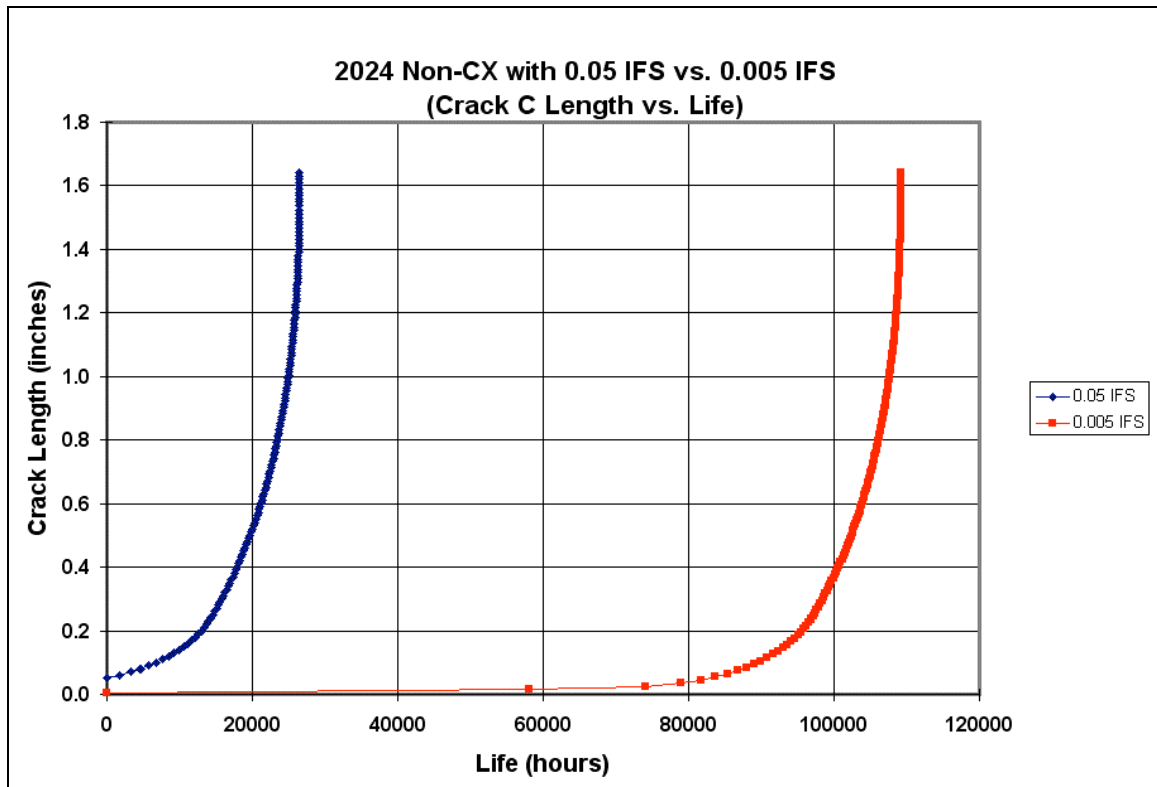
Fig. 5 Crack growth curve for 2024-T351 aluminum alloy with reduced initial flaw size correction and standard approaches. Plot produced using AFGROW.

The basic LEFM model consists of an infinitely wide plate with a crack in the center. To allow for the application of LEFM in real world situations β corrections are commonly used to adjust for geometric configuration, loading condition and fatigue crack interaction. Fig. 6 illustrates a few of the geometric considerations that can be accounted for with the use of a β correction. With the use of a β correction it is possible to modify the fatigue crack growth behavior from that seen in an infinite plate with a center crack to a plate with a hole of radius R in the center of it, or a component with a surface crack. These situations are commonly used in fatigue crack growth analysis problems.
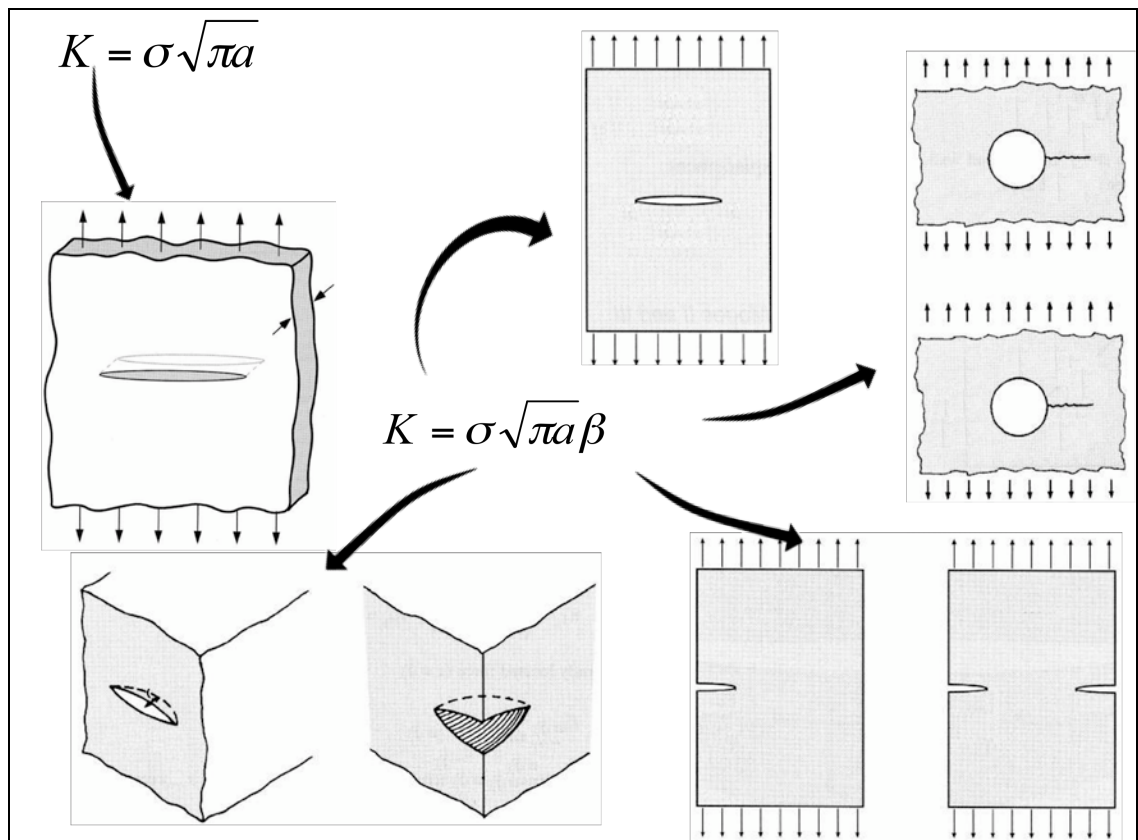
Fig. 6 Application of a β correction to adjust the standard LEFM model for use in real life situations.

1.4.1.1 β Correction Application for Crack Growth Adjustments

In order to provide a more accurate prediction of the crack growth behavior of a component that has been processed by cold expansion the use of a β correction has been theorized to possibly provide an accurate point-by-point correction as the crack propagates through the residual stress field. This type of application based approach to model and predict fatigue crack growth behavior has been applied in the past to predict crack growth for cracks that propagate through spar webs in aircraft.[27]

In order to develop these β corrections, specimen fatigue testing would need to be performed on the material in question. The testing would require both specimens that had not been cold expanded for a baseline and specimens that had been cold expanded to allow for the comparison of fatigue crack growth behaviors. This type of fatigue crack growth comparison has been well established in the LEFM field and a schematic of the process can be seen in Fig. 7. Fig. 7 illustrates the similitude principle, which states that for a given material and geometric configuration at a given crack growth rate (da/dN) the stress intensity (ΔK) for that configuration will be the same for two different testing specimens.

The process outlined in Fig. 7 shows how it is possible to extrapolate a scalar β correction by the difference in stress intensities (ΔK) at a given crack growth rate on a da/dN versus ΔK plot. By the use of the similitude principle a β correction can be extrapolated by the difference in stress intensities between the
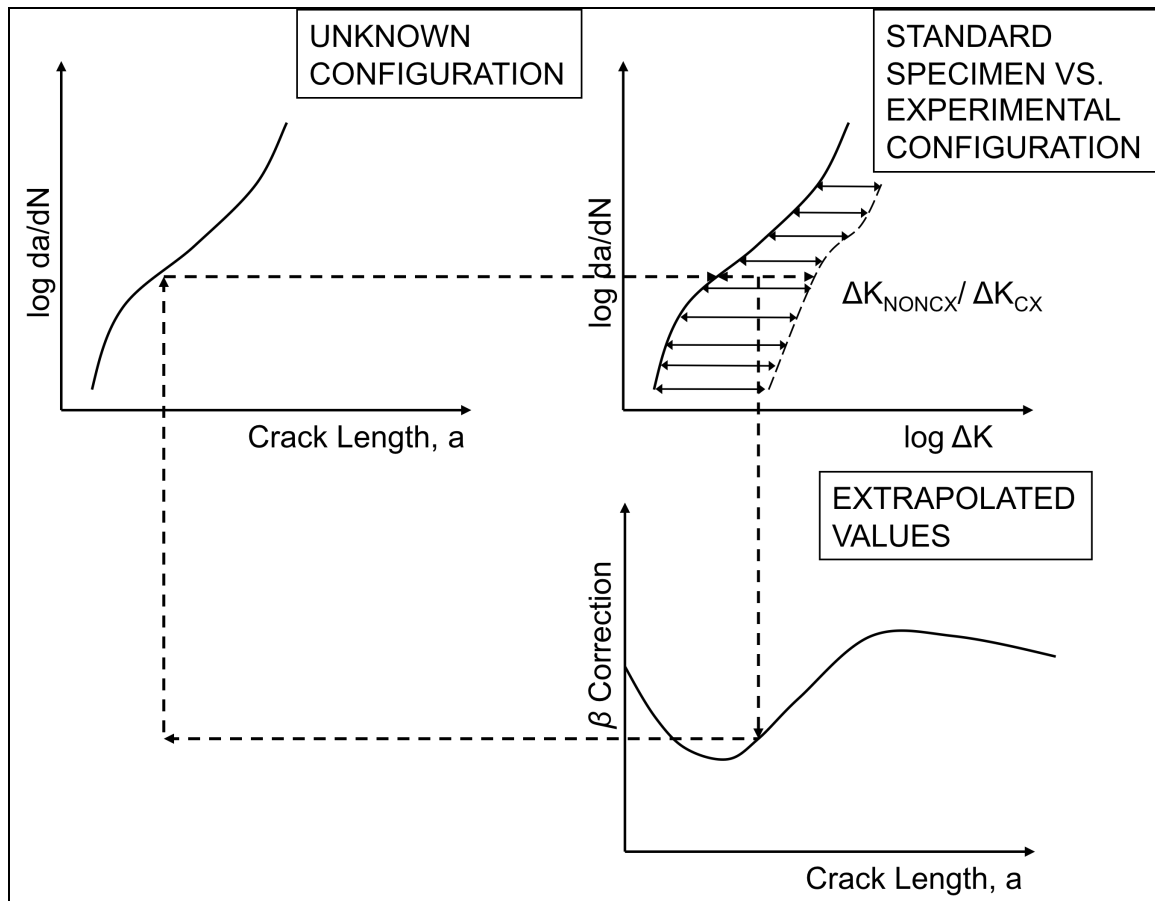
Fig. 7 Schematic of the fatigue crack growth method used for obtaining β corrections.

baseline noncold expanded specimens and the processed cold expanded

specimens.

The application of a β correction in a fatigue crack growth analysis would

make it possible to predict the fatigue behavior of a tested material under a

tested load or spectrum with a much greater accuracy than if other methods were

used such as residual stress superposition or simply reducing the initial flaw size

at the start of the analysis.

<u>1.5 Research Project Outline</u>

1.5.1 Fatigue Crack Growth Testing

This research program investigated the possibility of using a β correction as a point-by-point correction to model and predict the fatigue crack growth behavior of an aluminum alloy that had been processed by Split Sleeve Cold Expansion™. In order to calculate this β correction the fatigue crack growth behavior of the aluminum 2024-T351 alloy had to be known. To do this fatigue testing was performed on 2024-T351 aluminum in three phases. The ASTM standard E 647 was used as a guide for all testing and the specimen geometry was determined based on its guidance.[28] Each specimen was 16 inches long by 4 inches wide by 1 inch thick. All specimens were cut in the long-transverse direction, allowing the grain orientation to run the length of the specimen. Both the noncold expanded and cold expanded specimens had a 0.50 inch hole in the center of it with a corner electro discharge machining (EDM) notch on the cold expansion mandrel exit side. One specimen had the EDM placed on the exit side of the hole by accident and its fatigue crack growth characteristics will also be outlined.

<u>1.5.1.1 ASTM Standard E 647 Specimens</u>

The first phase of the fatigue testing program was the testing of ASTM standard E 647 middle tension specimens. Two specimens were tested to ensure that all testing equipment and procedures were within the required specification outlined in the E 647 testing procedure. The fatigue crack growth

data acquired during this phase of the research project were compared to data produced by the Southwest Research Institute (SwRI).[29]

1.5.1.2 Baseline Noncold Expanded Specimens

Phase two was the fatigue testing of noncold expanded specimens. These specimens had not undergone the cold expansion process and therefore allowed for a baseline or control for comparison.

1.5.1.3 Cold Expanded Specimens

The final phase of experimentation was the testing of cold expanded specimens. These specimens had been processed using Fatigue Technologies Inc. standard process for a 0.50 inch hole. After the testing of both the processed and unprocessed specimens it was possible to calculate a point-by-point β correction as a function of crack length for the cold expanded specimens. After the β correction is calculated it can be applied as a scalar correction to adjust the stress intensity to match the crack growth rate of the unprocessed noncold expanded material. This correction is applied using Equation 2.

$$K = \sigma\sqrt{\pi a}\beta_{Geometry}\beta_{ColdExpansion} \tag{2}$$

1.6 Research Program Objectives

Listed are the objectives proposed for this research project.

1. Determine the baseline fatigue crack growth behavior of the aluminum alloy 2024-T351.

2. Determine and compare the fatigue crack growth behavioral differences between the baseline noncold expanded configuration and the cold expanded configuration.

3. Understand the fatigue crack propagation geometry and its effects on the fatigue life and stress intensities along the crack front.

4. Develop a β correction as a function of crack length along the EDM entrance surface and down the primary EDM side of the bore.

5. Determine the feasibility of using a β correction to model and predict the fatigue crack growth behavior of cold expanded holes in Al 2024-T351.

6. Develop a relationship between the cold expanded β correction and the residual stress field induced into the material through this process.

7. Compare and contrast this calculated residual stress field with those calculated using finite element modeling.

2 FATIGUE TEST SETUP AND TESTING PROCEDURES

2.1 Fatigue Testing Specimen Specifications

2.1.1 Testing Specimen Material

The material selected for this research project was 2024-T351 aluminum. This material was selected for testing because it is one of the most common materials used in the aerospace industry for aircraft structure. This would make the research performed have widespread application not only to the USAF but also to other aerospace companies. 2024-T351 was first introduced by ALCOA in 1931 and has been used in the aerospace industry for over four decades[30]. With such a long history and its extensive use in the aerospace industry 2024 aluminum has a significant material testing data base. Aluminum 2024-T351 is the plate designation for Al 2024. The alloy's nominal chemical composition is 0.5% Si, 0.5% Fe, 3.8-4.9% Cu, 0.3-0.9% Mn, 1.2-1.8% Mg, 0.1% Cr, 0.25% Zn, 0.15% Ti with 0.15% total of other constituents and the balance being aluminum.

2.1.2 Material Procurement

The raw material used for this research was purchased by the United States Air Force Academy's (USAFA) Center for Aircraft Structure Life Extension (CASTLE) group from Kaiser Aluminum. The raw aluminum material came to the CASTLE group in one 4 by 6 feet sheet. All the material procured for this

research project is described in Appendix A. From this raw sheet material the CASTLE group manufactured the fatigue test specimens.

2.1.3 Testing Specimen Geometry

The test specimen geometry was based off on ASTM E 647 testing guidance for specimen geometry.[28] The standard geometry for all test specimens was 16 inches long by 4 inches wide by 0.25 inch thick. This specimen geometry would allow for easy visual access while being tested in the fatigue machine. Also it would allow for simple stress calculations to be performed due to its 1 inch cross sectional area.

2.1.3.1 ASTM Standard E 647 Testing Specimens

To ensure that the testing methods, fatigue machine and material were all performing properly two ASTM standard E 647 specimens were manufactured and tested. These specimens were manufactured to the ASTM E 647 specifications. The standard testing geometry was used for these specimens but each was modified to have a 0.100 inch diameter center hole with two through-thickness EDM notches on each side of the hole. The EDM notches ranged in length from 0.100 inch to 0.150 inch. Each ASTM E 647 specimen was measured to ensure conformance to the standard. Fig. 8 is the manufacturing draft of the E 647 specimen, which was given to the USAFA's CASTLE group for the manufacturing of these specimens.

O .100 THRU
0.020 EDM BOTH SIDES
(SEE DETAIL)

<1> ROLLING DIRECTION

2.000

4.000

SPECIMEN ID

EDM   0.020

DRILLED
HOLE

0.020

EDM/HOLE DETAIL

8.00

16.00

250

SPECIMEN TYPE	MATERIAL	QUANTITY	THICKNESS	SPECIMEN IDENTIFICATION
A	2024-T351	2	0.250	CC2024-X (1 TO 2)
B	7075-T651	2	0.250	CC7075-X (1 TO 2)

<1> ROLLING DIRECTION IS CRITICAL FOR ALL SPECIMENS

<2> ALL SPECIMENS OF SAME MATERIAL TYPE SHOULD
COME FROM THE SAME PLATE

<3> DEBURR AND POLISH EDGES OF SPECIMEN. DO NOT
CHAMFER OR RADIUS EDGE OF HOLE. POLISH AREA
AROUND HOLE.

<4> STEEL STAMP SPECIMEN ID ON BOTH ENDS

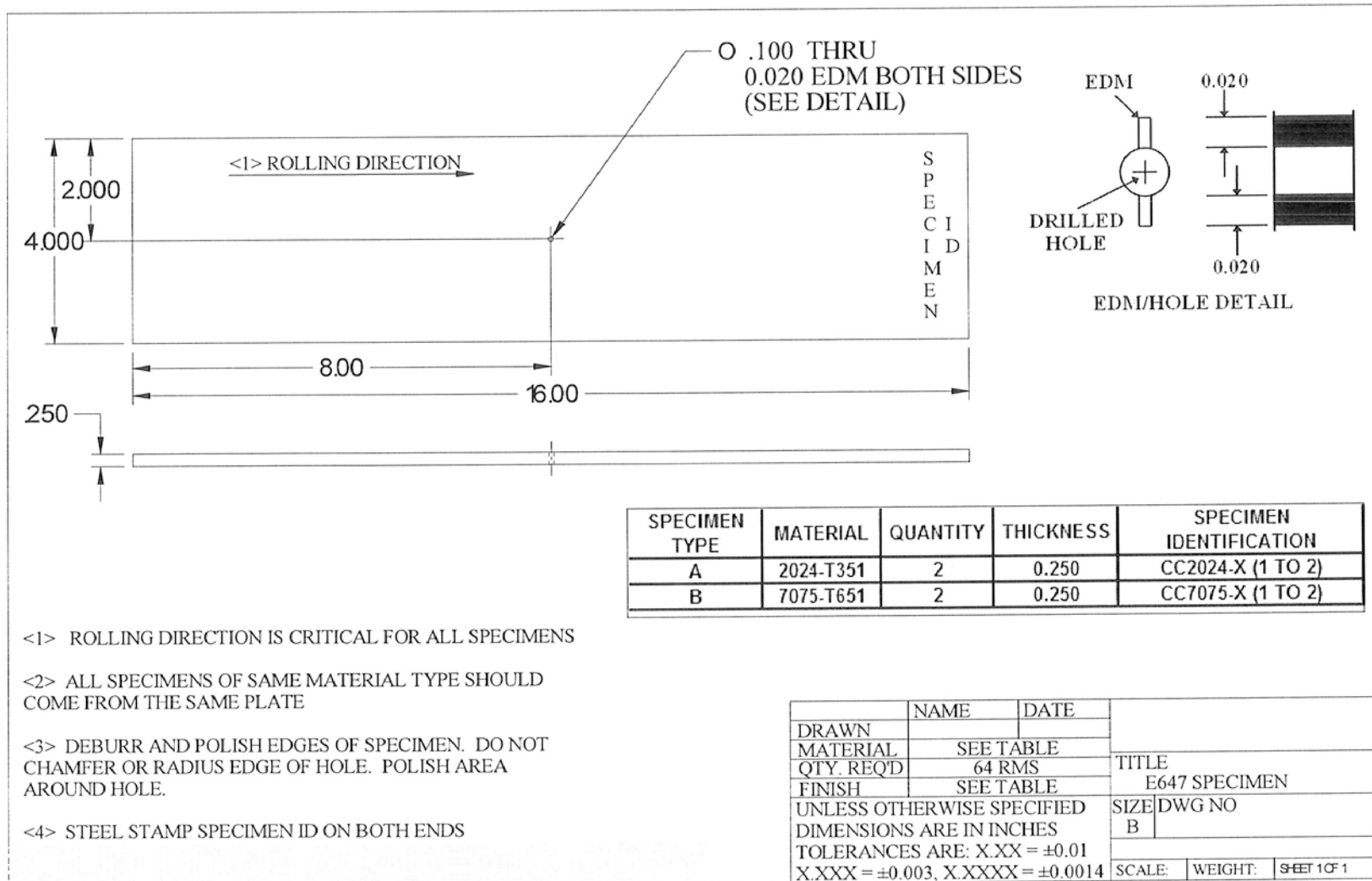|	NAME	DATE		
DRAWN				
MATERIAL	SEE TABLE		TITLE	
QTY. REQ'D	64 RMS		E647 SPECIMEN	
FINISH	SEE TABLE			
UNLESS OTHERWISE SPECIFIED			SIZE DWG NO	
DIMENSIONS ARE IN INCHES			B	
TOLERANCES ARE: X.XX = ±0.01				
X.XXX = ±0.003, X.XXXX = ±0.0014		SCALE:	WEIGHT:	SHEET 1 OF 1

Fig. 8 Manufacturing drawing of ASTM Standard E 647 fatigue specimens.

2.1.3.2 Baseline Noncold Expanded Testing Specimens

As a baseline for fatigue crack growth behavior there were four baseline, noncold expanded specimens manufactured. These test specimens were manufactured out of the same basic material blank as the ASTM E 647 specimens but varied from them in that instead of a 0.100 inch hole and two through-thickness EDM notches in the center of the test specimen these baseline specimens had a center hole of diameter 0.474 – 0.477 inch and a 0.010 inch EDM corner notch in them in the three o'clock position of the hole. Fig. 9 is the drawing provided to the CASTLE group for the manufacturing of the baseline noncold expanded specimens. The hole diameter of 0.474 – 0.477 inch corresponds with the industry standard established by Fatigue Technologies Incorporated (FTI) for the precold expansion hole diameter for a 0.500 inch hole.[9] FTI is one of the leading developers of the Split Sleeve Cold Expansion™ process and is the current contracting firm with the USAF for this process. Therefore it was desirable to follow the FTI standard specifications for Split Sleeve Cold Expansion™ in this research to ensure that it matched as much as possible the current USAF methodology.

2.1.3.3 Cold Expanded Testing Specimens

The final specimen configuration for this research project was the cold expanded specimen. These specimens like the ASTM E467 specimens and the noncold expanded specimens were cut from the same material blank.
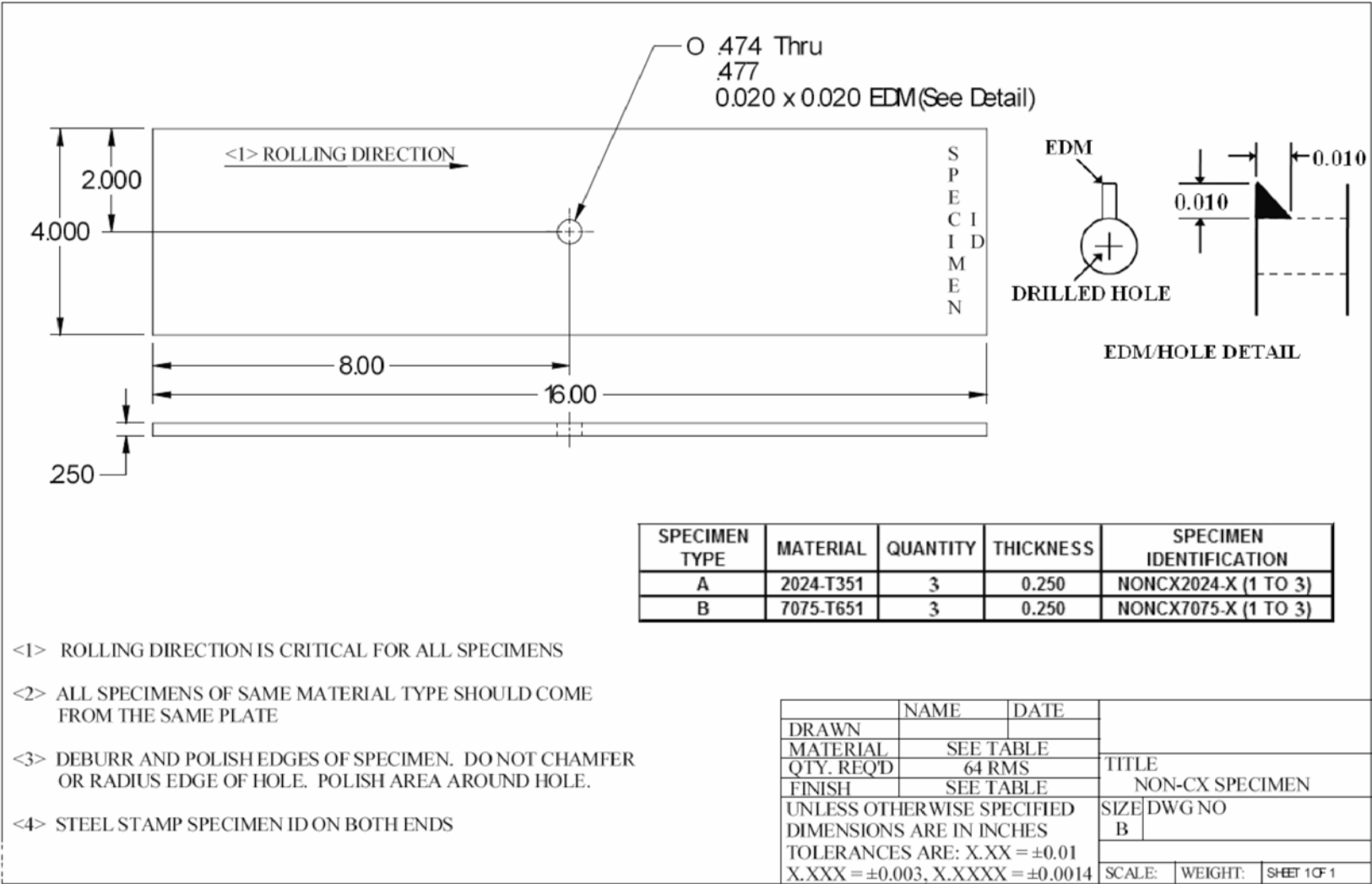
Fig. 9 Manufacturing drawing for noncold expanded baseline specimens.

In the drawing:

○ .474 Thru
.477
0.020 x 0.020 EDM (See Detail)

<1> ROLLING DIRECTION

2.000
4.000
8.00
16.00
250

S P E C I M E N   I D

EDM
DRILLED HOLE
EDM/HOLE DETAIL
0.010
0.010

SPECIMEN TYPE	MATERIAL	QUANTITY	THICKNESS	SPECIMEN IDENTIFICATION
A	2024-T351	3	0.250	NONCX2024-X (1 TO 3)
B	7075-T651	3	0.250	NONCX7075-X (1 TO 3)

<1> ROLLING DIRECTION IS CRITICAL FOR ALL SPECIMENS

<2> ALL SPECIMENS OF SAME MATERIAL TYPE SHOULD COME FROM THE SAME PLATE

<3> DEBURR AND POLISH EDGES OF SPECIMEN. DO NOT CHAMFER OR RADIUS EDGE OF HOLE. POLISH AREA AROUND HOLE.

<4> STEEL STAMP SPECIMEN ID ON BOTH ENDS

	NAME	DATE	
DRAWN			
MATERIAL	SEE TABLE		
QTY. REQ'D	64 RMS		TITLE
FINISH	SEE TABLE		NON-CX SPECIMEN

UNLESS OTHERWISE SPECIFIED
DIMENSIONS ARE IN INCHES
TOLERANCES ARE: X.XX = ±0.01
X.XXX = ±0.003, X.XXXX = ±0.0014

SIZE B   DWG NO
SCALE: WEIGHT: SHEET 1 OF 1

These specimens also

had a precold expansion center hole in them with a diameter of 0.474 – 0.477 inch and a 0.010 inch corner EDM notch in the three o'clock position of the hole. After the hole was drilled it was cold expanded using FTI's Split Sleeve Cold Expansion™ process. After the cold expansion process was complete the hole diameter was increased to 0.480 – 0.484 inch. Appendix B provides a table outlining the precold expansion hole size and calculated residual expansion for all cold expanded specimens tested during this research project. Once the specimens were cold expanded they were marked to allow an easy visual reference for which side of the specimen was the entrance side of the cold expansion mandrel and which was the exit. This will be the reference used in this paper for the designation of the specimen surfaces. It was required that the specimen be EDMed on the entrance side of the specimen.

To minimize the likelihood of fatigue cracks nucleating at the ends of the specimens where the fatigue machine grips attached to them, tabs were bonded onto the ends of the specimens. These tabs were made from 6064 aluminum sheet material and were bonded onto the 2024-T351 specimen using Hysol EA 9696, 0.06 psf adhesive. This was done due to the fact that previous fatigue research performed by the USAFA's CASTLE group showed that there was a high probability that fatigue cracks could nucleate at the grip locations on the specimens and propagate to failure if no additional material is present in this location.[11] Fig. 10 is an image of the standard specimen configuration for all cold expanded specimens. The tabs can be seen at the top and the bottom of the specimen and the 0.50 inch hole is in the center of the specimen. Fig. 11 is
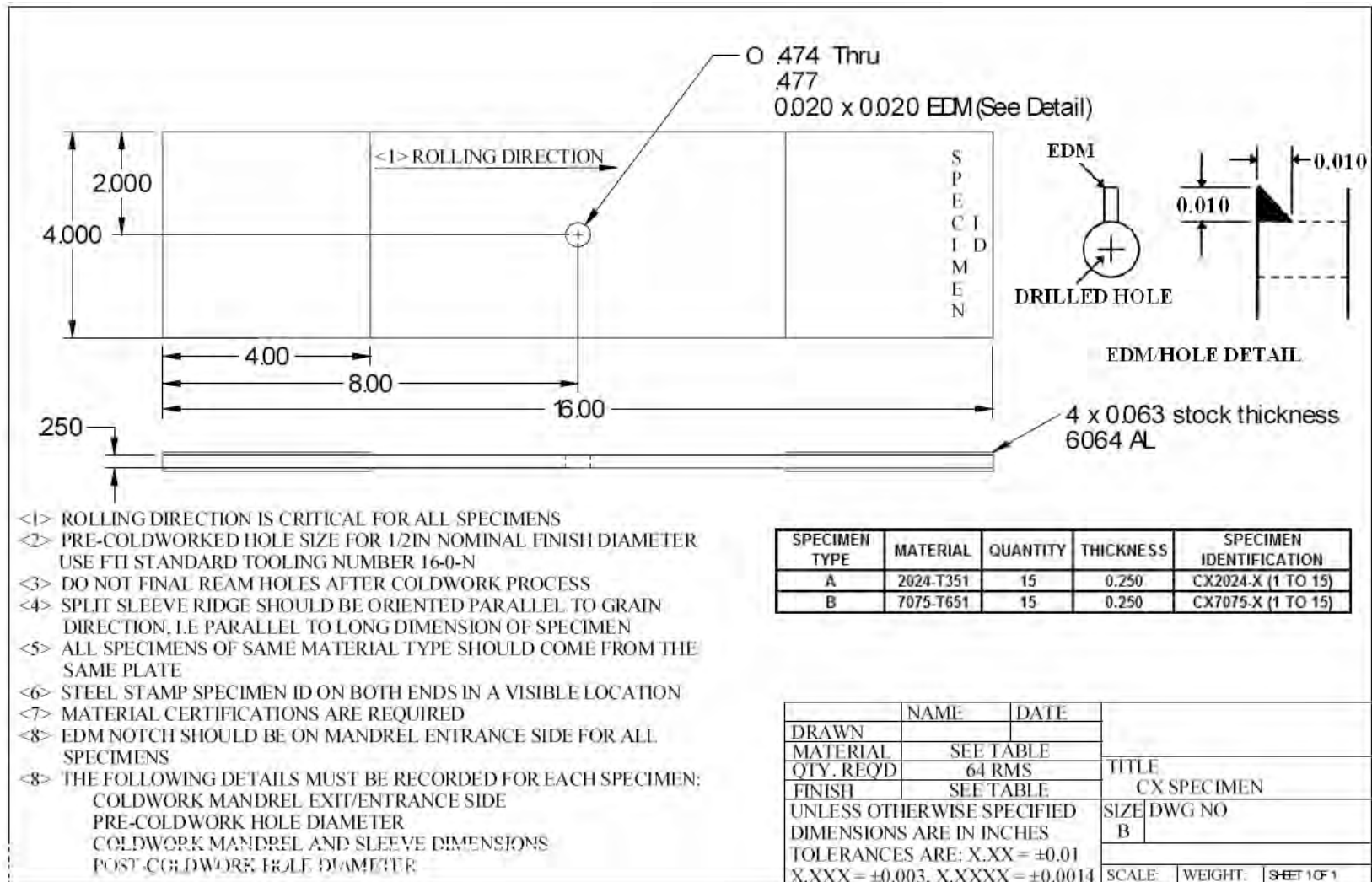
Fig. 10 Standard cold expanded specimen set-up.

Fig. 11 Manufacturing drawing for cold expanded fatigue testing specimens.

the drawing provided to the CASTLE group for the manufacturing of these cold

expanded specimens.

2.2 Fatigue Testing Equipment and Testing Setup

All of the testing for this research program was performed at Hill Air Force

Base (AFB) in the Materials Testing Laboratory.

2.2.1 Interlaken Series 3300 55 kip Fatigue Machine

Hill AFB acquired the Interlaken 55 kip fatigue machine in the early 1990s

and it was recalibrated on August 18, 2007. When the research program began

this machine had a set of Interlaken hydraulic grips installed however, these grips

only allowed for testing of specimens that were no wider than 2.50 inches. New

grips were requested from Wright-Patterson AFB but in order to install the new

grips threaded bushings had to be installed into the attachment locations for the

grips to the machine. Next a step-stud had to be threaded through the bushing

to allow for the proper stud diameter for both the Interlake fatigue machine and

the new MTS grips.

2.2.2 55 kip MTS 647 Hydraulic Wedge Grips

With the need to test specimens that were over the 2.50 inches allowable

width available from the Interlaken grips a set of MTS 55 kip hydraulic grips were

acquired from the Materials Directorate testing lab at Wright Patterson AFB.

These grips would allow for the testing of specimens in excess of 2.5 inches in

width. Once the grips were installed it was determined that a hydraulic intensifier

was needed to increase the pressure supplied to the grips for holding the test specimen.

2.2.3 MTS Model 685.60 Hydraulic over Hydraulic Intensifier

As the testing setup continued it was determined that a hydraulic intensifier was needed to increase the hydraulic pressure supply, of 3 ksi to around 6.5 ksi. This increased pressure would allow for a greater force to be exerted onto the surface of the specimen by the wedges within the MTS grips ensuring that the piston within the grips would not pull out by the high loads induced during testing. The intensifier used was manufactured by MTS and was designed to increase the pressure from the standard lab pressure of 3 ksi to 10 ksi. The intensifier used a "hydraulic over hydraulic" pump mechanism to perform this function. During the testing of the fatigue specimens the hydraulic intensifier was set to 6.5 ksi and this allowed for adequate pressure to hold the specimen in place without causing permanent deformation of the grip ends.

2.2.4 Instron 8800 FastTrack Testing Controller and Software

The Interlaken fatigue machine was controlled by an Instron 8800 FastTrack controller. Two pieces of software were used to produce the waveform used for the testing. These two programs were WaveMaker Editor and the Fatigue Crack Propagation – da/dN software packages. The WaveMaker Editor was used at the start of the testing phase but it had limitations in its ability to pause the test to take crack length measurements. The Fatigue Crack Propagation – da/dN software allowed the user to pause the test for a given amount of time and during this pause hold the load at either mean or maximum.

The Fatigue Crack Propagation – da/dN software was then used for the entire duration of testing.

2.2.5 Visible Crack Growth Tracking Equipment

To be able to capture the crack growth rates during testing a set of Gaertner traveling microscopes were mounted to the frame of the Interlaken fatigue machine. A fixture was fabricated to allow for the scopes to be mounted in front of the testing specimen. Fig. 12 shows the testing setup.

A set of microscopes and traveling slides were mounted to both the front and back of the fatigue machine to allow for visual crack measurements to be taken of the front surface, bore and back surface of the specimen. The Gaertner traveling microscopes allowed for a 10X magnification of the specimen surface.

Fig. 12 Testing Setup with MTS Hydraulic Grips and Gaertner Traveling Microscopes

This allowed for crack measurements to be taken at an accuracy of 0.0005 – 0.001 inch. This level of accuracy was well within the allowable guidelines established by ASTM E 647 standard.

2.2.6 Fatigue Testing Machine Calibration and Certification

The test frame and load cell were serviced, calibrated, and certified by an Instron technician on 09/18/2007 and were valid until 09/18/2008, which covered the certification during the testing. In order to check concentricity of the MTS hydraulic grips, a dial indicator was attached to the upper grip and the runout was checked as the lower grip was rotated. The maximum runout was recorded as 0.021 inch. Due to the difficulties with adjusting the Interlaken test frame, this runout value was noted but considered acceptable.

2.3 Fatigue Testing Procedures

2.3.1 Testing Specimen Preparation

In an attempt to minimize the effects caused by the manufacturing of the test specimens each specimen was prepared for testing by being sanded and polished. This specimen preparation process helped to ensure that fatigue cracks would nucleate only at the desired hole location and not at other stress concentration factors such as corner or even gouges and nicks. By driving the fatigue crack to nucleate at the EDM it made it more possible to drive out other factors that come into play during the fatigue crack growth process. These other factors, like multiple crack interaction or multiple crack nucleation are extremely difficult to model and induce error into the test that can not be accounted for.

Thus by inducing a crack starter into the material it makes it more likely that the

crack will behave in a manner that is possible to model and predict.

2.3.1.1 Sanding and Polishing of Testing Specimen

Once the fatigue test specimens were received from the CASTLE group at

the USAFA they were thoroughly sanded. The sanding process was made up of

two different phases. Each phase was done by hand with a sanding block to

allow for even sanding of the specimen. This would ensure that no area on the

surface of the specimen was of a smaller thickness than the specified 0.25 inch

requirement.

The first phase used a 320 grit sandpaper to eliminate the oxide film that

was on the surface of the specimen as well as any other nicks or scratches that

were present on the surface of the specimen. The removal of the oxide film was

to allow greater ability to visually see the fatigue crack on the surface of the

specimen. It was also necessary to remove any nicks or scratches on the

surface of the specimen where fatigue cracks could nucleate and propagate to

failure.

Once this first sanding process was finished a less abrasive, 500 grit

sandpaper was used on both the entrance and exit surfaces of the specimen

around the hole to prepare the specimen for the polishing. The finer grit paper

made it easier to polish the specimen to a mirror finish.

The polishing of the specimen was performed using an electric Dremel

with a polishing wheel attached to it. To aid in the polishing a diamond paste

slurry was used. The slurry came in two different diamond sizes, 5 micron and

10 micron. Both slurries were used to produce a mirror finish around the hole and then out to the edges. This would allow for greater accuracy in measuring the length of the fatigue crack as it propagated out from the hole.

Both the sanding and polishing process were not only applied to the entrance and exit surfaces of the specimen but also to the hole. Visual crack measurements were taken down the bore of the hole during the fatigue testing. Each hole had to be polished to a mirror finish to allow for the measurements to be taken accurately. Also a mirror finish would help to prevent fatigue cracks from nucleating at nicks in the hole from the cutting process.

2.3.2 Precracking and Final Reaming of Testing Specimens

It was determined that each test should simulate as much as possible the types of fatigue cracks that we see in the field that nucleate and propagate out of cold expanded holes. To do this, each specimen was precracked and then final reamed to the FTI specified final hole diameter of 0.500 inch. This would allow the final testing of the specimen to be free of any effects that can be caused by the EDM notch. These effects can include a heat-affected zone around the EDM notch. This zone can alter the fatigue crack growth behavior and therefore must be either taken into consideration or removed. It was decided that removing its effects by reaming out the EDM was preferred.

2.3.2.1 Precracking of Testing Specimen

Precracking of each specimen was performed in accordance with the guidelines outlined in ASTM Standard E 647. Appendix C contains all the pre-

cracking information, including load, stress, frequency and cycles. The final

crack size desired for the precracking stage ranged between 0.020 – 0.030 inch.

This would allow for a postfinal ream crack size of below 0.050 inch from the

edge of the hole. This would mean that depending on the size of the EDM there

would be some residual EDM left or there would be no EDM left, only a pure

fatigue crack. Either way it was determined that if a fatigue crack had

propagated to roughly two times the length of the EDM that all effects of the heat

effect zone would be minimal and not have to be considered within the scope of

this project.

2.3.2.2 Final Reaming of Testing Specimen

After the specimens were precracked and marked to show which side was

the precracked EDM side, they were reamed at the University of Utah's

Department of Mechanical Engineering machine shop. The final ream process

was performed on a standard mill with a 10-flute reamer. The final reaming

process was performed at 1,000 RPM and hand-fed to ensure that the surface

integrity was held to the highest quality. During the reaming process it was

determined that to reduce the chatter effects of the reamer on the EDM side of

the specimen the reamer should enter on the exit side of the specimen. This

would allow the reamer to be settled in by the time that it exited the hole. At the

feed rate and rotation speed this seemed to dramatically increase the surface

integrity of the bore surface and the edge of the hole. In turn this decreased the

time needed to produce a high quality surface during final sanding and polishing

stage of the specimen preparation.

2.3.3 Sanding and Final Polishing of Testing Specimen

After the final reaming was completed the specimens were taken back to

the Hill AFB Materials Lab and sanded and polished for a final time. This

process was performed in the same manner as the first stage sanding and

polishing as outlined previously. The final sanding and polishing stage focused

on producing as close to a mirror finish as possible. This would allow for the

visual tracking of the fatigue crack to be accomplished much easier both along

the surface of the specimen and along the bore. The sanding and polishing for

this final stage also focused on the areas right around the hole and out to the

edge of the specimen. This would be the main region of crack growth during the

testing. Fig. 13 shows a specimen prior to final testing.
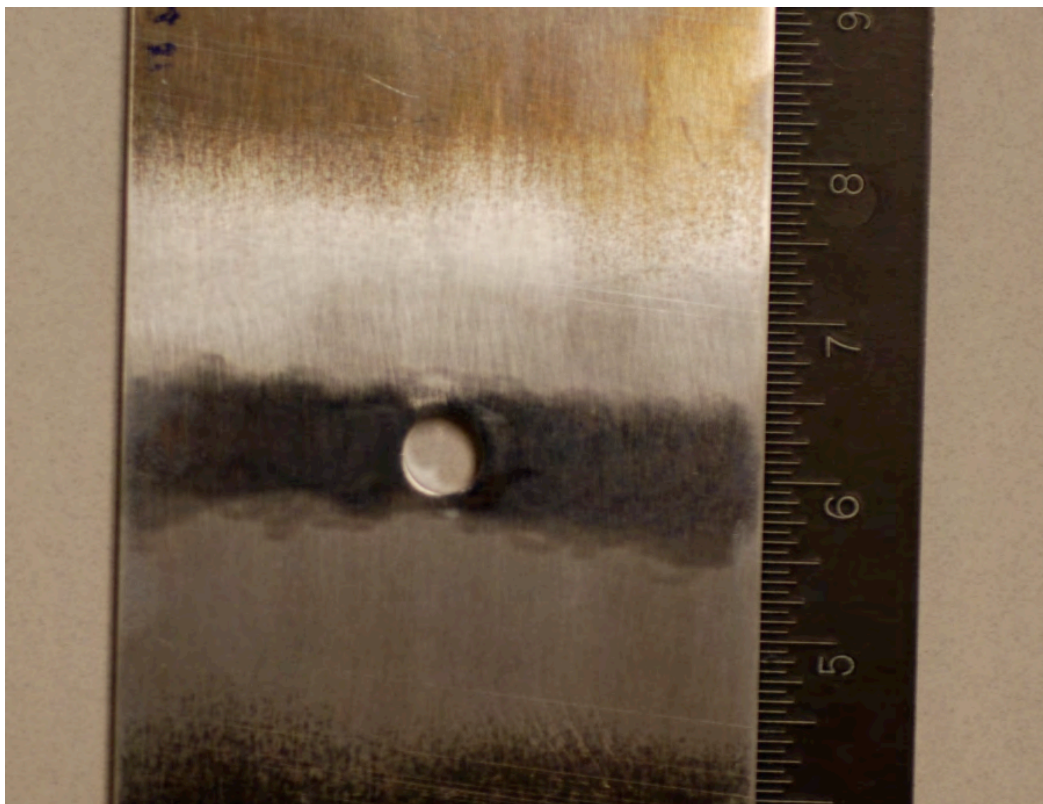

Fig. 13 Polished crack surface. Prepared by sanding and polishing.

2.3.4 Final Fatigue Testing to Failure

The final testing of all specimens was performed at different maximum stresses to capture the greatest range of ΔK as possible. Appendix C outlines the loading conditions for all specimens tested during this research project. All specimens were tested at a stress ratio of 0.1 and at 20 Hz, except for the E 647 specimens which were tested at 15 Hz. At this load and frequency the Instron controller had no problem with initial effects or tuning.   There were no environmental effects introduced into the test. The testing area was held at a relatively constant temperature of 71 degrees F and a humidity of 50 percent.

2.3.4.1 Testing to Failure

2.3.4.1.1 Specimen Installation and Visual Crack Growth

Once the surface was prepared the specimen was mounted into the two MTS open face hydraulic grips. The specimen had to be installed so that the hole could be seen through both the front and back traveling microscope. This was accomplished by first having the lower, actuator grip hold the specimen and then moving the actuator up and down to position the specimen properly. Once this was accomplished the upper grip was tightened and the specimen was held in place. To tighten the grips onto the specimen the MTS intensifier was used instead of the Interlaken gripping mechanism. This would allow the grips to exert a greater force on the specimen, holding it in place while the test was being tested at the higher loads.

With the specimen locked in place the back traveling microscope had to be turned to face the EDM side of the bore. This made it possible to track the fatigue crack as it propagated through the bore of the specimen.

To calculate the length of the fatigue crack down the bore a simple calculation had to be performed to use the angle of the microscope and the thickness of the specimen to calculate an accurate crack measurement. Fig. 14 along with Equation (3) show how this was accomplished. In order to accomplish this the rear side traveling microscope was twisted to an unknown angle in reference to the face of the specimen. This angle was then calculated by the use of the known relationships that occur in right triangles. By turning the microscope and then using it to measure the thickness of the specimen and comparing that to the known thickness a ratio could be determined and the angle could be solved for.

$$\theta = (\sin^{-1}) \times (\mathrm{Re}\,ading\,/\,Thickness) \times (180\,/\,\pi) \tag{3}$$

Fig. 14 Method of calculating the angle of the traveling microscope to correct the crack growth measurement.

With θ known, all crack measurements were then multiplied by the θ value and the visual crack length was then converted to represent how long the fatigue crack was through the bore of the specimen. This was a very simple way to measure the crack length through the bore of the specimen and worked very well.

2.3.4.1.2 Fatigue Testing and Visual Crack Growth Measurement

Once the setup was complete, the specimen was tested to failure. During the testing process the test was paused to allow for visual crack measurements to be taken. To take this visual crack measurement the cross hairs of the traveling microscope was set to the tip of the fatigue crack and a measurement was taken off of the measurement marks on the Gaertner scope. Also, at each crack measurement the traveling microscope was brought back to the edge of the hole or EDM notch if present and the crack growth measurement was based on that location. This ensured that each measurement was reset to the baseline dimension of the edge of the hole or EDM notch.

Crack growth measurements were taken on five surfaces during the length of each test. These measurement surfaces were on the Entrance EDM surface, Entrance Secondary surface, EDM Bore surface, Exit EDM surface and Exit Secondary surface. Appendix C contains crack growth measurement sheets for all specimens tested during this project.

2.3.5 Postfailure Testing Specimen Preparation

Once the testing specimen had failed it was removed from the upper and lower grips and examined. The specimen name was then written upon the entrance surface of the specimen next to the hole to allow for future reference. The EDM side was also marked on the surface of the specimen to make sure that the main crack location was known.

2.3.5.1 Fracture Surface Extraction and Examination

Once these markings were completed the fracture surface was extracted with a band saw. Each specimen was then cut about 1 inch away from the hole to allow for ease of storage and fractography. With the specimens cut to a shorter 1 inch length they were prepared for fractography.

3 FATIGUE TESTING DATA COLLECTION AND PROCESSING

3.1 Visual Crack Measurements

During the testing of each specimen visual crack growth measurements were taken. These measurements were taken on five surfaces of the specimen; the Entrance EDM surface, Entrance Secondary surface, EDM Bore surface, Exit EDM surface and the Exit Secondary surface. During the testing of each specimen the Entrance EDM surface was the crack length that was the main focus. The objective was to take crack growth measurements at a consistent rate for given crack lengths. This measurement rate would change as the crack grew and propagated more rapidly. By moving the cross hairs of the traveling microscope to the desired crack length and then watching the crack propagate to that point a consistent crack grow measurement could be accomplished. This was done throughout the test to ensure consistent crack growth measurements were taken.

3.2 Calculating Fatigue Crack Growth Rates

Crack growth rates were calculated using the secant method as outlined in ASTM E 647.[28] This method calculates da/dN by the slope of a straight line between two data points on the crack length versus cycles curve (a versus N).

Equation 4 calculated the change in crack length versus number of cycles is an average crack growth rate over the increment of ($a_{i-1} - a_i$).

$$(da/dN)_{\bar{a}} = \Delta a/\Delta n = (a_{i+1} - a_i)/(N_{i+1} - N_i) \tag{4}$$

3.3 Crack Front Geometry From Cold Expanded Holes

As the fatigue crack growth testing continued it was realized that the shape of the crack front in a cold expanded specimen propagated away from the hole differently than that of a noncold expanded specimen. This difference was previously unknown before testing and had to be understood and documented before further testing could be performed. Therefore, it was determined that a specimen would be marker banded to allow for documentation of how fatigue cracks grow in a residual stress field caused by cold expansion.

3.3.1 Marker Bands

Marker bands are commonly used in testing to aid in the determination of how fatigue cracks propagate through materials that are undergoing cyclic loading. The marks are produced on the surface of the specimen by changing the loading spectrum to either a higher or lower load and changing the frequency of that load. This change causes a mark to be imposed on the surface of the specimen due to the changes in the crack driving force. An example of this can be seen in Fig. 15. This image is of an aluminum alloy that underwent a spectrum loading experimentation. The visual bands on the surface are locations where the fatigue crack experienced a change in the loading sequence.
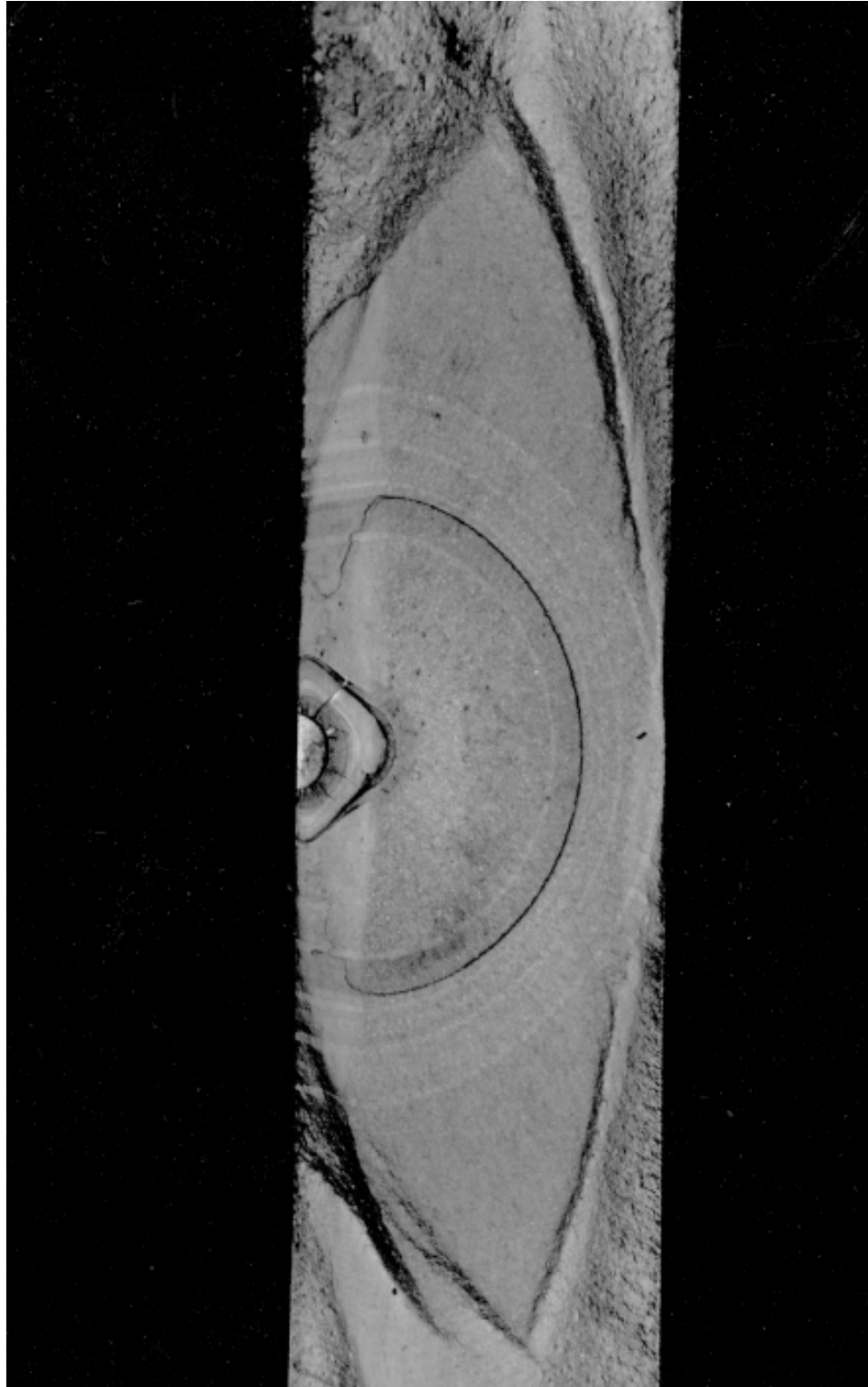
Fig. 15 Marker banding of from surface flaw. Courtesy of Hoeppner.[31]

3.3.1.1 Purpose for Marker Bands

When a material like 2024 aluminum is cold expanded the residual stresses that are induced into the material are significant enough to dramatically alter the fatigue crack growth shape. This was not well understood by the research community before this research project began. In a noncold expanded specimen the crack propagates in an elliptical shape from the nucleation site through the thickness of the material. The fatigue crack then changes to an elliptical shaped through-thickness crack and finally to a straight through crack. This type of fatigue crack propagation is well understood and documented.[32,33]

In a material that has been cold expanded however the crack does not propagate in this manner. Therefore, in order to accurately model and calculate the stress intensities for the cold expanded crack front geometry a specimen was tested under a unique loading spectrum to band the fatigue crack surface without changing the fatigue crack growth behavior of the material.

3.3.1.2 Marker Band Loading Spectrum

To successfully marker band the 2024 material the loading sequence or spectrum was changed periodically. Fig. 16 shows this loading spectrum. The spectrum was broken up into two main loading blocks. The main block was the same as the standard loading spectrum of maximum stress of 25 ksi and a stress ratio of 0.1 at 20 Hz. The banding spectrum had the same maximum stress of 25 ksi however the stress ratio was changed to 0.9 and the frequency was raised to 40 Hz. Table 1 shows the loading spectrum for this specimen.
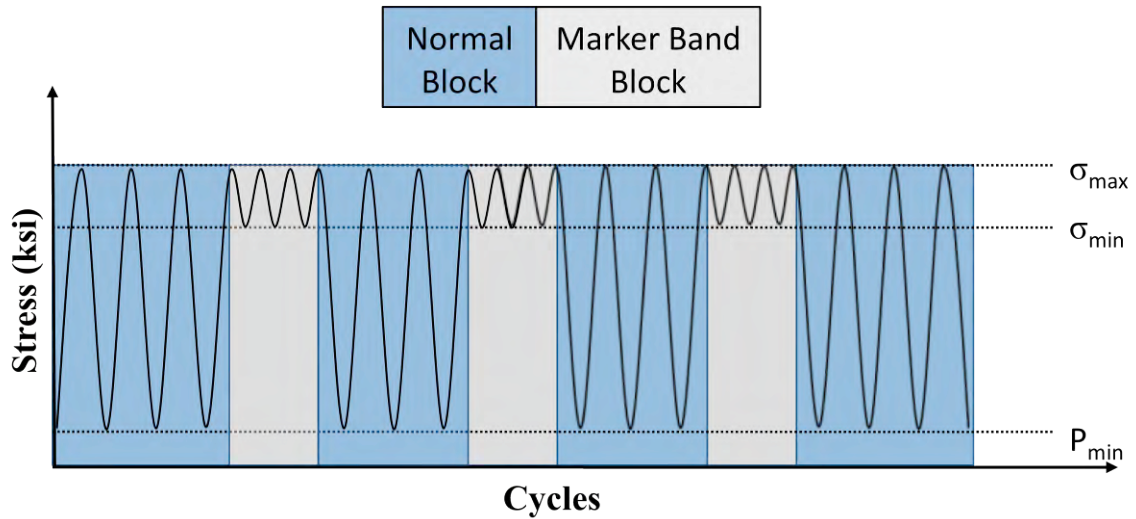
Fig. 16 Marker banding loading spectrum for aluminum 2024-T351.

Table 1 Loading Blocks for Marker Banding of Al 2024-T351 Specimen

Block	Stress Ratio	Minimum Stress	Maximum Stress	Frequency
Normal Block	0.1	2.5 ksi	25 ksi	20 Hz
Marker Band Block	0.9	22.5 ksi	25 ksi	40 Hz

The number of cycles in each block changed to allow enough cycles to either propagate the fatigue crack enough to have significant distance between each band or enough cycles in the banding spectrum to allow a visual reference to where the mark was on the fracture surface.

3.3.1.3 Marker Banding Results

Three specimens were designated to be marker banded. These specimens were CX 2024-08, CX 2024-10 and CX 2024-18. Specimen CX 2024-08's fracture surface was banded but the bands were too faint to be able to accurately determine the location of the crack front at given cycle counts. Fig. 17 is a fracture surface image of this specimen. It can be seen that the fatigue
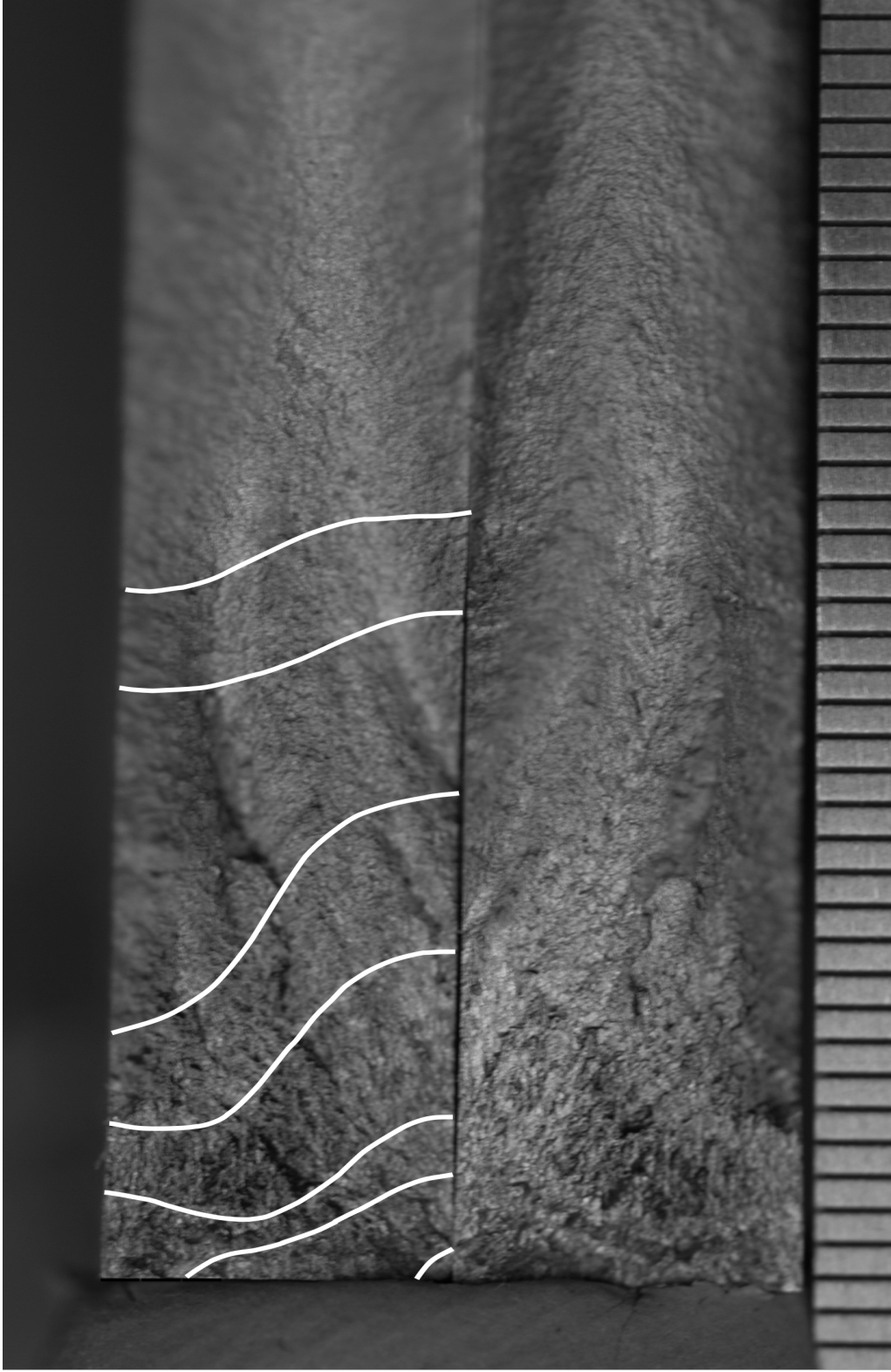
Fig. 17 Image of marker banded specimen CX 2024-08 with marker bands highlighted.

crack propagation shape changes as the crack propagates through the specimen. This shape was documented to allow for the accurate calculations of the stress intensities.

After CX 2024-08 had been tested and documented it was determined that another specimen must be tested in an attempt to band the specimen with a greater degree of clarity. Thus, the next specimen, CX 2024-10 was tested at longer intervals in the banding blocks. This would increase the length of the band on the fracture surface and produce a more pronounced marker band. This specimen, however, did not band properly and therefore this test had to be redone to produce accurate marker bands.

The final specimen that was banded for this project was CX 2024-18. During the marker banding of this specimen the banding blocks were extended in time to allow for a greater number of cycles to be imposed on the fracture surface of the specimen. During this test the crack was tracked on all three main fracture surfaces. This allowed for a reconstruction of the fatigue crack propagation from the crack length locations measured on the surface of the specimen. Fig. 18 shows the reconstruction of the fatigue crack front propagation through a residual stress field caused by cold expansion. 3.4 Determining Stress Intensities (K)

3.4 Determining Stress Intensities (K)

With a firm understanding of the physics of the crack propagation behavior through both the cold expanded and noncold expanded specimens the next task
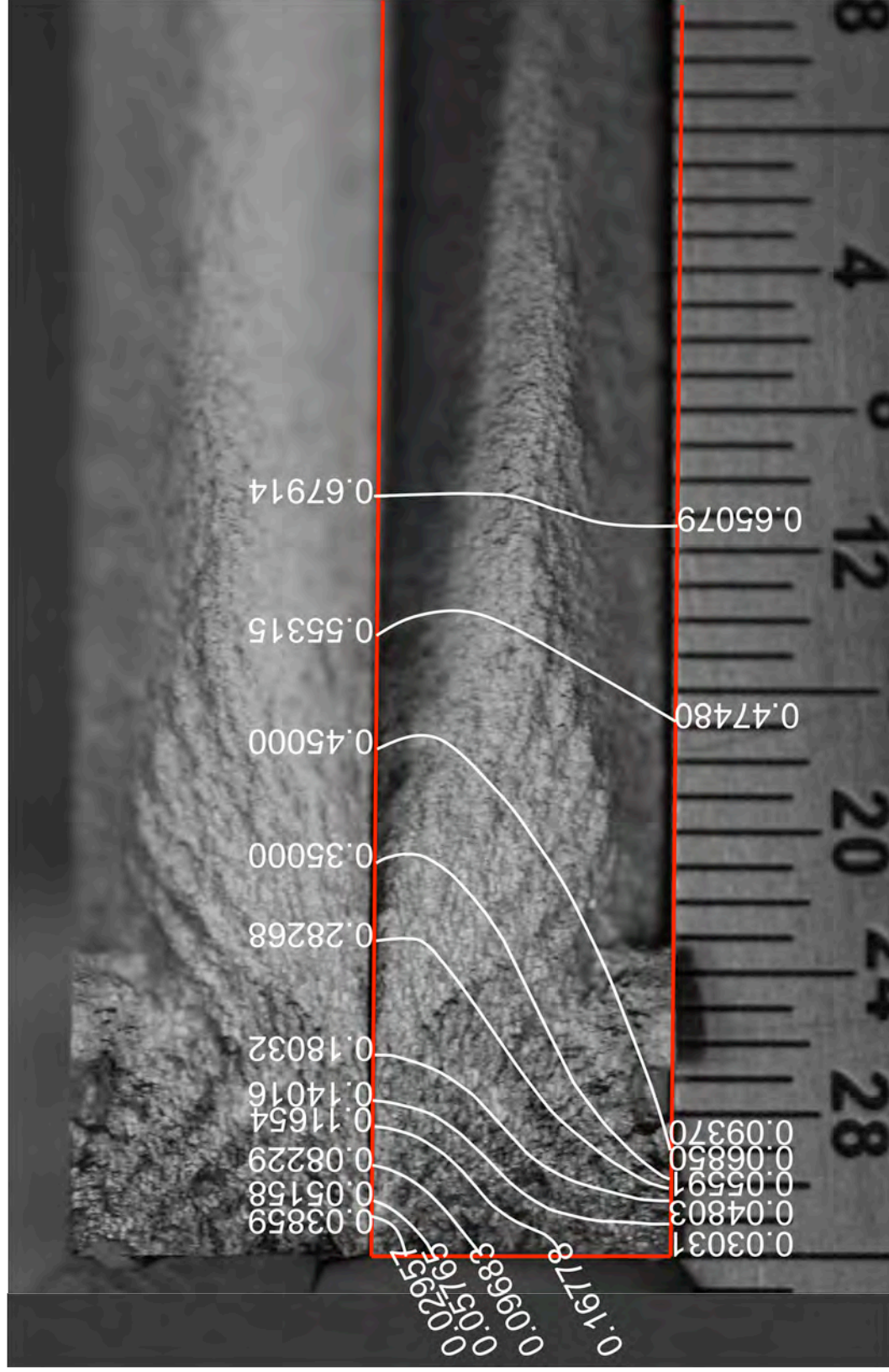
Fig. 18 Image of marker banded specimen CX 2024-18 with marker bands highlighted with surface and bore lengths (all dimensions in inches).

was to model these crack geometries using finite element analysis to compute the stress intensities. Each stress intensity would be specific for the given fatigue crack shape and length. The modeling of the stress intensities for this project were performed using StressCheck® and AFGROW.

3.4.1 Finite Element Modeling with StressCheck®

The next phase in the calculation of the stress intensities was to input the crack front geometry along with the testing specimen specifications into the finite element modeling software StressCheck®. StressCheck® is a polynomial based, p-version Finite Element Analysis (FEA) software that allows the user to impose onto the model a simulated crack front. As a p-version FEA software, StressCheck®uses a polynomial based refinement method that increases the order of the basis function that describes the geometry of the element edges. This type of finite element software differs from the standard h-version finite element program in that h-version software refines the elements by increasing the number of elements in a model rather than increasing the basis function. By increasing the number of elements in the mesh it provides a greater degree of accuracy in high strain gradients. This can be very labor intensive and time consuming and is also very sensitive to the types of elements used in the model.

StressCheck® allows for a p-level range from one to eight that can increase the accuracy when modeling high strain gradients without increasing the number of elements in the model. This makes it possible to solve for the given model without having to refine the mesh. The maximum p-level used for this project was five.

3.4.1.1 StressCheck® Modeling Methodology

       To calculate the stress intensities in StressCheck®, FEA models first had to be developed. These models were based on the testing geometry and loading conditions. The model dimensions, crack dimensions, applied loads, Young's Modulus, and Poisson's ratio were input as parameters into the FEA model to allow for repeated use and ease of updating the parameters and automatic regeneration of the model geometry and mesh.

3.4.1.1.1 Specimen Model Geometry

       A symmetric model was used to represent the specimen geometry. This reduced the computation time needed to calculate the solutions. Fig. 19 provides an overview of the model geometry and loading condition used in the FEA models. To simulate a crack in the finite element model, elliptical lines were imposed onto the symmetry surface to represent the crack front.

3.4.1.1.2 Specimen Model Loads and Constraints

       In order for the finite element model to provide stress intensity solutions for the testing configurations produced during testing proper model loads and constraints needed to be applied. Fig. 20 shows the loads and constraints applied to the finite element model produced in StressCheck®. To accurately model the testing conditions seen in the experimentation phase of this project the plane of symmetry at the centerline of the specimen was constrained with a symmetric boundary conditions.
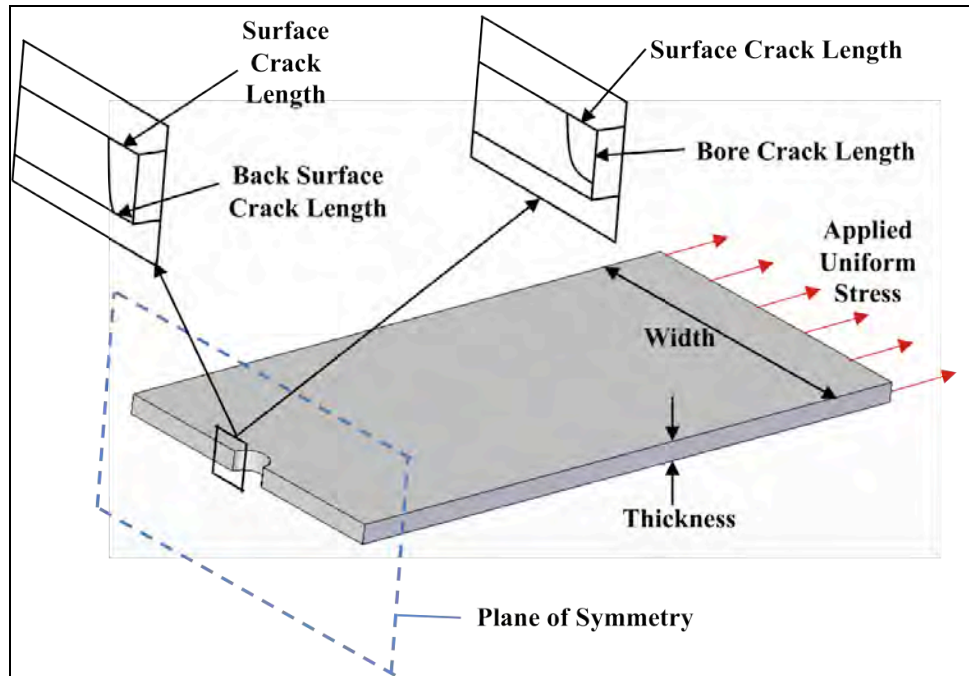
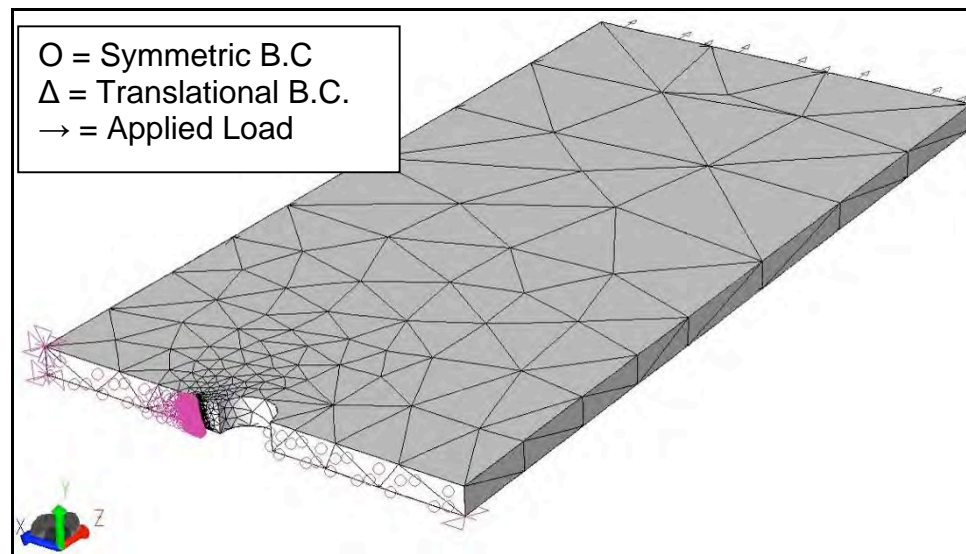Fig. 19 Overview of StressCheck® FEA model geometry and loading.

Fig. 20 StressCheck® model with loads and constraints applied to simulate testing conditions.

The crack face, however, was left unconstrained to allow the modeled crack front to propagate naturally as observed during testing. Translational constraints were applied to the symmetric boundary. This would eliminate out of plane rotations and movement. The crack face was unconstrained to represent a free surface. Finally a uniform stress was applied to the far end of the specimen to simulate the applied loading conditions seen in the test.

3.4.1.1.3 Specimen Model Mesh

The MeshSim automeshing feature in StressCheck® was used to mesh the model geometry. This automeshing feature, developed by Simmetrix, Inc., utilizes 10-node tetrahedral elements. The default global automeshing parameters were selected for the models with the exception of midside nodes. The automeshing feature in StressCheck® also has boundary layer refinement capabilities which can be used to control the mesh density at given geometric features without affecting the global mesh. This boundary layer refinement capability was utilized to refine the mesh at the crack tip. The allowed for a more accurate model to be produced.

3.4.1.1.3.1 Boundary layer refinement methodology. The boundary layer refinement methodology followed specific guidelines provided by Prost-Demasky of Analytical Processes and Engineering Solutions (APES) to make sure there is adequate mesh refinement throughout the model and at the crack tip[34]. These guidelines involved the following criteria:

1. The crack front should have four layers of elements of progressive smaller size

2. The refined boundary layer that is farthest from the crack front should be approximately 15% of the average crack size
3. The layer next to the crack front should be 15% of the width of the largest layer

The boundary layer parameters available in StressCheck®, which are used to manipulate the boundary layer refinement, are *Ratio*, *Layers*, *To*, *T-Total*, and *Side*. These parameters were utilized to meet the boundary layer refinement guidelines described above. The boundary layers were constructed in a geometric progression that was based upon the thickness of the first layer *To* and the total thickness of the boundary layer *T-Total*. Fig. 21 provides an illustration of the boundary layer refinement at the crack front.

3.4.1.1.3.1.1 Ratio. This parameter controls the ratio of the longest attached element edge to the length of the geometric edge or face. This value was used to control the mesh density at the boundary layer as the curvature of the crack front changed. The goal was to achieve a consistent mesh density at the crack tip to allow for accurate solutions without an overly dense mesh. For the models generated, Ratio values ranged from 0.02 to 1.0.

3.4.1.1.3.1.2 Layers. This parameter controls the number of layers of elements generated at the crack front. For the models generated, this value was set to 4.

3.4.1.1.3.1.3 To. This parameter controls the thickness of the first layer of elements next to the crack front. For the models generated, this value, based on the guidelines illustrated above, was set using Equation 5 where a and b are the surface crack dimensions.

$$T_O = 0.15 \times 0.15 \times ((a+b)/2) \qquad\qquad (5)$$

3.4.1.1.3.1.4 T-Total. This parameter controls the total thickness of the boundary layer. In order to input this into the program T_o and the largest refined layer in the crack mesh had to be known. Once these were known they were back substituted in order to solve for T-Total. The constant 0.161249 is a constant that come out of this calculation/conversion. In order to meet the guidelines specified above, this value was set using Equation 6.

$$T - Total = 0.161249 \times (a+b) \qquad\qquad (6)$$

3.4.1.1.3.1.5 Side. This parameter controls whether the boundary layer refinement will be generated on both or just one side of the crack front. This value was set to 0.00 which generates a boundary layer refinement on both sides of the crack front.

3.4.1.1.4 Model of Fatigue Crack

In order to produce the most accurate stress intensity solutions for the testing conditions seen during the experimental phase of the research program, three different finite element models were developed to represent the crack front geometry as seen from the marker banding specimen. These models would provide the basis for the development of the da/dN versus ΔK plots for both the baseline specimens and the processed specimen configuration. Fig. 22 provides a reference for these three models. All three models were referenced using either an angle or a distance from the entrance surface.
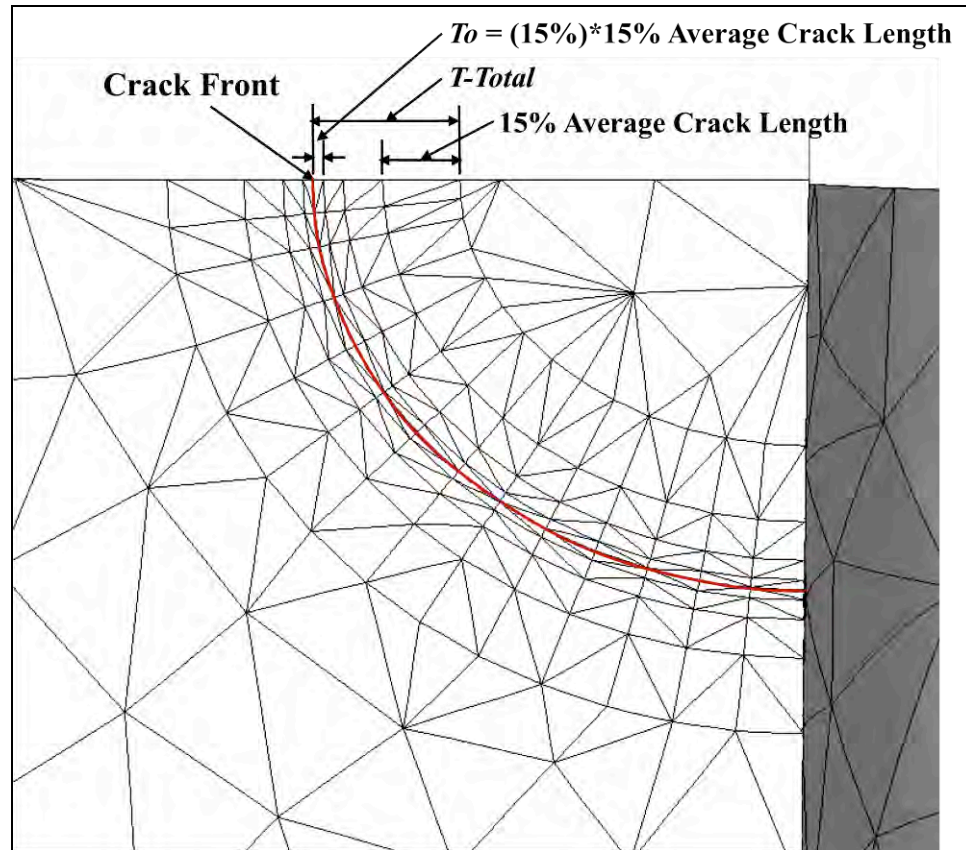
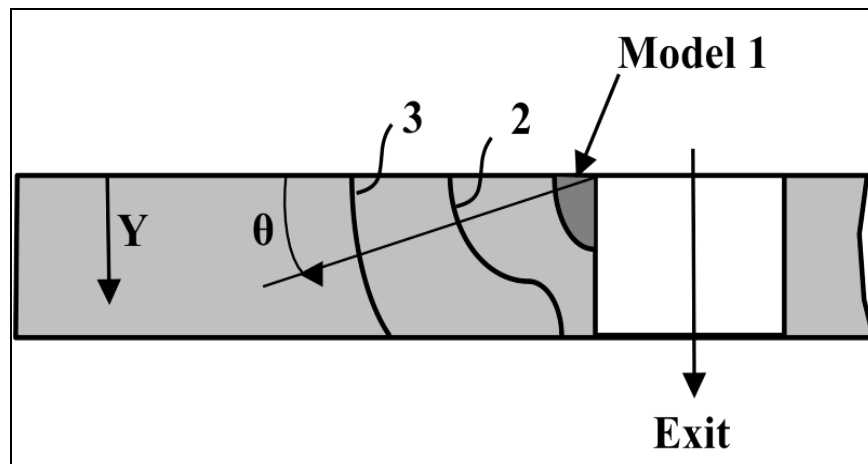Fig. 21 Simulated crack dimensional guidelines for StressCheck®.

Fig. 22 Diagram of FEA models showing the fatigue crack front geometry developed for StressCheck®.

3.4.1.1.4.1 Elliptical corner crack (Model 1). As seen in Fig. 18, the marker banded specimen, the crack front propagated from the EDM notch in an elliptical shape until it propagated through the thickness of the specimen. Therefore the initial stages of the crack propagation were modeled with a non-through-thickness elliptical corner crack. Fig. 23, which is an image taken from StressCheck®, shows an elliptical corner crack at the edge of the simulated fastener hole.

3.4.1.1.4.2 P-Shaped through crack (Model 2). Once the fatigue crack had propagated through the thickness of the specimen the model was changed from an elliptical corner crack to a P-shaped through-thickness crack. Model 2 was composed of two ellipses that were connected by a point on the crack front. This point was calculated from a between the relationship of the entrance surface crack length and the exit surface crack length by the Equation 7. Where y is the intersection height of the two ellipses and x is the primary entrance surface crack length. This equation was solved using Microsoft Excel and the marker banded crack front geometry to estimate the location of the crack inflection point. From the marker banded specimen a coordinate grid system was produced and from that an approximate location of the inflection point was found. This inflection point was then plotted in Microsoft Excel. The constants seen in Equation 7 are the constants extrapolated from the curve fit feature in Microsoft Excel.

Model 2 was used for primary entrance surface cracks that ranged in length from 0.00 inch to 0.35 inch. Fig. 24 is an image taken from StressCheck® of this model.
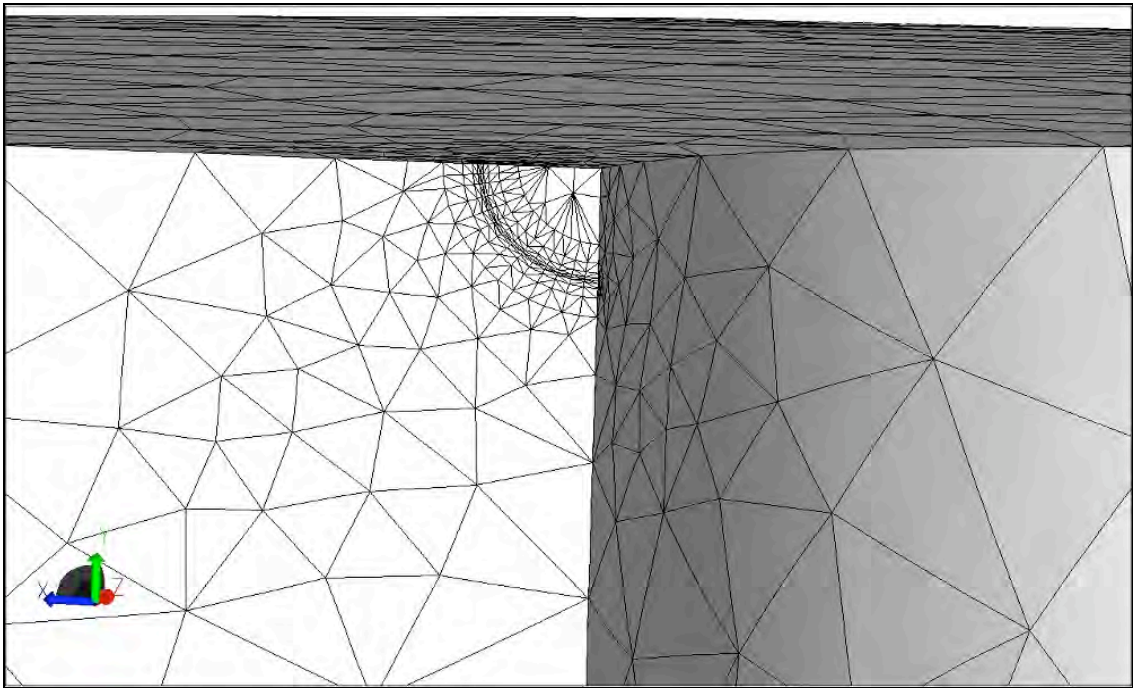
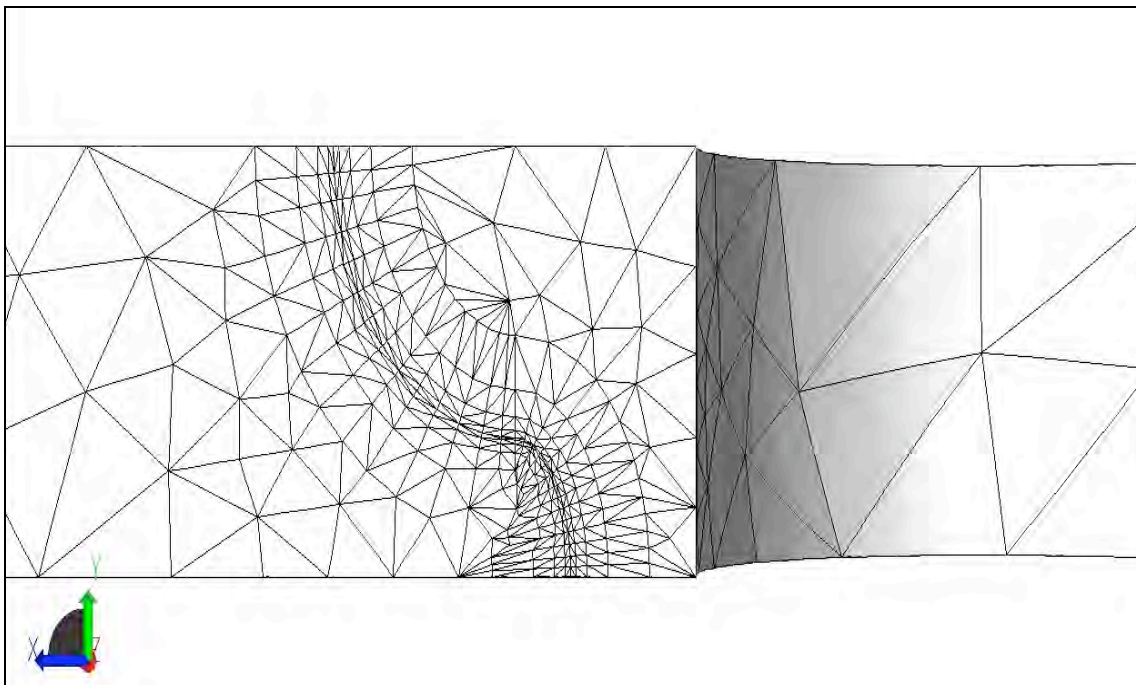Fig. 23 Model 1, non-through-thickness corner crack model for StressCheck®.

Fig. 24 Model 2, p-shaped through-thickness crack front model for StressCheck®.

$$y = 0.378 \times x^2 - 0.2568 \times x + 0.1668 \tag{7}$$

3.4.1.1.4.3 Elliptical through crack (Model 3). The third and final model used to simulate the crack front geometry in the finite element analysis was an elliptical through-crack model. Model 3 was used for cracks that had propagated beyond the bounds of the p-shaped crack model of 0.35 inch to the final fatigue crack length measured during testing. The elliptical through-crack was composed of one ellipse that passed through the thickness of the specimen and dimensioned to the crack lengths of the primary entrance and primary exit surfaces. Fig. 25 is an image taken in StressCheck® of this finite element model.

3.4.1.1.5 StressCheck® Stress Intensities for Analytical Models

StressCheck® uses a contour integral method to extract the stress intensities along the crack tip geometry. To perform this integration the user must input a contour integral radius. In order to follow the procedures outlined by Scott Prost-Demasky and APES[34] the contour integral radius had to pass through the middle of the second layer of the elements at the crack tip. In order to fulfill this requirement the contour integral radius was manually input into StressCheck® as Equation 8. Equation 8 has four main constants. The 0.15 breaks down the 15 percent requirement for mesh refinement between layers and the 0.50 takes the last layer and reduces it by 50 percent. The final constant 2.111 was solved for using the same methodology as that used to solve for T-Total.
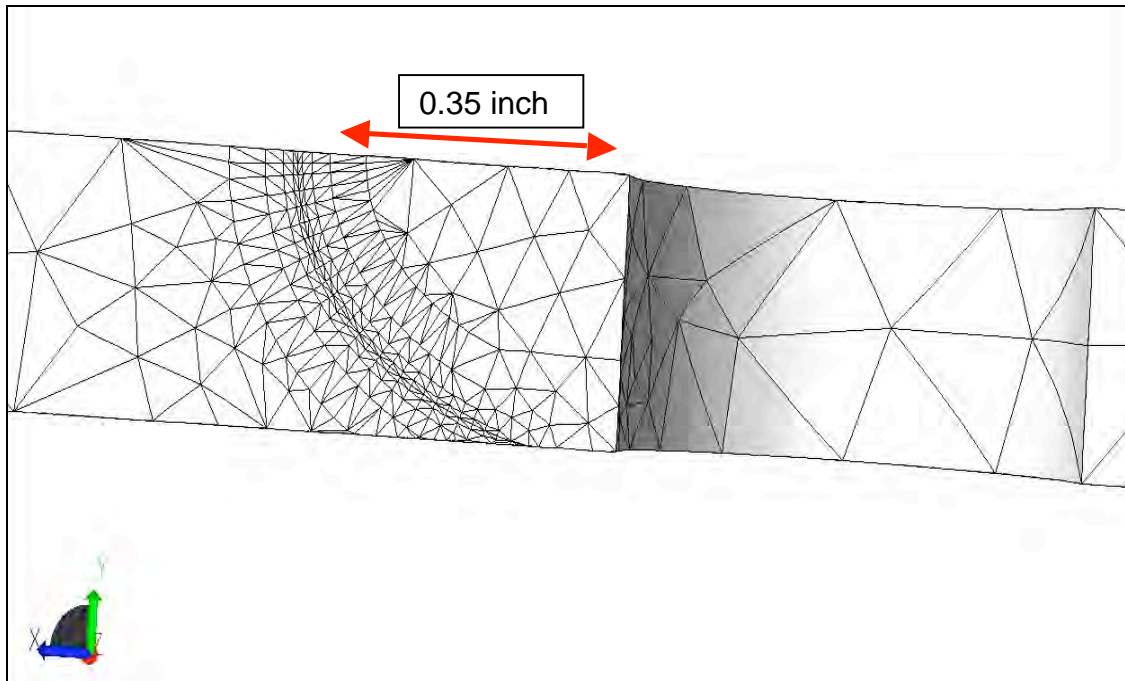
Fig. 25 Model 2, elliptical through crack front model for StressCheck® used when entrance side crack length exceeded 0.35 inch.

$$radius = 2.111 \times 0.15 \times 0.15 \times 0.5 \times (a + b) \qquad (8)$$

In this equation a is equal to the primary entrance surface crack length and b is equal to the primary exit surface crack length. Each of these crack lengths was visually measured during the fatigue testing of each specimen.

3.4.1.1.5.1 Location of stress intensities on model. Once the StressCheck® models were developed and processed it was determined that the stress intensities for each crack geometry should be calculated at the point where the crack front intersected the surface of the specimen. This would give a stress intensity at the surface of the primary entrance surface and the primary bore surface or once the fatigue crack had propagated through-thickness it would be at both the entrance and exit surfaces. The decision to chose the surface

edge for the location of the stress intensity was reached after speaking with Fawaz and discussing what was used in the development of AFGROW.[35]

   3.4.1.1.5.2 Stress intensity plots. Shown in Fig. 26 through Fig. 29 are examples of the solutions from StressCheck® for its calculations of the stress intensities along the crack front for both a baseline noncold expanded specimen and a cold expanded specimen. Each set of data represents the two surface crack measurements that were observed during fatigue testing. Two separate plots are shown for each specimen. One plot represents crack geometries along the EDM entrance surface and primary bore surface and the other represents after the fatigue crack after it had propagated through the thickness and therefore the measurements were taken on the EDM entrance and exit surfaces. From these plots all the stress intensities were derived. These plots were essential in the development of the da/dN versus ΔK plots. This would in-turn allow for the development of a *β* correction to represent the residual effects of the cold expansion process. Each plot has in the upper left corner a legend. This legend gives a breakdown of each crack length that was observed during the testing. The thru at the end of some crack lengths means that the crack had propagated through the thickness of the specimen and therefore a new set of coordinates were then used to measure from. The two types of coordinates can be seen in Fig. 22; one was based off of an angle from the entrance surface and the other was a distance from the entrance surface through the thickness of the specimen.

   The crack front geometry has a key role in the crack growth behavior in virtually all fatigue applications. This can be seen in these stress intensity plots.
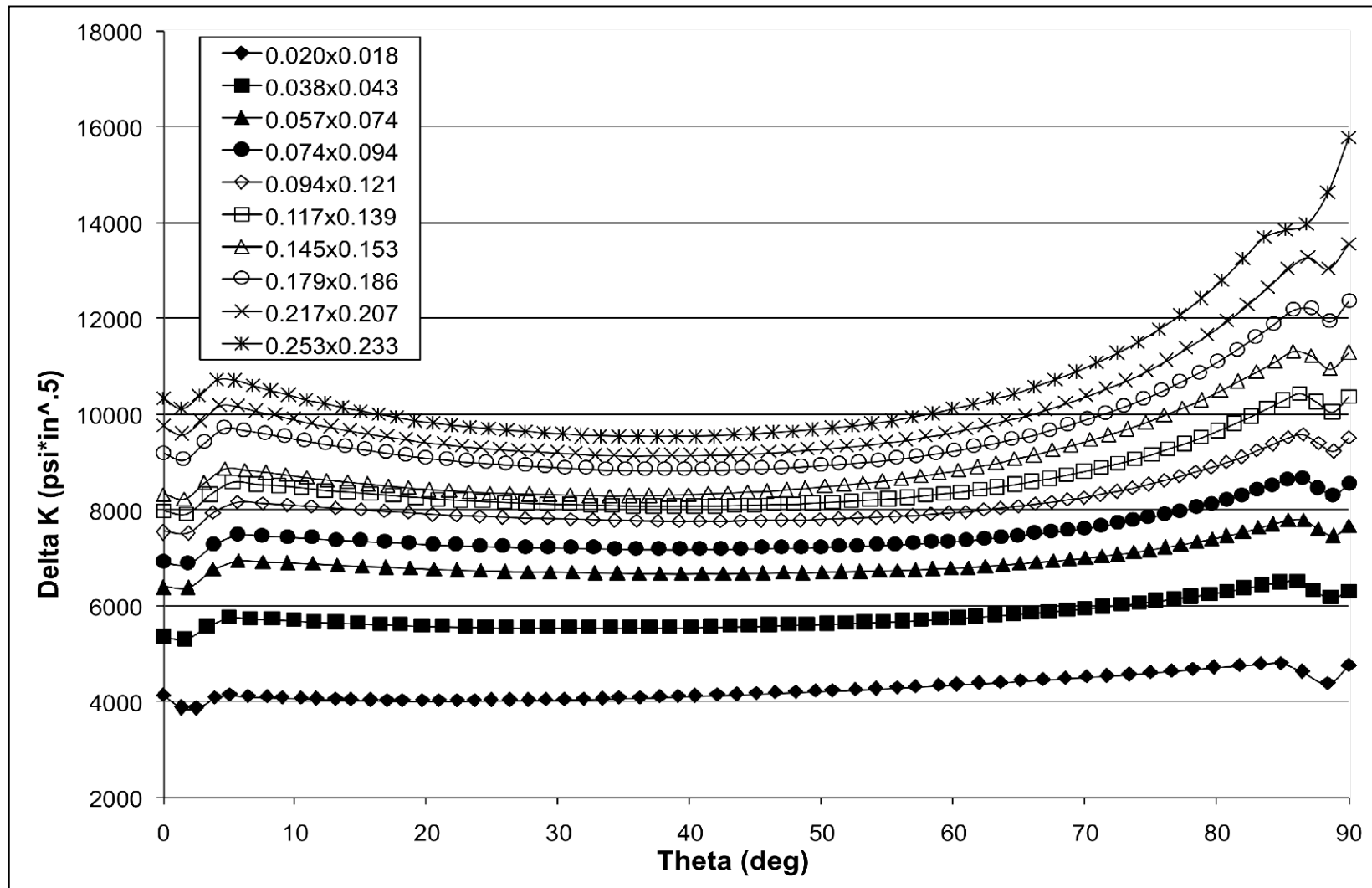
Fig. 26 StressCheck stress intensity solutions along the crack front for the non-through-thickness elliptical corner cracks modeled for specimen NON CX 2024-04. FEA modeled at σ_{max} = 10 ksi.
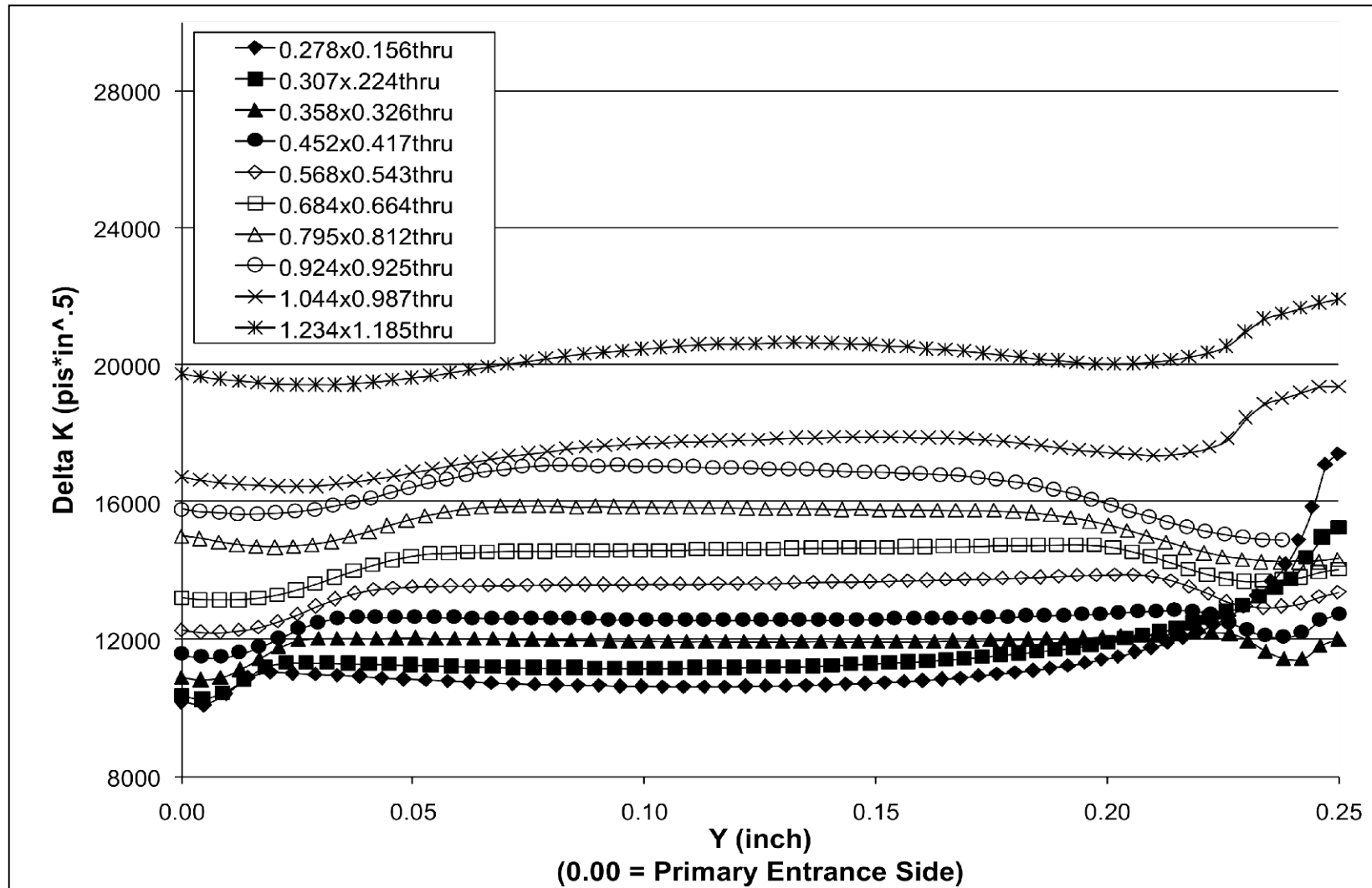
Fig. 27 StressCheck stress intensities along the crack front for the elliptical through cracks modeled for specimen NON CX 2024-04. FEA modeled at σ_{max} = 10 ksi.
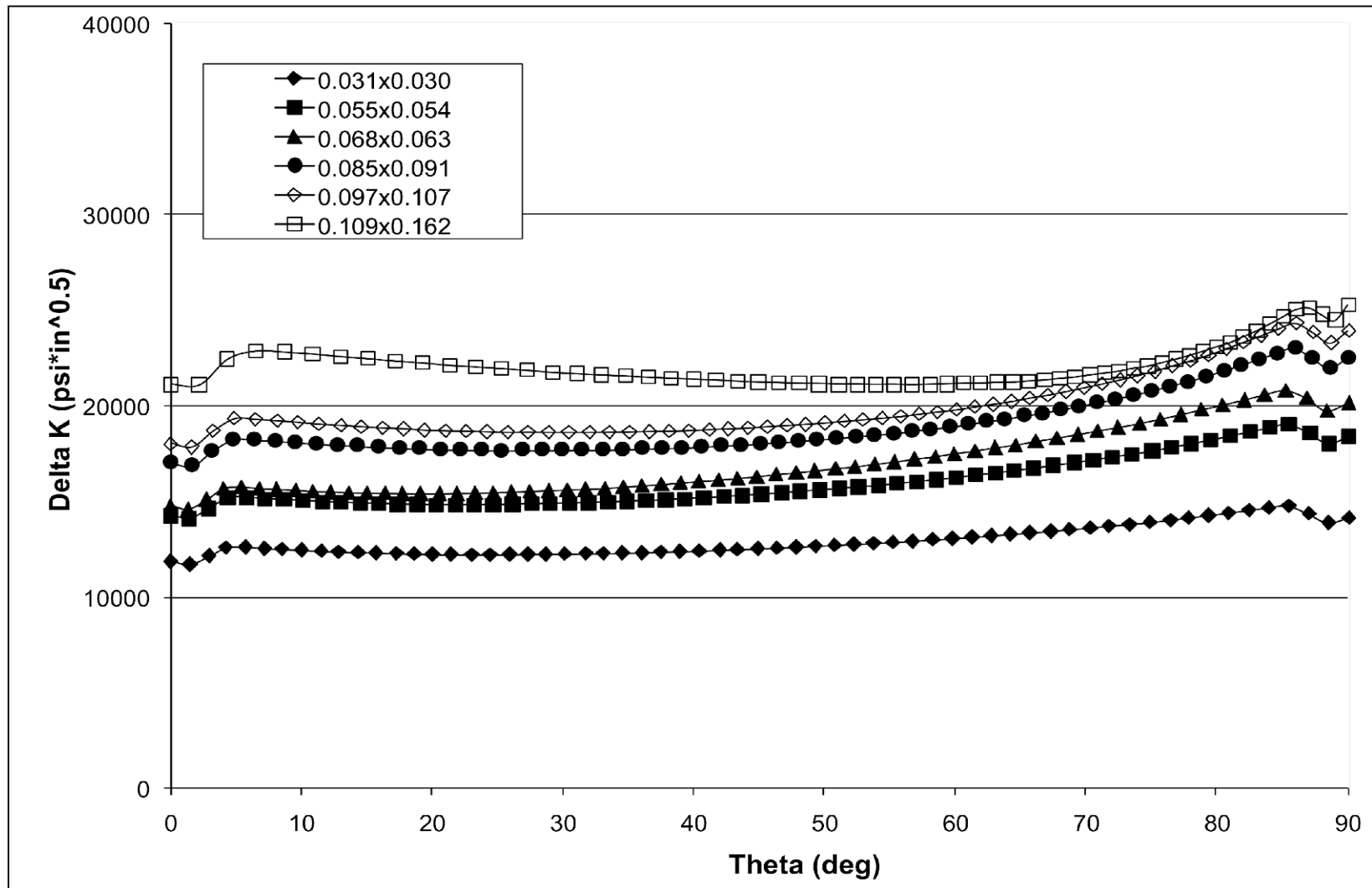
Fig. 28 StressCheck stress intensities along the crack front for the non-through-thickness elliptical corner cracks modeled for specimen CX 2024-04. FEA modeled at σ_{max} = 25 ksi.
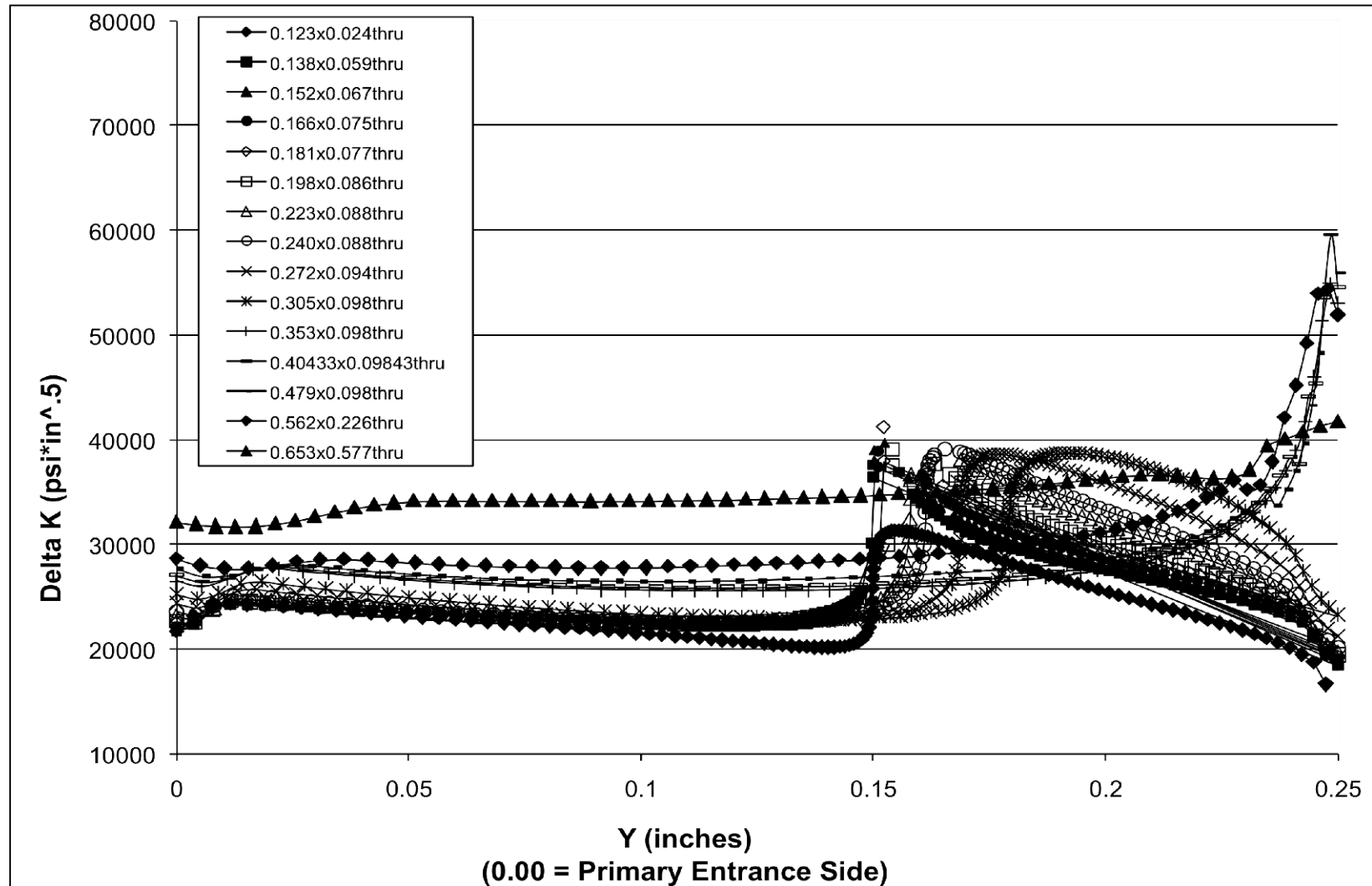
Fig. 29 StressCheck stress intensities along the crack front for the p-shaped and elliptical through cracks modeled for specimen CX 2024-04. FEA modeled at σ_{max} = 25 ksi.

As the stress intensity increases the crack has a greater desire to propagate through the material. This was easily seen when the entrance surface crack was on the order of 0.3 inch and the exit surface crack was still around 0.06 inch. When this would occur the stress intensity would increase dramatically until the crack would finally propagate rapidly through the material to allow the material to be more in equilibrium. This behavior can be seen in these plots. Fig. 29 shows a unique plot characteristic at roughly 0.15 inch. This drastic change in stress intensity is due the sudden change in the crack front geometry as seen in Fig. 24. This sudden change in crack shape causes a discontinuity in the model at this point. This does not, however, affect the results at the surfaces and this is where all the stress intensities were being taken from.

3.4.2 Determination of Stress Intensities Using AFGROW

AFGROW was also used to check the calculation of stress intensities at the surface of the specimen for different crack lengths. AFGROW is one of the United States Air Force's fatigue crack growth and life prediction software tools. It implements five different material models (Forman Equation, Walker Equation, Tabular lookup, Harter-T Method and NASGRO Equation) to determine crack growth per applied cyclic loading. AFGROW includes useful tools such as: user-defined stress intensity solutions, user-defined β modification factors (ability to estimate stress intensity factors for cases, which may not be an exact match for one of the stress intensity solutions in the AFGROW library), a residual stress analysis capability, cycle counting, and the ability to automatically transfer output data to Microsoft Excel. AFGROW Modeling Methodology."[36]

3.4.2.1 Specimen Model Geometry

Two different AFGROW models were used to calculate the stress intensity solutions at the surface edges of the crack front. The first model that was used was a single corner crack at a hole. This model was used for all non-through-thickness cracks. The second was for an oblique through crack at a hole. This model was used to model all cracks that had gone through the thickness of the testing specimen. These two model configurations are used frequently in the USAF to model common fatigue crack types during fatigue analysis performed on the structure of aircraft. Fig. 30 and Fig. 31 show how a user inputs these geometric parameters into AFGROW.
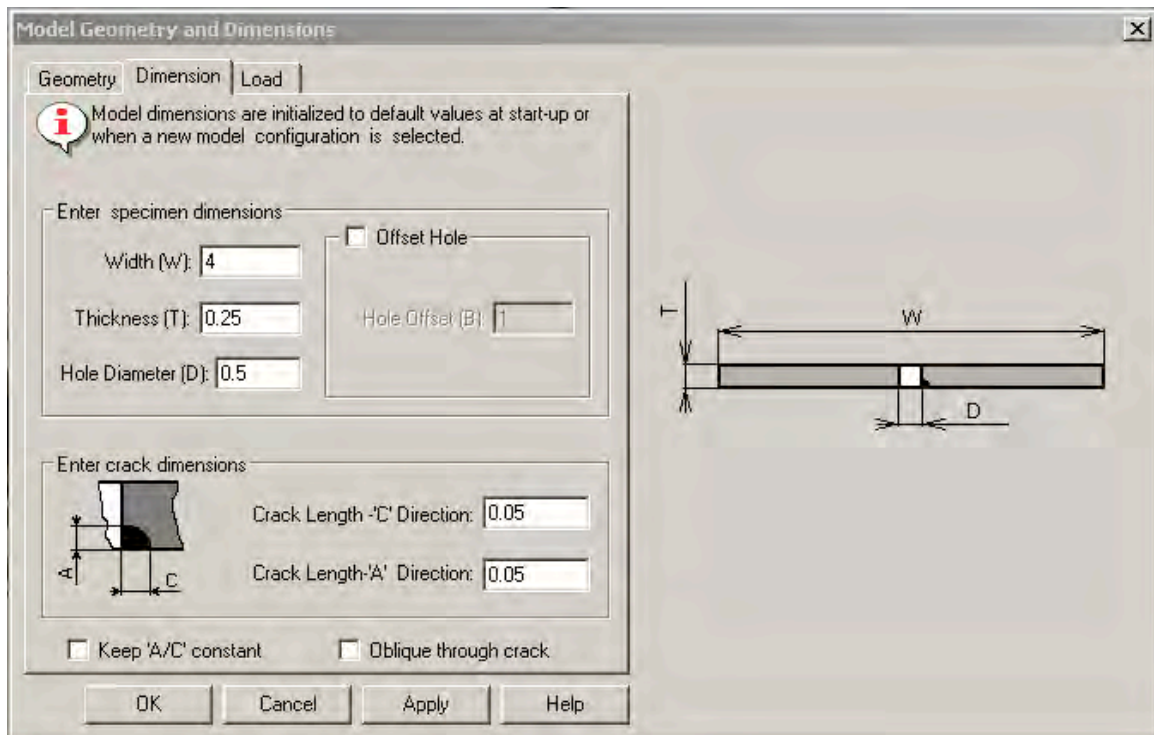

Fig. 30 AFGROW model geometric and dimensional input tab for non-through-thickness elliptical corner crack at a hole.

3.4.2.2 Specimen Model Loads

All loads input into AFGROW were the same as those seen by the test specimen during the fatigue testing phase of this project. Maximum stresses are input onto AFGROW along with a stress ratio. Fig. 32 shows how this is input into AFGROW.

3.4.2.3 AFGROW Stress Intensities for Model

AFGROW stress intensities were calculated by performing single runs of the software under the fatigue testing stresses and geometries. The solutions for the single corner elliptical crack at a hole were developed by Newman and Raju and were calculated using the tabular data from their research.[33] The oblique through-thickness crack at a hole solutions were developed by Fawaz and are calculated at a given location in reference to the surface and bore of the specimen.[33]

It should be noted that for the oblique through-thickness cracks several measured testing crack lengths were outside the bounds set for this model by Fawaz.[33]

3.5 Calculation of β Corrections

After the stress intensities had been calculated in StressCheck® and the location was determined for the specific location where the K would be taken from along the curve, the da/dN versus ΔK curves were calculated and plotted. These plots allowed for the comparison of multiple specimens, tested at different stresses to determine the effect of cold expansion on the fatigue crack growth.
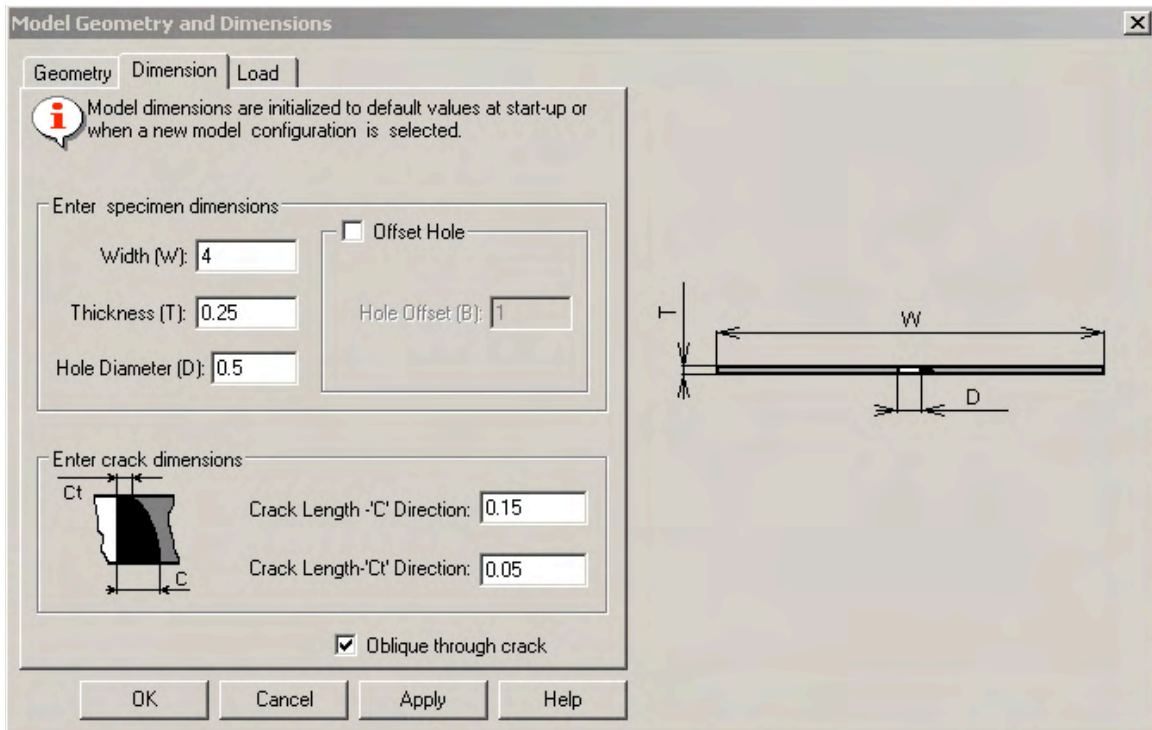
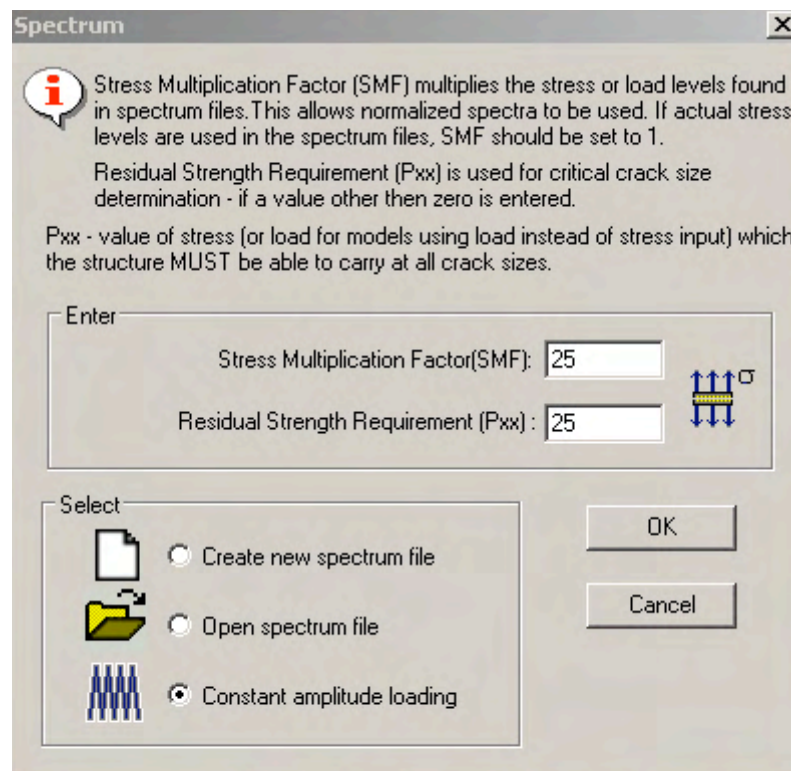Fig. 31 AFGROW model geometric and dimensional input tab for oblique through-thickness cracks at a hole.

Fig. 32 AFGROW stress input for either constant amplitude or spectrum loading. Stress ratio is set to 0.1 for stress intensities for fatigue testing conditions.

The basic process used to extract a β correction from the da/dN versus ΔK curves of the baseline noncold expanded specimens and the cold expanded specimens is called the similitude principle. This principle, which is used in fracture mechanics, states that if every parameter of both specimens is the same except for the one parameter being tested for, in this research project that parameter is the cold expansion process, then at the same crack growth rate, da/dN, the same ΔK should be seen in each specimen. If there is a shift in the two curves then this shift is an artifact of the process being tested for, i.e. the cold expansion process. Fig. 33 shows how an unknown stress intensity configuration can be solved for using the similitude. The unknown configuration in this research is the cold expanded specimen.

The standard is the noncold expanded and by comparing their fatigue crack growth characteristics at a given crack growth rate the unknown shift in stress intensities can be solved for.

To calculate a β correction that would represent the residual stress field induced into the material by the cold expansion process first an average da/dN versus ΔK curve fit had to be calculated for the noncold expanded baseline specimen's. This was performed by taking horizontal cross-sections at small increments along the curve and calculating the mean value at that cross section. In order to perform this task all the data was input into Microsoft Excel and functions were produced to allow for this calculation. Once this was performed the average values were then used.
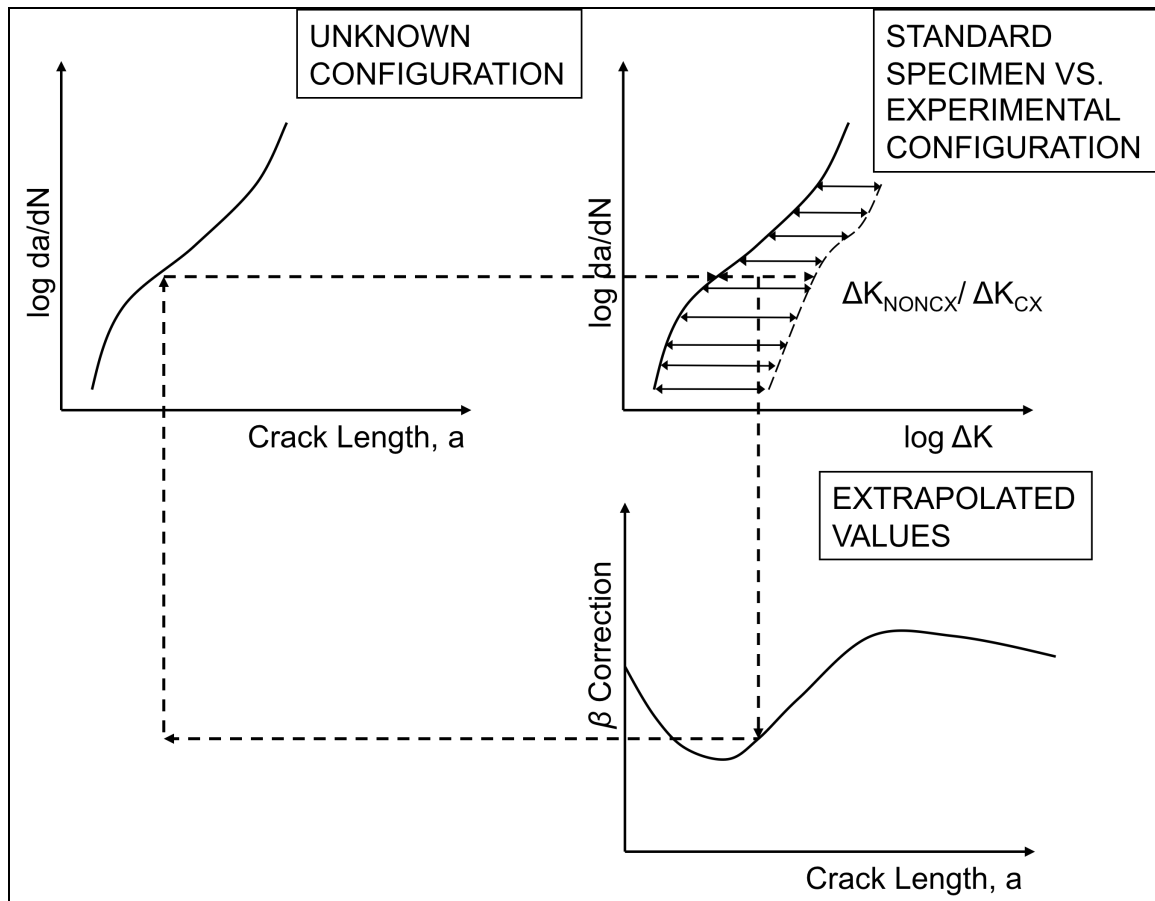
Fig. 33 Illustration of the similitude principle for the calculation for the β correction as a function of da/dN versus ΔK.

With this average da/dN versus ΔK curve produced for the noncold expanded specimens, the da/dN versus ΔK curve was plotted for the cold expanded specimens. This allowed for a direct comparison of crack growth rate of both the noncold expanded and cold expanded specimens. Using the similitude principles, which states that for a fixed geometry and material type at a given da/dN the stress intensity at that location should be identical. However, due to the residual stress present in the cold expanded material there is a dramatic shift in the stress intensity at the same crack growth rate (da/dN). The horizontal percent difference between the noncold expanded average curve and

the cold expanded da/dN versus ΔK curve was computed using Equation 9 and

represents the shift in the crack driving force caused by the residual stress. The

process used to calculate the $\beta_{ColdExpansion}$ is outlined in Fig. 34

$$\beta_{ColdExpansion} = \Delta K_{NonColdExpanded} / \Delta K_{ColdExpanded} \tag{9}$$
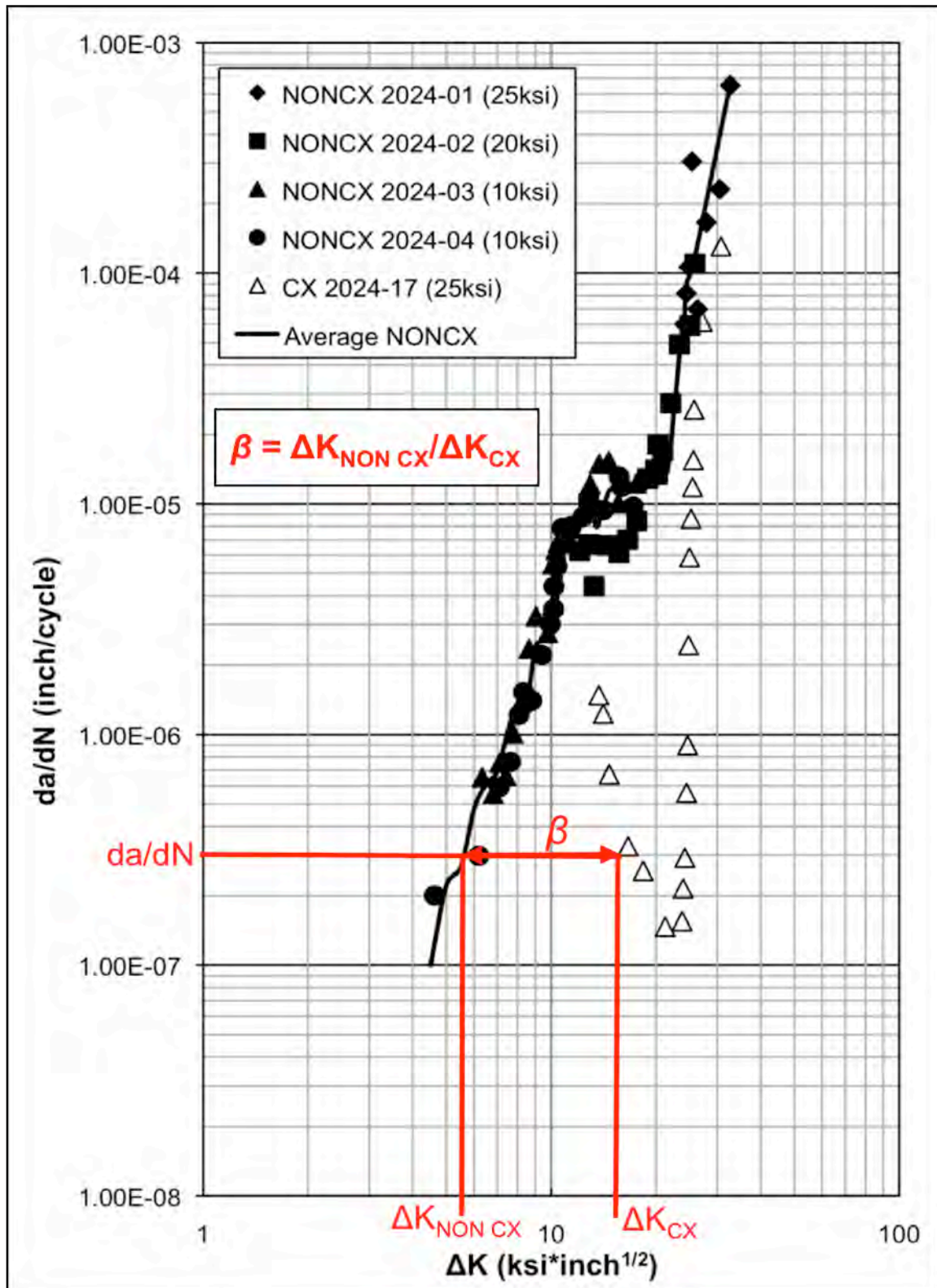
Fig. 34 Illustration of the similitude principle used to calculate the β correction for cold expansion using the same da/dN.

4 FRACTOGRAPHY

To document the fracture surfaces of all specimens both macro images and micro images were obtained. This allowed for further research to be accomplished by the inspection of the unique fracture surface characteristics found on the cold expanded and noncold expanded specimens.

Certain regions of the fracture surface were focused on in the documentation of the specimens. These regions included the nucleation area around the EDM notch, the smoother, more flat fatigue region, the unique tear-through feature on the exit side of the hole, and finally the transition region from fatigue to fast fracture.

It was also important that the specimens tested to produce marker bands on the fracture surface be documented. This made it possible to produce a fracture surface map of how a fatigue crack propagated through a residual stress field produced by the cold expansion process.

4.1 Macro Images

4.1.1 Nikon D80 with 60 mm Macro Lens

In order to document the fracture surface morphology of the testing specimens it was required that macro images be taken of all fracture surfaces. For a complete documentation of all fracture surfaces reference Appendix D.

Photographs of ASTM Standard E 647 2024-01, noncold expanded specimens, NCX 2024-04, NCX 2024-02 and cold expanded specimens CX 2024-17, 2024-02 are shown in the report.

All macro pictures were taken using a 10.2 mega pixel Nikon D80 SLR digital camera and a Nikon Nikkor 60 mm macro/micro lens. The camera was mounted to a standard tripod to allow for a more stable platform for taking the fracture surface images. All specimens were mounted using standard modeling clay which allowed for different angles to be shot without moving the angle of the camera.

All images were captured using the manual setting on both the Nikon D80 camera and the Nikkor 60 mm lens. This allowed for greater versatility when capturing images of the fracture surface. Different color backdrops were used to reduce the reflection and increase the contrast of the fracture surface.

4.1.1.1 ASTM E 647 Standard Specimens

All ASTM Standard E 647 specimens were photographed for documentation. These specimens were tested at a lower relative stress than those tested for the standard test. This allowed for a much longer fatigue crack to propagate through the specimen and a much smoother, more flat fracture surface. The ASTM E 647 standard specimen configuration also allowed for cracks to nucleate on both sides of the small hole and propagate through the thickness of the specimen in a much more symmetric manner. This can be seen in Fig. 35.
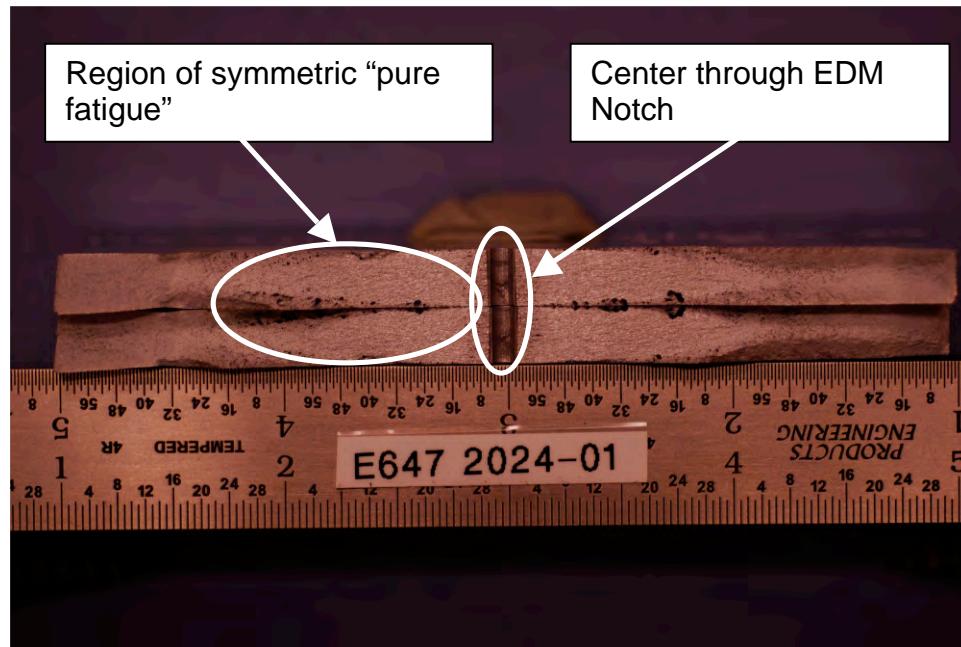
Fig. 35 ASTM Standard E 647 CC 2024-01 middle tension fracture surfaces. Specimen tested at a σ_{max} of 11.1ksi, R = 0.1, f = 15 Hz, and lab air.

4.1.1.2 Noncold Expanded Specimens

The noncold expanded baseline specimens were tested at different stresses than the cold expanded specimens. These specimens also were able to propagate farther than the cold expanded specimens because of the lower stresses applied. These specimens also exhibited a unique characteristic at lower stresses. As seen in Fig. 36, it was possible to nucleate a crack on the EDM side and have only that side propagate to failure. In order to extract the fracture surface from the specimen it was cut using a band saw. This was not seen in any of the cold expanded specimens but was of great use for this research because it provided a true baseline crack growth curve for only one side of the hole and this is what was being analyzed in this research.

Fig. 36 NON CX 2024-04, noncold expanded baseline specimen pair fracture surface. Specimen was tested at a σ_{max} of 10 ksi, R = 0.1, f = 20 Hz, and lab air. Fracture occurred only on one side of the specimen.

Fig. 37 is a good representation of the fracture surface of all the noncold expanded baseline specimens. The fatigue crack nucleated from a corner EDM that is circled. The EDM side shows a much rougher surface than that of the opposite side of the hole. This is most likely due to the high stress applied during testing. At the higher stress there is less evidence of fatigue and more evidence of pure ductile tearing of the material around the hole. Also the end of the fatigue zone of the fracture surface is outlined to allow for reference to the point of fast fracture.

4.1.1.3 Cold Expanded Specimens

The cold expanded specimens exhibited very unique fracture surface morphologies. The fatigue cracks that nucleated out of the EDM did not propagate in the same manner as those that nucleated in the noncold expanded
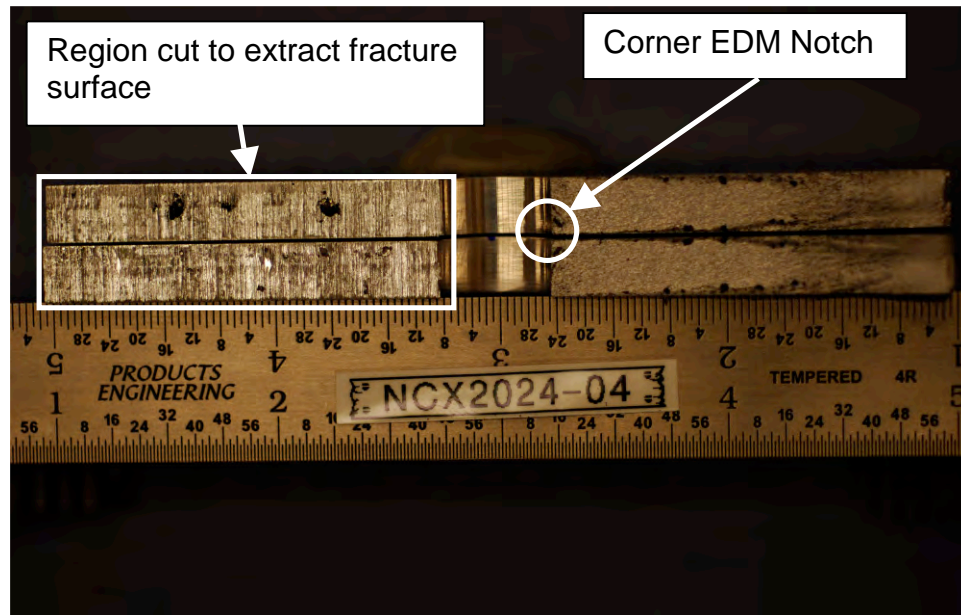
Fig. 37 NON CX 2024-02, noncold expanded baseline specimen, pair fracture surface. Specimen was tested at a σ_{max} = 20 ksi, R = 0.1, f = 20 Hz, and lab air. EDM notch location is highlighted.

specimens. At a macro level Fig. 38 shows this difference. The EDM notch location is highlighted in the image to give a reference to where the fatigue crack nucleated and also the lines give reference to where the fatigue crack propagation ended and fast fracture began. The fatigue crack nucleated in the EDM notch and then propagated along the entrance surface of the specimen and through the bore at a similar rate. As the fatigue crack propagated through the thickness of the bore it would become difficult to track the main crack due to multiple cracks nucleating through the bore and propagating along with the main crack. Once the main fatigue crack reached about 0.18 to 0.21 inch through the bore the crack would "pop" through-thickness and then propagate only a very short distance on the exit surface of the specimen. Once the fatigue crack was through the thickness of the specimen it would continue to propagate on the entrance surface but would not propagate on the exit surface.
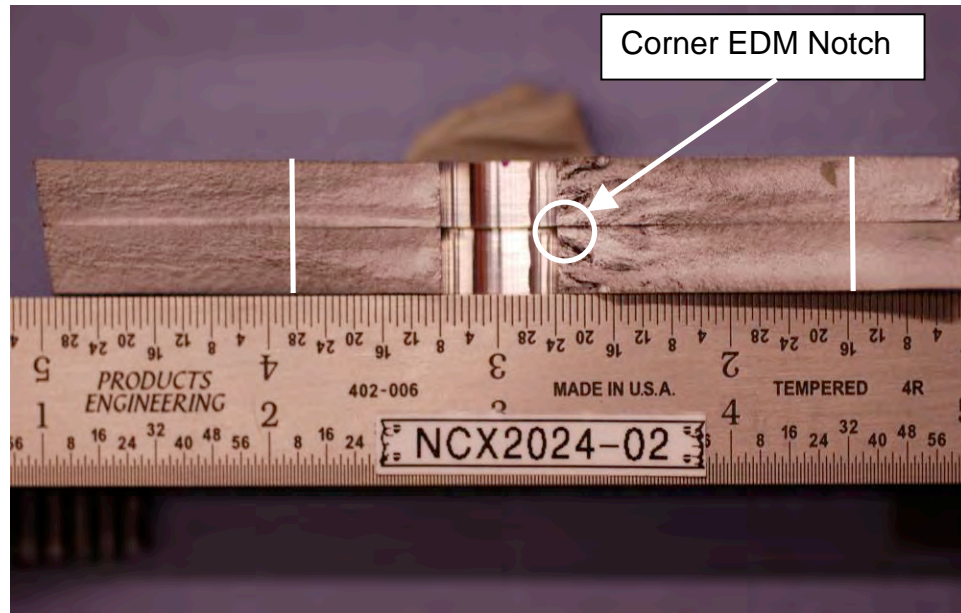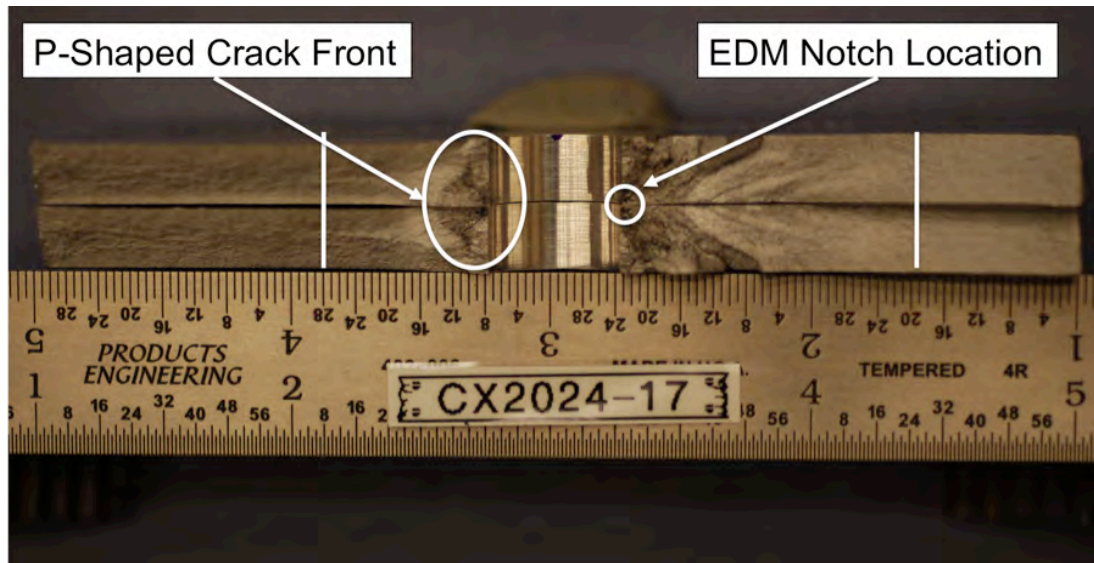
Fig. 38 CX 2024-17, cold expanded specimen, pair fracture surface. Specimen was tested at a σ_{max} = 25 ksi, R = 0.1, f = 20 Hz, and lab air. EDM notch is and fatigue zone are highlighted along with the P-shaped crack front typical in cold expanded holes.

The reason for this resistance to fatigue crack propagation on the exit surface is due to the presence of a higher residual stress located on this surface. This region of higher residual stress was imposed into the material by the cold expansion process. As the mandrel passes through the hole a portion of the material in the hole is pulled to the exit surface. This additional material causes an increase in the resistance of the balk material to plastic deformation caused by the cold expansion process. This unique fracture morphology is illustrated in Fig. 38.

Another one of the unique fracture surface features is shown in Fig. 39. This surface feature is produced due to the residual stress profile along the bore and then through the thickness of the material. As the crack propagated through the specimen it reached the maximum residual stress location in the material and then propagated around this location. Once the fatigue crack had propagated
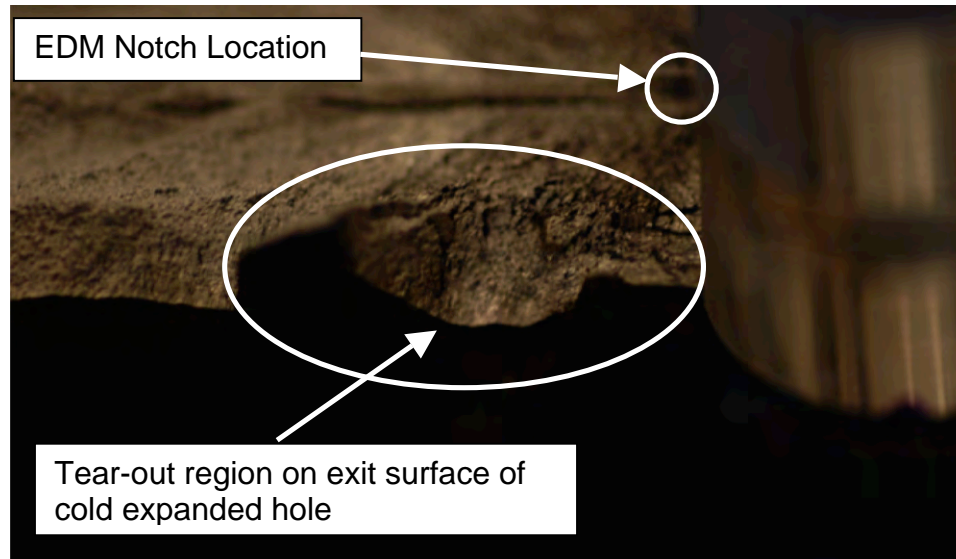
Fig. 39 CX 2024-17 cold expanded specimen, bottom of exit surface with tear-out shown. Specimen was tested at a σ_{max} = 25 ksi, R = 0.1, f = 20 Hz, and lab air.

around this intense residual stress zone it would cause the material to tear and thus cause the fracture surface seen in Fig. 39. This figure shows a close up view of the exit surface of the specimen at the edge of the cold expanded hole. This type of fracture surface morphology was very common in cold expanded specimens that were tested at a σ_{max} = 25 ksi. The severity to which it occurred was different but most of the specimens showed this same type of fracture. Fig. 40 is a macro view of the same fracture surface.

4.1.2 Olympus Stereoscope

An Olympus SZX10 stereoscope was used to take macro/micro images of the fracture surfaces of NON CX 2024-02, NON CX 2024-04, and CX 2024-04. The stereoscope allows the user to change the magnification from 6.3 X magnification to as high as 25 X. Images were taken at varying magnification to allow for a greater perspective of the fracture surface morphology.
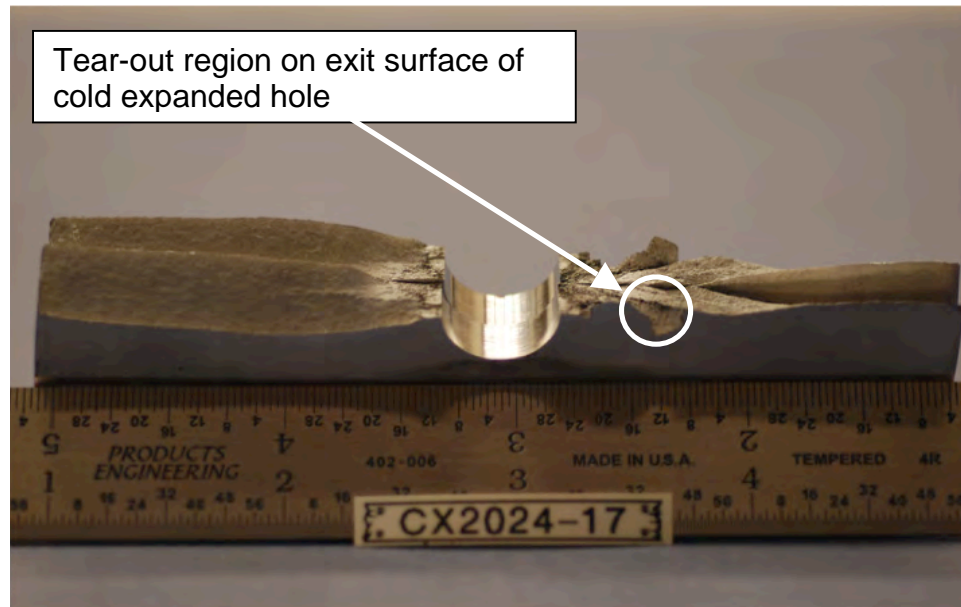
Fig. 40 CX 2024-17 cold expanded specimen pair fracture surface showing the unique tearing of the exit surface due to the residual stress field caused by the cold expansion process. Specimen was tested at a σ_{max} = 22 ksi, R = 0.1, f = 20 Hz, and lab air.

4.1.2.1 Fracture Surface Morphology

All specimens were notched with a corner EDM to aid in the nucleation of the fatigue crack. However, after the final ream process was performed the EDM was often no longer present. The location of the EDM notch was always tracked to provide reference to the location where the fatigue crack nucleated.

The fracture morphology shown in Fig. 41 is unique in that specimen NON CX 2024-02 was tested at a σ_{max} = 20 ksi. This high stress level caused the fracture surface to exhibit more ductile failure features than was expected. This ductile tearing of the material can be seen in Fig. 42. Fig. 43 shows the difference in the fracture surfaces of a noncold expanded specimen that was tested at a lower σ_{max} = 10 ksi compared to that seen in Fig. 42. The fracture surface of specimen NON CX 2024-04 is more flat and is smoother than the
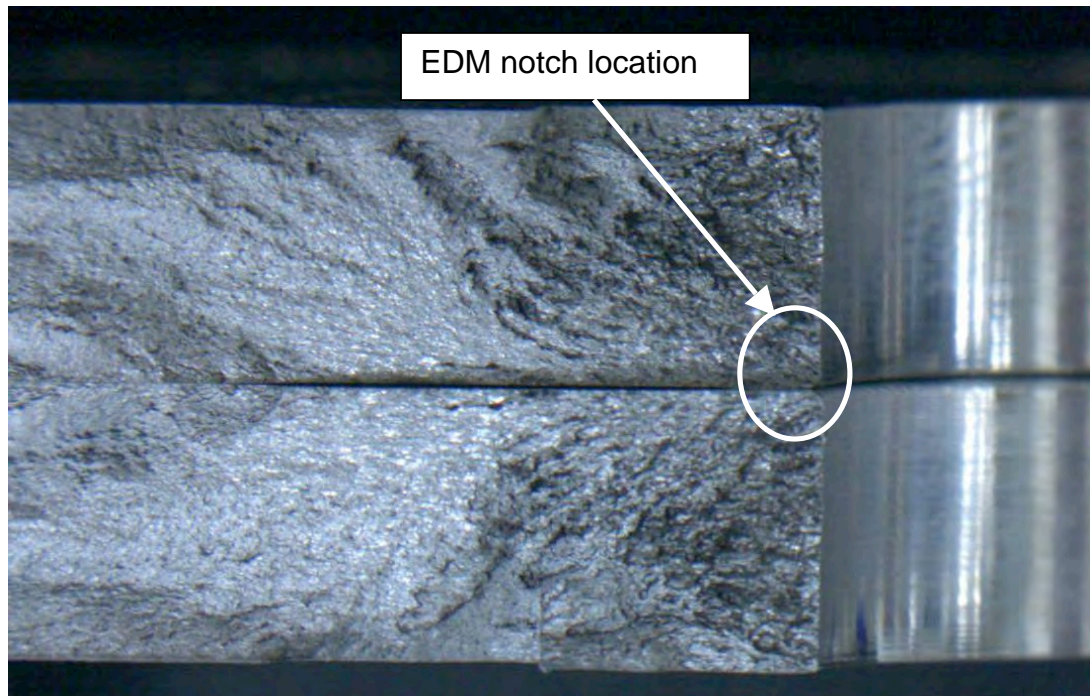
Fig. 41 NON CX 2024-02 fracture surface. EDM side is shown with the notch location circled. Image at 6.3 X magnification.

surface seen in Fig. 42. This type of fracture surface is typical for aluminum under cyclical loading.[32]

The cold expanded specimens exhibited both fatigue and ductile failure zones on the fracture surface. The reason for this is because of the high stress the specimens needed to be tested at to propagate a fatigue crack through the residual stress zone adjacent to the hole.

Fig. 44 and Fig. 45 are close-up images of specimen CX 2024-04. These images highlight some of the important areas on the fracture surface observed during testing. The EDM notch is circled and the region adjacent to the notch exhibits a more flat fatigue morphology. The dark region that is seen in the figure is from fatigue debris that is produced during testing.
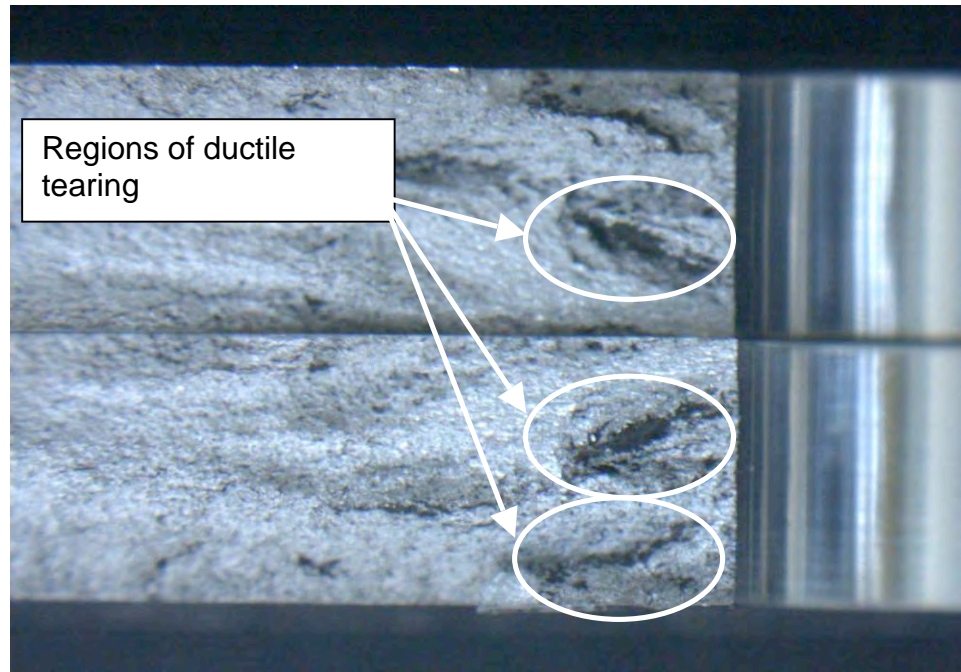
Fig. 42 NON CX 2024-02 fracture surface with ductile failure regions highlighted. Image at 8.0 X magnification. Specimen tested at σ_{max} = 20 ksi, R = 0.1, f = 20 Hz, and lab air.
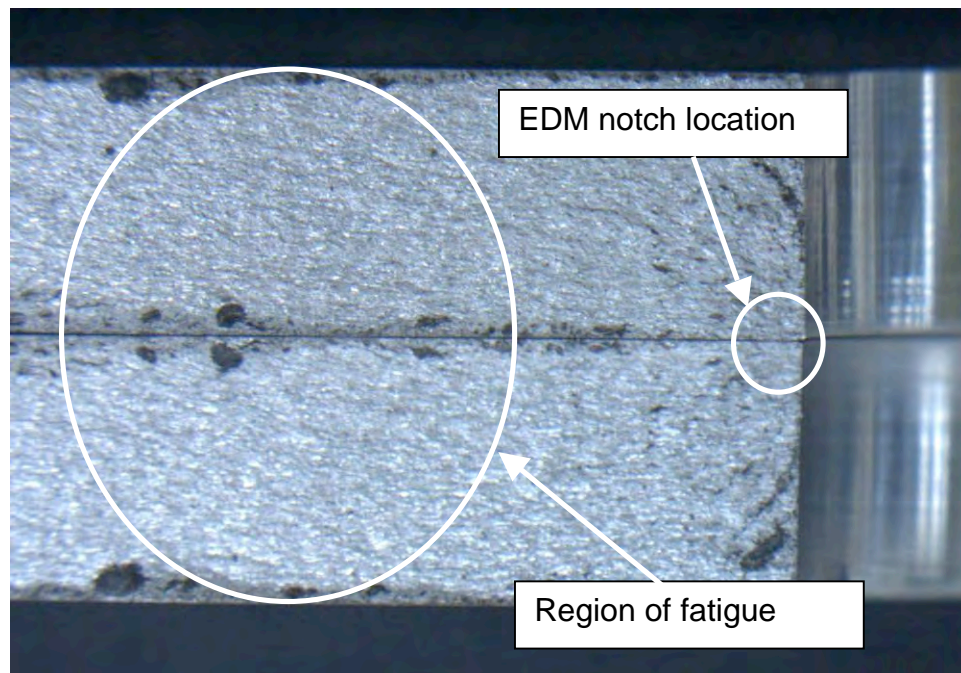
Fig. 43 NON CX 2024-04 fracture surface. EDM corner notch is highlighted along with pure fatigue region of failure surface. Image at 8.0 X magnification. Specimen tested at σ_{max} = 10 ksi, R = 0.1, f = 20 Hz, and lab air.
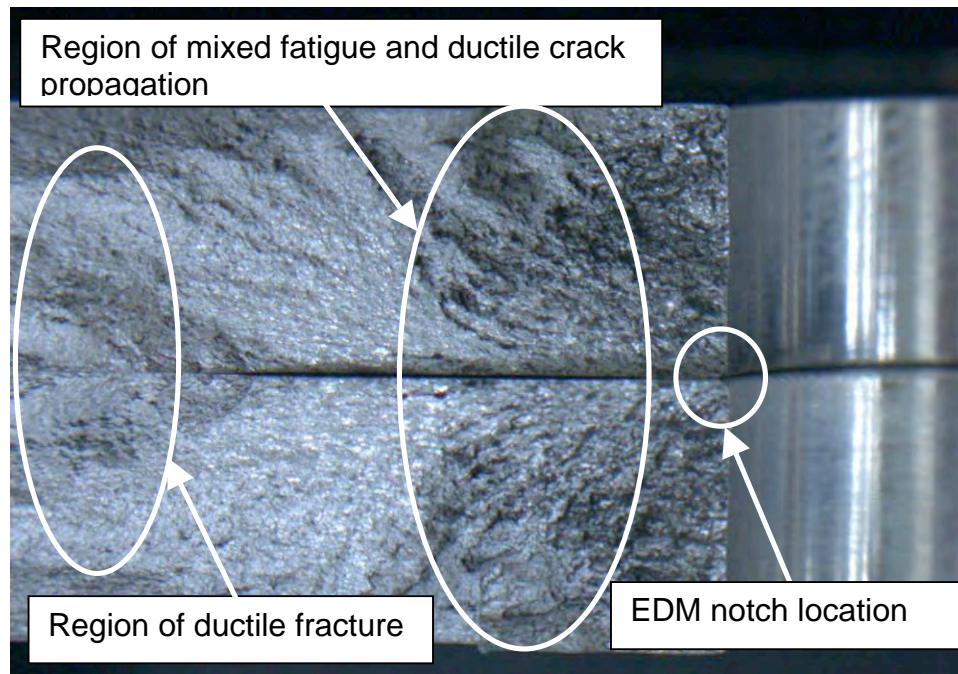
Fig. 44 CX 2024-04 fracture surface. EDM corner notch is highlighted along with region of mixed fatigue and ductile crack propagation. Image at 6.3 X magnification. Specimen tested at σ_{max} = 25 ksi, R = 0.1, f = 20 Hz, and lab air.

This is typical and at times the debris could be seen coming out of the fatigue crack as it opened and closed during the fatigue process. As the fatigue crack propagated away from the corner notch the high stress caused the crack to propagate by ductile tearing along with the fatigue. This is evident in the fracture surface as it begins to transition from a flat, mode I fatigue surface to an out-of-plane, mode II like, fatigue propagation. The fatigue crack would then transition to a ductile failure type at approximately 0.75 inch.

The final image, Fig. 46, provides an image of one of the unique fracture characteristics found during the fatigue testing of the cold expanded specimens. This figure shows the type of tear-out on the exit side of the specimen that was seen in multiple specimens.
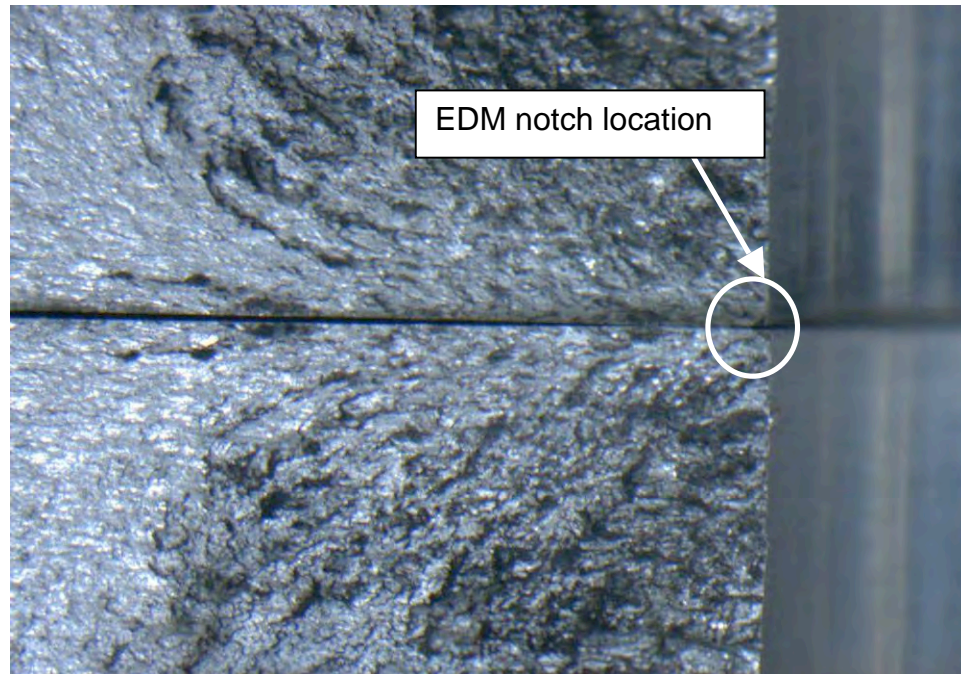
Fig. 45 CX 2024-04 close-up of corner EDM notch. Image at 16 X magnification. Specimen tested at σ_{max} = 25 ksi, R = 0.1, f = 20 Hz, and lab air.

This tear-out would occur at the latter end of the fatigue test. The exit surface crack would propagate to approximately 0.08 inch and would then propagate rapidly to catch up with the entrance surface. The region of tear-out has correlated to the location of highest residual stress found in the specimen from the cold expansion process. This high residual stress would prevent the fatigue crack from propagating through the exit surface and would therefore drive the crack around this region and cause this tear-out effect. The amount of tear-out was greatest on the specimens that were tested at the higher stress of σ_{max} = 25 ksi. On specimens that were run at lower stresses the tear-out region was much less severe and at times not even visible to the unaided eye. This tear-out phenomena was observed to be more extreme on the 2024-T3 alloy than on the 7075-T6 alloy.
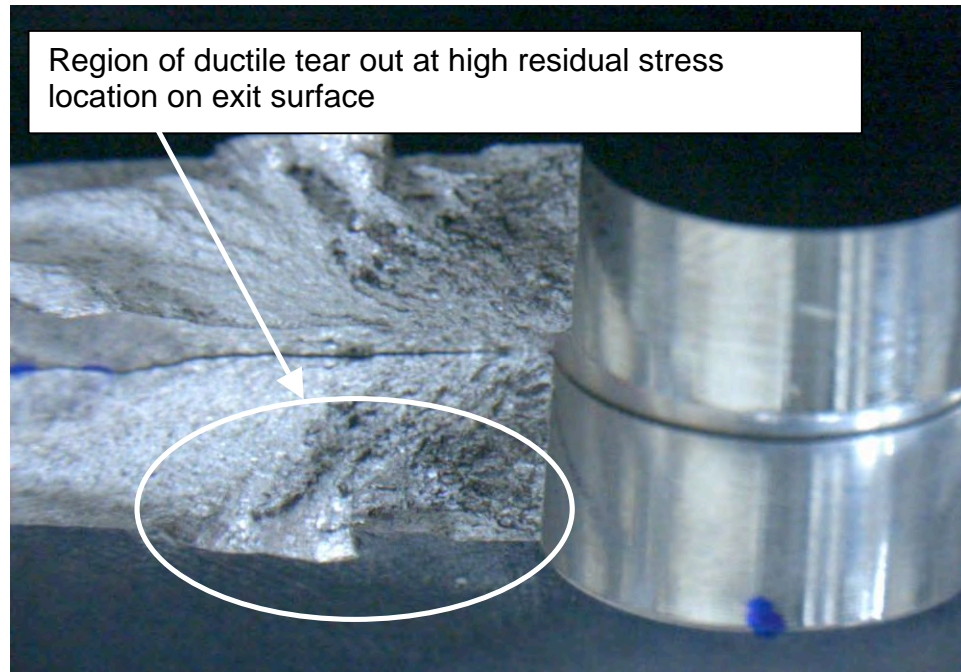
Fig. 46 CX 2024-04 close-up of exit surface showing region of ductile tearing. Image at 10 X magnification. Specimen tested at σ_{max} = 25 ksi, R = 0.1, f = 20 Hz, and lab air.

4.2 Micro Images

### 4.2.1 Scanning Electron Microscope (SEM) Images

The fracture surface of specimen CX 2024-17 was examined under a

Hitachi model 2600 scanning electron microscope (SEM) which is located at the

University of Utah's Materials Behavior Laboratory (MABEL). The purpose of

examining the fracture surface under a SEM was to understand the capabilities

and operational characteristics of a SEM. Then an examination of the fracture

surface was performed at a microscopic level to observe evidence of fatigue at a

high level of magnification.

To begin this process a macro image of the specimen was used to select

locations on the fracture surface for examination in the SEM. Fig. 47 was used

as a reference for the selection of specific locations to view under the higher

Fig. 47 Macro image of CX 2024-17 used for reference in SEM. Markers show locations selected for further examination under the SEM. Short/Transverse grain orientation shown.

magnification of the SEM. When the specimen was mounted into the SEM it had to be twisted to fit in the mounting bracket. Therefore all the images are twisted at a slight angle but rolling orientation is shown as Short (S) and Transverse (T). This allows for a reference to the major grain orientation for the plate. The specific grain orientation is not shown as this can differ from grain to grain and additional research would be require that was outside of the scope of this research project.

Location 1 on Fig. 47 is located close to the EDM notch and allow for a close-up view of what the fracture surface looks like in a more pure fatigue region Fig. 48, which is at 300 X magnification, shows a general fatigue crack propagation direction away for the cold expanded hole. This image also shows some small dark dots on the surface of the specimen that look like pits. These are particle constituents of other elements that compose the 2024 aluminum alloy. Fig. 49 is a 1,500X magnified view of the outlined section in Fig. 48 and shows a more zoomed in view of this striation field.
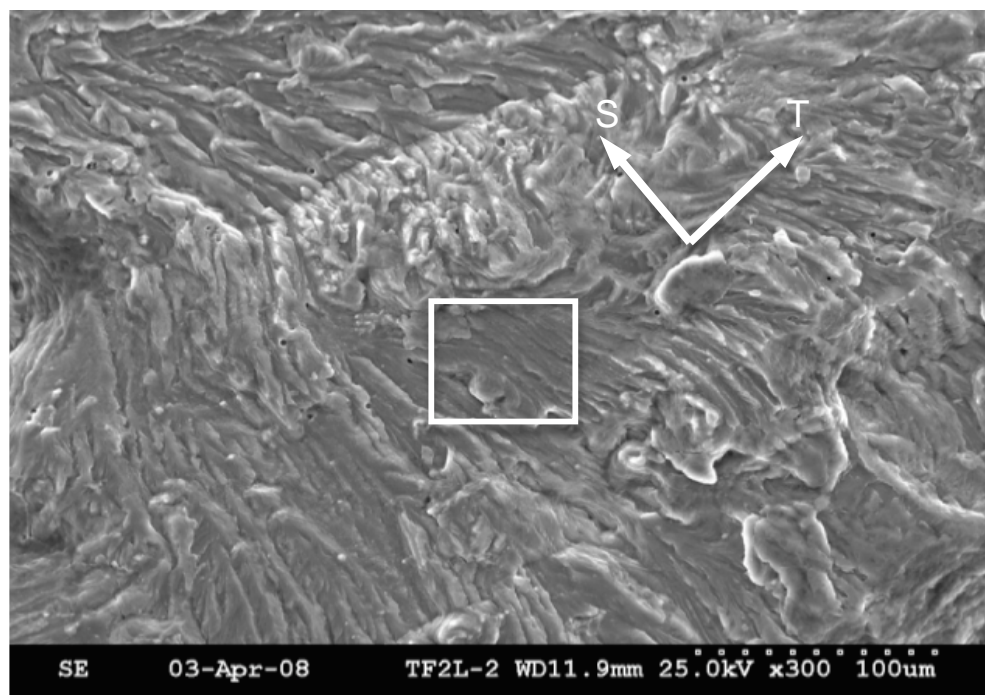
Fig. 48 SEM image of CX 2024-17 at location 1 from Fig. 47. Image is at 300 X magnification.
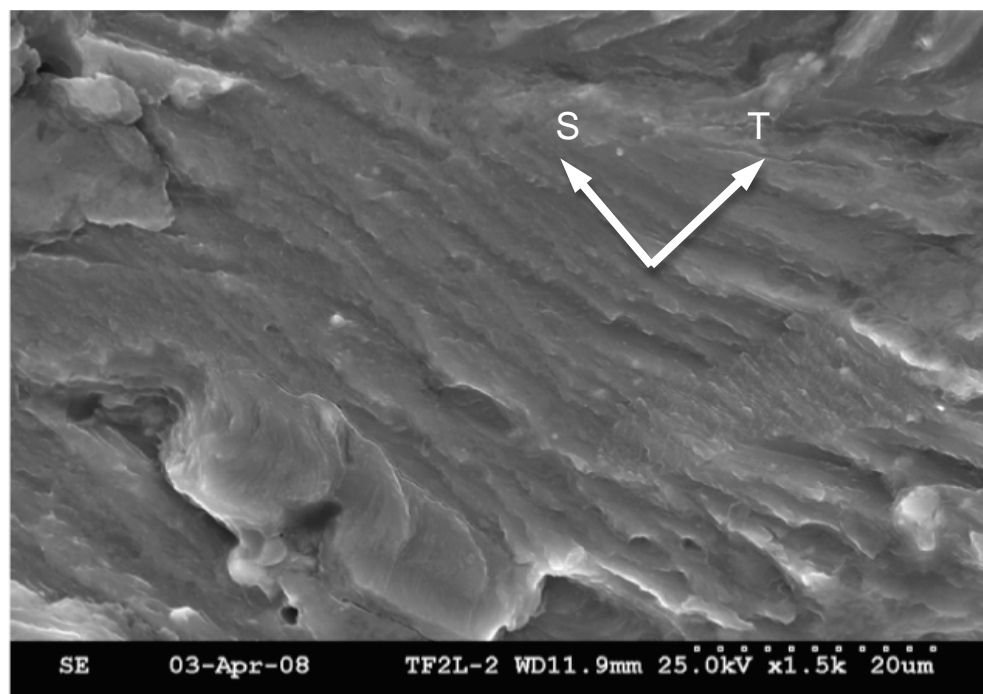
Fig. 49 SEM image of CX 2024-17 at location 1, zoomed in at boxed region of Fig. 48. Image is at 1,500 X magnification.

Fig. 50, which is marked in Fig. 47 under the 2, shows another of the unique alloy characteristics. This image shows not only the fatigue striations but also how these striations propagate through grain boundaries and into voids caused by the transition between pure fatigue and ductile tearing.

The last location selected for images from the SEM was close to the point at which the fatigue crack propagated more slowly due to the high residual stress at the exit surface of the specimen and then rapidly propagated through the material. This location, seen in Fig. 51 and Fig. 52, is designated as point 3 in Fig. 47. Fig. 51 shows signs of both fatigue, as highlighted in Fig. 52 but also shows signs of ductile failure. This area is highlighted by the circle in the top right corner of the image. This helps to show that at this point the fatigue crack began to tear the material apart along with propagating by fatigue.
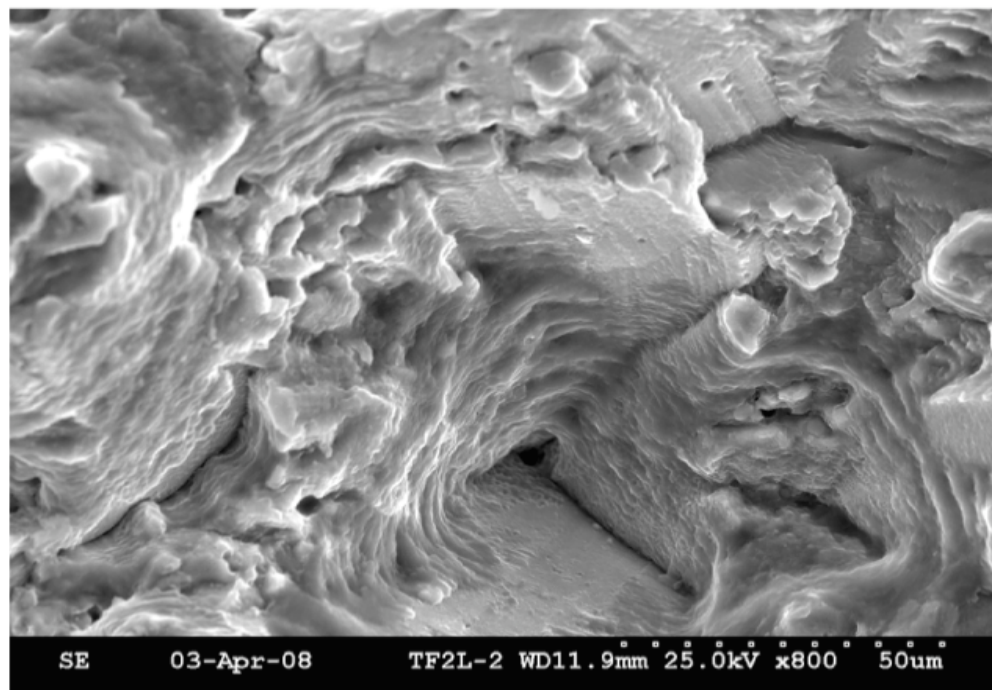
Fig. 50 SEM image of CX 2024-17. Image location is shown in Fig. 47 as 2. Image is at 800 X magnification.
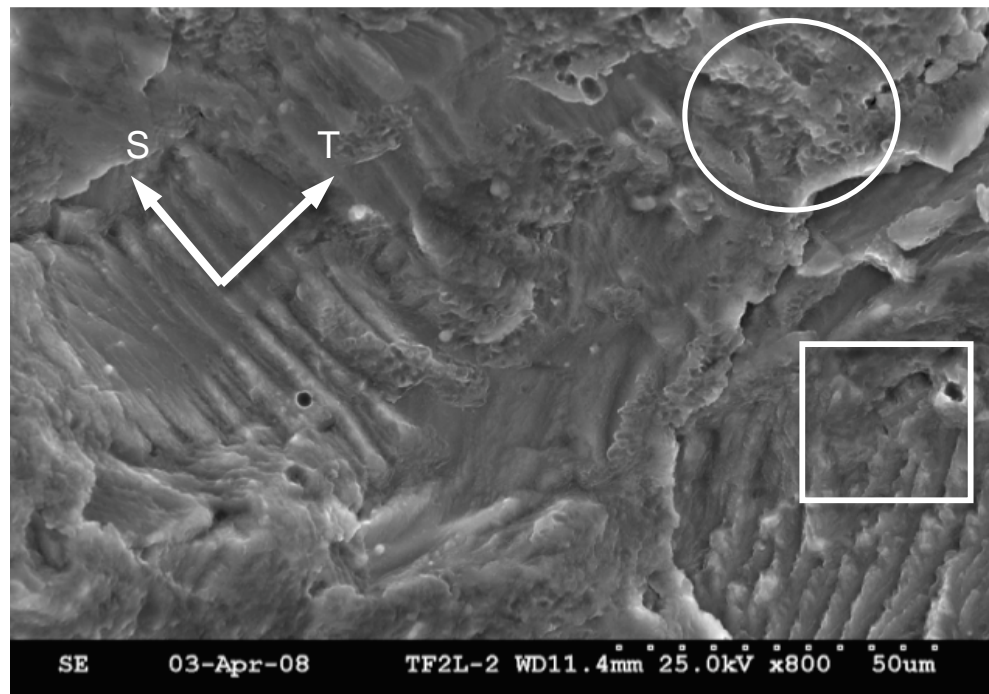
Fig. 51 SEM image of CX 2024-17. Image location is shown in Fig. 47 as location 3. Image is taken at 800 X magnification.
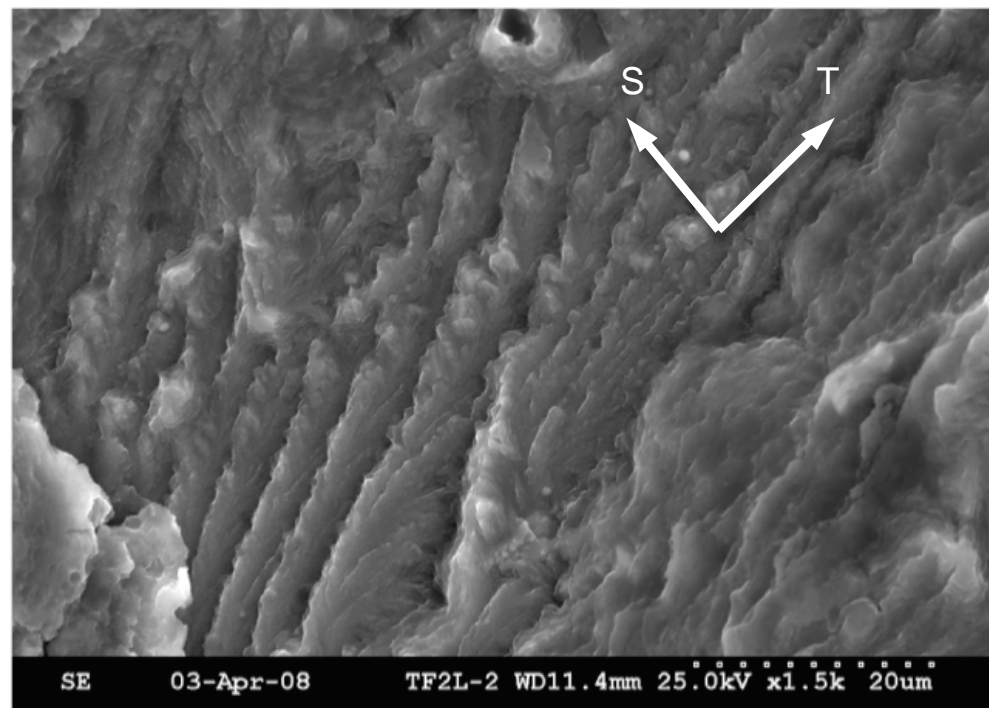
Fig. 52 SEM image of boxed area in Fig. 35. Image shows striation markings in the direction of crack propagation. Image is taken at 1,500 X magnification.

5 RESULTS

5.1 Fatigue Crack Growth Testing Data Sheets

The testing matrix for this research program is shown in Table 2. A total of 23 specimens were tested in three different phases. During the testing of each specimen a crack growth data sheet was used to record specific specimen information such as specimen thickness, hole diameter, surface area, maximum load and maximum stress. Before each specimen was tested to failure the initial crack length was recorded and then measured again at specimen specific crack growth intervals. A typical crack growth data sheet is shown in Table 3.

5.2 Crack Length Versus Number of Cycles Plots (a Versus N)

With the data collected the first set of plots produced were crack length (a) versus cycle count (N) plots. These are simple plots that allow one to see the propagation of the fatigue crack over the number of cycles performed during the test. They are however the starting block for all fatigue data analysis. All other data produce for this research is based upon the data collected from these a versus N plots. It is therefore important to establish and show these plots as a starting point for each of the following progressive steps in the data analysis portion of this research project.

Table 2 Testing Matrix for Al 2024-T351 Alloy

Specimen ID	Specimen Type	Test Date	Test Data Results	Max Stress	Cycles
CC2024-01	E 647 M(T)	7/24/07	Good Data	11.1 ksi	422121
CC2024-02	E 647 M(T)	7/26/07	Good Data	11.1 ksi	410081
NONCX2024-01	M(T) Non-Cold Expanded Central Hole	12/4/07	Good Data	25 ksi	7443
NONCX2024-02		1/14/08	Good Data	20 ksi	47443
NONCX2024-03		2/25/08	Good Data	10 ksi	279806
NONCX2024-04		2/25/08	Good Data	10 ksi	425336
CX2024-1	M(T) Cold Expanded Central Hole	10/9/07	Failed at Tab - Useful Data	25 ksi	498000
CX2024-2		10/11/07	Good Data	25 ksi	415770
CX2024-3		11/1/07	Failed at Tab - Useful Data	25 ksi	316314
CX2024-4		12/20/07	Good Data	25 ksi	469000
CX2024-5		12/21/07	Good Data	25 ksi	467735
CX2024-6		11/15/07	Good Data	25 ksi	676518
CX2024-7		2/15/08	Failed on South Side - Unsure of Data	25 ksi	453117
CX2024-8		2/7/08	Marker Band Specimen - Worked	25 ksi	1850009
CX2024-9		1/31/08	Failed on South Side - Unsure of Data	25 ksi	792834
CX2024-10		1/25/08	Marker Band Specimen - Didn't Work	25 ksi	815000
CX2024-11		1/4/08	Good Data	25 ksi	638302
CX2024-12		1/2/08	Good Data	25 ksi	478899
CX2024-13		1/3/08	Good Data	25 ksi	436391
CX2024-14		1/8/08	Good Data	25 ksi	490705
CX2024-15		1/11/08	Good Data	25 ksi	524172
CX2024-16			Spare	25 ksi	
CX2024-17		3/4/08	Spare	25 ksi	
CX2024-18		2/21/08	Marker Band	25 ksi	
CX2024-19			Good Data at Larger Crack Lengths	12 ksi	1532182

Table 3 Fatigue Crack Growth Testing Data Sheet

Spec. I.D. CX 2024-04   Loading Condition: Constant Amplitude R = 0.1

Width: 4.000 in   Thick: 0.254 in   Area: 1.028 in^2   Frequency: 20 Hz

Precrack Information:

Hole Dia: 0.4874 in   Peak Stress: 25.0 ksi   Date: September 25, 2007

Surface EDM Length: 0.01457 in

Test Information:

Hole Dia: 0.50118 in   Peak Stress: 25.0 ksi   Date: December 27, 2008

Surface EDM Length: 0.00787 in

Cycles	Crack Length (inches)				Bore	Comments
	Surface of Hole					
	Entracne		Exit			
	North	South	North	South		
0						Precracking
125011						
0	0.0311				0.0540	Testing
13053	0.0551				0.0633	
20783	0.0689				0.0919	
67991	0.0850	0.0378			0.1073	
85317	0.0972	0.0524			0.1621	
121487	0.1094	0.0732				Through Bore
159072	0.1236	0.0854	0.0248	0.0260		
225008	0.1390	0.1043	0.0591	0.0472		
278239	0.1528	0.1181	0.0673	0.0520		
330814	0.1665	0.1319	0.0756	0.0634		
367003	0.1811	0.1429	0.0780	0.0689		
399305	0.1988	0.1535	0.0866	0.0709		
419904	0.2236	0.1587	0.0886	0.0728		
434611	0.2402	0.1661	0.0890			
447221	0.2728	0.1697	0.0941			
454319	0.3055	0.1744	0.0984	0.0776		
459234	0.3539	0.1748				
462320	0.4043	0.1760				
465253	0.4799	0.1846				
467099	0.5626	0.1882	0.2264	0.0866		
468225	0.6539	0.1957	0.5780	0.0976		
469000	Final Specimen Fracture					

The a versus N plots were performed for all specimens tested during this project, however only nine plots will be shown in this section. For a complete listing of all a versus N plots refer to Appendix E.

5.2.1 ASTM Standard E 647 Specimens

A combined plot of both ASTM Standard E 647 specimens is shown in Fig. 53. This plot was produced using the ASTM E 647 procedures for the middle tension specimen configuration. This standard requires that all four crack lengths be averaged and plotted versus the number of cycles. These tests were performed to allow for the fatigue machine set-up and data collection process to be checked for accuracy. The ASTM E 647 test provided a baseline starting point for the comparison of collected data to that found in the current aerospace material property database. These tests also allowed for the testing of the visual crack measurement equipment to insure that this type of technique would provide crack measurements that would be within the required range outlined in the Standard. Both of the E 647 specimens were tested at a σ_{max} = 11.1 ksi, frequency = 15 Hz and a stress ratio = 0.1. As seen in Fig. 53 the two specimens show a very good correlation between each other and the number of cycles to failure was well within the range expected.

5.2.2 Baseline Noncold Expanded Specimens

The fatigue crack growth curves for all of the baseline noncold expanded specimens are shown in Fig. 54 through Fig. 58. From these noncold expanded specimens were developed all the baseline curves for da/dN versus ΔK and
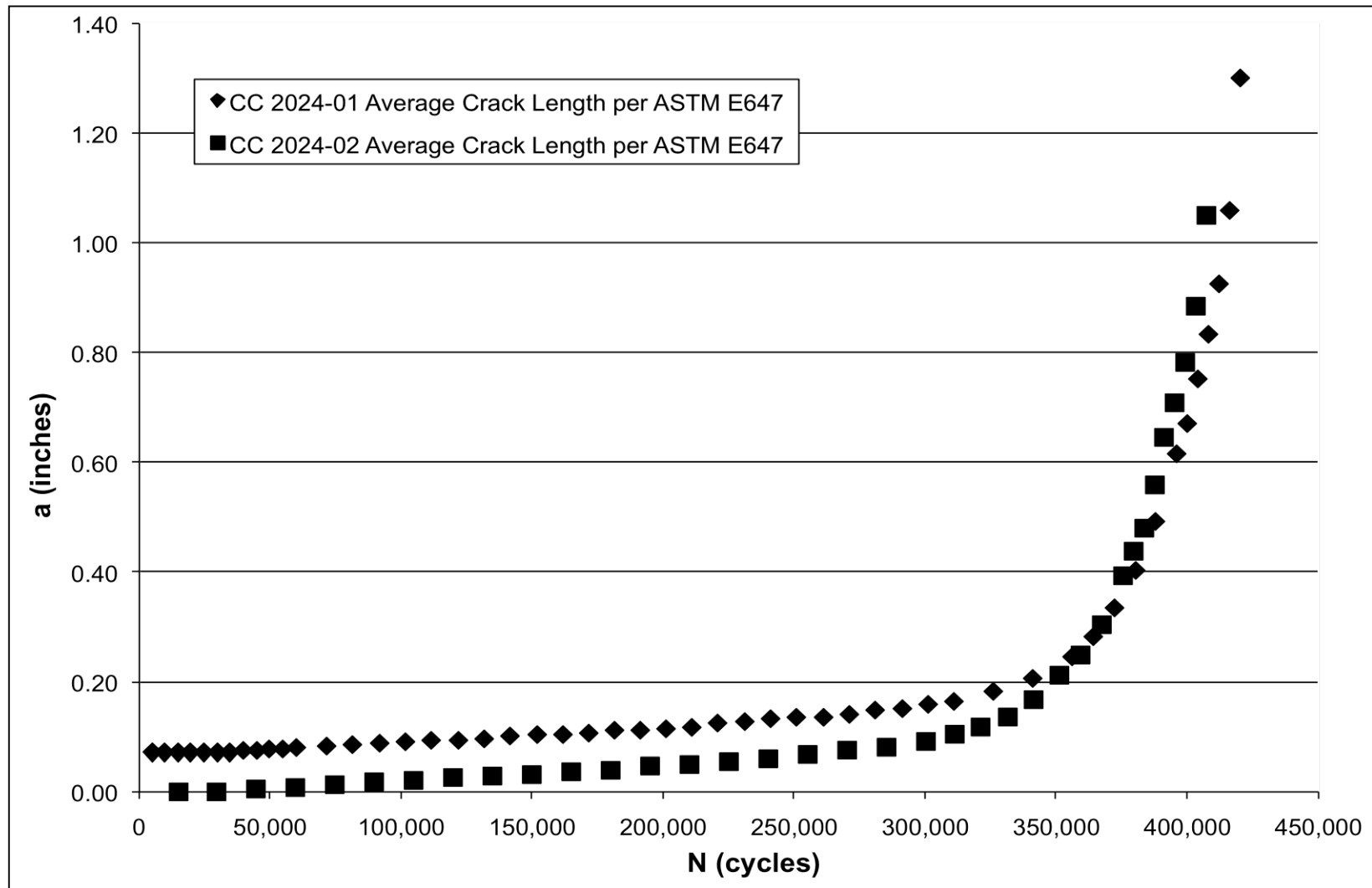
Fig. 53 Cycles versus crack length (a versus N) plot for ASTM Standard E 647 test of Al 2024-T351 middle tension specimen. Specimens tested at σ_{max} = 11.1 ksi, R = 0.1, f = 15 Hz and lab air.
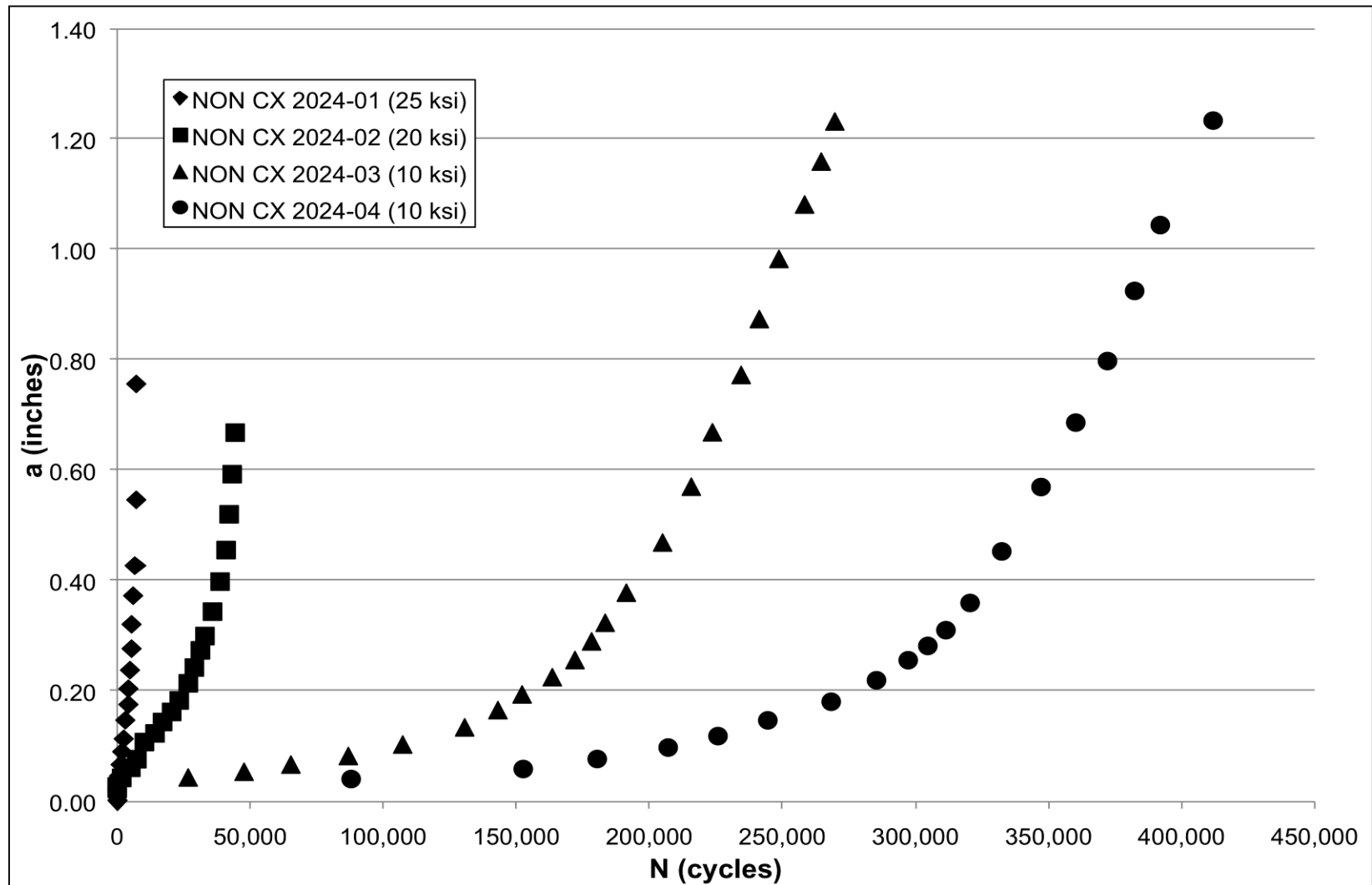
Fig. 54 Crack growth curve (a versus N) for all noncold expanded baseline specimen's EDM entrance surface. Specimens were tested at varying maximum stresses but all at R = 0.1, f = 20 Hz and lab air.

Fig. 55 Crack growth curve (a versus N) for NON CX 2024-01 all primary surfaces. Specimen was tested at σ_{max} = 25 ksi, R = 0.1, 20 Hz and lab air.

Fig. 56 Crack growth curve (a versus N) for NON CX 2024-02 all primary surfaces. Specimen was tested at σ_{max} = 20 ksi, R = 0.1, 20 Hz and lab air.

Fig. 57 Crack growth curve (a versus N) for NON CX 2024-03 all primary surfaces. Specimen was tested at 10 ksi, R = 0.1, 20 Hz and lab air.

Fig. 58 Crack growth curve (a versus N) for NON CX 2024-04 all primary surfaces. Specimen was tested at 10 ksi, R = 0.1, 20 Hz and lab air.

finally for β. All crack measurements were recorded as crack lengths adjacent to the hole. The crack measurements were recorded on the five main surfaces of the specimen. These surfaces were: EDM entrance surface, secondary entrance surface, primary bore surface, EDM exit surface and secondary exit surface. However, for this project the EDM surface was examined and the plots are composed of these surfaces. Fig. 54 through Fig. 58 provide the crack growth curves for these specimens. Fig. 59 is an example of an a versus N plot for all fives surfaces is provided at the end of this section. Fig. 54 shows the four noncold expanded specimens that were tested and their individual fatigue crack growth lives. It can be seen that as the stress was decreased the life was extended and this in turn provided a more stable crack growth behavior. Fig. 55 through Fig. 58 show all the noncold expanded baseline crack growth curves. These curves again are required to provide a baseline for the development of additional plots needed to calculate and produce the da/dN versus ∆K curves as well as the β corrections. Fig. 55 shows the relatively short life of NON CX 2024-01 because of the high stress. Fig. 56 through Fig. 58 all show an increase in life as the stress decreases. In all of these plots however, one characteristic that should be noted is the behavior of the three main primary surfaces. The entrance surface is the main crack that propagated to failure. The primary bore nucleated and propagated within a short number of cycles and then once that crack propagated through the thickness the exit surface was tracked. Fig. 59 provides an example of how all five surfaces behaved under the high
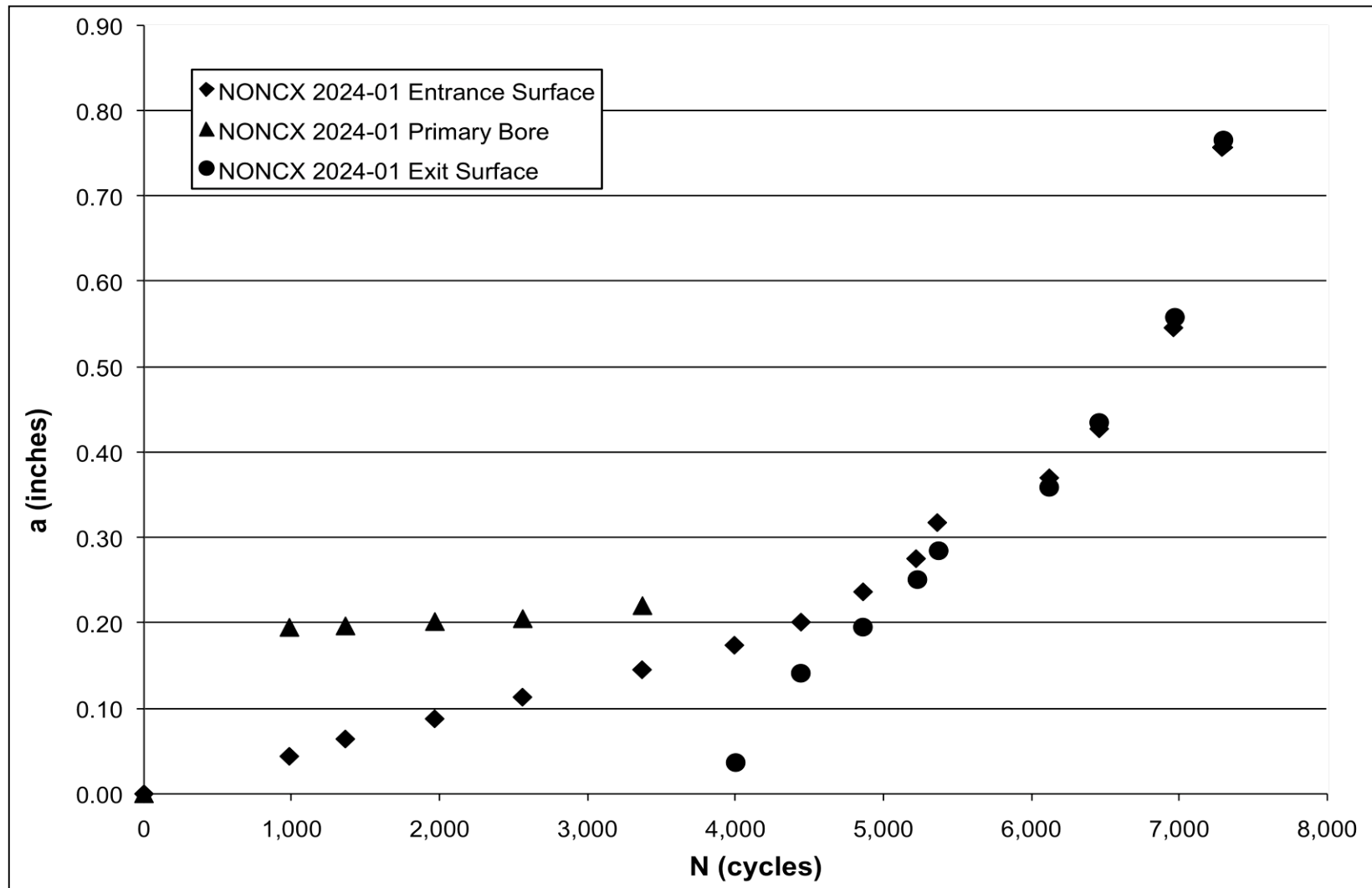
Fig. 59 Crack growth curve (a versus N) for NON CX 2024-01 all primary and secondary surfaces. Specimen was tested at σ_{max} = 25 ksi, R = 0.1, 20 Hz and lab air.

stress loading condition. This figure gives an insight into when the secondary

cracks nucleated and how long they were when failure occurred.

5.2.3 Cold Expanded Specimens

The crack growth curves for all of the cold expanded specimens that were

tested during this research can be found in Appendix D. Once all the fatigue

testing was complete it was determined that three specimens were to be selected

to develop all the da/dN versus ΔK curves as well as the β correction

extrapolation. The three specimens that were selected represented the lower,

middle and upper ranges of fatigue life seen during data collected. This would

allow for the greatest capture of the variability seen during the fatigue testing

phase. The three cold expanded specimens selected were CX 2024-04, CX

2024-15 and CX 2024-17. The fatigue crack growth curves for these three

specimens can be seen in Fig. 60 through Fig. 62.

Like the noncold expanded baseline specimens all crack measurements

were taken from the five main surfaces of the fatigue specimen. These surfaces

were: EDM entrance surface, secondary entrance surface, primary bore surface,

EDM exit surface and secondary exit surface. However for this project the EDM

surface was examined and all a versus N, da/dN versus a and da/dN versus ΔK

plots are composed of these three primary surfaces.

An example of an a versus N plot for all fives surfaces is provided in Fig.

63. This allows for a simple means to determine the crack growth on each

surface in relation to the other four surfaces. From these plots one can

determine when the secondary cracks nucleated and how large they were at final
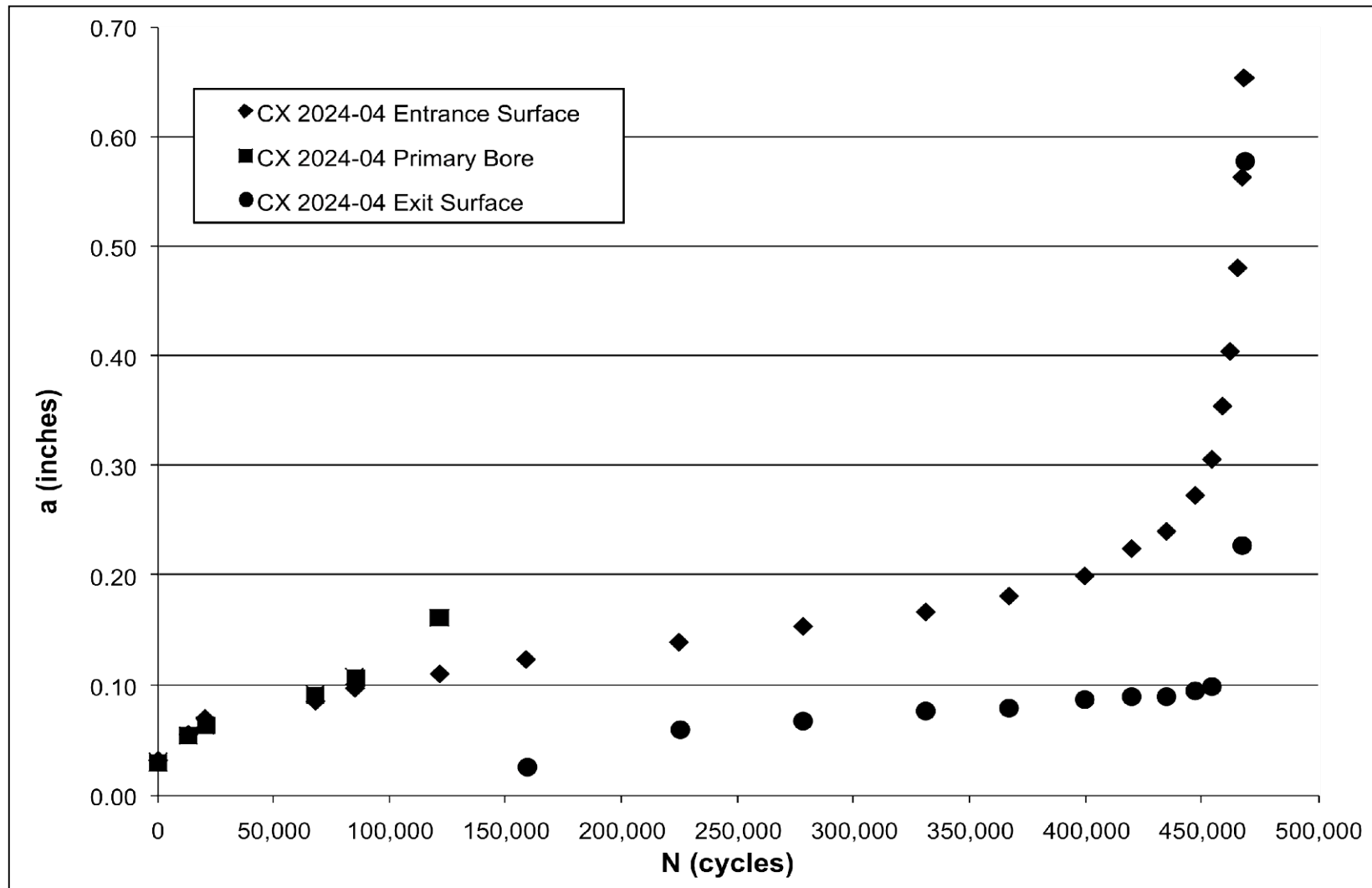
Fig. 60 Crack growth curve (a versus N) CX 2024-04 all primary surfaces. Specimen was tested at σ_{max} = 25 ksi, R = 0.1, 20 Hz and lab air.

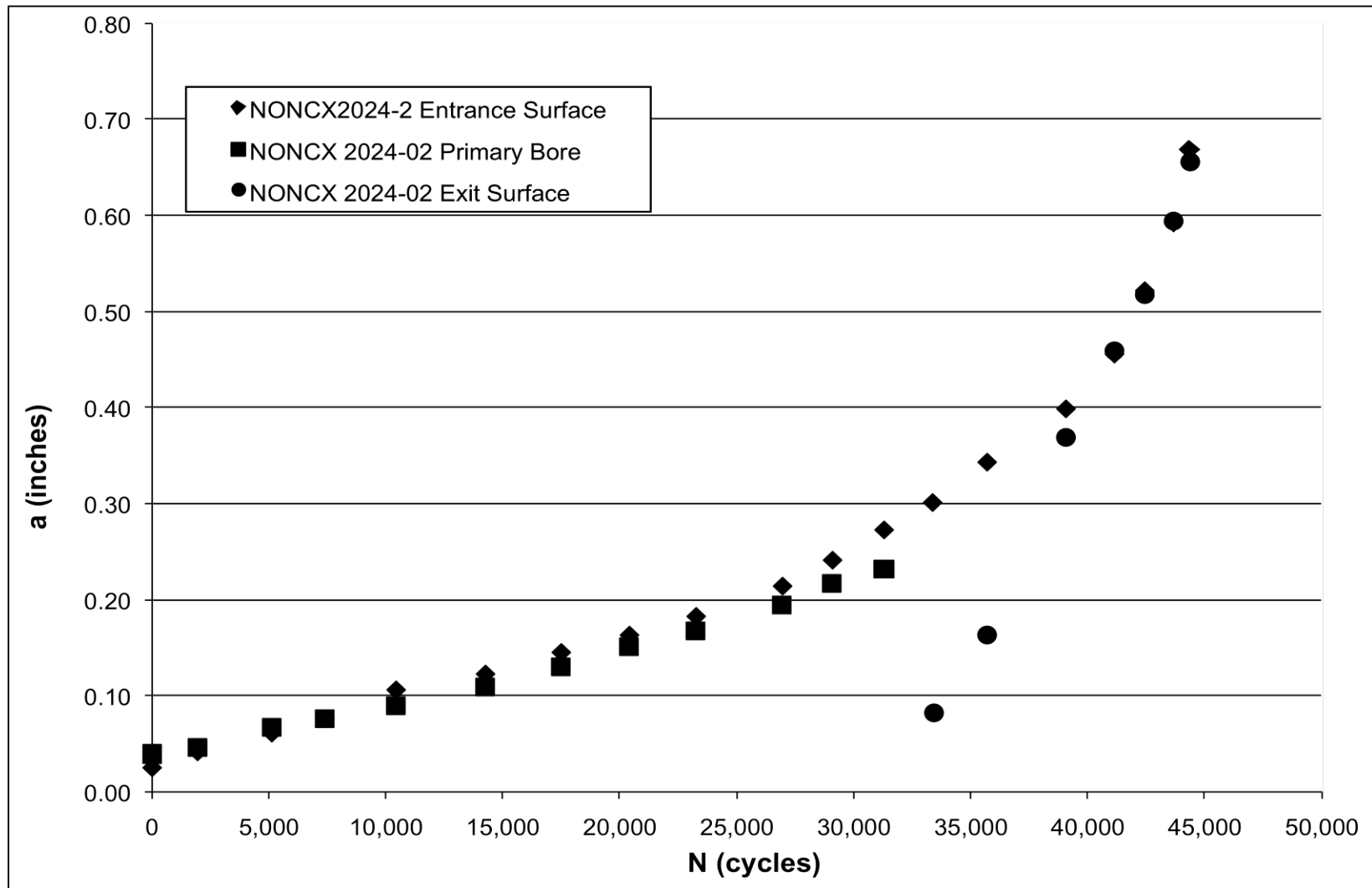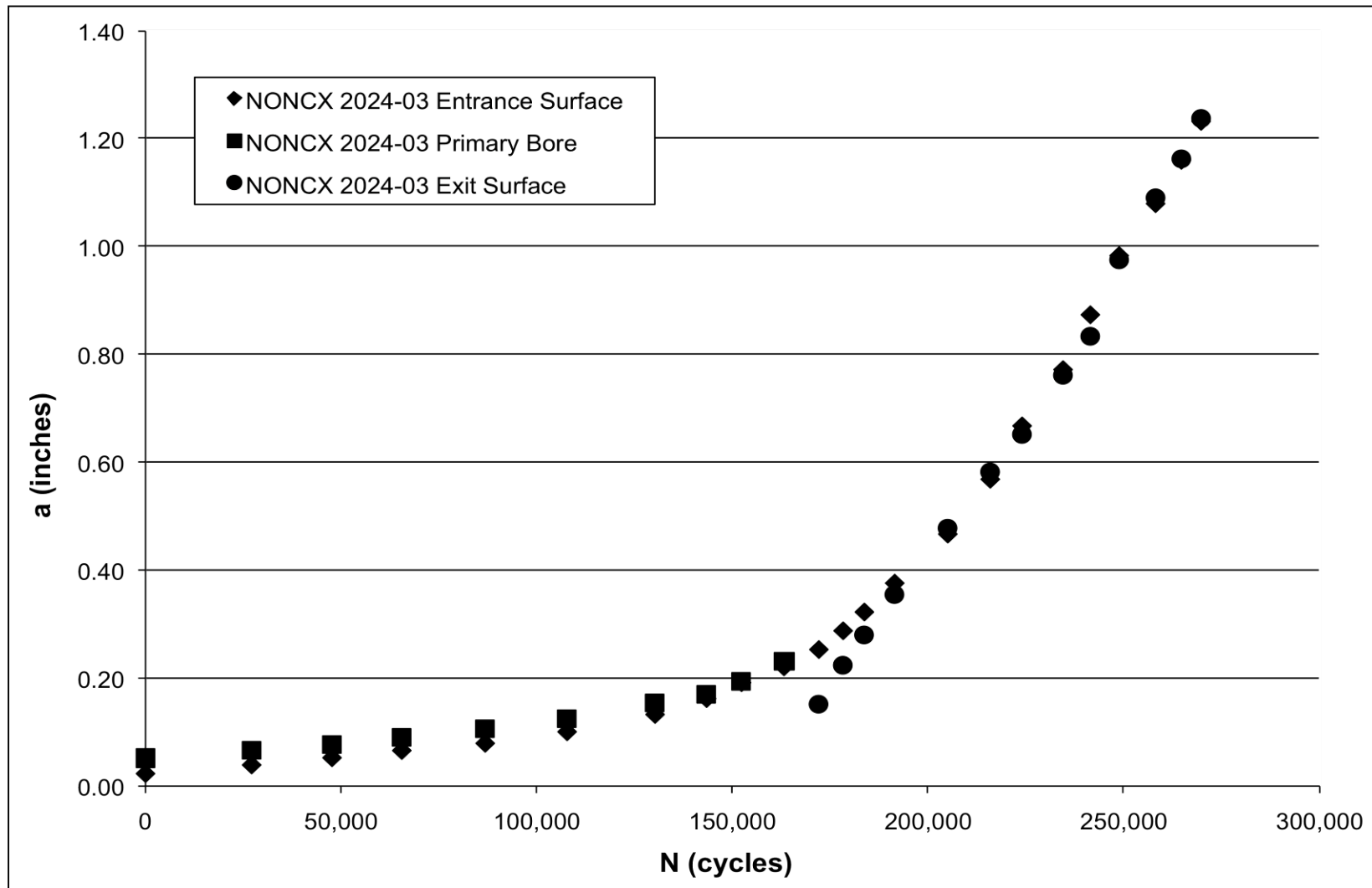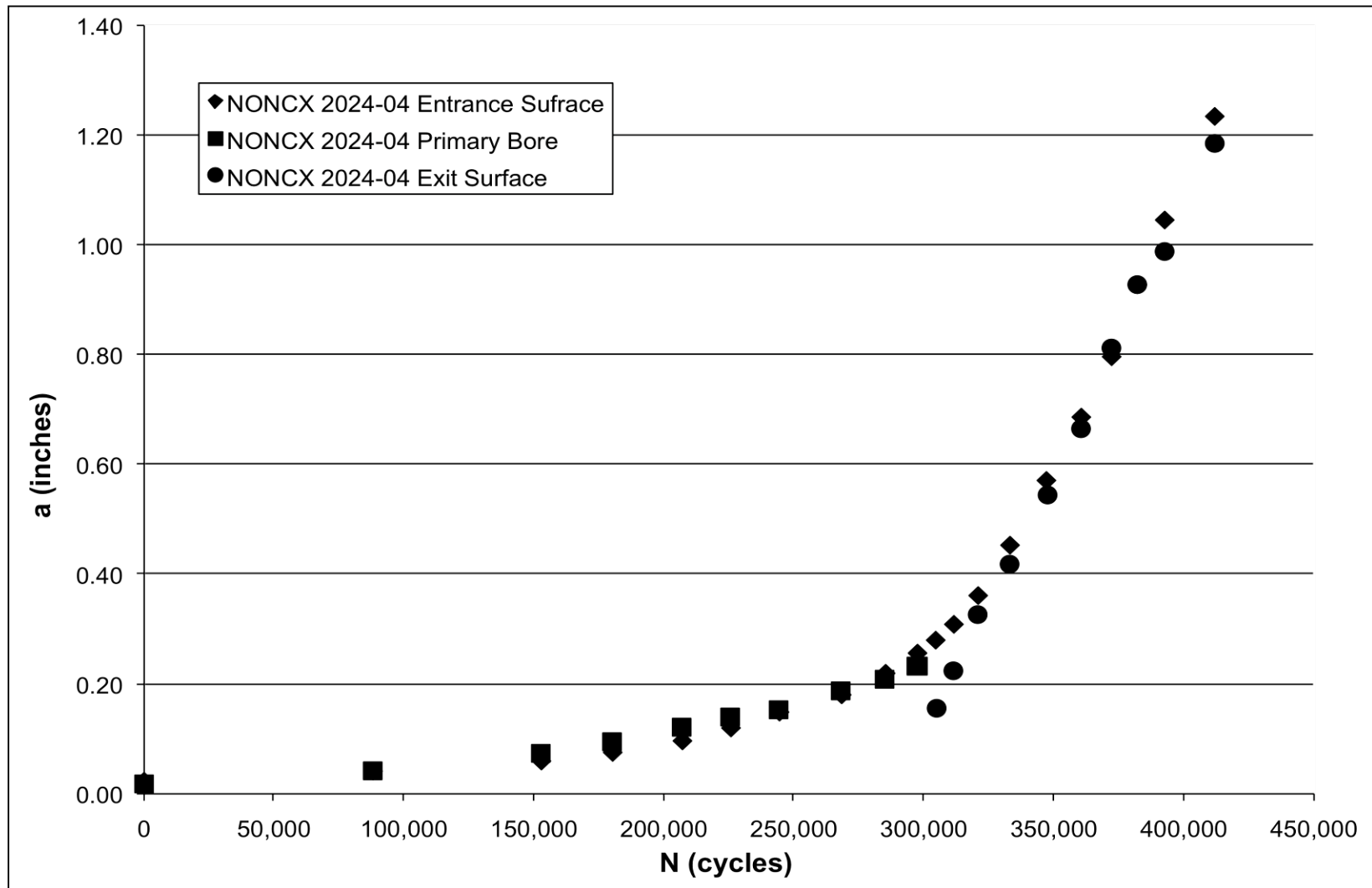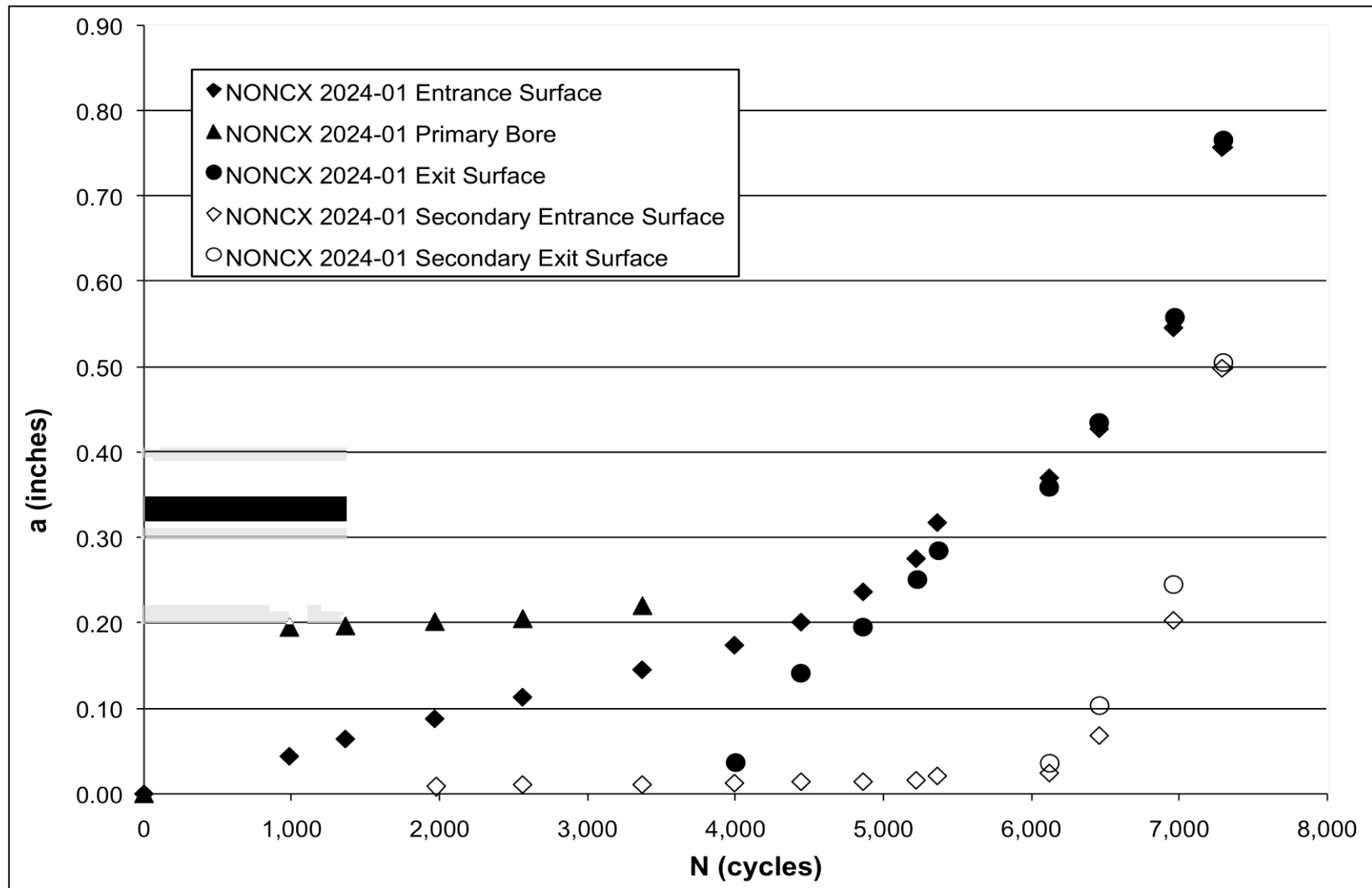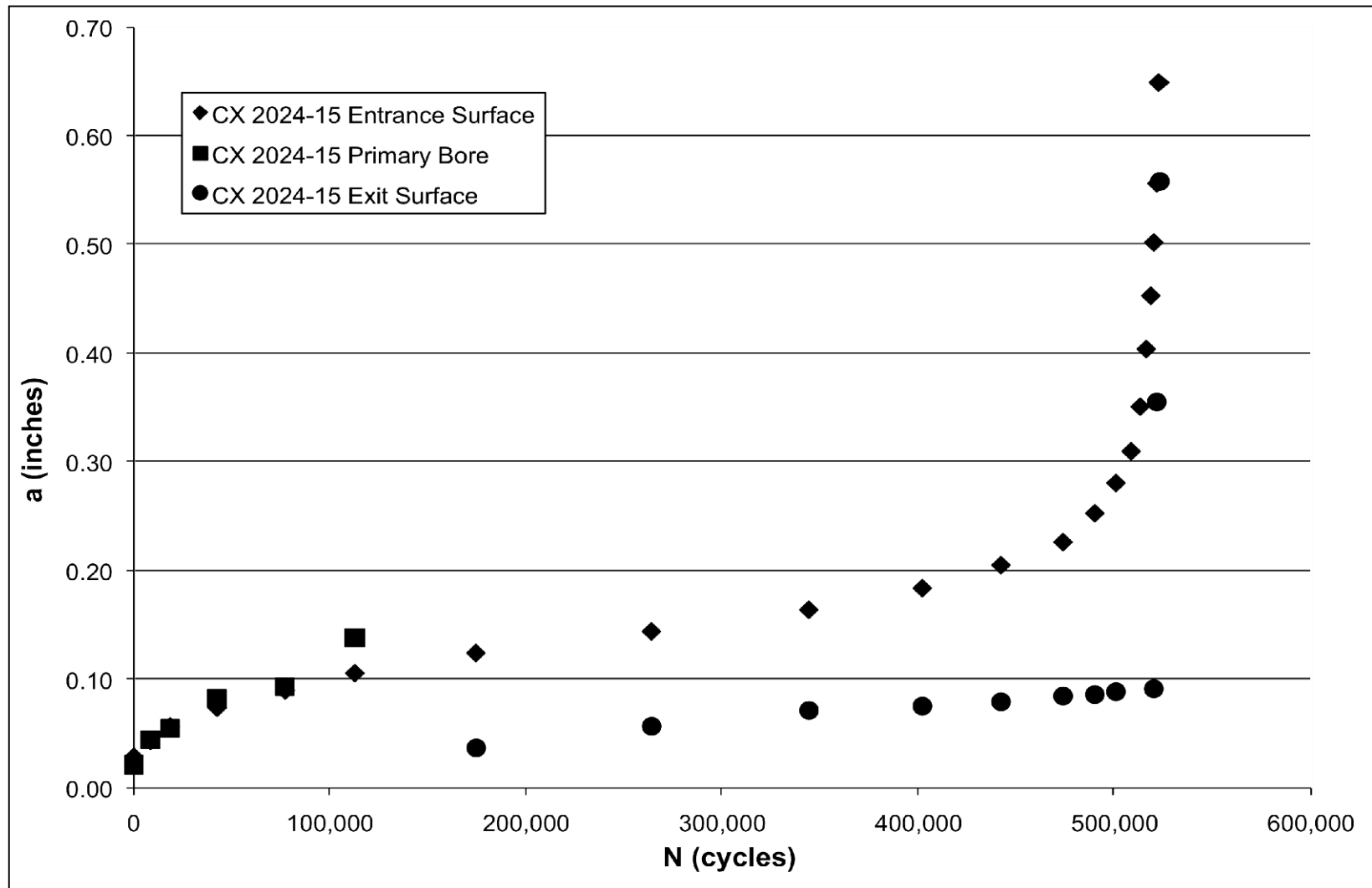Fig. 61 Crack growth curve (a versus N) CX 2024-15 all primary surfaces. Specimen was tested at σ_{max} = 25 ksi, R = 0.1, 20 Hz and lab air
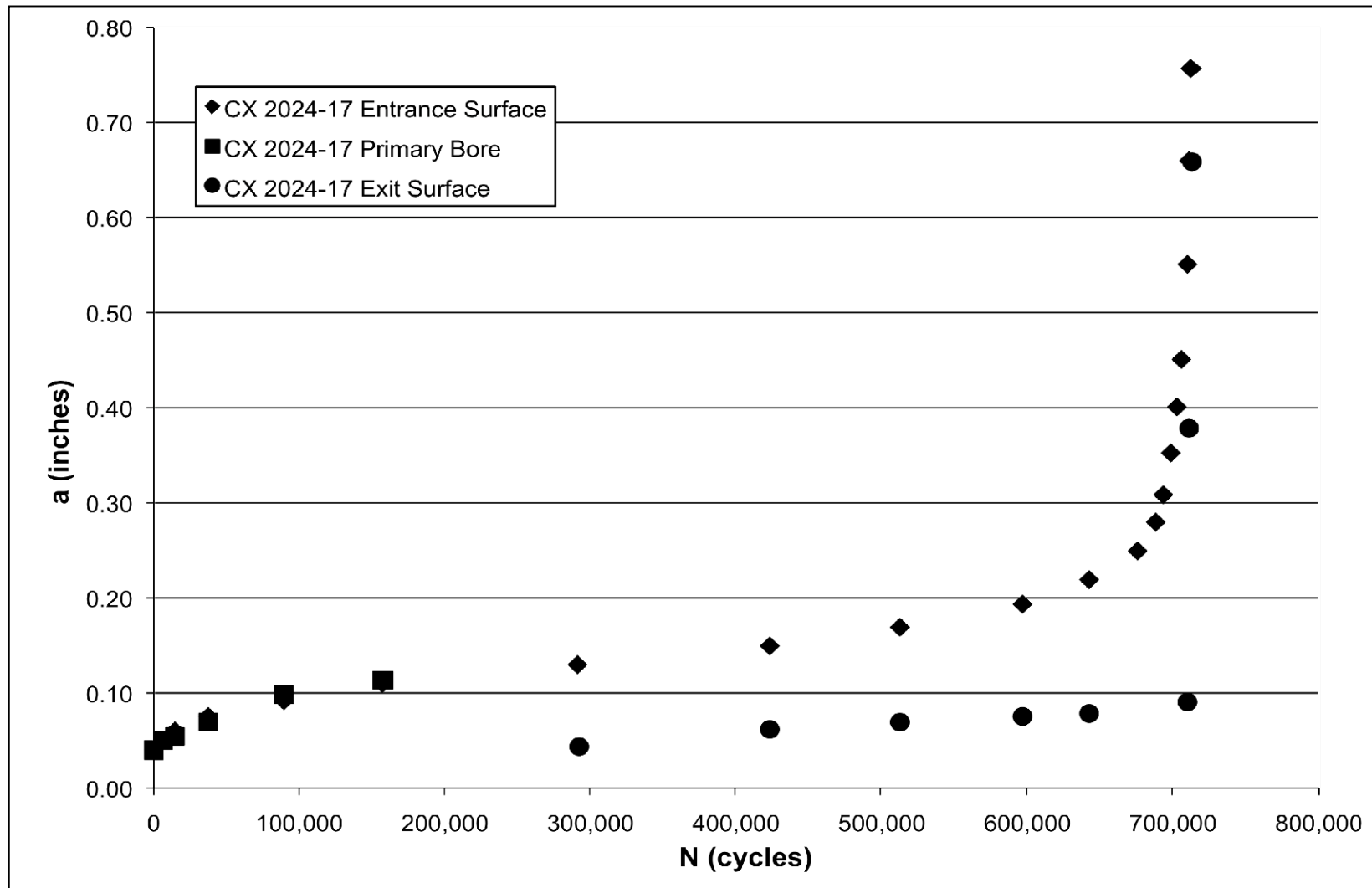
Fig. 62 Crack growth curve (a versus N) CX 2024-17 all primary surfaces. Specimen was tested at σ_{max} = 25 ksi, R = 0.1, 20 Hz and lab air.
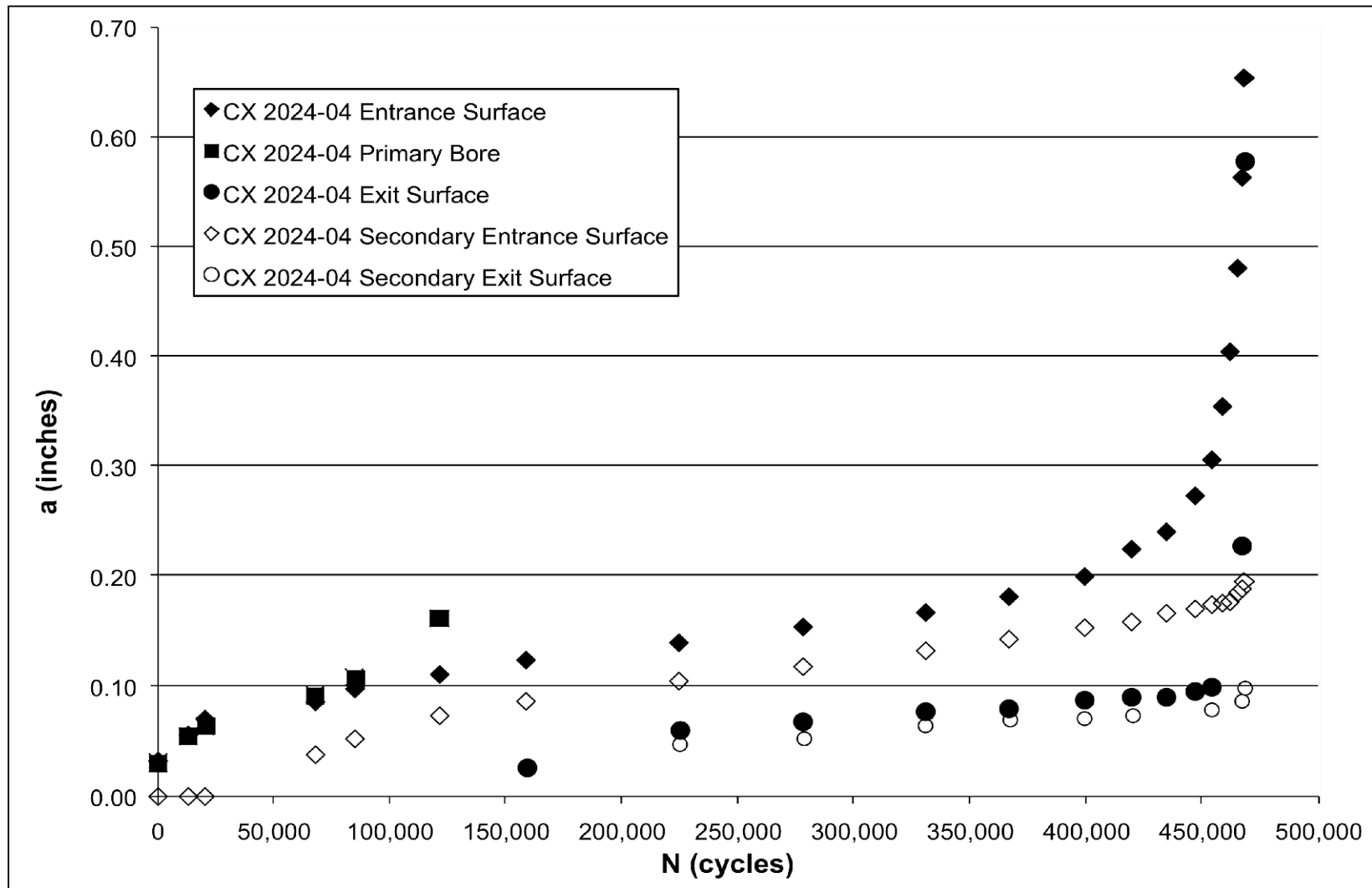
Fig. 63 Crack growth curve (a vs. N) CX 2024-04 all primary and secondary surfaces. Specimen was run at 25 ksi, R = 0.1, 20 Hz and lab air.

fracture. This figure provides the lower bound of the fatigue life seen during testing of the cold expanded specimens. Specimen CX 2024-04 only lasted approximately 475,000 cycles while specimen CX 2024-15, as seen in Fig. 61 lasted almost 550,000 and the longest of the cold expanded specimens, CX 2024-17 was able to run for over 700,000 cycles. The fatigue crack growth behavior of all three specimens was very similar; however, the number cycles until failure was dramatically different from specimen to specimen. These, like the noncold expanded specimens fatigue crack growth curves, are extremely important in the documentation and analysis of the fatigue crack growth behavior of the cold expanded material.

5.3 Crack Growth Rate Versus Crack Length Plots (da/dN Versus a)

Crack growth rate versus crack length (da/dN versus a) plots for all specimens were created for this research project. Only those specimens outlined in the previous section will be shown in this section. For plots of all specimens refer to Appendix F.

5.3.1 ASTM Standard E 647 Specimens

Fig. 64 shows the crack growth rate versus crack length (da/dN versus a) plots for the two ASTM Standard E 647 specimens. This plot was created using the standard secant method for the development of da/dN as outlined in the ASTM Standard.
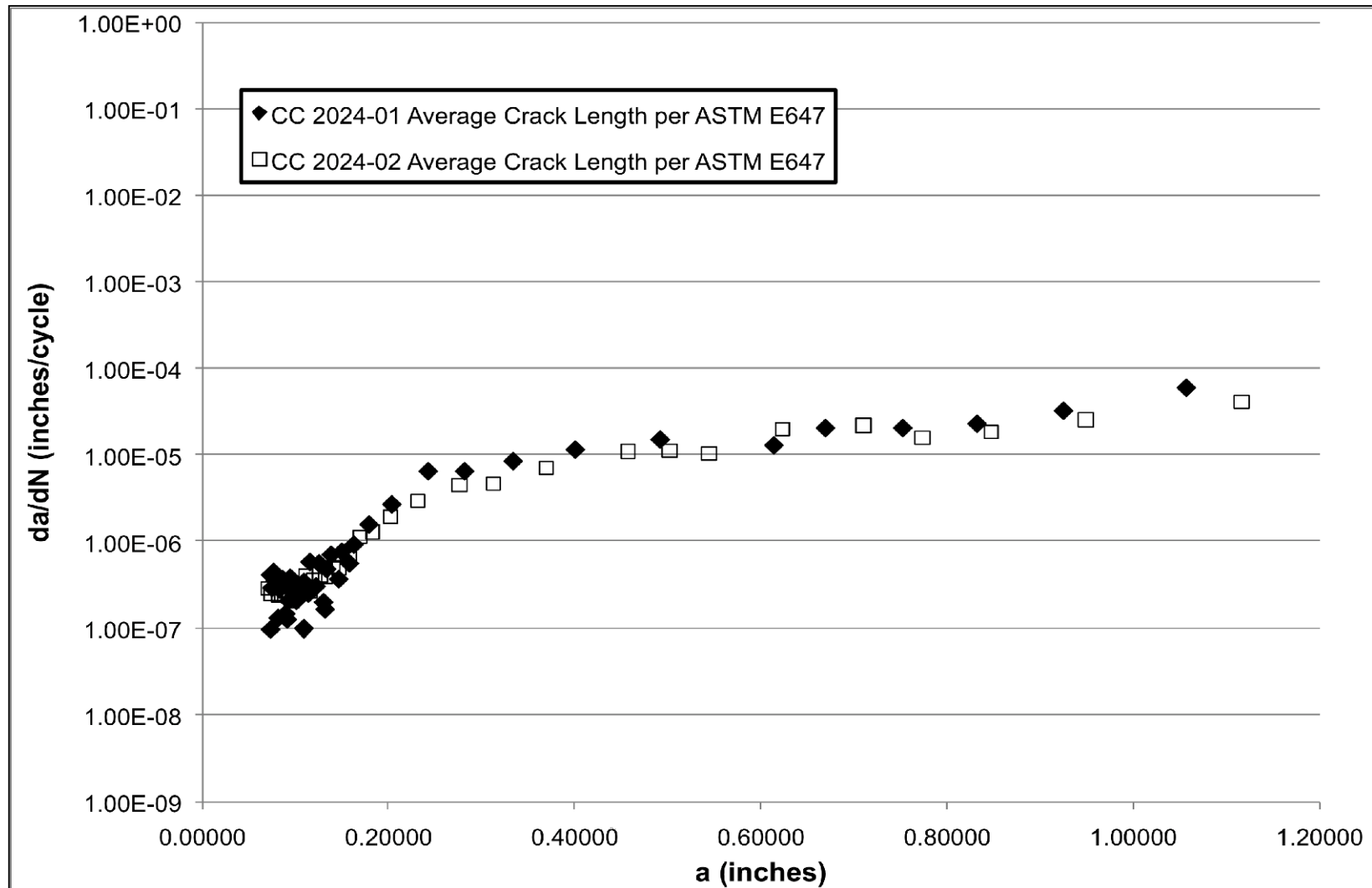
Fig. 64 da/dN versus a curve for CC 2024-01 and 02 ASTM Standard E 647 Specimens. Specimens were tested at σ_{max} = 11.1 ksi, R = 0.1, f = 15 Hz, and lab air. Crack lengths are averaged per the ASTM standard procedures.

As seen in the figure the crack growth rate starts out at a constant rate than increases to approximately 1.00E-5 inch per cycle and then stays at that rate until final failure of the specimen. There is also good correlation between the two specimens and this is because of the quality data that was taken and shown in the a versus N plots.

5.3.2 Baseline Noncold Expanded Specimens

Baseline noncold expanded specimens were tested at different stress levels to allow the greatest range of da/dN to be captured. For a full report of all da/dN versus a curves refer to Appendix F. During the testing of each specimen all primary and secondary surfaces were tracked, however only the primary surfaces are plotted in Fig. 65 through Fig. 68. Fig. 65 and Fig. 66 show the fatigue crack growth rates for specimens NON CX 2024-01 and -02. These specimens were tested at the higher stress of 25 ksi and 20 ksi. As it can be seen from these two plots they exhibit similar crack growth features, in that they have fairly constant da/dN rates as the crack propagated through the specimen. The rate for the NON CX 2024-01 was greater due to the higher stress it was tested at. The last two specimens NON CX 2024-03- and -04 were tested at a σ_{max} = 10 ksi. These specimens show a difference in their crack growth rates from that seen in the specimens tested at the higher stress. These two specimen start out at a much slower rate and then progress to a more rapid crack growth as the fatigue propagated through the specimen.
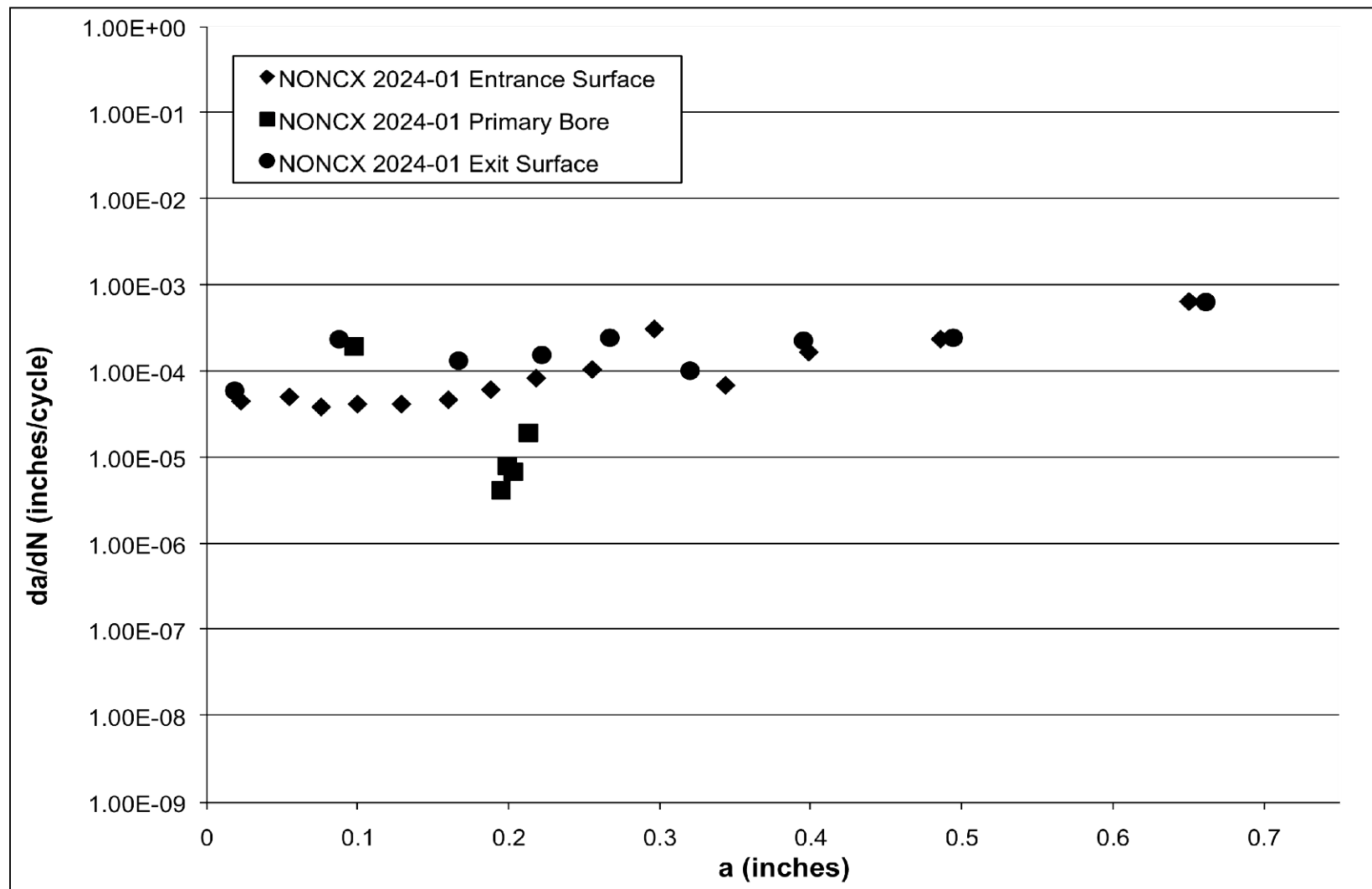
Fig. 65 Crack growth rate versus crack length (da/dN versus a) curve for base line NON CX 2024-01. Specimen was tested at σ_{max} = 25 ksi, R = 0.1, f = 20, and lab air.
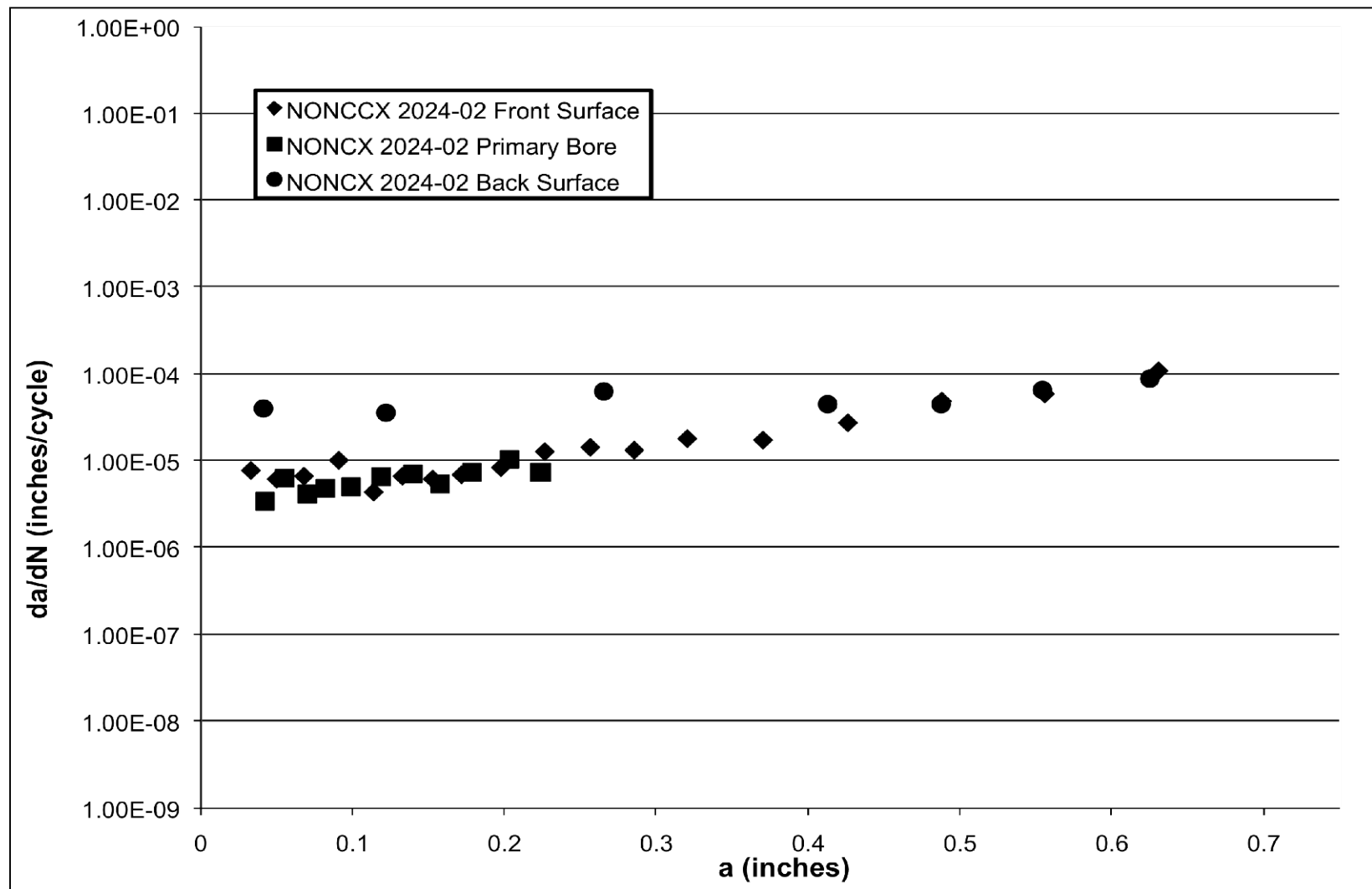
Fig. 66 Crack growth rate versus crack length (da/dN versus a) curve for base line NON CX 2024-02. Specimen was tested at σ_{max} = 20 ksi, R = 0.1, f = 20, and lab air.
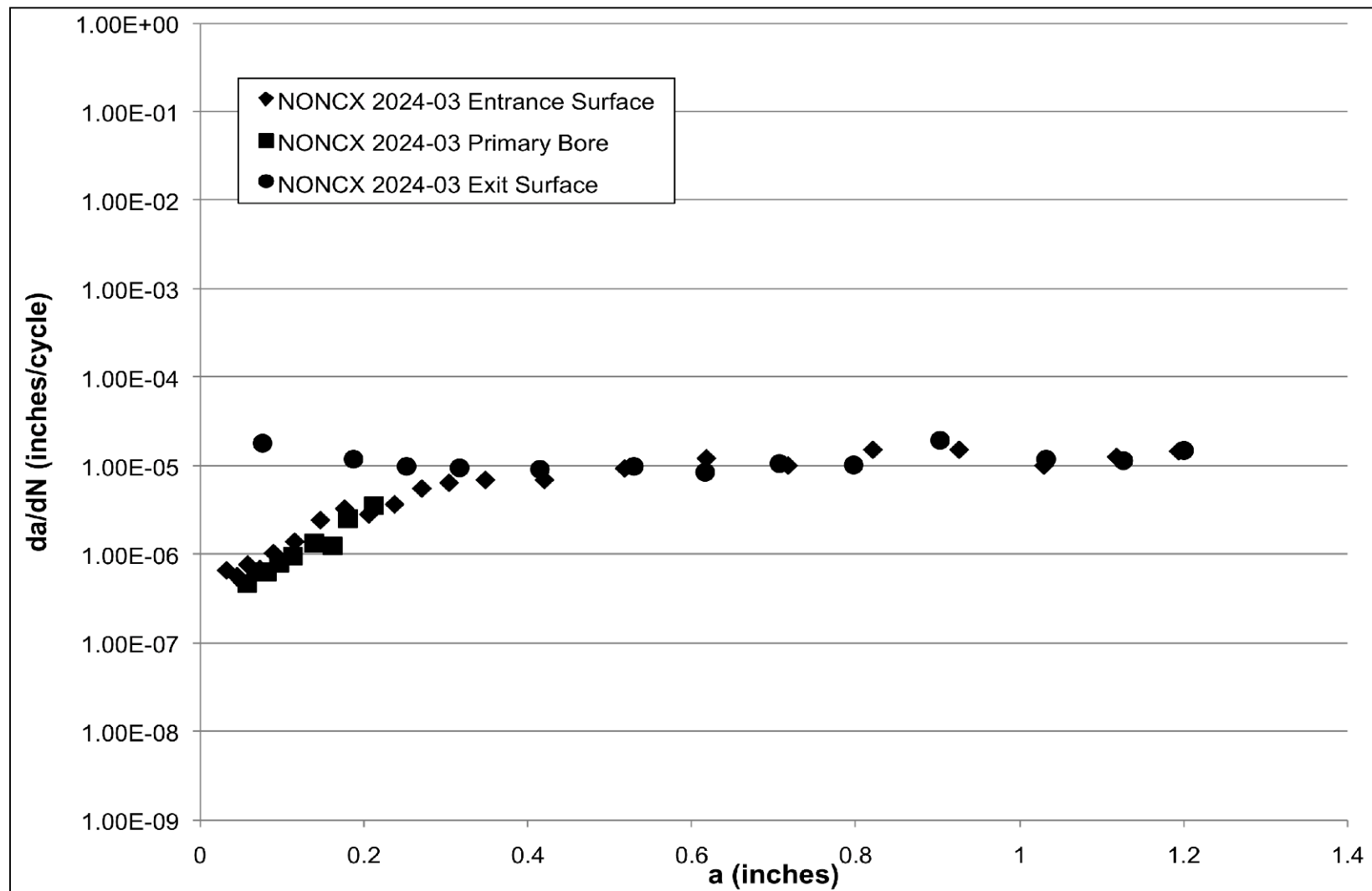
Fig. 67 Crack growth rate versus crack length (da/dN versus a) curve for base line NON CX 2024-03. Specimen was tested at σ_{max} = 10 ksi, R = 0.1, f = 20, and lab air.
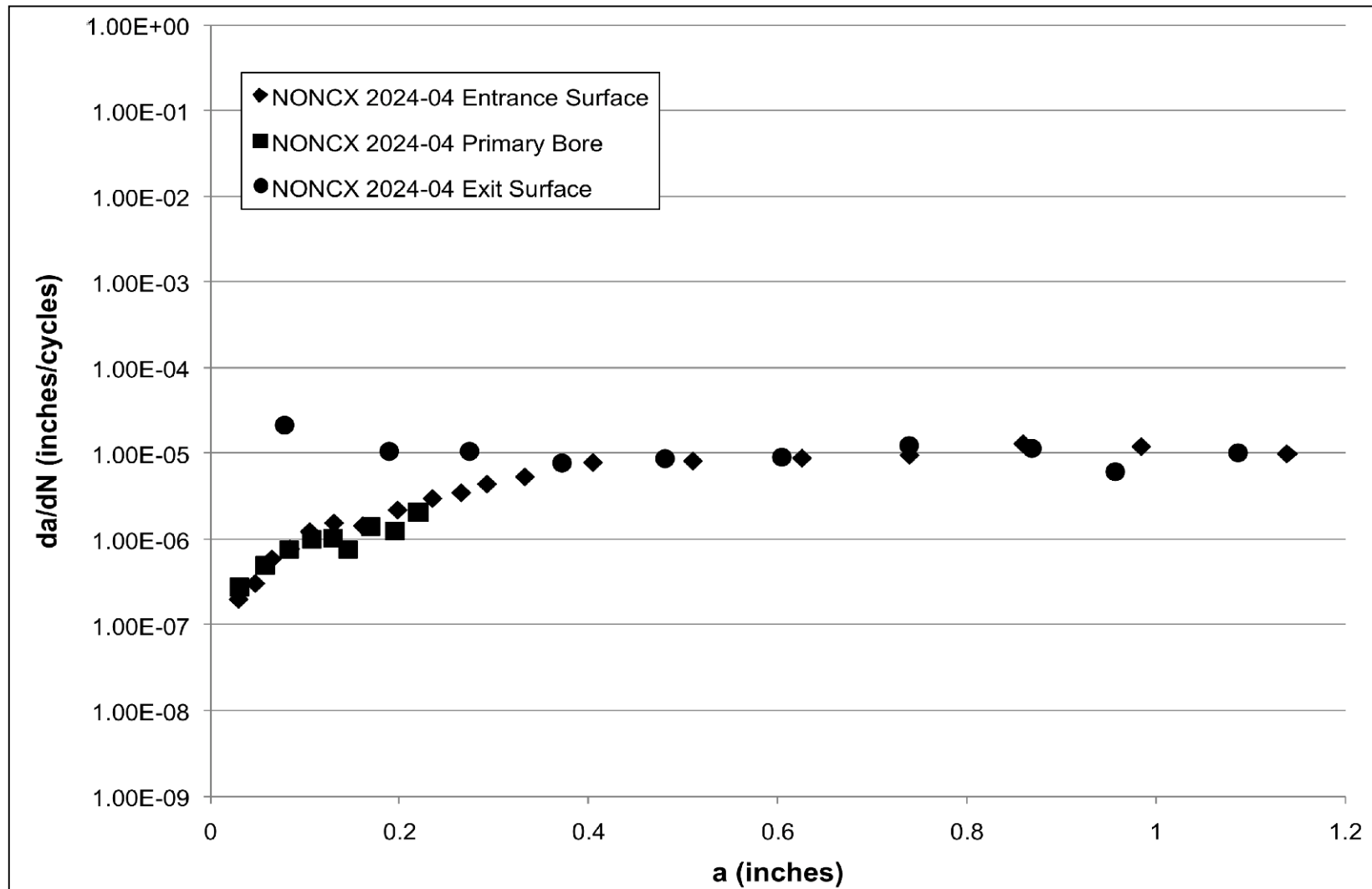
Fig. 68 Crack growth rate versus crack length (da/dN versus a) curve for base line NON CX 2024-04. Specimen was tested at σ_{max} = 10 ksi, R = 0.1, f = 20, and lab air.

5.3.3 Cold Expanded Specimens

5.3.3.1 EDM Entrance Surface da/dN versus a

To allow for a general overview of the crack growth rate versus crack length of the cold expanded specimens, Fig. 69 shows all the cold expanded specimens together. This figure provided an overview of fatigue crack growth behavior of all the cold expanded specimens that were tested at a σ_{max} = 25 ksi. The figure also provides a good insight into the overall trend exhibited by the cold expanded specimens. The data shows very good conformity with each data point. Fig. 70 is specific to the four cold expanded chosen to represent the total population tested. These specimens were chosen because the represented the upper, middle and lower bounds on the da/dN versus a plot. This in turn would provide data that captured the extremes and the middle without having to develop curves for all the cold expanded specimens. Specimen CX 2024-19 was tested at a lower σ_{max} = 12 ksi. This was done to allow for a greater range of da/dN to correlate with the noncold expanded specimens.

5.3.3.2 Primary Bore Surface da/dN versus a

The primary bore surface was also tracked and Fig. 71 illustrates the overall trend of all the cold expanded specimens crack growth rate versus crack length for this critical surface. This trend showed that there was a fairly constant fatigue crack growth rate through the bore. It was difficult to track the fatigue cracks through the bore because of multiple fatigue cracks that would nucleate in the bore as the fatigue crack propagated. As stated above in the section for the EDM entrance surface three specimens were selected to represent total

Fig. 69 Crack growth rate versus crack length (da/dN versus a) for all cold expanded specimen's EDM entrance surface. All specimens were tested at σ_{max} = 25 ksi, R = 0.1, f = 20, and lab air.
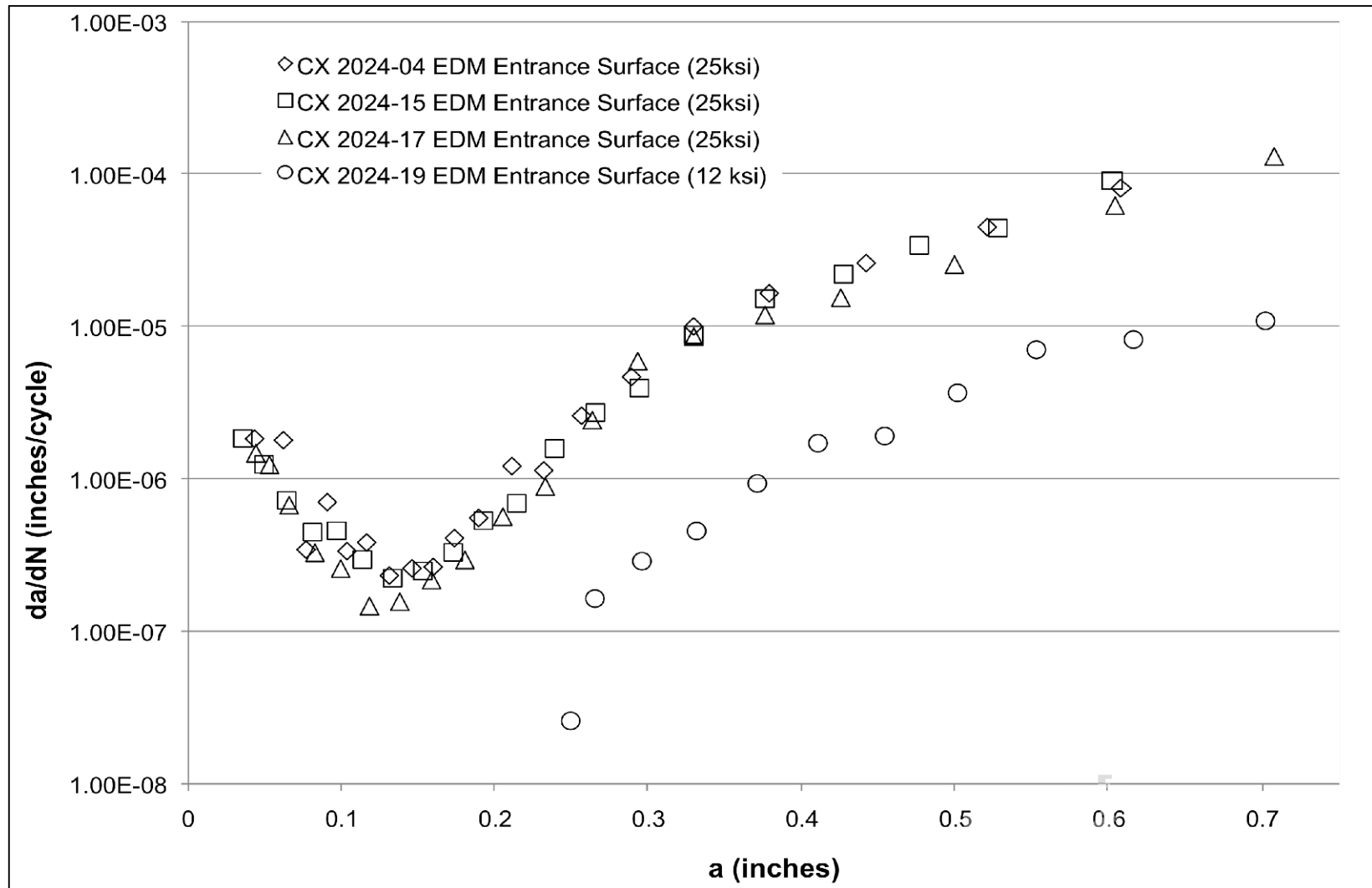
Fig. 70 Crack growth rate versus crack length (da/dN versus a) for selected cold expanded specimen's EDM entrance surface. Specimens were tested at varying σ_{max}, R = 0.1, f = 20, and lab air.
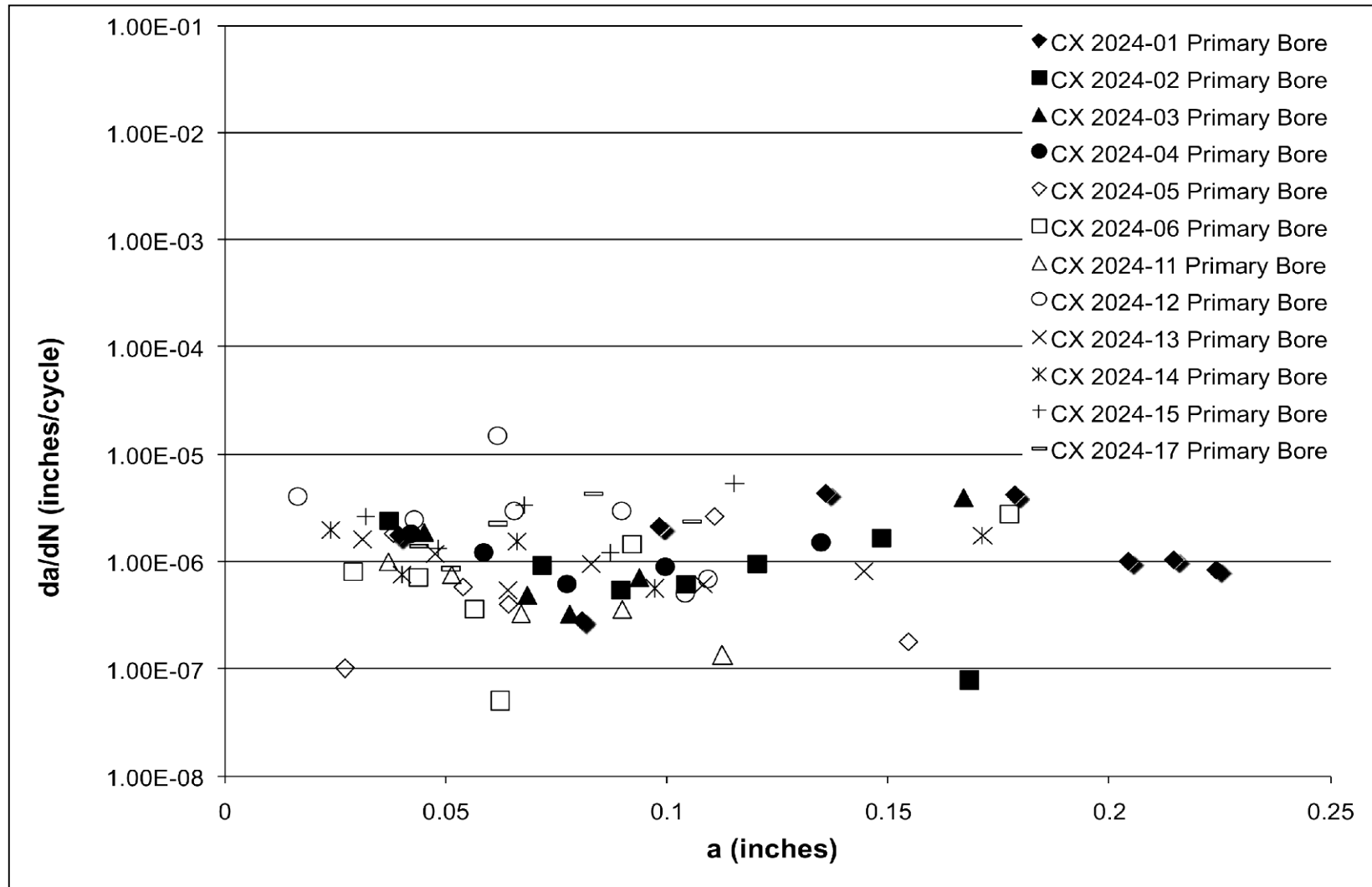
Fig. 71 Crack growth rate versus crack length (da/dN versus a) for all cold expanded specimen's primary bore surface. All specimens were tested at σ_{max} = 25 ksi, R = 0.1, f = 20, and lab air

population of data collected. These three specimens were CX 2024-04, -15 and

-17. These specimens represented the two extreme values found in the da/dN

versus a plot and one in the middle. Fig. 72 highlights these three specimen's

crack growth rate versus crack length for through bore cracks.

5.3.3.3 Primary Exit Surface da/dN versus a

The primary exit surface was tracked and can be seen in Fig. 73 and Fig.

74 illustrate the overall trend for this surface. From these plots it can be seen

that on the exit surface the fatigue crack growth rate decreases dramatically to

approximately 1.00E-07 inches per cycle as it propagates to approximately 0.06

to 0.08 inch from the edge of the cold expanded hole. The crack then stays that

that rate until the crack extends to over 0.12 – 0.14 inches. From this one can

see the dramatic influence this surface has on the overall fatigue crack growth

behavior of these specimens that had been processed by cold expansion.

5.4 Crack Growth Rate Versus Stress Intensities (da/dN Versus ΔK)

In fracture mechanics one of the standard plotting tools used to determine

the crack growth characteristics for a particular material is to use a da/dN versus

ΔK curve. This curve compares the crack growth rate to the stress intensity. A

da/dN versus ΔK plot was computed for all three phases of this research and are

shown.
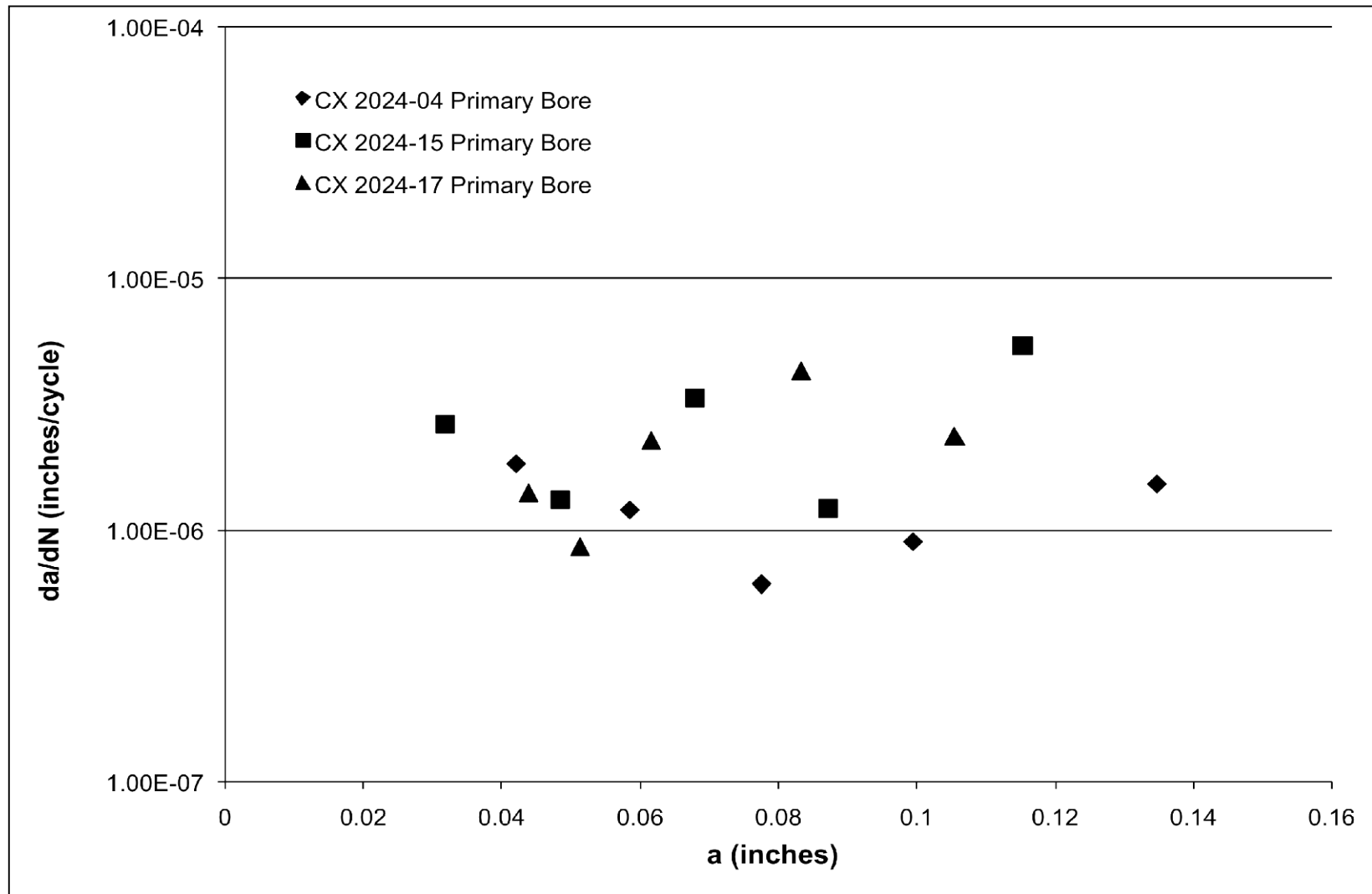
Fig. 72 Crack growth rate versus crack length (da/dN versus a) for selected cold expanded specimen's primary bore surface. All specimens were tested at σ_{max} = 25 ksi, R = 0.1, f = 20, and lab air

Fig. 73 Crack growth rate versus crack length (da/dN versus a) for selected cold expanded specimen's primary exit surface. All specimens were tested at σ_{max} = 25 ksi, R = 0.1, f = 20, and lab air
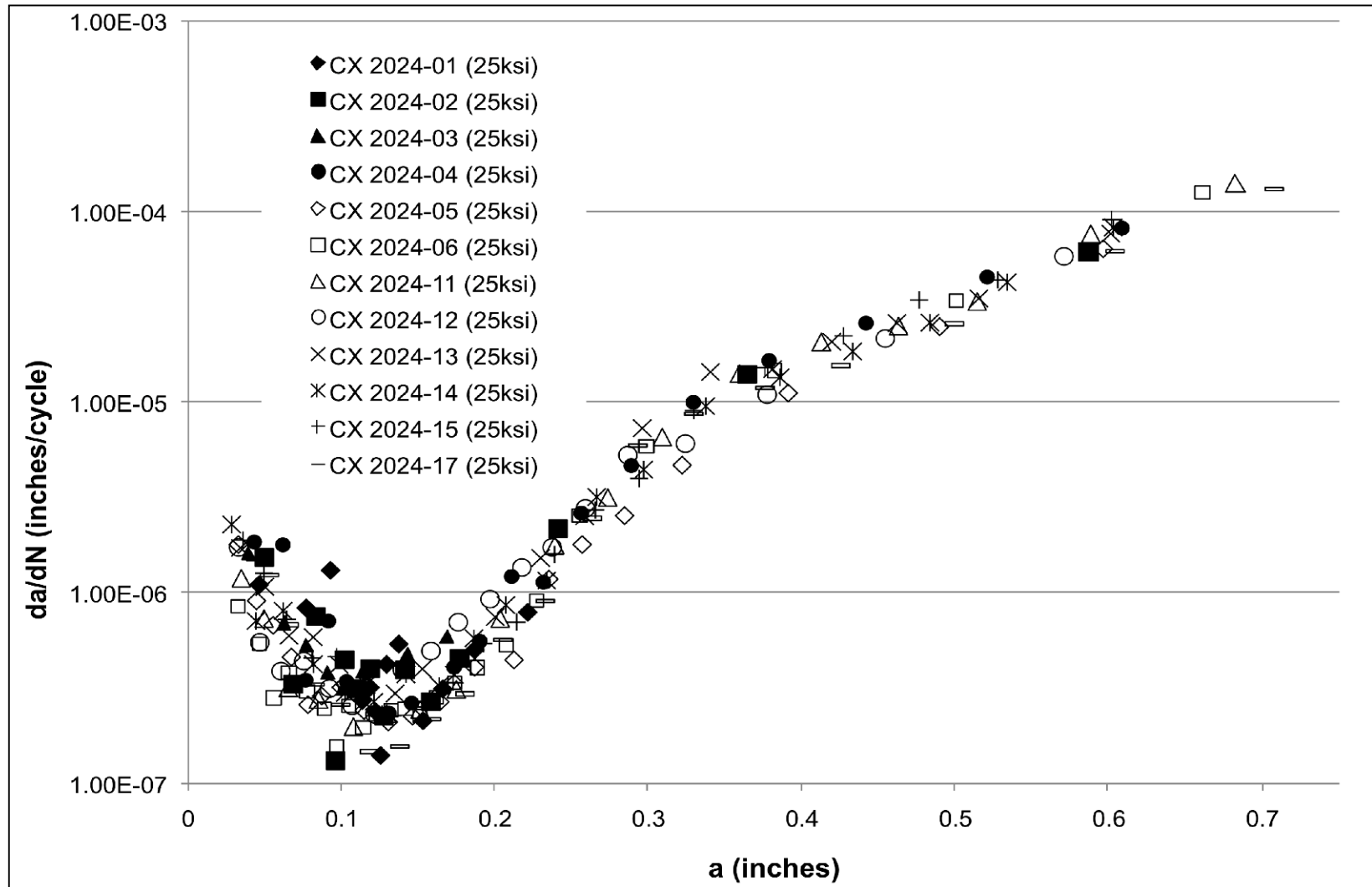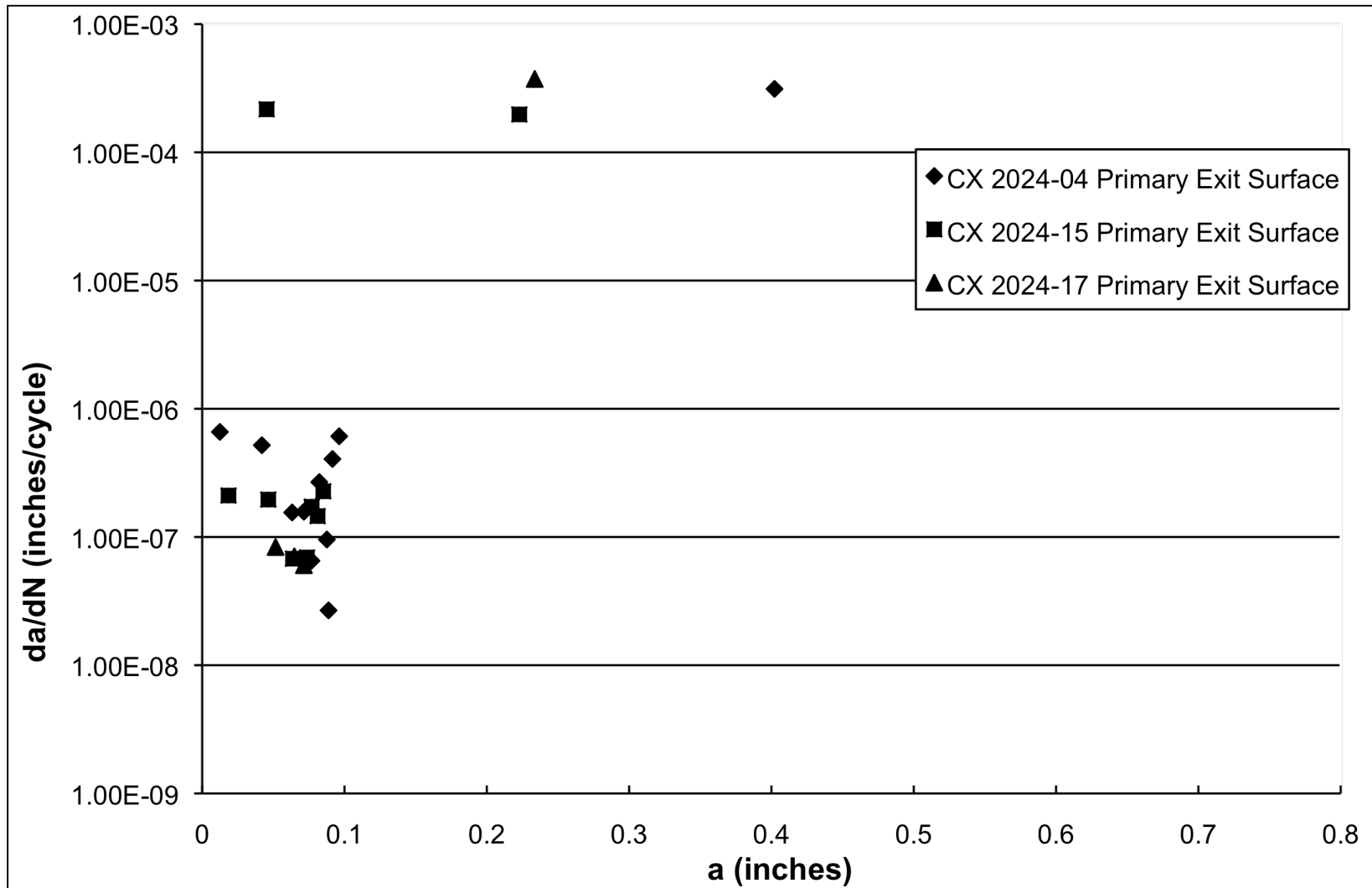
Fig. 74 Crack growth rate versus crack length (da/dN versus a) for selected cold expanded specimen's primary exit surface. All specimens were tested at σ_{max} = 25 ksi, R = 0.1, f = 20, and lab air

5.4.1 ASTM Standard E 647 Specimens

The ASTM E 647 specimen's da/dN versus ΔK curves were computed using the ASTM standard calculation for ΔK.[28] These data were then compared to known testing data provided from SwRI.[29] The results from this comparison can be seen in Fig. 75. As seen in Fig. 75, the ASTM Standard E 647 data collected correlate very well with the industry standard data provided by SwRI.

5.4.2 Baseline Noncold Expanded Specimens

All baseline specimens were used to develop the baseline noncold expanded da/dN versus ΔK curves for both the EDM entrance surface and the primary bore surface and can be seen in Fig. 76 through Fig. 77. The baseline curves were compared again to the SwRI and other industry standard data. This comparison provided a good correlation between data points. The baseline data were also compared to the NASGRO and Harter-T material data provided in AFGROW.[33] As seen in Fig. 77 the baseline noncold expanded data lay very well on top of the SwRI data at the bottom of the curve but then shifts and the Harter T data fit well in the middle section of the data. It can be seen that the data has a knee in it at around a crack growth rate of approximately 1.0E-5 inch per cycle. This made it difficult to fit any of the tabular or curve fit data shown in that figure to this characteristic. This type of knee in aluminum alloys is not uncommon and is a property of the alloy itself. This type of material characteristic is difficult to capture with equation driven curve fits like the Harter-T and NASGRO.
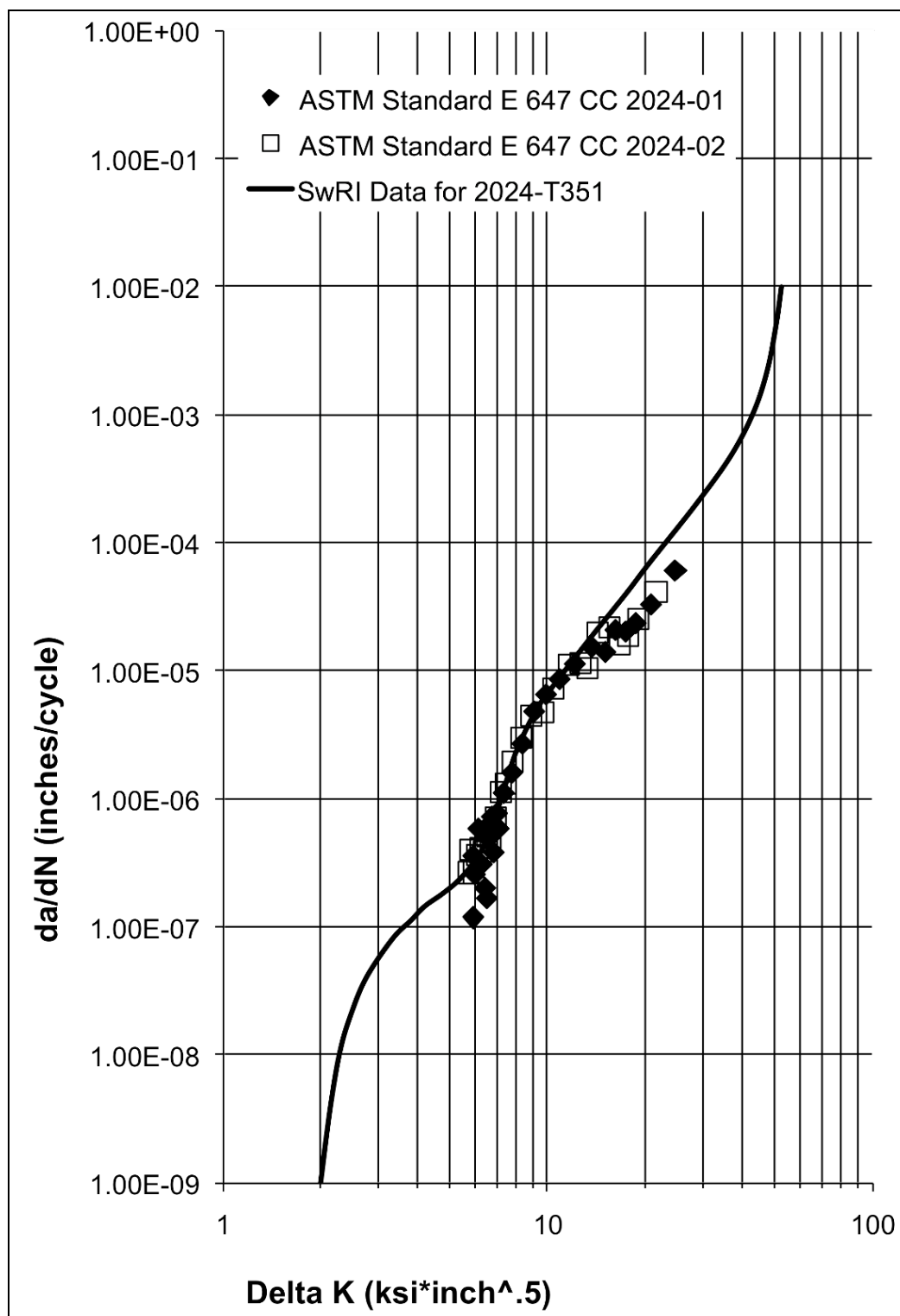
Fig. 75 da/dN versus ΔK for ASTM Standard E 647 middle tension specimens tested at σ_{max} of 11.1ksi, R = 0.1, f = 20 Hz, and lab air. SwRI comparison for 2024-T351 at R = 0.1.
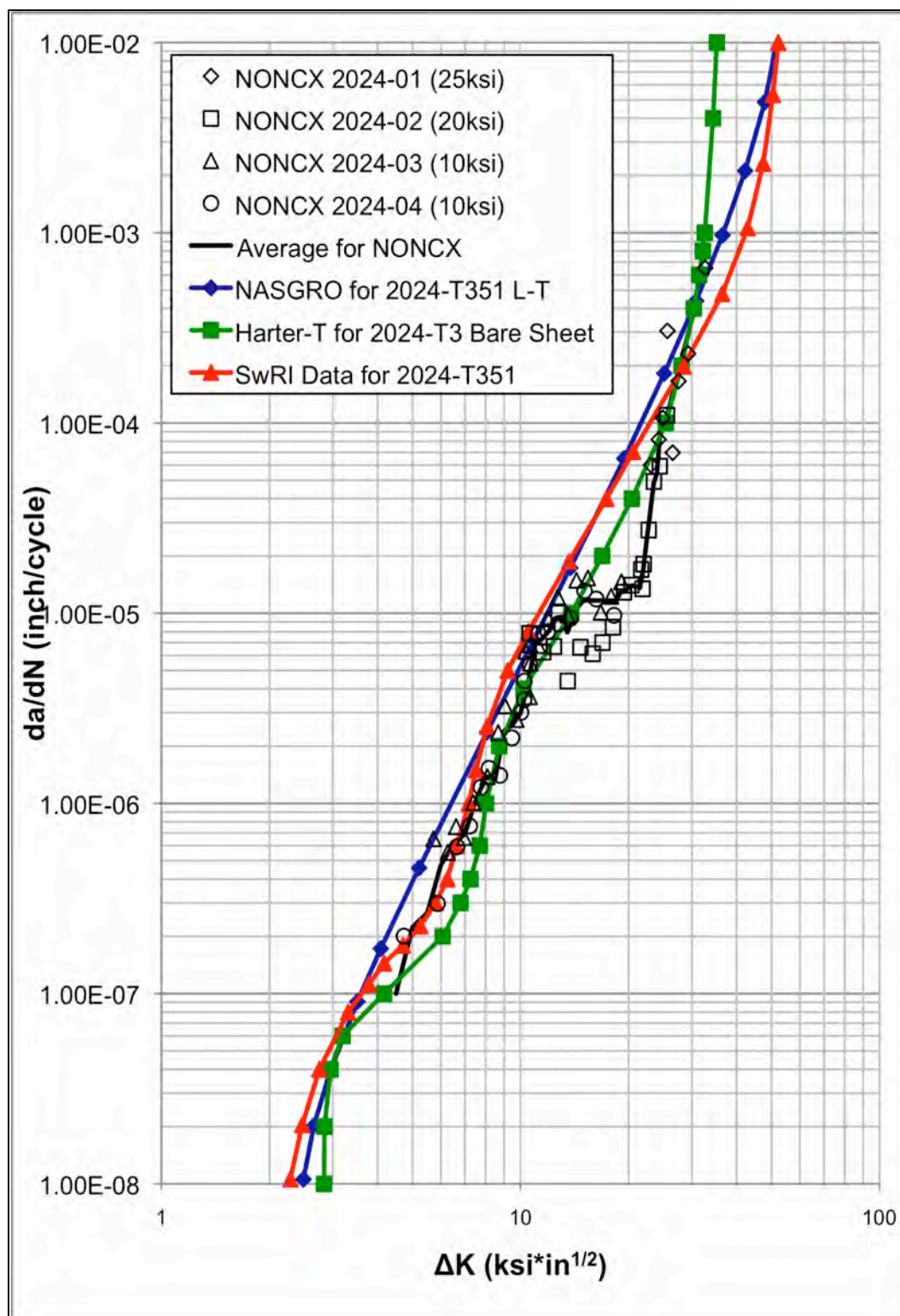
Fig. 76 da/dN versus ∆K for all noncold expanded baseline specimens EDM entrance surface. Tested at varying σ_{max}, R = 0.1, f = 20 Hz, and lab air. Compared to SwRI, NASGRO and Harter-T data.

Fig. 77 da/dN versus ΔK for all noncold expanded baseline specimens primary bore surface. Tested at varying σ_{max}, R = 0.1, f = 20 Hz, and lab air. Compared to SwRI, NASGRO and Harter-T data.

5.4.3 Cold Expanded Specimens

Only three cold expanded specimens were initially selected to perform the da/dN versus ΔK curves. These specimens CX 2024-04, -15, and -17 were all tested at a σ_{max} of 25 ksi. After the initial three specimens were tested it was determined that a lower stress was needed. CX 2024-19 was then tested. These four specimen's EDM entrance surface da/dN versus ΔK curves are plotted in Fig. 78. This figure shows the unique fatigue crack growth characteristic seen in the cold expanded specimens, where the crack begins to propagate out of the hole at a rate of approximately 2.0E-6 inch per cycle and then very quickly decreases as it enters into the high residual stress field caused by the cold expansion process and then progresses out of that field to higher stress intensity. Fig. 79 shows the da/dN versus ΔK plot for three of the cold expanded specimen's primary bore surface. CX 2024-19 is not shown because the bore was not tracked during testing. This plot shows the fatigue crack growth behavior of the bore under the same loading conditions seen in. The stress intensity stays relatively constant throughout the tests and shows good correlation between the three specimens. The final plot for the cold expanded specimens is shown in Fig. 80. This plot provides insight into the material behavior from the high residual stress found on that exit surface.

5.4.4 β Correction Versus Crack Size (β versus a) for Cold Expanded Specimens

Cold expansion β corrections were developed for all primary tracked surfaces and can be seen in Fig. 81 through Fig. 83. By the use of the
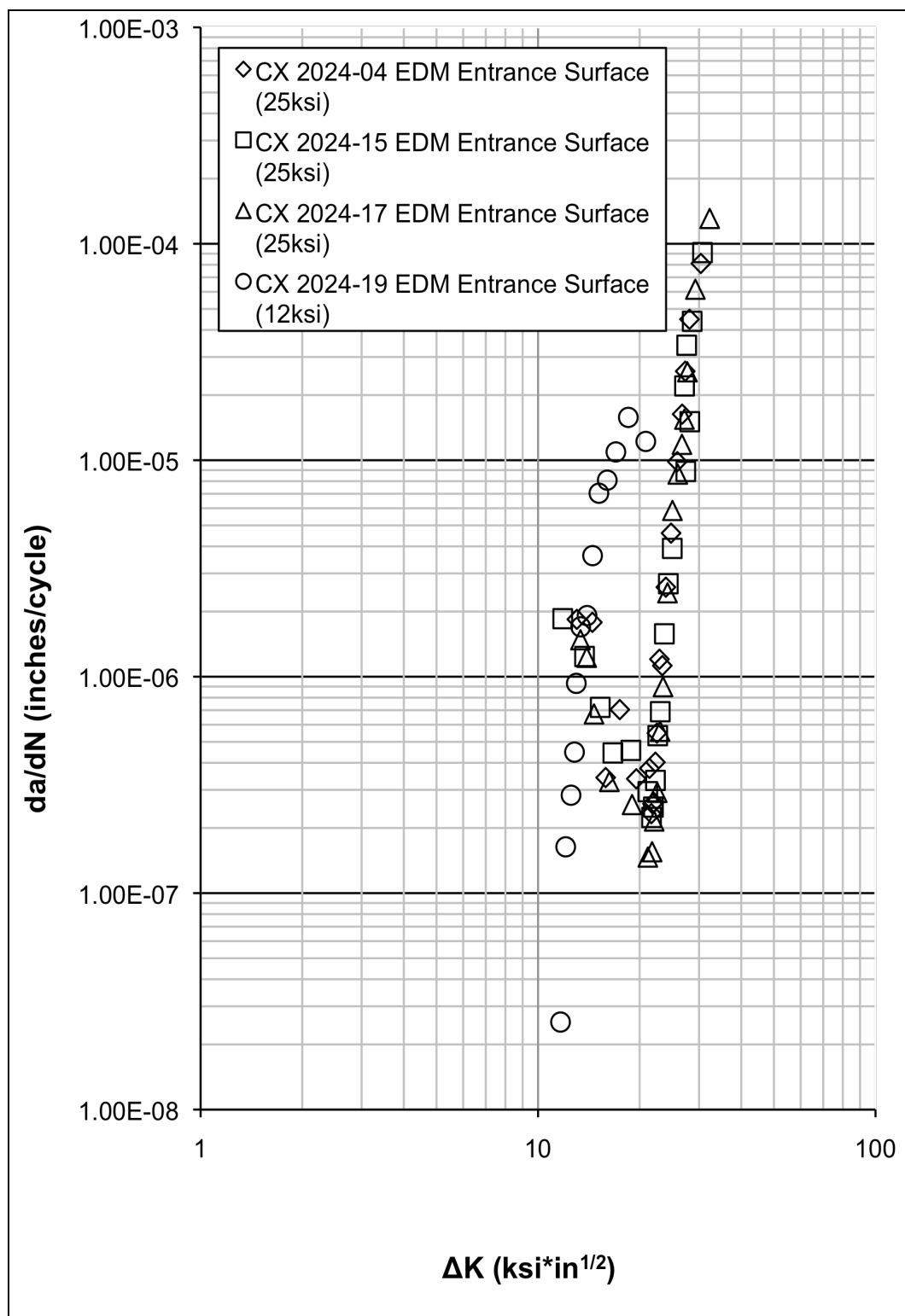
Fig. 78 da/dN versus ΔK for cold expanded specimens EDM entrance surface. All specimens were tested at at varying σ_{max}, R = 0.1, f = 20Hz, and lab air.
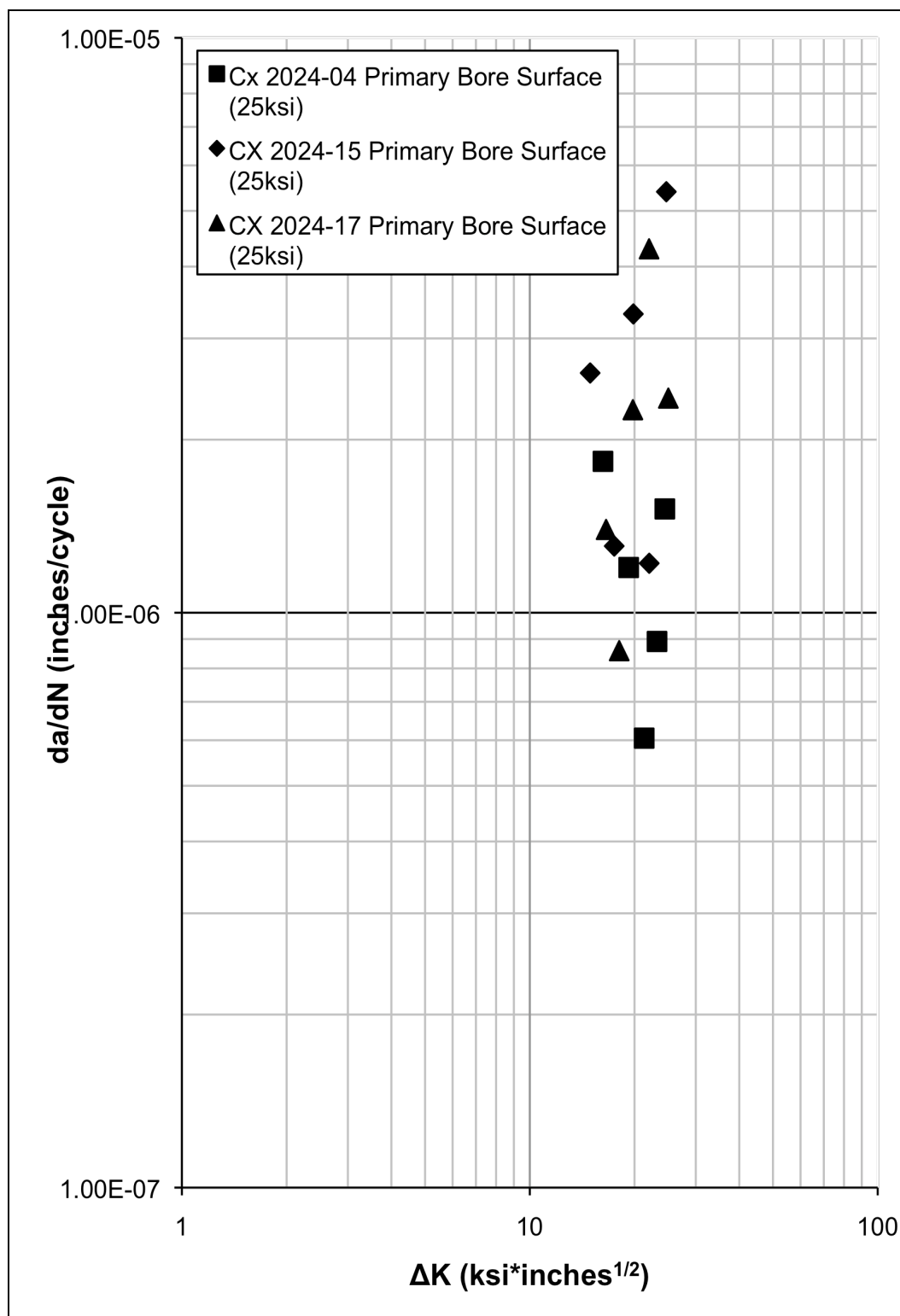
Fig. 79 da/dN versus ΔK for cold expanded specimens primary bore surface. All specimens were tested at at σ_{max} = 25ksi, R = 0.1, f = 20Hz, and lab air.
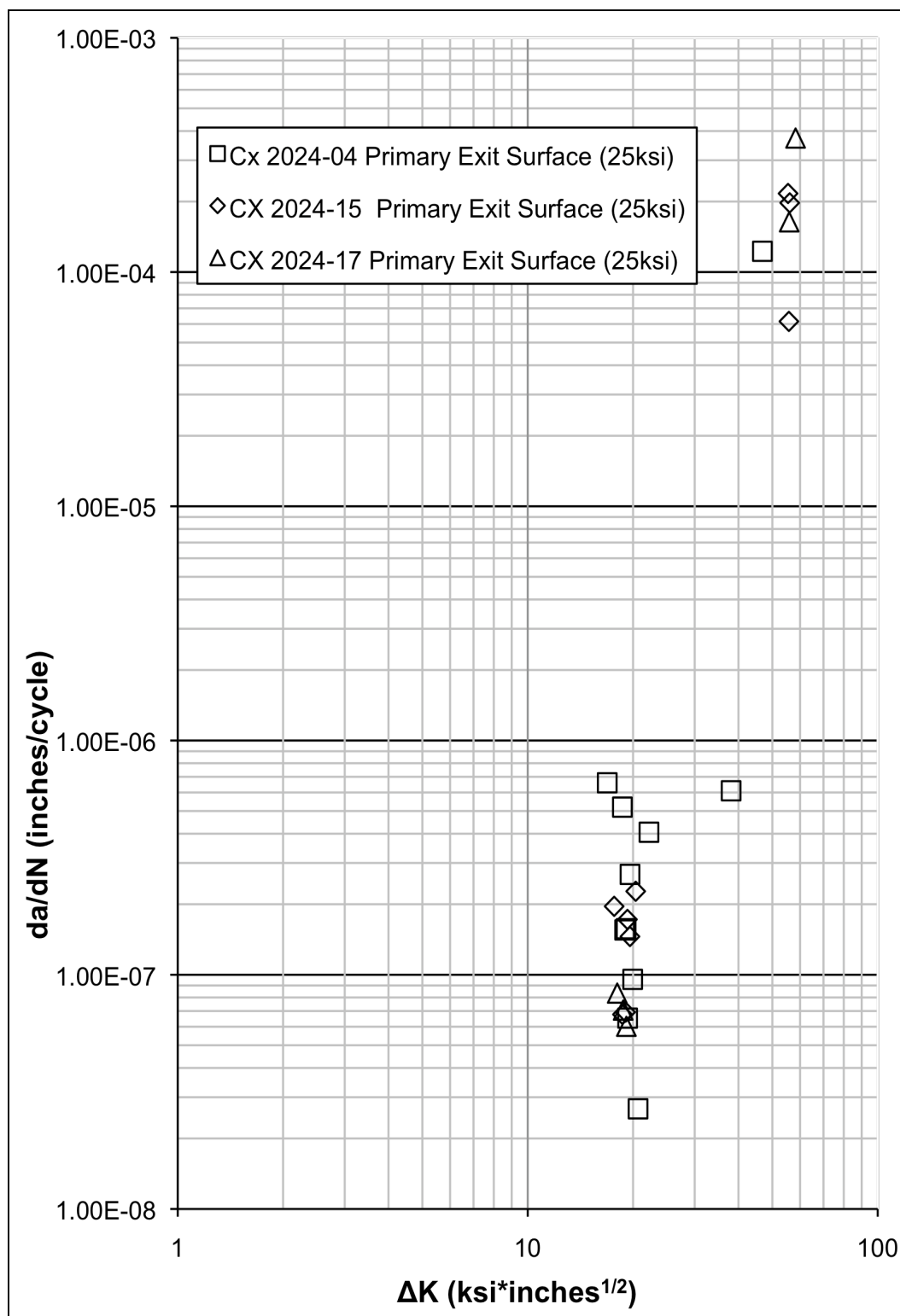
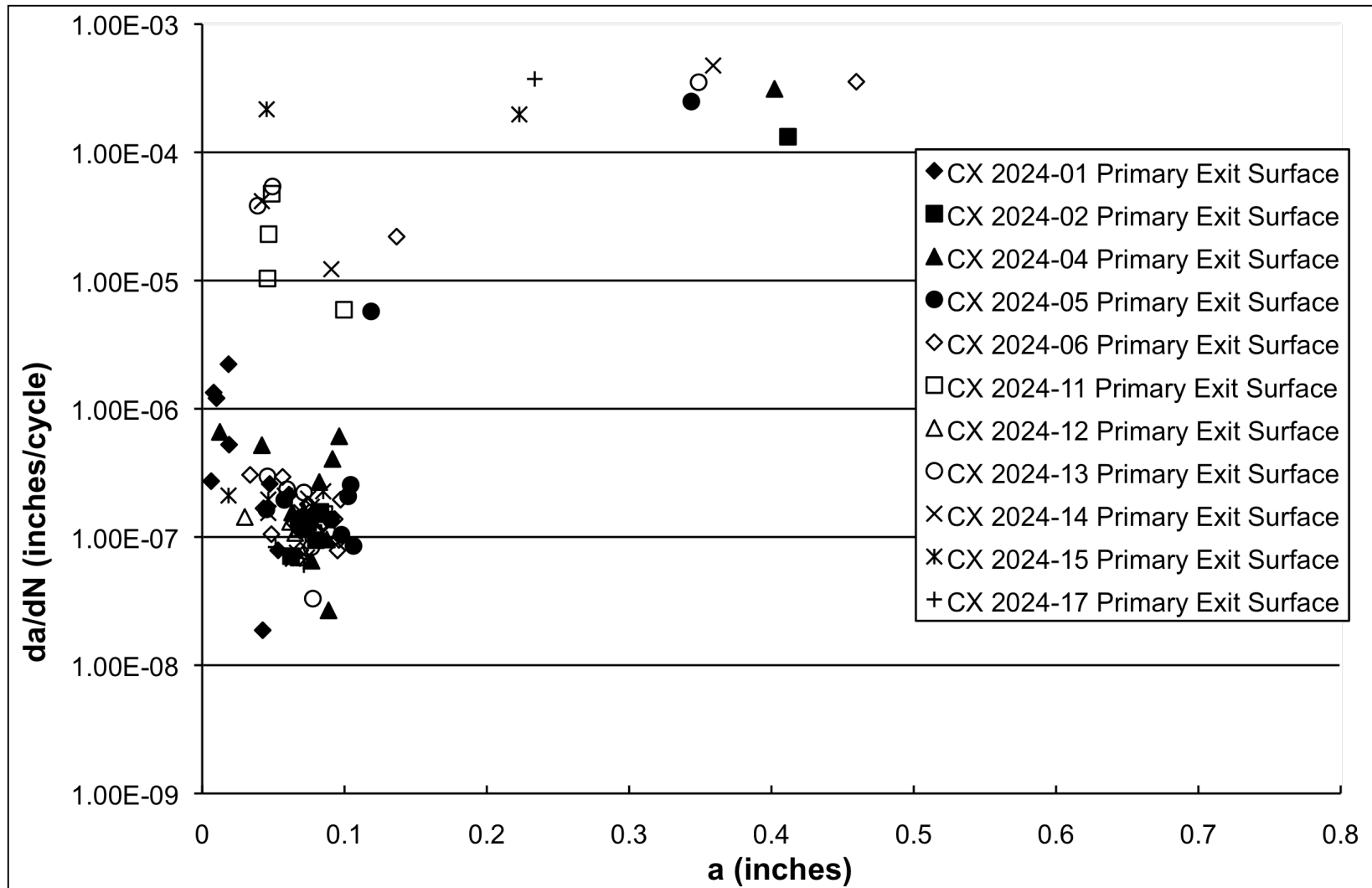Fig. 80 da/dN versus ΔK for cold expanded specimens primary exit surface. All specimens were tested at σ_{max} = 25ksi, R = 0.1, f = 20Hz, and lab air.
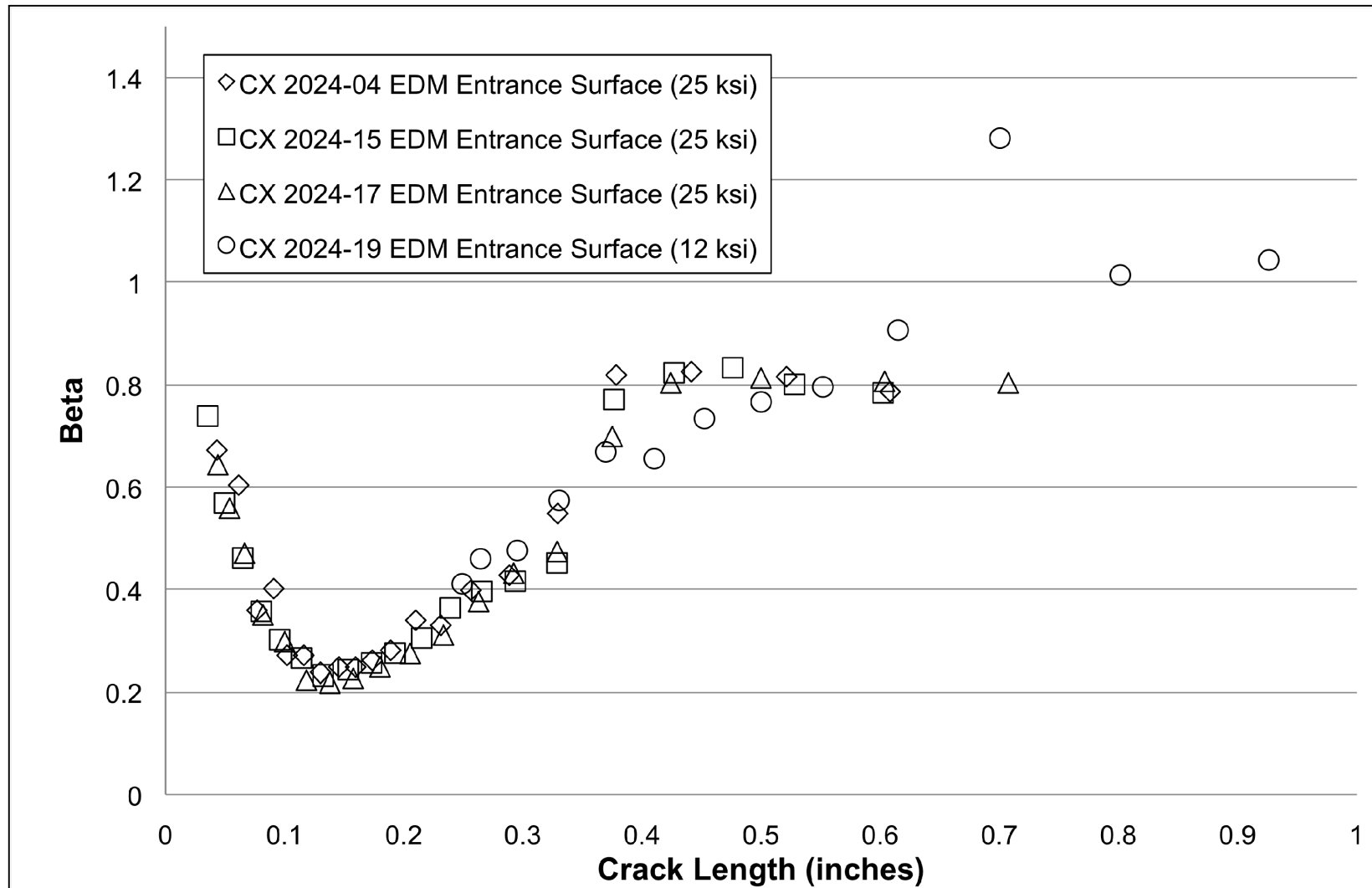
Fig. 81 β correction factors as a function of crack length along the EDM entrance surface for cold expanded specimens.
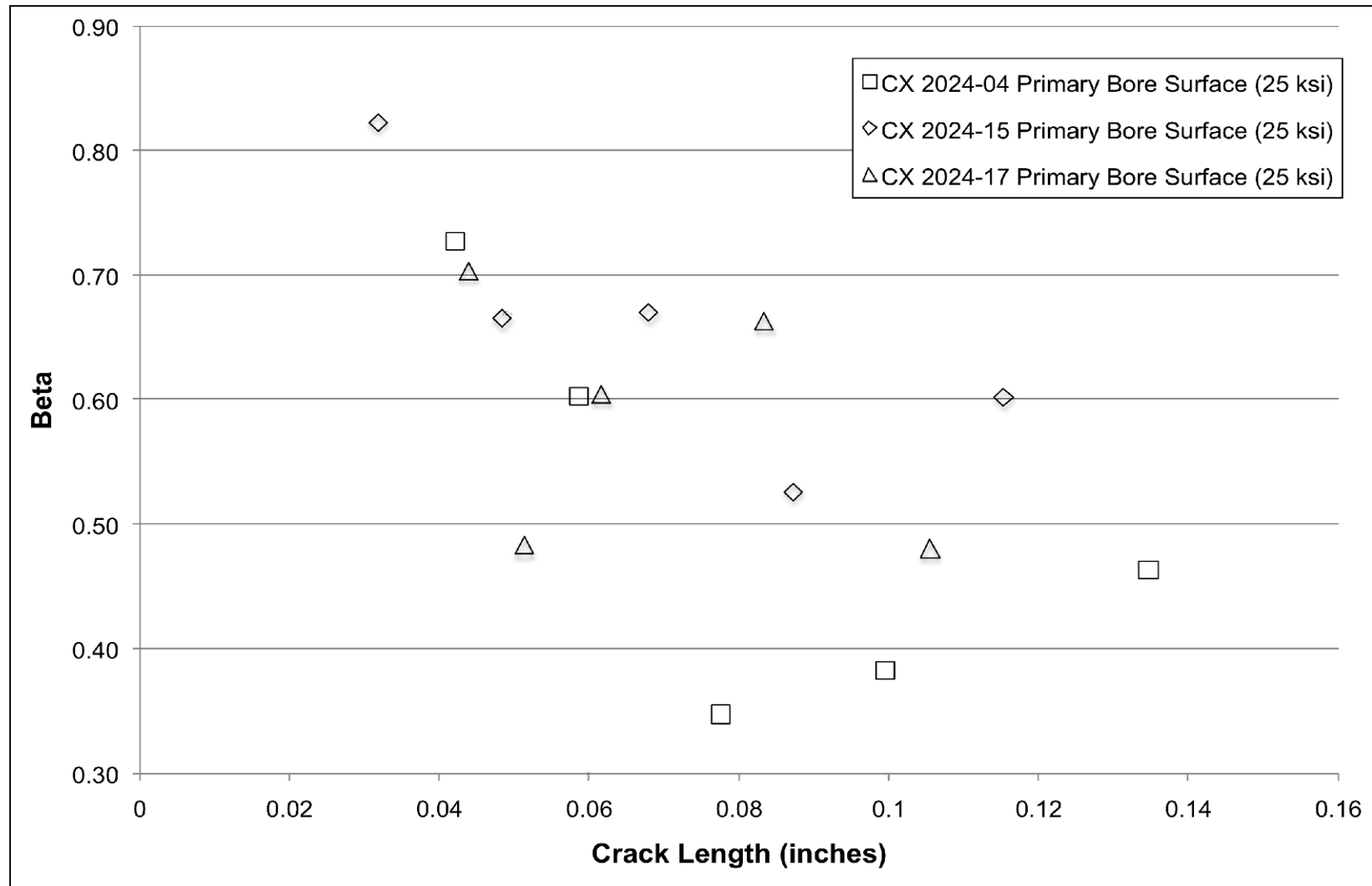
Fig. 82 β correction factors as a function of crack length along the primary bore surface for cold expanded specimens.

Fig. 83 β correction factors as a function of crack length along the EDM exit surface for cold expanded specimens.

similitude principle the β corrections are a direct correlation to the residual stress field induced in the material by the cold expansion process. By plotting the crack length against the β correction it allowed for the removal of any plotting effect, like those seen in Fig. 70 from the loading stress. This is one of the key beneficial features of using a scalar β correction to get a visual approximation of the effects caused by the cold expansion process. These three figures required the use of all the previous figures from a versus N to da/dN versus a to da/dN versus ΔK to calculate the β correction.

6 DISCUSSION

6.1 Fatigue Crack Growth Testing Observations

One of the primary objectives for this research project was to develop a greater understanding of the fatigue behavior of aluminum alloys. In order to accomplish this objective fatigue crack growth testing was performed and the data were correlated to established crack growth testing data used in industry. The testing portion of this research was performed in three main phases and their outcomes are discussed below.

During the fatigue testing of the cold expanded specimens two specimens failed prematurely from fatigue cracks that nucleated out of grinding marks found on the surface of the specimen. These grinding marks were present due to the method of surface preparation for the bonding of the specimen tabs. The data captured from these two specimens were not used in the calculations of crack growth rate and β. A macro image of one of these specimens can be found in Appendix D.

6.1.1 ASTM Standard E 647 Specimen Testing

The first phase of testing consisted of testing two middle tension specimens that were prepared according to the ASTM standard E 647 fatigue testing specifications. The fatigue crack growth rate curves calculated from these

tests correlated very well with established data provided by SwRI.[29] This

correlation provided an increase in the confidence in the ability of the fatigue test

machine and also for the process used to gather crack growth data and the

analysis of the gathered data. The fatigue crack growth curves can be seen in

Fig. 75 and the SwRI testing data for aluminum 2024-T351 are also shown.

<p style="text-align:center">6.1.2 Baseline Noncold Expanded Specimen Testing</p>

The second phase of the testing program was the testing of four noncold

expanded baseline specimens. For the first specimen tested, NON CX 2024-01,

it was determined that for consistency the specimen would be tested at a σ_{max} of

25 ksi. However, once the test was started it was determined that this stress was

too extreme to allow for accurate data to be gathered. The next specimen, NON

CX 2024-02 had already been precracked at a lower σ_{max} of 20ksi, therefore it

had to be tested at this stress. Even at this lower stress level it was still very

difficult to gather accurate data during the test. This region is highlighted as Area

1 in of Fig. 84. It was therefore decided that the final two noncold expanded

specimens would be tested a significantly lower σ_{max} of 10 ksi.

The data gathered from the final two noncold expanded specimens, NON

CX 2024-03 and -04, showed good correlation between the data processed using

the ASTM standard E 647 specimen configuration. There are, however, some

differences in the data shown in Fig. 84. This region of difference is highlighted

in Area 2 of Fig. 84.
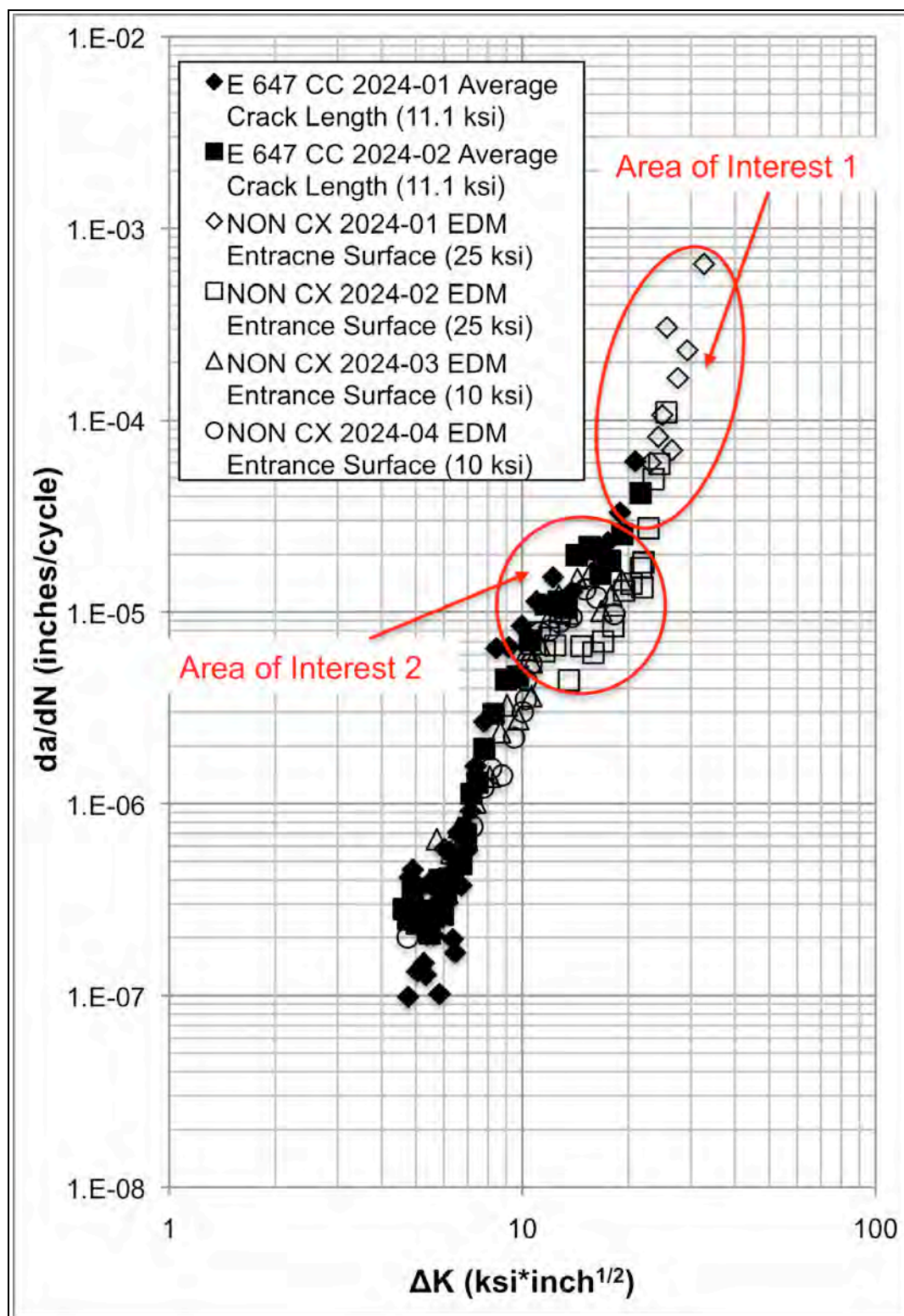
Fig. 84 Comparison of ASTM standard E 647 crack growth curve data, da/dN versus ΔK, and noncold expanded baseline specimens with circled areas of interest.

6.1.3 Cold Expanded Specimen Testing

The third and final phase of fatigue testing was that of the cold expanded specimens. The testing data gathered from these specimens showed a very high level of conformity as seen in Fig. 69. The crack growth curve showed a dramatic decrease in the crack growth rate as the fatigue crack entered the residual stress zone caused by the cold expansion process. The residual stress field had little influence on the crack growth rate when the fatigue crack was very close to the hole. As the crack moved away from the edge of the hole it began to dramatically impact the behavior of crack front. These effects can be seen in Fig. 69. As the crack propagated to around 0.10 inch it reached the center of the residual stress field adjacent to the hole.

In order to capture data at lower crack growth rates one cold expanded specimen was tested at a σ_{max} = 12 ksi. Crack growth da/dN versus a data for this specimen is shown along with the other three cold expanded specimens in Fig. 69. Testing a cold expanded specimen at this lower stress allowed for a greater correlation between the da/dN for the cold expanded specimens and the noncold expanded specimens. This would make it possible to calculate the β correction at a maximum number of locations.

6.2 Fatigue Crack Growth Prediction
Differences Found in Testing

One of the major finding from this research program was the significant effect cold expansion has on the fatigue life of Al 2024-T351 alloy. The increase in life was conservatively on the order of 10 to 20 times the fatigue life of that of a

specimen that had not been processed using Split Sleeve Cold Expansion™. This can be seen when examining the fatigue life of NON CX 2024-01 and CX 2024-17, which are shown in Fig. 55 for the noncold expanded specimen and Fig. 62 for the cold expanded specimen. The life of the two components differs by almost a factor 100.

6.2.1 Current USAF Approach Versus Testing Results

The current USAF approach to predict the fatigue life of a component that has been processed using Split Sleeve Cold Expansion™ is to reduce the initial flaw size from 0.05 inch to 0.005 inch.[26.29] It was found that this approach was extremely conservative in the prediction of the fatigue life of the 2024 aluminum alloy tested in this research project. Fig. 85 shows the three methods used during this research to predict the fatigue life of the cold expanded specimens. As one can see there is a dramatic difference in the fatigue life seen during testing and that predicted using the USAF's crack growth analysis tool, AFGROW.

The third line plotted in Fig. 85, "Beta Correction Applied" was produced using AFGROW and applying the β corrections calculated during this research. One of the main reasons that this line and the last, "Testing Results for CX 2024-15" is that AFGROW does not, at this time, allow the user to input β corrections for the backside or exit side of the component. It was determined that the exit side of the specimen had a dramatic influence on the fatigue crack growth behavior of the specimen. The exit side seemed to hold back the fatigue crack
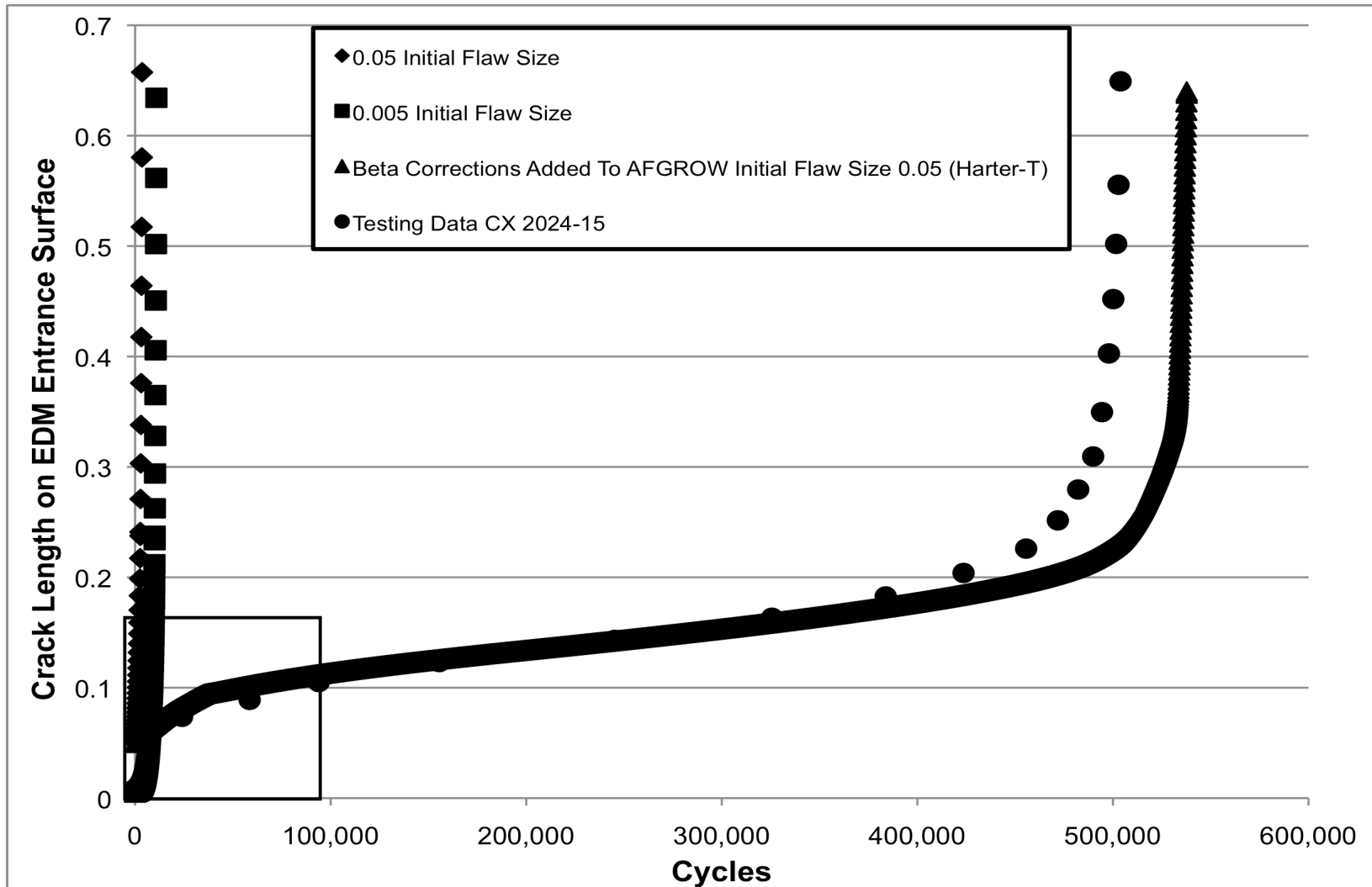
Fig. 85 Fatigue crack growth life predictions using AFGROW initial flaw size correction, β correction application and CX 2024-15 crack growth life from testing. Region of interest highlighted by black square.

from propagating through the specimen because of the high residual stress zone found on that surface.

This plot is where one can truly see the benefits of the cold expansion process and also where the DoD and the USAF are lacking in their ability to take advantage of this process properly. If the USAF could only increase their predicted fatigue life by two times that would have a dramatic cost savings on aircraft maintenance costs that are being incurred due their aging fleet.

Another key feature seen in Fig. 85 is the shape of the four curves at the far left hand side of the plot. This region is highlighted by the boxed out area and is shown in Fig. 86. This region show the dramatic difference in the fatigue crack growth behavior of what the USAF predicts for a cold expanded hole and what is actually seen during experimentation. This difference can have a significant impact on the life, shape and inspectability of the hole that has been cold expanded.

6.3 Crack Growth Geometry and Behavior

6.3.1 Overview of Crack Growth Geometry

6.3.1.1 Noncold Expanded Crack Growth Geometry

The fatigue crack propagation geometry has been well understood in the fracture mechanics field for materials that have not been processed by any type of residual stress inducing process. Fig. 87 shows the fatigue crack propagation geometry in an aluminum 2024 specimen that has not been cold expanded. The fatigue crack nucleates at a corner crack and propagates in an elliptical manner until it reaches through the thickness of the specimen.[32]
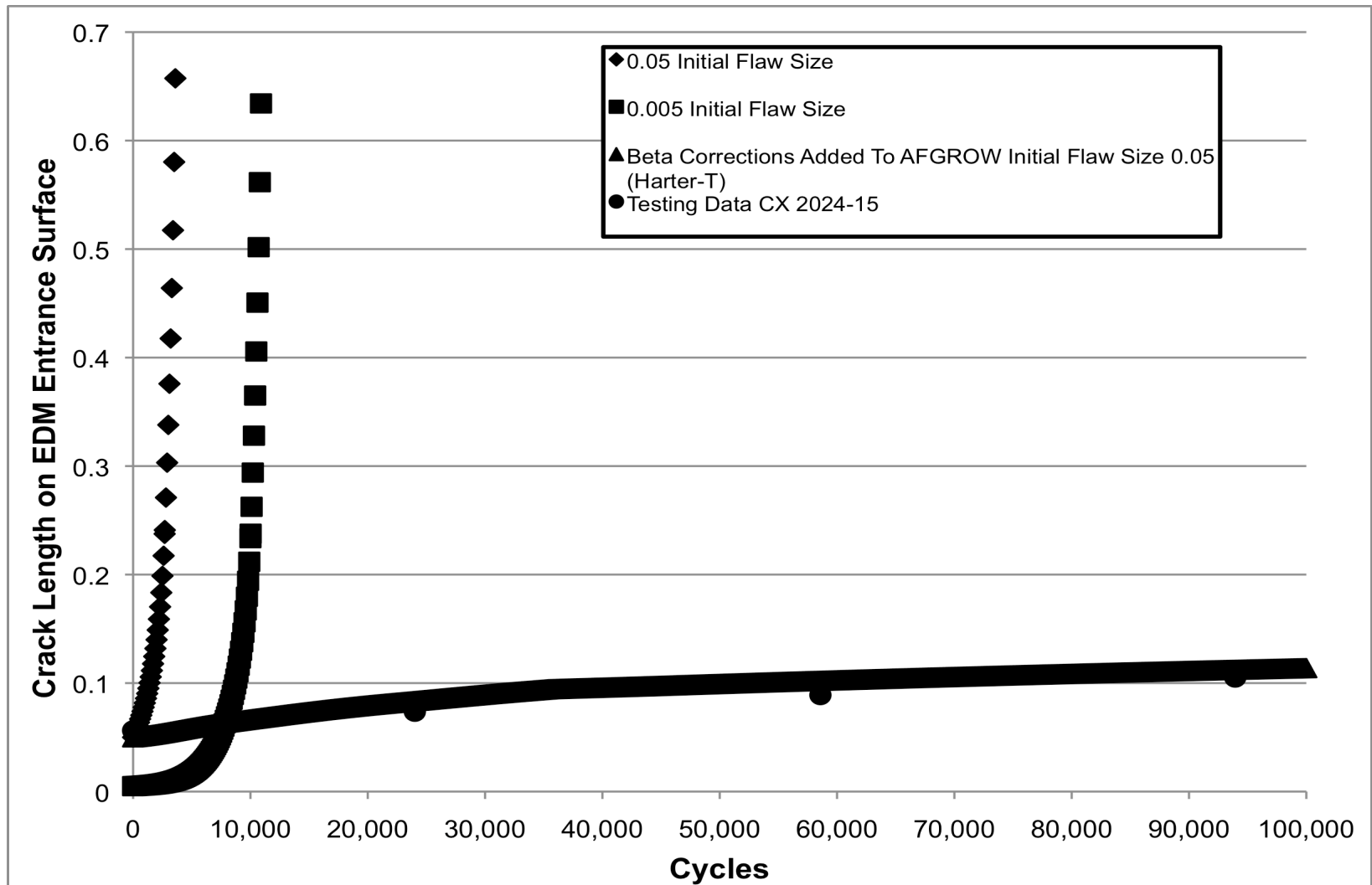
Fig. 86 Zoomed in redoing highlighted in Fig. 85 for CX 2024-15
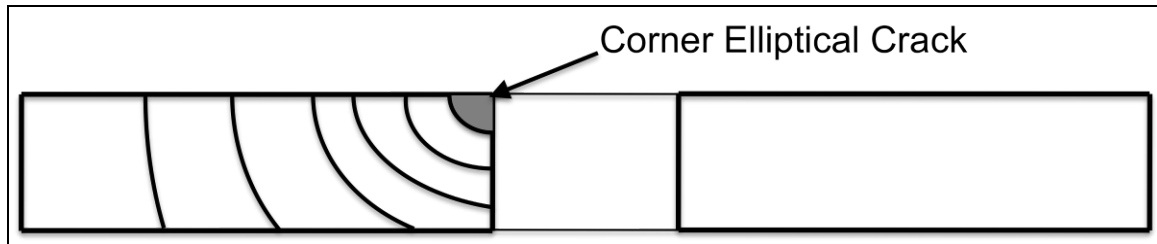
Fig. 87 Standard crack growth geometry for noncold expanded baseline Al 2024-T351 specimens

Once the fatigue crack has propagated through the thickness it can begin to tunnel through the center of the specimen, however it was found that the fatigue crack lengths on both the front and back surfaces had approximately the same crack lengths measured as the fatigue crack propagated through the thickness of the specimen.

6.3.1.2 Cold Expanded Crack Growth Geometry

The fatigue crack growth geometry of the aluminum 2024 alloy that has been processed by Split Sleeve Cold Expansion™ is quite different from the noncold expanded baseline specimen geometry. The cold expansion process produces a three-dimensional residual stress field that can dramatically influence the fatigue crack growth behavior. Fig. 88 illustrates how a fatigue crack grows through the residual stress field produced by cold expansion. This type of unique fatigue crack growth behavior has not been explored much in the fatigue and fracture mechanics research communities. This type of fatigue crack growth behavior has a dramatic influence on the entire crack front. It is important to think of this fatigue crack behavior as being a result of the total behavior of the
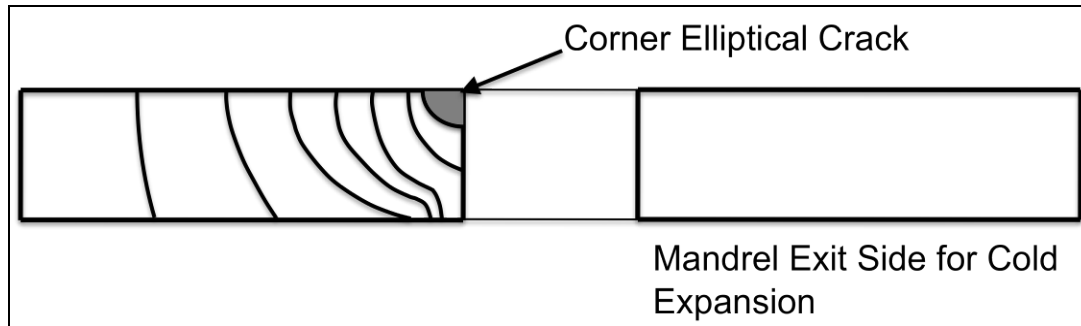
Fig. 88 Fatigue crack growth geometry for cold expanded Al 2024-T351 specimens.

combined crack front. Every part of the crack has an effect on the other portions of the crack front.

6.3.1.3 Crack Propagation Shape on Entrance Versus Exit Surfaces

As seen in Fig. 88 the fatigue crack exhibited a resistance to propagation on the exit surface of the EDM side of the specimen. This resistance to fatigue crack propagation is directly related to the higher residual stresses in this area produced from the cold expansion process. As the cold expansion mandrel is hydraulically pulled through the hole the material adjacent to the hole is plastically deformed in the radial direction out and away from the hole. The material within the hole is also pulled through the hole and produces a bulge on the exit surface around the hole. This material build up at the exit side of the hole produces a greater interaction between the plastically deformed material just adjacent to the hole and the elastically deformed material that is outside of this region. This elastic/plastic interaction is what produces the residual stress field and at the exit side of the hole just adjacent to the hole this elastic/plastic interaction reaches a maximum and thus creates the unique fatigue crack growth behavior seen during testing.

6.3.1.4 Nondestructive Inspection Implications

The unique fatigue crack growth behavior of components that have been processed by Split Sleeve Cold Expansion™ can have a tremendous impact on their inspectability. This can be seen in Fig. 89. It is possible for the fatigue crack to nucleate and propagate, slowly however, for an extended period of time without ever being able to detect it because of the orientation of a fastener or other component that might be overtop of it.

During the fatigue testing of the cold expanded specimens it was realized that this crack growth geometry could be both beneficial and detrimental for the inspectability and detection of fatigue cracks in locations where fasteners are located in the cold expanded hole. It was found that fatigue cracks that nucleated at the edge of a cold expanded hole propagated somewhat "rapidly", in comparison to when it reached the center of the cold expanded zone, on the cold expansion mandrel entrance surface to a crack length of between 0.08 inch and 0.14 inch.
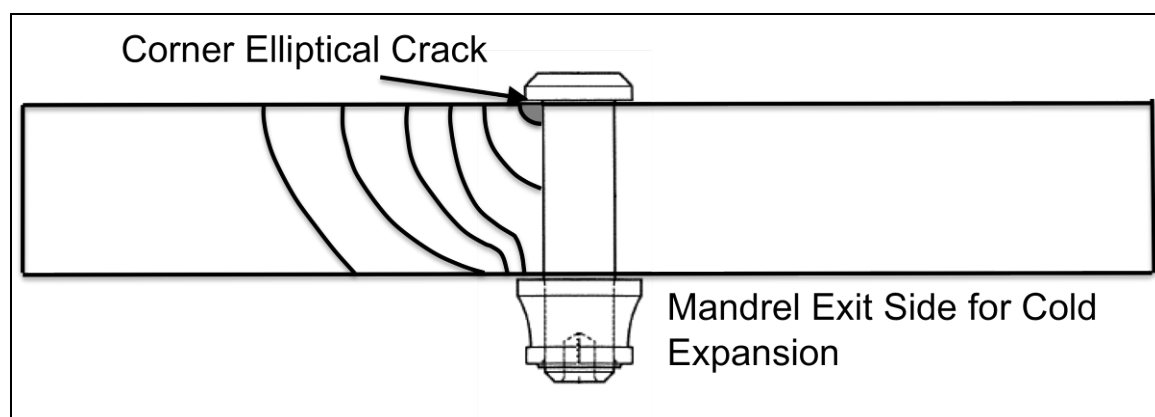
Fig. 89 Possible fatigue crack propagation geometry during inspection of aircraft structures.

The fatigue crack would spend approximately 75 to 85 percent of its time at this length on the entrance surface and would possibly provide a very high probability of detection. However, on the opposite side of the hole the fatigue crack would propagate to only approximately 0.06 inch to 0.08 inch before it would dramatically decrease its fatigue crack growth rate. At this length it would be virtually impossible to detect the fatigue crack under a fastener head as shown in Fig. 89. Therefore, if the hole being inspected was cold expanded and the mandrel exited the surface on the surface being inspected it would be quite possible to never detect the fatigue crack before the component had less than 10 percent of its life left. If this process were reversed however and the mandrel exited the opposite surface from that being inspected it would be possible to detect the fatigue crack with roughly 90 percent of the component's life left, depending on the detection thresholds.

This observation has significant implications within the NDI field. The NDI field at this time does not model the fatigue crack propagation of cold expanded holes using a P-shaped crack geometry.

6.3.1.5 Crack Growth Behavior of Cracks that Nucleate on Exit Side

During the fatigue testing of a Al 7075-T651 specimens it was determined that the corner EDM notch had been placed on the mandrel exit side of the hole. This was not according to the requested manufacturing process but provided a valuable insight into the behavior of this material if a fatigue crack nucleated on this side of the hole. As the fatigue crack began to propagate from the initial corner crack it rapidly propagated through the bore of the hole to the entrance

surface of the specimen. Once the fatigue crack had propagated through the thickness it proceeded to propagate on the non-EDM side or in this case the entrance surface at the same rate as if it had been EDMed on that side of the specimen. The EDMed side for this specimen being the mandrel exit surface did not propagate and acted much like the other specimens that had not been EDMed on the exit surface.

Even though this specimen was originally thought to be a total loss it was soon determined that it provide a unique insight into the behavior of fatigue cracks as they propagate through residual stress fields caused by Split Sleeve Cold Expansion™ and it can be reasonably assumed that Al 2024-T351 would behave in the same manner.

6.4 β Corrections for Cold Expanded Holes in Al 2024-T351 Alloy

As outlined in the results section of this report, three cold expanded specimens were selected to represent the total population of cold expanded specimens. For each of these specimens a β correction was calculated as a function of crack length and crack growth rate as seen in Fig. 90. These β corrections represent a direct correlation to the residual stress field produced by the cold expansion process and show that this residual stress field changes as it moves away from the cold expanded hole.

During the final development of the β correction curves it was determined that the data used to calculate the β corrections at long crack lengths had a high degree of variability. It was determined that an additional specimen should be fatigue tested at a lower stress. Specimen CX 2024-19 was therefore tested at
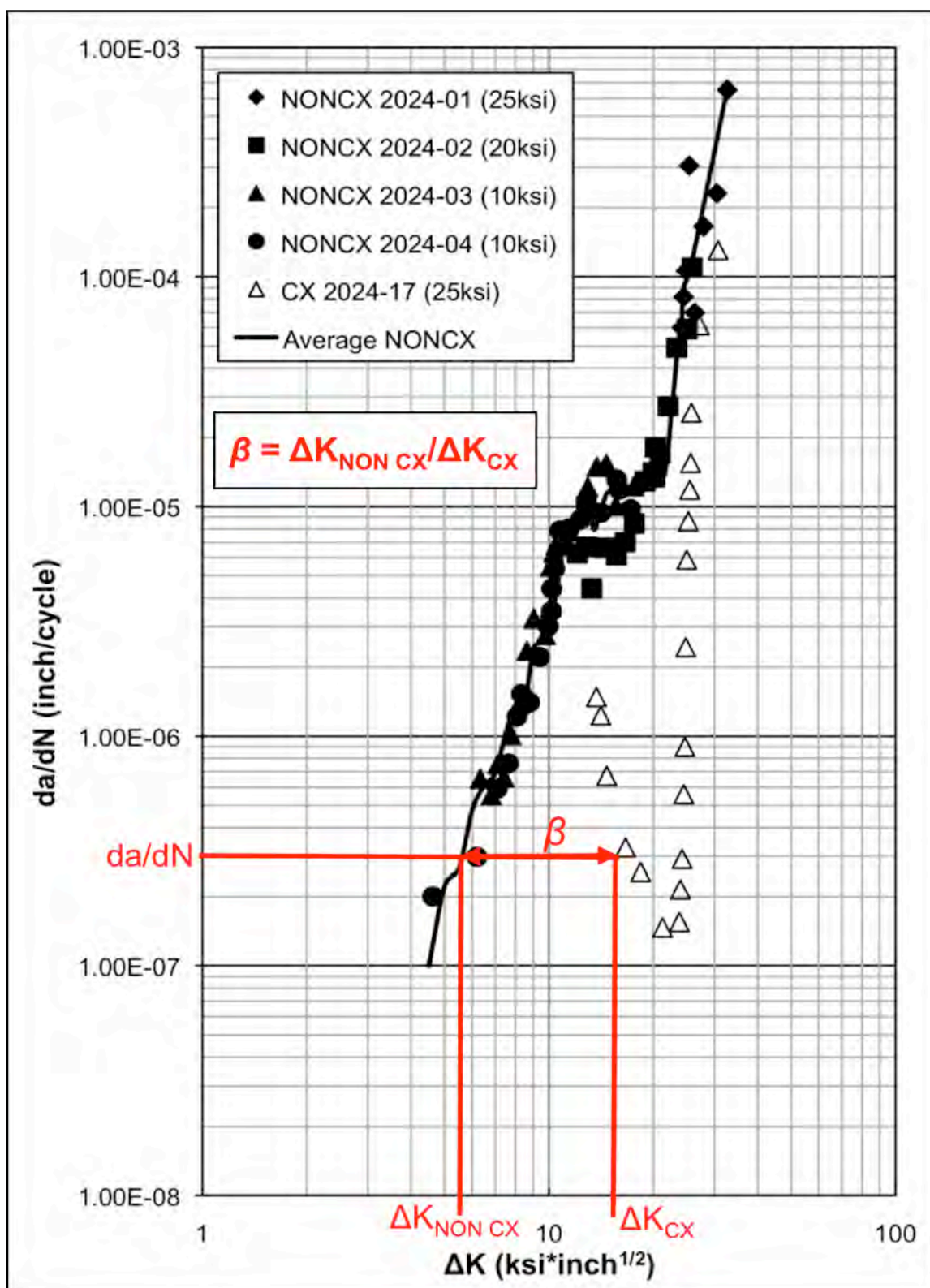
Fig. 90 Method used for the calculation of β corrections for cold expanded holes as a function of da/dN versus ΔK.

12 ksi. Crack measurements were taken at a crack length of 0.25 inch from the

edge of the hole until final failure. This additional test provided valuable

information on what the β corrections are at greater distances away from the

hole.

β corrections were computed for the three main surfaces observed during

this research project. Each of these surfaces will be discussed to highlight some

of their unique features.

6.4.1 EDM Entrance Surface β Corrections

The EDM entrance surface β correction curve shown in Fig. 91 has three

regions of interest. These regions are circled in the figure and will be discussed

below. The first area of interest, shown in Fig. 91 as Region of Interest 1, is

located next to the edge of the hole. It can be seen that next to the hole there is

a relatively little effect on the crack growth rate by the residual stress field. This

was seen during testing also. As the fatigue crack began to propagate from the

edge of the hole it did so at roughly the same rate as the cracks in the noncold

expanded specimens. This effect was not expected to be seen in these tests.

The current understanding of the residual stress field in a material processed by

cold expansion is that the residual stress profile is highly developed even very

close to the edge of the hole[25]. The slope of the β in this region is also unique. It

is much more gradual than what was expected. This means that the residual

stress profile is much more gradual than what was first expected.

The second region of interest, highlighted as Region of Interest 2 in Fig.

91, is the point at which the βs reach their lowest point on the plot. This again
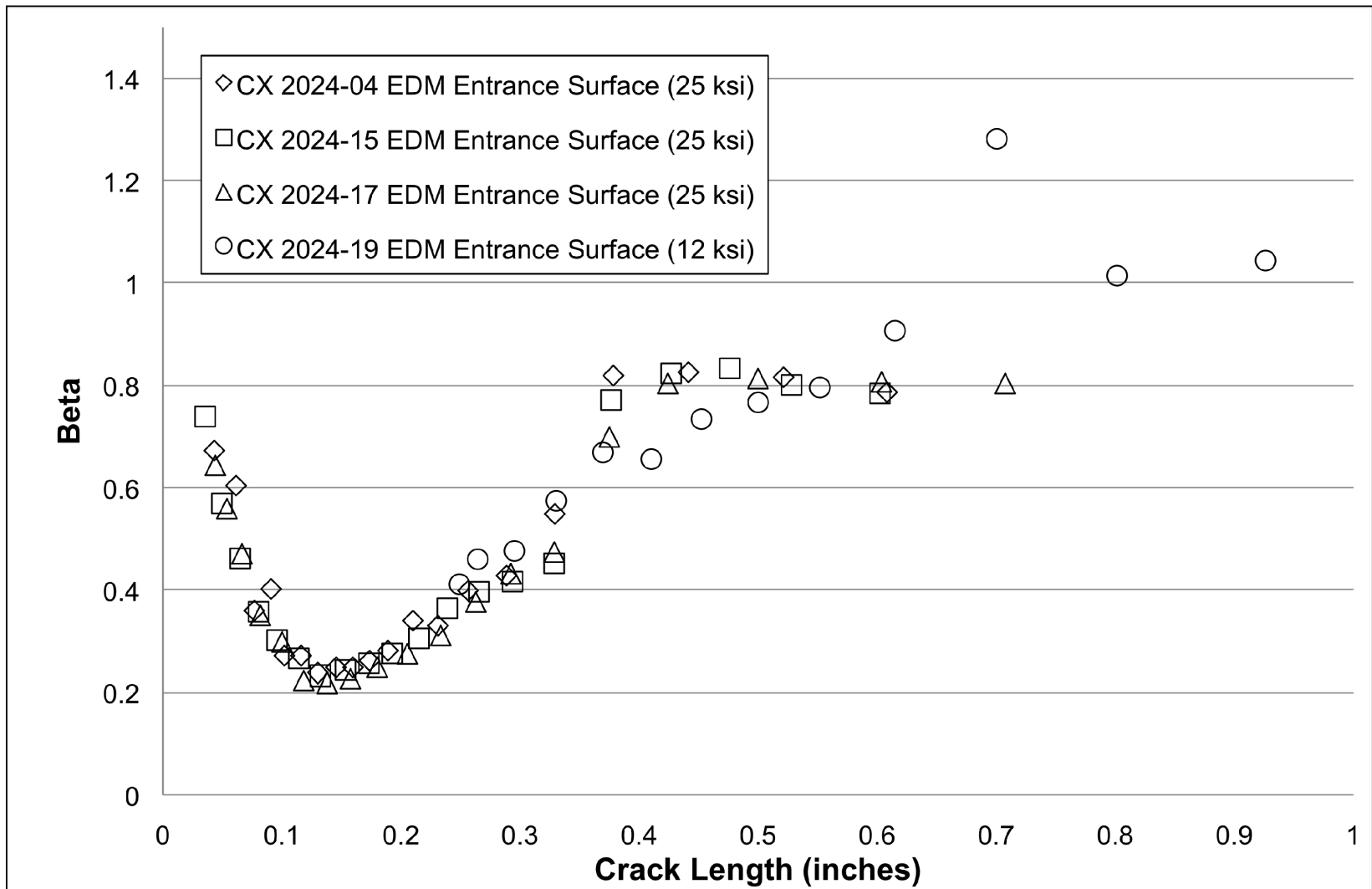
Fig. 91 EDM entrance surface β corrections as a function of crack length with regions highlighted for discussion.

correlates to the region of maximum residual stress in the material. This location, which is approximately 0.10 inch to 0.15 inch from the edge of the hole is specific to the Al 2024-T351 material tested. In this region the fatigue crack experienced the greatest resistance to fatigue crack growth. The effect of this deep residual stress field continues to effect the fatigue crack growth behavior of the material out to approximately 0.70 inch away from the processed hole.

The final region of interest is region 3 in Fig. 91. This area of the curve was produced at a lower stress to allow for the capture of data at longer crack lengths. The purpose of this was to determine if the residual stress field which produces the β would have no effect on the fatigue crack growth behavior on larger cracks. As seen in Fig. 91 at a crack length of approximately 0.70 inch the β correction takes a substantial jump from over 1.0 to approximately 1.28 and then reduces to around 1.0. This jump in the β at this large crack length indicates that a possible tension field is located at the edge of the residual compressive stress field. This would be in accordance to most literature that discusses the stress fields produced by the Split Sleeve Cold Expansion™ process. [25]

7 SUMMARY

7.1 Conclusions

The primary conclusions of this thesis are presented below in the order they were stated in the objectives. Further comments concerning the findings related to the overall project are also included.

7.1.1 Testing Procedure

The testing procedures and equipment used during the fatigue testing phase of this research provided highly accurate data that correlated well with established crack growth data for the 2024-T351 aluminum alloy. The use of traveling microscopes made it possible to track the fatigue crack with precision up to 0.001 inch which was well within the ASTM E647 guidelines. In order to track cracks that propagated through the bore of the specimen a technique was developed in which no additional hardware was needed. By simply turning the microscope to roughly a 30 degree angle to the bore it was possible to scan the bore surface of the specimen with ease and accuracy.

7.1.2 Fatigue Crack Growth Life of Cold Expanded Specimens

The fatigue life of the 2024 aluminum specimens that were processed using Spit Sleeve Cold Expansion™ was 10 to 20 times greater than the life of the nonprocessed specimens. This life extension exceeded FTI's prediction of

approximately three times. It was also determined that the life estimations

calculated using the current DoD/USAF procedure of reducing the initial flaw size

had a high degree of error. These predictions were an order of magnitude below

the fatigue life seen during testing. With such a high degree of discrepancy

between the testing data and the calculations performed in AFGROW it is the my

opinion that the fatigue life calculations that are being preformed using AFGROW

grossly underestimate the life of a cold expanded hole. Thus requiring aircraft to

be brought back from the field and inspected prematurely and inducing an

increase in maintenance costs.

7.1.3 Fatigue Crack Geometry

The fatigue crack growth geometry of the cold expanded specimens was

quite different from that seen in the non-processed specimens. In the author's

opinion the crack geometry of the cold expanded specimens can have a

tremendous impact on the detectability of fatigue cracks propagating from

fastener holes. If a fastener hole has been processed using cold expansion and

the mandrel exit side is the surface that will be inspected during the life of the

component it is possible that the fatigue crack will never be detected either

visually or by NDI before the fatigue crack propagates to a critical length and the

component fails. However, if the inspectable surface is the entrance surface it is

possible to detect a fatigue crack very early in the fatigue life of the component

and have adequate time to track and remove the fatigue crack before it

propagates to a critical size. The difference in fatigue crack growth behavior

between the entrance and exit surface was unknown to the author at the time this

research project began and was also unknown to the NDI team at Hill AFB. Also, the NDI team at Hill AFB was unaware of this fatigue crack propagation geometry and therefore have not integrated this behavior into their fatigue crack growth models. If this behavior were integrated into the NDI standard modeling specifications it would provide greater capability to know the behavior of fatigue cracks that propagate from cold expanded holes.

7.1.4 Development of β Corrections

The development of β corrections was the final stage of this project. These corrections provide an insight into how the crack driving force changes as the fatigue crack propagates through the residual stress field. At its peak the correction showed that cold expansion could reduce the crack driving force by up to 80 percent. This peak location was also at a bit of a surprising location. Most models researched by the author showed that the maximum residual stress was located very close to the edge of the hole. This was not the case with the material tested. The maximum residuals stress was located between 0.10 and 0.16 inch away from the edge of the hole. It can also be inferred that the residuals stress at this maximum location did not exceed the yield stress of the material. This can be concluded due to the fact that fatigue crack propagation continued to occur through this region of high residual stress.

The development of a β correction allows the analysis to adjust the fatigue crack growth model to match the testing results seen during testing. The crack growth curves produced using AFGROW had a much higher degree of correlation to the actual testing data than those produced using the DoD

standard method of reducing the initial flaw size. These results are encouraging. However the testing data acquired during this research program can be applied only to the material tested and the loading spectrum used. The β corrections would therefore need to be produced either by additional testing or by the use of finite element modeling that has a greater degree of accuracy in its correlation to testing data. This process will be neither easy nor inexpensive. However, this data can provide a more accurate approach to predict the fatigue crack growth behavior of critical aircraft components. With this increased accuracy it may be possible to increase the time between inspections and thus decrease the high costs associated with structural repairs and replacements.

7.2 Significance

This research project contributes to the fracture mechanics field in two main areas. First, by the development of β corrections that represent the residual stress field induced by the cold expansion process. The use of β corrections to represent geometric, loading or even fatigue crack interaction has long been standard in the field of fracture mechanics. However, it has yet to be applied as a means to modify the fatigue crack growth behavior through residual stress fields. This is revolutionary in the field and can have wide sweeping effects on the methods used to predict the life of critical components that have been processed by cold expansion. The method of using a β correction is not limited to cold expansion. There are other processes that this type of methodology can be applied to. One of the current issues the USAF is dealing with is foreign object debris damage on jet engine compressor and turbine

blades. This serious problem is being solved by the use of two new and very exciting processes known as Laser Shock Peening (LSP) and Low Plasticity Burnishing (LPB). Both of these processes, like Split Sleeve Cold Expansion™, induce a deep residual stress field into the material to help prevent fatigue crack nucleation and propagation. Currently the USAF is trying to develop a type of superposition technique that will allow for finite element models to be produced that approximate the total stress imposed on the blade during use. These calculated net stresses then allow for an increased minimal allowable flaw size on the blade. This allows the inspections to be performed by finger feel instead of with a line of dental flaws. However, this technique does not take into account the effects the crack has on the residual stress field as it propagates through. With a better understanding of the loading state on a turbine or fan disc it would be possible to apply the same type of β correction approach to these critical engine components.

The second significant finding of this research is the fatigue crack growth geometry of a fatigue crack as it propagates through the residual stress field adjacent to a cold expanded hole. This was not previously known to the community in the depth that it has been documented here in this paper. The unique fatigue crack growth characteristics have significant implication in the NDI community. This community does not at this time have a model that accurately predicts the fatigue crack growth characteristics of aluminum that has been cold expanded. As the findings from this research project are integrated into the NDI community, it will be possible to provide to the inspector a greater understanding

of what to look for as he or she is looking for fatigue cracks that propagate from cold expanded hole. This will increase the likelihood of finding cracks and eliminate them before they propagate to a critical size.

In conclusion, the use of a β correction to predict and model the fatigue crack growth behavior of materials that have been processed to induce a residual stress field can provide a more accurate representation of the fatigue behavior than other methods used today. Also, with a greater understanding of the fatigue crack growth geometry of materials that have been processed the NDI community can have a greater probability of detecting fatigue cracks that nucleate and propagate through residual stress fields adjacent to cold expanded holes. Even with fatigue testing's high up-front testing costs the long-term benefits can provide greater aircraft safety and lower long-term maintenance and inspection costs

7.3 Recommendations

1. Additional research is needed to develop a mathematical correlation between β and residual stress.

2. To increase the knowledge of the fatigue crack growth geometry of materials that have been processed by cold expansion, the author recommends that further testing be performed to develop a marker banding spectrum for the 2024-T351 aluminum alloy.   Once this spectrum has been developed it is recommended that further testing be performed to statistically characterize the fatigue crack growth geometry. This was

not performed during this research project. Only one specimen was tested and recorded.

3. It is recommended that further research be applied to the development of NDI techniques that can capture in-situ the fatigue crack growth behavior of materials being tested in fatigue. This would allow for a more accurate characterization of the fatigue crack growth geometry.

4. Research must be performed using spectrum loading. It is unknown what the fatigue characteristics of cold expanded specimens are like under variable loading. This can be determined only by fatigue testing of specimens using the loading spectrum that component would seen in service.

5. Other materials must also be tested. These materials may include titanium alloys, nickel based super alloys or even newer aerospace grade aluminum alloys. Each material will have its own unique fatigue crack growth characteristics and this must be captured and statistically analyzed.

6. Testing needs to be performed on varying hole diameters, thicknesses, maximum stress values, and stress ratios.

7. Finite element models need to be produced that more accurately represent what is truly happening in the material during the cold expansion process and the changes in the residual stress profile when a far-field load is applied.

8. Testing is also needed to gain a greater understanding of the effects of oversizeing a previously cold expanded hole and how the fatigue crack growth behavior is modified by this process.

9. β corrections can also be calculated to model the fatigue crack growth behavior of hybrid materials such as GLARE and TiGr. In order to accomplish this fatigue testing must be performed to characterize how fatigue crack propagate through these types of composite structures.

10. As fatigue testing continues it is recommended that greater attention be given to the preparation of the fatigue specimens. The bonding techniques need to provide adequate stress relief but must not induce into the material additional locations where fatigue cracks can nucleate and propagate to failure.

APPENDIX A

MATERIAL CERTIFICATION SHEET

Fig. 92 Material certification test report from Kaiser Aluminum. Part 1.

KAISER
ALUMINUM
Trentwood Works - Spokane, WA 99215
Phone: (800) 367-2586

CERTIFIED TEST REPORT

Serial Number
4035329

CERTIFICATION

KAISER ALUMINUM & CHEMICAL CORPORATION (KAISER) HEREBY CERTIFIES THAT METAL SHIPPED UNDER THIS ORDER WAS MANUFACTURED IN THE U.S.A. AND HAS BEEN INSPECTED, TESTED, AND FOUND IN CONFORMANCE WITH THE REQUIREMENTS OF THE APPLICABLE SPECIFICATIONS AS INDICATED HEREIN. ALL METAL WHICH IS SOLUTION HEAT-TREATED COMPLIES WITH AMS 2772 (MIL-H-6088). ANY WARRANTY IS LIMITED TO THAT SHOWN ON KAISER'S STANDARD GENERAL TERMS AND CONDITIONS OF SALE. TEST REPORTS ARE ON FILE, SUBJECT TO EXAMINATION. ISO-9001:2000 CERTIFIED

BILL POYNOR, LABORATORIES SUPERVISOR

Page 2 of 2

Fig. 93 Material certification test report from Kaiser Aluminum. Part 2.

APPENDIX B

RESIDUAL COLD EXPANSION TABLE

Part Number	Hole Size Before CX	Sleve Size Before CX	Madrel Diameter	Hole Size After CX	Applied Expansion (%)	Residual Expansion (%)	Hole Size After CX	Residual Expansion (%)
CX2024-1	0.4740	0.0110	0.4700	0.4885	3.7975	3.0591	0.4866	2.6582
CX2024-2	0.4745	0.0110	0.4700	0.4885	3.6881	2.9505	0.4877	2.7819
CX2024-3	0.4745	0.0110	0.4700	0.4890	3.6881	3.0558	0.4874	2.7187
CX2024-4	0.4745	0.0110	0.4700	0.4885	3.6881	2.9505	0.4874	2.7187
CX2024-5	0.4745	0.0110	0.4700	0.4890	3.6881	3.0558	0.4878	2.8030
CX2024-6	0.4745	0.0110	0.4700	0.4890	3.6881	3.0558	0.4874	2.7187
CX2024-7	0.4745	0.0110	0.4700	0.4885	3.6881	2.9505	0.4870	2.6344
CX2024-8	0.4745	0.0110	0.4700	0.4885	3.6881	2.9505	0.4874	2.7187
CX2024-9	0.4745	0.0110	0.4700	0.4890	3.6881	3.0558		-100.0000
CX2024-10	0.4745	0.0110	0.4700	0.4885	3.6881	2.9505		-100.0000
CX2024-11	0.4745	0.0110	0.4700	0.4885	3.6881	2.9505	0.4898	3.2244
CX2024-12	0.4750	0.0110	0.4700	0.4885	3.5789	2.8421	0.4882	2.7789
CX2024-13	0.4750	0.0110	0.4700	0.4885	3.5789	2.8421	0.4882	2.7789
CX2024-14	0.4750	0.0110	0.4700	0.4885	3.5789	2.8421	0.4866	2.4421
CX2024-15	0.4745	0.0110	0.4700	0.4885	3.6881	2.9505	0.4874	2.7187
CX2024-16	0.475	0.009	0.470	0.489	2.737	2.947		-100.000
CX2024-17	0.475	0.009	0.470	0.489	2.737	2.947	0.488	2.693
CX2024-18	0.475	0.009	0.470	0.490	2.737	3.158		-100.000
CX2024-19	0.475	0.009	0.470	0.490	2.737	3.158		-100.000
CX7075-1	0.4745	0.0110	0.4700	0.4860	3.6881	2.4236	0.4858	2.3815

Fig. 94 Cold Expansion data sheet for all processed specimens. Cold expansion process was performed at the USAFA's CASTLE Group.

APPENDIX C

FATIGUE CRACK GROWTH DATA SHEETS

Spec. I.D. CC 2024-01   Loading Condition: Constant Amplitude R = 0.1
Width: 4.000 in   Thick: 0.254 in   Area: 1.016 in^2   Frequency: 15 Hz

Testing Information:

Hole Dia: 0.1050 in   Peak Stress: 11.1 ksi   Date: July 24, 2007

EDM Through Notch Length (mm)

Front: North: 0.26 mm   South: 0.85 mm

Back: North: 0.47 mm   South: 0.24 mm

Cycles	Crack Length (inches)				Bore	Comments
	Surface of Hole					
	Entrance		Exit			
	North	South	North	South		
5000	0.0000	0.0000	0.0000	0.0000	N/A	
10000	0.0000	0.0000	0.0000	0.0000		
15000	0.0000	0.0000	0.0000	0.0000		
20000	0.0000	0.0000	0.0000	0.0000		
25000	0.0000	0.0000	0.0000	0.0000		
30000	0.0000	0.0000	0.0000	0.0000		
35000	0.0016	0.0000	0.0000	0.0000		
40000	0.0028	0.0035	0.0000	0.0039		
45000	0.0039	0.0028	0.0020	0.0035		
50000	0.0035	0.0039	0.0043	0.0087		
55000	0.0055	0.0094	0.0055	0.0059		
60000	0.0083	0.0091	0.0102	0.0079		
71837	0.0106	0.0094	0.0142	0.0118		
81837	0.0134	0.0098	0.0157	0.0130		
91837	0.0130	0.0165	0.0165	0.0173		
101837	0.0146	0.0205	0.0205	0.0224		
111837	0.0161	0.0213	0.0224	0.0240		
121837	0.0213	0.0185	0.0248	0.0244		
131837	0.0236	0.0205	0.0264	0.0268		
141837	0.0256	0.0276	0.0295	0.0299		
151837	0.0303	0.0291	0.0327	0.0311		
161837	0.0327	0.0303	0.0350	0.0335		
171837	0.0327	0.0358	0.0386	0.0362		
181837	0.0354	0.0374	0.0437	0.0390		
191101	0.0382	0.0390	0.0425	0.0402		
201101	0.0413	0.0445	0.0441	0.0441		
211101	0.0425	0.0469	0.0480	0.0469		
221101	0.0484	0.0547	0.0563	0.0480		
231101	0.0520	0.0543	0.0610	0.0524		
241101	0.0559	0.0610	0.0650	0.0602		
251101	0.0591	0.0650	0.0650	0.0610		
261101	0.0602	0.0669	0.0650	0.0646		

Continued Below

271101	0.0654	0.0705	0.0685	0.0717		
281101	0.0689	0.0732	0.0843	0.0780		
291101	0.0724	0.0740	0.0850	0.0878		
301101	0.0787	0.0811	0.0890	0.1012		
311101	0.0823	0.0815	0.0965	0.1126		
326101	0.0957	0.0913	0.1146	0.1366		
341101	0.1220	0.1055	0.1382	0.1665		
356101	0.1642	0.1543	0.1740	0.2004		
364101	0.2024	0.1961	0.2094	0.2354		
372101	0.2610	0.2102	0.3012	0.2807		
380101	0.3248	0.3228	0.3240	0.3520		
388101	0.4150	0.4016	0.4264	0.4437		
396101	0.5496	0.5307	0.5248	0.5673		
400101	0.6126	0.6075	0.5744	0.6016		
404101	0.6787	0.6673	0.6740	0.7043		
408101	0.7476	0.7197	0.7780	0.8016		
412101	0.8744	0.8106	0.8650	0.8669		
416101	0.9354	0.9961	1.0051	1.0083		
420101	1.1342	1.2429	1.1795	1.3646		
422121	Specimen Final Failure					

Spec. I.D. CC 2024-02   Loading Condition: Constant Amplitude R = 0.1

Width: 4.000 in   Thick: 0.255 in   Area: 1.016 in^2   Frequency: 15 Hz

Testing Information:

Hole Dia: 0.1060 in   Peak Stress: 11.1 ksi   Date: July 24, 2007

EDM Through Notch Length (mm)

Front: North: 0.40 mm   South: 0.42 mm

Back: North: 0.26 mm   South: 0.26 mm

Cycles	Crack Length (inches)				Bore	Comments
	Surface of Hole					
	Entrance		Exit			
	North	South	North	South		
0	0.0000	0.0000	0.0000	0.0000	N/A	
15000	0.0000	0.0000	0.0000	0.0000		
30000	0.0000	0.0000	0.0000	0.0000		
45000	0.0043	0.0051	0.0035	0.0039		
60000	0.0079	0.0083	0.0087	0.0071		
75000	0.0114	0.0165	0.0122	0.0122		
90000	0.0161	0.0169	0.0165	0.0169		
105000	0.0181	0.0209	0.0205	0.0217		
120000	0.0256	0.0240	0.0228	0.0244		
135000	0.0264	0.0283	0.0287	0.0287		
150000	0.0295	0.0311	0.0307	0.0335		
165000	0.0339	0.0374	0.0366	0.0335		
180000	0.0366	0.0409	0.0417	0.0382		
195000	0.0465	0.0457	0.0453	0.0441		
210000	0.0492	0.0488	0.0496	0.0496		
225000	0.0559	0.0512	0.0575	0.0539		
240000	0.0591	0.0547	0.0634	0.0657		
255000	0.0630	0.0626	0.0701	0.0705		
270000	0.0689	0.0665	0.0819	0.0791		
285000	0.0748	0.0701	0.0917	0.0890		

Cycles	Crack Length (inches)				Bore	Comments
	Surface of Hole					
	Entrance		Exit			
	North	South	North	South		
5000	0.0000	0.0000	0.0000	0.0000	N/A	
10000	0.0000	0.0000	0.0000	0.0000		
15000	0.0000	0.0000	0.0000	0.0000		
20000	0.0000	0.0000	0.0000	0.0000		
25000	0.0000	0.0000	0.0000	0.0000		
30000	0.0000	0.0000	0.0000	0.0000		
35000	0.0016	0.0000	0.0000	0.0000		
40000	0.0028	0.0035	0.0000	0.0039		
45000	0.0039	0.0028	0.0020	0.0035		
50000	0.0035	0.0039	0.0043	0.0087		
55000	0.0055	0.0094	0.0055	0.0059		
60000	0.0083	0.0091	0.0102	0.0079		
71837	0.0106	0.0094	0.0142	0.0118		
81837	0.0134	0.0098	0.0157	0.0130		
91837	0.0130	0.0165	0.0165	0.0173		
101837	0.0146	0.0205	0.0205	0.0224		
111837	0.0161	0.0213	0.0224	0.0240		
121837	0.0213	0.0185	0.0248	0.0244		
131837	0.0236	0.0205	0.0264	0.0268		
141837	0.0256	0.0276	0.0295	0.0299		
151837	0.0303	0.0291	0.0327	0.0311		
161837	0.0327	0.0303	0.0350	0.0335		
171837	0.0327	0.0358	0.0386	0.0362		
181837	0.0354	0.0374	0.0437	0.0390		
191101	0.0382	0.0390	0.0425	0.0402		
201101	0.0413	0.0445	0.0441	0.0441		
211101	0.0425	0.0469	0.0480	0.0469		
221101	0.0484	0.0547	0.0563	0.0480		
231101	0.0520	0.0543	0.0610	0.0524		
241101	0.0559	0.0610	0.0650	0.0602		
251101	0.0591	0.0650	0.0650	0.0610		
261101	0.0602	0.0669	0.0650	0.0646		

Continued Below

300000	0.0882	0.0791	0.1008	0.0992		
311187	0.1016	0.0858	0.1130	0.1173		
321187	0.1087	0.0996	0.1311	0.1299		
331187	0.1232	0.1213	0.1547	0.1472		
341187	0.1594	0.1476	0.1807	0.1764		
351187	0.2020	0.1957	0.2252	0.2189		
359187	0.2488	0.2441	0.2555	0.2409		
367187	0.3016	0.3098	0.3000	0.3051		
375187	0.3787	0.4012	0.3898	0.3972		
379187	0.4370	0.4402	0.4350	0.4354		
383187	0.4846	0.4811	0.4862	0.4634		
387187	0.5591	0.5563	0.5508	0.5661		
391187	0.6122	0.6413	0.6405	0.6866		
395187	0.6902	0.6941	0.7228	0.7268		
399187	0.7409	0.7567	0.8138	0.8177		
403187	0.8102	0.9020	0.8984	0.9248		
407187	1.0232	1.0354	1.0504	1.0925		
410081	Specimen Final Failure					

Spec. I.D. NON CX 2024-01   Loading Condition: Constant Amplitude R = 0.1

Width: 4.000 in   Thick: 0.255 in   Area: 1.020 in^2   Frequency: 20 Hz

Precrack Information:

Hole Dia: 0.4764 in   Peak Stress: 25.0 ksi   Date: October 18, 2007

Surface EDM Length: 0.0185 in

Test Information:

Hole Dia: 0.50354 in   Peak Stress: 25.0 ksi   Date: December 4, 2007

Surface EDM Length: EDM Was Removed During Final Ream

Cycles	Crack Length (inches)				Bore	Comments
	Surface of Hole					
	Entrance		Exit			
	North	South	North	South		
0						Precracking
3101	0.0201					
0						
987	0.0449				0.1947	
1370	0.0646				0.1963	
1976	0.0882				0.2011	
2562	0.1126				0.2051	
3370	0.1457				0.2204	
4000	0.1748	0.0366	0.0366			Through Bore
4445	0.2016	0.1398	0.1398			
4868	0.2362	0.1953	0.1953			
5231	0.2748	0.2500	0.2500			
5373	0.3181	0.2843	0.2843			
6123	0.3705	0.3579	0.3579	0.0358		
6462	0.4268	0.4339	0.4339	0.1020		
6972	0.5449	0.5567	0.5567	0.2449		
7297	0.7571	0.7657	0.7657	0.5051		
7443	Final Specimen Failure					

Spec. I.D. NON CX 2024-02   Loading Condition: Constant Amplitude R = 0.1

Width: 4.001 in   Thick: 0.254 in   Area: 1.016 in^2   Frequency: 20 Hz

Precrack Information:

Hole Dia: 0.4779 in   Peak Stress: 20.0 ksi   Date: December 19, 2007

Surface EDM Length: 0.0149 in

Test Information:

Hole Dia: 0.5023 in   Peak Stress: 20.0 ksi   Date: January 14, 2007

Surface EDM Length: EDM Was Removed During Final Ream

Cycles	Crack Length (inches)				Bore	Comments
	Surface of Hole					
	Entrance		Exit			
	North	South	North	South		
0						Precracking
50190	0.0267					
0	0.0252		0.0000		0.0388	
1961	0.0406		0.0000		0.0456	
5178	0.0606		0.0000		0.0658	
7416	0.0756		0.0000		0.0751	
10438	0.1059		0.0000		0.0894	
14287	0.1228		0.0000		0.1089	
17498	0.1441		0.0000		0.1300	
20456	0.1622		0.0000		0.1510	
23265	0.1819		0.0000		0.1662	
26951	0.2130		0.0000		0.1932	
29119	0.2409		0.0000		0.2160	
31305	0.2717		0.0000		0.2321	
33414	0.3000		0.0823			Through Bore
35739	0.3421		0.1634			
39057	0.3984		0.3681			
41130	0.4551		0.4591			
42457	0.5205		0.5169			
43666	0.5921		0.5937			
44365	0.6689		0.6559			
47443	**Final Specimen Failure**					

Spec. I.D. NON CX 2024-03   Loading Condition: Constant Amplitude R = 0.1

Width: 4.002 in   Thick: 0.254 in   Area: 1.0165 in^2   Frequency: 20 Hz

Precrack Information:

Hole Dia: 0.4755 in   Peak Stress: 10.0 ksi   Date: January 18, 2007

Surface EDM Length: 0.0129 in

Test Information:

Hole Dia: 0.5023 in   Peak Stress: 10.0 ksi   Date: February 25, 2007

Surface EDM Length: EDM Was Removed During Final Ream

Cycles	Crack Length (inches)				Bore	Comments
	Surface of Hole					
	Entrance		Exit			
	North	South	North	South		
0						Precracking
810030	0.0247					
0	0.0232				0.0506	
27170	0.0409				0.0635	
47821	0.0524				0.0764	
65567	0.0657				0.0876	
87001	0.0799				0.1045	
107638	0.1008				0.1238	
130447	0.1323				0.1535	
143316	0.1626				0.1696	
152384	0.1921				0.1921	
163372	0.2224				0.2315	
171931	0.2535		0.1520			Through Bore
178206	0.2878		0.2252			
183627	0.3220		0.2791			
191596	0.3764		0.3539			
205036	0.4673		0.4772			
215943	0.5693		0.5827			
223964	0.6669		0.6512			
234553	0.7705		0.7626			
241395	0.8724		0.8331			
248614	0.9831		0.9748			
258227	1.0803		1.0898			
264617	1.1587		1.1626			
269677	1.2327		1.2382			
279806	**Final Failure of Specimen**					

Spec. I.D. NON CX 2024-04   Loading Condition: Constant Amplitude R = 0.1

Width: 4.001 in   Thick: 0.253 in   Area: 1.0122 in^2   Frequency: 20 Hz

Precrack Information:

Hole Dia: 0.4748 in   Peak Stress: 10.0 ksi   Date: January 18, 2007

Surface EDM Length: 0.0135 in

Test Information:

Hole Dia: 0.50236 in   Peak Stress: 10.0 ksi   Date: February 26, 2007

Surface EDM Length: EDM Was Removed During Final Ream

Cycles	Crack Length (inches)				Bore	Comments
	Surface of Hole					
	Entrance		Exit			
	North	South	North	South		
0						Precracking
50015	0.0287					
0	0.0205		0.0000		0.0180	
88291	0.0382		0.0000		0.0427	
153106	0.0575		0.0000		0.0741	
180379	0.0736		0.0000		0.0943	
207318	0.0941		0.0000		0.1205	
225766	0.1165		0.0000		0.1392	
244554	0.1453		0.0000		0.1534	
268377	0.1787		0.0000		0.1864	
285471	0.2165		0.0000		0.2073	
297632	0.2531		0.0000		0.2328	
304829	0.2783		0.1559			Through Bore
311364	0.3071		0.2240			
320903	0.3583		0.3256			
332865	0.4520		0.4169			
347386	0.5681		0.5433			
360565	0.6843		0.6642			
372388	0.7953		0.8122			
382267	0.9248		0.9256			
392346	1.0445		0.9878			
411818	1.2342		1.1850			
425336	**Final Specimen Failure**					

Spec. I.D. CX 2024-01   Loading Condition: Constant Amplitude R = 0.1

Width: 4.000 in   Thick: 0.254 in   Area: 1.016 in^2   Frequency: 20 Hz

Precrack Information:

Hole Dia: 0.4866 in   Peak Stress: 20.0 ksi   Date: September 12, 2007

Surface EDM Length: 0.01457 in

Test Information:

Hole Dia: 0.50275 in   Peak Stress: 25.0 ksi   Date: October 9, 2007

Surface EDM Length: 0.0039 in

Cycles	Crack Length (inches)				Bore	Comments
	Surface of Hole					
	Entrance		Exit			
	North	South	North	South		
0	0.0000				N/A	
92402	0.0201					
0	0.0213				0.0000	
45452	0.0709				0.0787	
60060	0.0831				0.0829	
75023	0.1028				0.1143	
85027					0.1581	
95014					0.1995	
105009					0.2096	
115206		0.0307			0.2202	
124996		0.0386			0.2285	
140175		0.0547			0.2303	
152009	0.1122	0.0618	0.0126			
165008	0.1158	0.0705	0.0161			
180999	0.1209	0.0776				
196006	0.1244	0.0835	0.0201	0.0122		
210010	0.1264	0.0906	0.0370			
225017	0.1327	0.0894		0.0382		
241996	0.1417	0.0945	0.0378	0.0402		
259998		0.1008	0.0472	0.0457		
281001	0.1484	0.1039	0.0476	0.0500		
324993	0.1579	0.1165	0.0591	0.0575		
375000	0.1736	0.1299	0.0630	0.0654		
428308	0.2004	0.1402	0.0744	0.0713		
480995	0.2417	0.1547	0.0803	0.0807		
498000	Specimen Final Failure					

Spec. I.D. CX 2024-02   Loading Condition: Constant Amplitude R = 0.1

Width: 4.000 in   Thick: 0.255 in   Area: 1.020 in^2   Frequency: 20 Hz

Precrack Information:

Hole Dia: 0.4877 in   Peak Stress: 20.0 ksi   Date: September 12, 2007

Surface EDM Length: 0.0185 in

Test Information:

Hole Dia: 0.50315 in   Peak Stress: 25.0 ksi   Date: October 11, 2007

Surface EDM Length: 0.0338 in

Cycles	Crack Length (inches)				Bore	Comments
	Surface of Hole					
	Entrance		Exit			
	North	South	North	South		
0	0.0000					
107276	0.0221					Precracking
0	0.0339				0.0123	
20524	0.0650				0.0619	
42086	0.0721				0.0815	
72446	0.0949	0.0126			0.0981	
93336	0.0976	0.0496			0.1109	
113774	0.1067	0.0622			0.1300	
136484	0.1138	0.0791			0.1673	
160030	0.1232	0.0866			0.1692	
200002	0.1323	0.1016	0.0606	0.0472		Through Bore
249992	0.1520	0.1173	0.0642	0.0571		
301577	0.1658	0.1374	0.0713	0.0681		
350000	0.1878	0.1520	0.0776	0.0744		
400032	0.2953	0.1744	0.0823	0.0846		
410066	0.4343	0.1835	0.0839	0.0000		
415020	0.7398	0.2094	0.7394	0.0933		
415770						

Spec. I.D. CX 2024-03   Loading Condition: Constant Amplitude R = 0.1

Width: 4.000 in   Thick: 0.255 in   Area: 1.020 in^2   Frequency: 20 Hz

Precrack Information:

Hole Dia: 0.4874 in   Peak Stress: 20.0 ksi   Date: September 27, 2007

Surface EDM Length: 0.0169 in

Test Information:

Hole Dia: 0.5086 in   Peak Stress: 25.0 ksi   Date: November 1, 2007

Surface EDM Length: Removed During Final Reaming

Cycles	Crack Length (inches)				Bore	Comments
	Surface of Hole					
	Entrance		Exit			
	North	South	North	South		
0	0.0000					
100007	0.0287					Precracking
0	0.0232				0.0265	
20014	0.0555				0.0636	
39994	0.0693				0.0734	
69999	0.0850	0.0252			0.0831	
100001	0.0965	0.0602			0.1048	
131153	0.1063	0.0850			0.2292	
171003	0.1217	0.1059	0.0461	0.0390		Through Bore
210023	0.1307	0.1173	0.0717	0.0512		
259952	0.1543	0.1280	0.0858	0.0638		
307013	0.1819	0.1445	0.1000	0.0732		
316314	Specimen Failed at Top Tab from Grinding Mark					

Spec. I.D. CX 2024-04   Loading Condition: Constant Amplitude R = 0.1

Width: 4.000 in   Thick: 0.254 in   Area: 1.028 in^2   Frequency: 20 Hz

Precrack Information:

Hole Dia: 0.4874 in   Peak Stress: 20.0 ksi   Date: September 25, 2007

Surface EDM Length: 0.0169 in

Test Information:

Hole Dia: 0.5011 in   Peak Stress: 25.0 ksi   Date: December 20, 2007

Surface EDM Length: 0.00787 in

Cycles	Crack Length (inches)				Bore	Comments
	Surface of Hole					
	Entrance		Exit			
	North	South	North	South		
0	0.0000					
125011	0.0244					Precracking
0	0.0311				0.0301	
13053	0.0551				0.0540	
20783	0.0689				0.0633	
67991	0.0850	0.0378			0.0919	
85317	0.0972	0.0524			0.1073	
121487	0.1094	0.0732			0.1621	
159072	0.1236	0.0854	0.0248	0.0260		Through Bore
225008	0.1390	0.1043	0.0591	0.0472		
278239	0.1528	0.1181	0.0673	0.0520		
330814	0.1665	0.1319	0.0756	0.0634		
367003	0.1811	0.1429	0.0780	0.0689		
399305	0.1988	0.1535	0.0866	0.0709		
419904	0.2236	0.1587	0.0886	0.0728		
434611	0.2402	0.1661	0.0890			
447221	0.2728	0.1697	0.0941			
454319	0.3055	0.1744	0.0984	0.0776		
459234	0.3539	0.1748				
462320	0.4043	0.1760				
465253	0.4799	0.1846				
467099	0.5626	0.1882	0.2264	0.0866		
468225	0.6539	0.1957	0.5780	0.0976		
469000	Specimen Final Failure					

Spec. I.D. CX 2024-05   Loading Condition: Constant Amplitude R = 0.1

Width: 3.998 in   Thick: 0.254 in   Area: 1.0154 in^2   Frequency: 20 Hz

Precrack Information:

Hole Dia: 0.4878 in   Peak Stress: 25.0 ksi   Date: October 18, 2007

Surface EDM Length: 0.02126 in

Test Information:

Hole Dia: 0.5023 in   Peak Stress: 25.0 ksi   Date: December 21, 2007

Surface EDM Length: 0.0126 in

Cycles	Crack Length (inches)				Bore	Comments
	Surface of Hole					
	Entrance		Exit			
	North	South	North	South		
0	0.0000					
14966	0.0217					Precracking
0	0.0260				0.0268	
7222	0.0390				0.0275	
19412	0.0500				0.0492	
35814	0.0610				0.0586	
64814	0.0744	0.0295			0.0702	
95301	0.0823	0.0445			0.1512	
132283	0.0929	0.0634			0.1578	
176492	0.1071	0.0764	0.0398	0.0323		Through Bore
241227	0.1228	0.0917	0.0504	0.0484		
315992	0.1386	0.1122	0.0650	0.0504		
387910	0.1547	0.1287	0.0752	0.0650		
460263	0.1740	0.1429	0.0862	0.0677		
523563	0.2000	0.1535	0.0949	0.0756		
580279	0.2252	0.1697	0.1008	0.0843		
597347	0.2453	0.1720	0.1043	0.0854		
610442	0.2689	0.1764		0.0874		
622783	0.3004	0.1791	0.1059	0.0886		
632027	0.3433	0.1854		0.0890		
640526	0.4382	0.1898	0.1067	0.0894		
644706	0.5413	0.1969	0.1307	0.0913		
646417	0.6508	0.2051	0.5567	0.0921		
647735	Specimen Final Failure					

Spec. I.D. CX 2024-06   Loading Condition: Constant Amplitude R = 0.1

Width: 3.998 in   Thick: 0.253 in   Area: 1.0115 in^2   Frequency: 20 Hz

Precrack Information:

Hole Dia: 0.480 in   Peak Stress: 25.0 ksi   Date: October 18, 2007

Surface EDM Length: 0.02126 in

Test Information:

Hole Dia: 0.50275 in   Peak Stress: 25.0 ksi   Date: November 15, 2007

Surface EDM Length: 0.00394 in

Cycles	Crack Length (inches)				Bore	Comments
	Surface of Hole					
	Entrance		Exit			
	North	South	North	South		
0	0.0000					
26009	0.0224					Precracking
0	0.0240				0.0211	
20000	0.0409				0.0369	
40510	0.0520				0.0512	
69986	0.0602				0.0617	
100018	0.0717	0.0346			0.0632	
140014	0.0839	0.0555			0.1212	
180052	0.0937	0.0736			0.2334	
220012	0.1000	0.0843	0.0276	0.0295		Through Bore
260008	0.1102	0.0941	0.0398	0.0370		
300015	0.1181	0.1031	0.0465	0.0409		
341205	0.1276	0.1150	0.0508	0.0469		
380004	0.1370	0.1224	0.0622	0.0492		
419997	0.1469	0.1299	0.0673	0.0539		
460002	0.1559	0.1386	0.0705	0.0579		
501614	0.1677	0.1500	0.0780	0.0630		
540000	0.1807	0.1571	0.0823	0.0697		
580857	0.1972	0.1705	0.0874	0.0756		
620003	0.2181	0.1858	0.0917	0.0835		
639993	0.2362	0.2071	0.0945	0.0858		
655047	0.2744	0.2102	0.0957	0.0874		
663349	0.3232	0.2138	0.0965	0.0882		
671410	0.4409	0.2244	0.0980	0.0898		
674917	0.5602	0.2421	0.1752	0.0941		
676518	0.7618	0.2673	0.7441	0.1205		

Spec. I.D. CX 2024-07   Loading Condition: Constant Amplitude R = 0.1

Width: 4.000 in   Thick: 0.255 in   Area: 1.020 in^2   Frequency: 20 Hz

Precrack Information:

Hole Dia: 0.4870 in   Peak Stress: 25.0 ksi   Date: January 16, 2007

Surface EDM Length: 0.01850 in

Test Information:

Hole Dia: 0.50079 in   Peak Stress: 25.0 ksi   Date: February 15, 2007

Surface EDM Length: 0.00149 in

Cycles	Crack Length (inches)				Bore	Comments
	Surface of Hole					
	Entrance		Exit			
	North	South	North	South		
0	0.0000					
114160	0.0181					Precracking
0	0.0343	0.0000	0.0000	0.0000	0.0300	
17584	0.0496	0.0000	0.0000	0.0000	0.0609	
46909	0.0685	0.0047	0.0000	0.0000	0.0771	
76222	0.0764	0.0260	0.0000	0.0000	0.0869	
173742	0.0957	0.0732	0.0409	0.0000	0.0000	Through Bore
276218	0.1177	0.1047	0.0539	0.0390	0.0000	
336386	0.1311	0.1177	0.0579	0.0453	0.0000	
447841	0.1500	0.1472	0.0681	0.0606	0.0000	
453117	0.1508	0.1512	0.0000	0.0000	0.0000	
	Secondary Crack Longer Than Primary Crack					

Spec. I.D. CX 2024-08   Loading Condition: Constant Amplitude R = 0.1

Width: 4.000 in   Thick: 0.255 in   Area: 1.020 in^2   Frequency: 20 Hz

Precrack Information:

Hole Dia: 0.4874 in   Peak Stress: 25.0 ksi   Date: January 16, 2007

Surface EDM Length: 0.01929 in

Test Information:

Hole Dia: 0.5000 in   Peak Stress: 25.0 ksi   Date: February 7, 2007

Surface EDM Length: EDM Removed During Final Reaming

Specimen Used for Marker Banding

Spec. I.D. CX 2024-09   Loading Condition: Constant Amplitude R = 0.1

Width: 3.999 in   Thick: 0.254 in   Area: 1.0157 in^2   Frequency: 20 Hz

Precrack Information:

Hole Dia: 0.4874 in   Peak Stress: 20.0 ksi   Date: January 17, 2007

Surface EDM Length: 0.01435 in

Test Information:

Hole Dia: 0.5004 in   Peak Stress: 25.0 ksi   Date: January 31, 2007

Surface EDM Length: 0.01181 in

Cycles	Crack Length (inches)				Bore	Comments
	Surface of Hole					
	Entrance		Exit			
	North	South	North	South		
0	0.0000					
106709	0.0221					Precracking
0	0.0346				0.0213	
28659	0.0496				0.0563	
76277	0.0681				0.0722	
144246	0.0846				0.1430	
235281	0.0988				0.1475	
328299	0.1201	0.0949	0.0307	0.0669		Through Bore
459345	0.1390	0.1232	0.0516	0.0843		
558573	0.1594	0.1445	0.0618	0.1063		
664846	0.1791	0.1717	0.0717	0.1244		
754254	0.2051	0.2287	0.0811	0.1441		
784884	0.2240	0.3866	0.0854	0.1555		
790203	0.2425	0.5039	0.0886	0.3618		
792834	Specimen Final Failure					

Spec. I.D. CX 2024-10   Loading Condition: Constant Amplitude R = 0.1

Width: 4.002 in   Thick: 0.254 in   Area: 1.0165 in^2   Frequency: 20 Hz

Precrack Information:

Hole Dia: 0.48819 in   Peak Stress: 20.0 ksi   Date: January 17, 2007

Surface EDM Length: 0.01417 in

Test Information:

Hole Dia: 0.5003 in   Peak Stress: 25.0 ksi   Date: January 25, 2007

Surface EDM Length:

Specimen Used for Marker Banding

Spec. I.D. CX 2024-11   Loading Condition: Constant Amplitude R = 0.1

Width: 4.002 in   Thick: 0.254 in   Area: 1.0165 in^2   Frequency: 20 Hz

Precrack Information:

Hole Dia: 0.4898 in   Peak Stress: 20.0 ksi   Date: December 17, 2007

Surface EDM Length: 0.0122 in

Test Information:

Hole Dia: 0.50197 in   Peak Stress: 25.0 ksi   Date: January 3, 2007

Surface EDM Length: EDM Removed During Final Reaming

Cycles	Crack Length (inches)				Bore	Comments
	Surface of Hole					
	Entrance		Exit			
	North	South	North	South		
0	0.0000					
113131	0.0209					Precracking
0	0.0264				0.0301	
13599	0.0425				0.0438	
34549	0.0579				0.0596	
81433	0.0728				0.0746	
168573	0.0969	0.0567			0.1055	
275539	0.1181	0.0850			0.1198	
373245	0.1406	0.1039	0.0634	0.0382		Through Bore
460740	0.1618	0.1197	0.0736	0.0642		
544869	0.1882	0.1378	0.0827	0.0787		
586591	0.2185	0.1465	0.0890	0.0878		
610250	0.2602					
619090	0.2882	0.1543	0.0917	0.0902		
625690	0.3311					
629746	0.3882	0.1587	0.0933	0.0906		
632137	0.4374		0.0000			
634190	0.4886	0.1622	0.0976	0.1177		
635746	0.5409	0.1646		0.3134		
636996	0.6358	0.1713		0.5705		
637661	0.7295	0.1776	0.1016	0.7280		
638302	Specimen Final Failure					

Spec. I.D. CX 2024-12   Loading Condition: Constant Amplitude R = 0.1

Width: 4.000 in   Thick: 0.254 in   Area: 1.016 in^2   Frequency: 20 Hz

Precrack Information:

Hole Dia: 0.48819 in   Peak Stress: 20.0 ksi   Date: December 17, 2007

Surface EDM Length: 0.01417 in

Test Information:

Hole Dia: 0.5012 in   Peak Stress: 25.0 ksi   Date: January 2, 2007

Surface EDM Length: 0.00394 in

Cycles	Crack Length (inches)				Bore	Comments
	Surface of Hole					
	Entrance		Exit			
	North	South	North	South		
0	0.0000					
96390	0.0217					Precracking
0	0.0256				0.0000	
8228	0.0398				0.0329	
33431	0.0535				0.0532	
71368	0.0681				0.0777	
107326	0.0839				0.1022	
158987	0.1000	0.0268			0.1064	
217436	0.1150	0.0496			0.1120	
281630	0.1295	0.0709				
331605	0.1492	0.0799			0.1239	
367932	0.1669	0.0878	0.0598	0.0535		Through Bore
395431	0.1862	0.0945	0.0638	0.0591		
419466	0.2083	0.0996	0.0669	0.0622		
434132	0.2280	0.1024	0.0685	0.0654		
445502	0.2476	0.1043	0.0693	0.0669		
453821	0.2705	0.1055		0.0697		
460111	0.3032					
467074	0.3449					
473092	0.4098					
477284	0.4992	0.1118	0.0776	0.0717		
479727	0.6417	0.1157	0.5339	0.0736		
480000	Specimen Final Failure					

Spec. I.D. CX 2024-13   Loading Condition: Constant Amplitude R = 0.1

Width: 3.998 in   Thick: 0.255 in   Area: 1.019 in^2   Frequency: 20 Hz

Precrack Information:

Hole Dia: 0.4882 in   Peak Stress: 20.0 ksi   Date: December 18, 2007

Surface EDM Length: 0.01496 in

Test Information:

Hole Dia: 0.5000 in   Peak Stress: 25.0 ksi   Date: January 4, 2007

Surface EDM Length: 0.00669 in

Cycles	Crack Length (inches)				Bore	Comments
	Surface of Hole					
	Entrance		Exit			
	North	South	North	South		
0	0.0000					
127600	0.0213					Precracking
0	0.0264				0.0240	
8676	0.0413				0.0381	
24703	0.0587				0.0572	
50626	0.0740				0.0713	
75486	0.0886	0.0224			0.0947	
120858	0.1075	0.0587			0.1222	
175914	0.1256	0.0795			0.1667	
239461	0.1445	0.0972	0.0394	0.0323		Through Bore
283233	0.1618	0.1071	0.0524	0.0472		
345032	0.1846	0.1201	0.0669	0.0642		
385759	0.2150	0.1307	0.0760	0.0744		
404655	0.2437	0.1394	0.0776	0.0780		
416561	0.2736	0.1417	0.0780	0.0791		
422656	0.3177	0.1433		0.0815		
425853	0.3634	0.1461		0.0823		
428193	0.3980	0.1484				
430226	0.4402	0.1504		0.0846		
431873	0.4831					
433698	0.5465	0.1563	0.0988	0.0890		
435118	0.6555	0.1618	0.5988	0.0941		
436391	Specimen Final Failure					

Spec. I.D. CX 2024-14   Loading Condition: Constant Amplitude R = 0.1

Width: 4.002 in   Thick: 0.255 in   Area: 1.021 in^2   Frequency: 20 Hz

Precrack Information:

Hole Dia: 0.4866 in   Peak Stress: 20.0 ksi   Date: December 17, 2007

Surface EDM Length: 0.01614 in

Test Information:

Hole Dia: 0.50275 in   Peak Stress: 25.0 ksi   Date: January 8, 2007

Surface EDM Length: EDM Removed During Final Reaming

Cycles	Crack Length (inches)				Bore	Comments
	Surface of Hole					
	Entrance		Exit			
	North	South	North	South		
0	0.0000					
108168	0.0213					Precracking
0	0.0197				0.0165	
7439	0.0366				0.0313	
30912	0.0531				0.0487	
53906	0.0717				0.0835	
103739	0.0925	0.0264			0.1114	
172451	0.1130	0.0740			0.2315	
238229	0.1307	0.0949	0.0417	0.0413		Through Bore
299644	0.1535	0.1118	0.0512	0.0488		
365319	0.1748	0.1280	0.0650	0.0547		
407050	0.1988	0.1406	0.0681	0.0594		
427267	0.2161	0.1433	0.0713	0.0622		
458852	0.2524	0.1563	0.0776	0.0626		
467833	0.2807	0.1614				
475218	0.3134	0.1618				
480319	0.3618	0.1638		0.0634		
483854	0.4091	0.1665				
486465	0.4571	0.1724				
488481	0.5098		0.0839			
489605	0.5571	0.1756	0.0976	0.0669		
490705	0.6480	0.1807	0.6205			
49100.0000	Specimen Final Failure					

Spec. I.D. CX 2024-15   Loading Condition: Constant Amplitude R = 0.1

Width: 4.000 in   Thick: 0.253 in   Area: 1.012 in^2   Frequency: 20 Hz

Precrack Information:

Hole Dia: 0.4874 in   Peak Stress: 20.0 ksi   Date: December 17, 2007

Surface EDM Length: 0.01732 in

Test Information:

Hole Dia: 0.5000 in   Peak Stress: 25.0 ksi   Date: January 11, 2007

Surface EDM Length: 0.0086 in

Cycles	Crack Length (inches)				Bore	Comments
	Surface of Hole					
	Entrance		Exit			
	North	South	North	South		
0	0.0000					
90241	0.0201					Precracking
0	0.0276				0.0207	
8496	0.0433				0.0429	
18974	0.0563				0.0540	
42987	0.0736				0.0821	
77556	0.0890				0.0925	
112914	0.1051				0.1383	
174477	0.1232		0.0370	0.0276		Through Bore
264231	0.1433	0.0433	0.0559	0.0402		
344627	0.1634	0.0650	0.0717	0.0476		
402780	0.1827	0.0787	0.0756	0.0504		
442586	0.2039	0.1213	0.0783	0.0520		
474589	0.2260	0.1220	0.0839	0.0563		
490811	0.2516	0.1280	0.0862	0.0598		
501211	0.2795	0.1319	0.0886	0.0602		
508854	0.3094					
513379	0.3496					
516907	0.4028					
519140	0.4520	0.1343		0.0646		
520611	0.5020	0.0000	0.0906			
521833	0.5555	0.1346	0.3551	0.0673		
522862	0.6492	0.1386	0.5583	0.0693		
524172	Specimen Final Failure					

Spec. I.D. CX 2024-17   Loading Condition: Constant Amplitude R = 0.1

Width: 4.000 in   Thick: 0.254 in   Area: 1.016 in^2   Frequency: 20 Hz

Precrack Information:

Hole Dia: 0.4878 in   Peak Stress: 25.0 ksi   Date: December 17, 2007

Surface EDM Length: 0.00748 in

Test Information:

Hole Dia: 0.5012 in   Peak Stress: 25.0 ksi   Date: January 11, 2007

Surface EDM Length: EDM Removed During Final Reaming

Cycles	Crack Length (inches)				Bore	Comments
	Surface of Hole					
	Entrance		Exit			
	North	South	North	South		
0	0.0000					
46534	0.0386					Precracking
0	0.0390				0.0392	
6645	0.0488				0.0485	
14661	0.0587				0.0542	
37486	0.0740				0.0692	
90355	0.0913				0.0977	
157895	0.1087	0.0602			0.1134	
292053	0.1283	0.0941	0.0421	0.0480		Through Bore
423923	0.1488	0.1201	0.0610	0.0555		
513527	0.1681	0.1382	0.0685	0.0685		
597144	0.1925	0.1539	0.0744	0.0720		
642902	0.2181	0.1665	0.0772	0.0764		
676625	0.2484	0.1780		0.0787		
689207	0.2791	0.1827				
694045	0.3075	0.1850				
699066	0.3508					
703255	0.4004					
706436	0.4496					
710341	0.5496		0.0894			
712103	0.6583		0.3780			
712855	0.7567		0.6587			
713581	**Specimen Final Failure**					

Spec. I.D. CX 2024-18   Loading Condition: Constant Amplitude R = 0.1

Width: 4.000 in   Thick: 0.254 in   Area: 1.016 in^2   Frequency: 20 Hz

Precrack Information:

Hole Dia: 0.4831 in   Peak Stress: 25.0 ksi   Date: February 12, 2007

Surface EDM Length: 0.01417 in

Test Information:

Hole Dia: 0.5000 in   Peak Stress: 25.0 ksi   Date: February 20, 2007

Surface EDM Length: EDM Removed During Final Reaming

Specimen Used for Marker Banding

Spec. I.D. CX 2024-19   Loading Condition: Constant Amplitude R = 0.1

Width: 4.003 in   Thick: 0.253 in   Area: 1.012 in^2   Frequency: 20 Hz

Precrack Information:

Hole Dia: 0.48661 in   Peak Stress: 25.0 ksi   Date: January 11, 2007

Surface EDM Length: 0.01102 in

Test Information:

Hole Dia: 0.50118 in   Peak Stress: 25.0 ksi   Date: March 17, 2007

Surface EDM Length: 0.00354 in

Cycles	Crack Length (inches)				Bore	Comments
	Surface of Hole					
	Entrance		Exit			
	North	South	North	South		
0	0.0000					
100000	0.0270					Precracking
0	0.0276					
520278	0.1988	0.1551	0.0661	0.0862		
577679	0.2087					
712118	0.2228					
783865	0.2323					
847010	0.2394					
906242	0.2480					Through Bore
983828	0.2500	0.1563	0.0665	0.0858		
1169100	0.2803		0.0665			
1278853	0.3114		0.0665			
1366700	0.3508		0.0665			
1408974	0.3902		0.0665			
1433067	0.4311		0.0665			
1456296	0.4756		0.3323			
1470308	0.5264	0.1563	0.4453	0.0874		
1477745	0.5787		0.5209			
1486749	0.6516		0.6311			
1495942	0.7520		0.7299			
1502231	0.8512		0.7815			
1514515	1.0012		1.0193			
1524295	1.1492		1.1453			
1532182	Specimen Final Failure					

APPENDIX D

FRACTOGRAPHY IMAGES
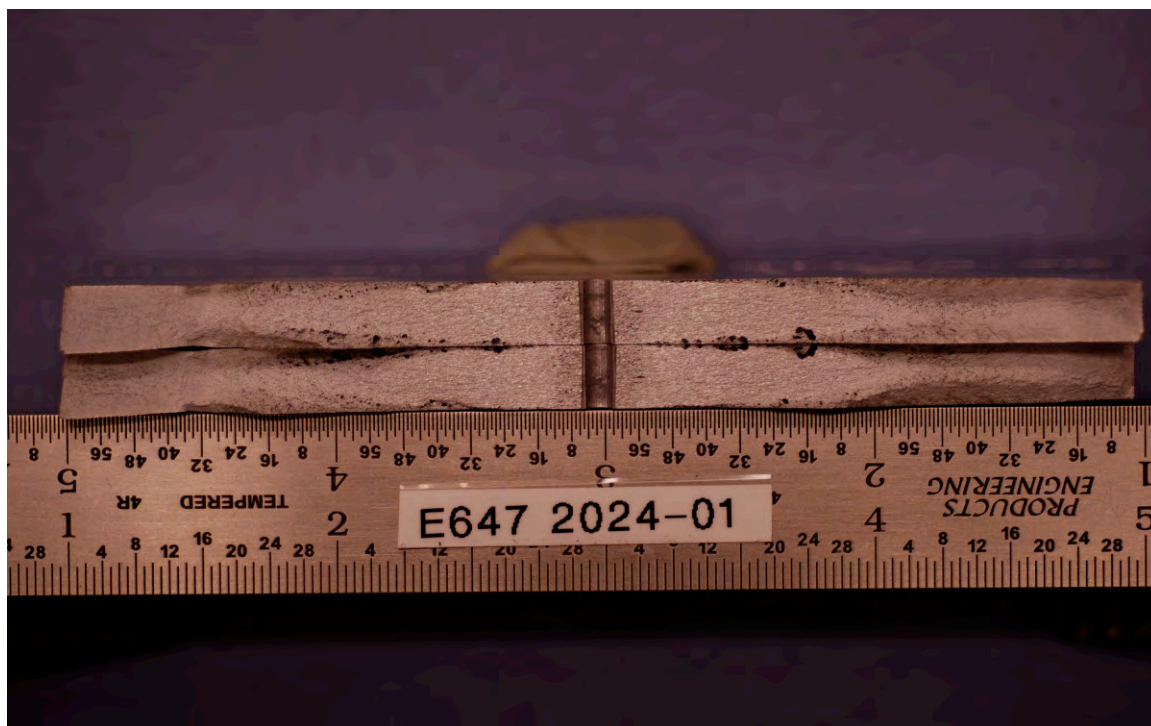
Fig. 95 CC E 647 2024-01 specimen. Specimen tested at σ_{max} = 11.1 ksi, R = 0.1, f = 15 Hz, and lab air.
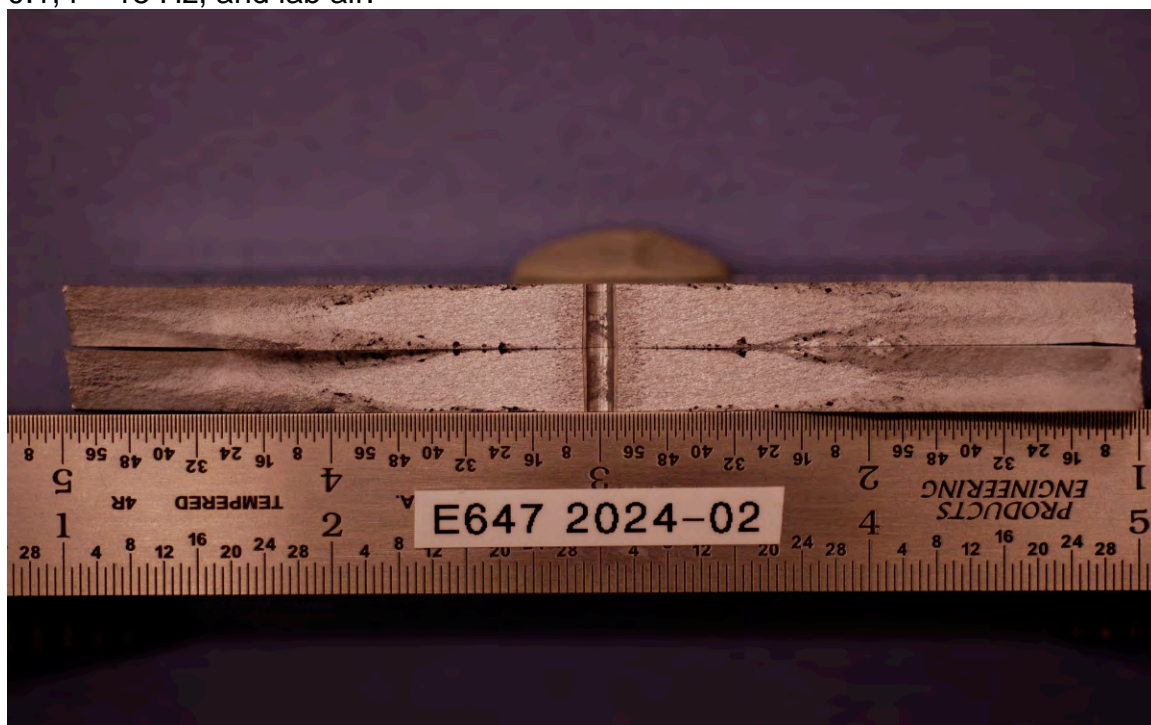
Fig. 96 CC E 647 2024-02 specimen. Specimen tested at σ_{max} = 11.1 ksi, R = 0.1, f = 15 Hz, and lab air.
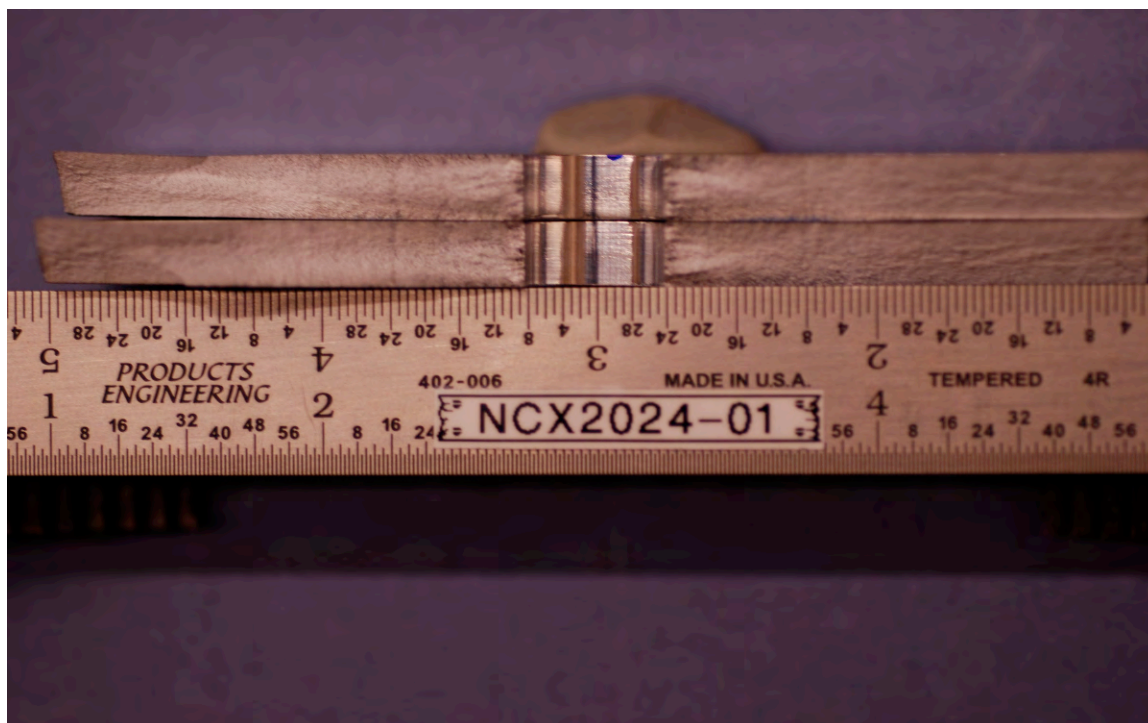
Fig. 97 NON CX 2024-01 specimen. Specimen tested at σ_{max} = 25 ksi, R = 0.1, f = 20, and lab air.
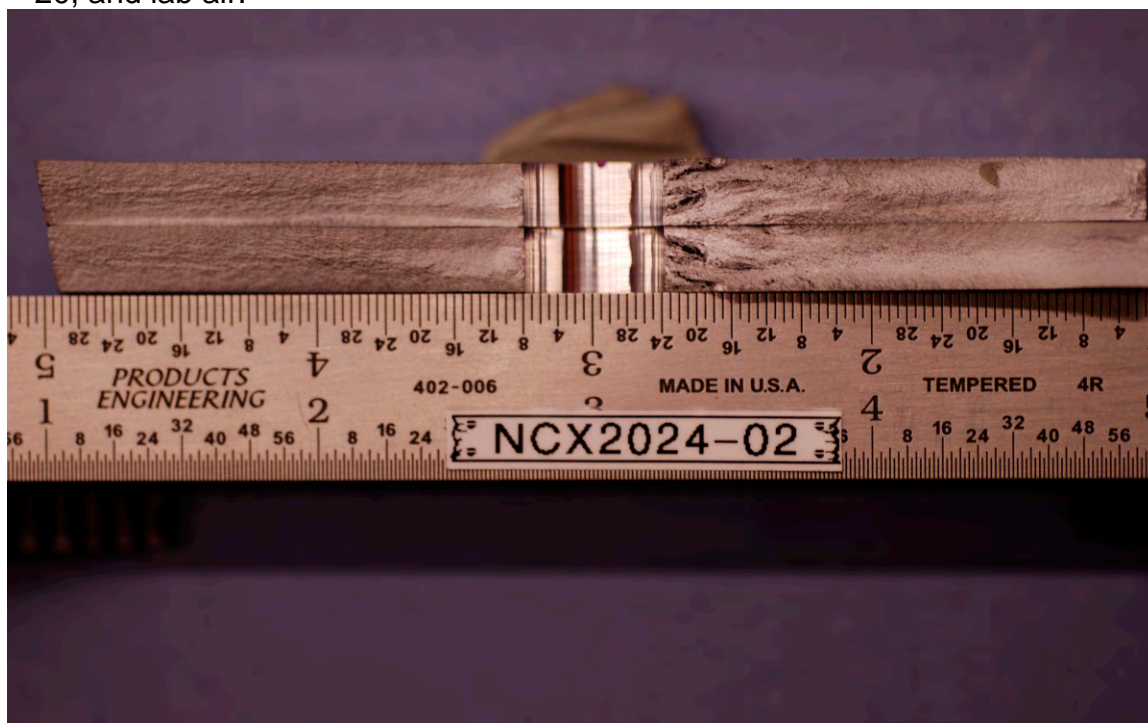
Fig. 98 NON CX 2024-02 specimen. Specimen tested at σ_{max} = 20 ksi, R = 0.1, f = 20, and lab air.
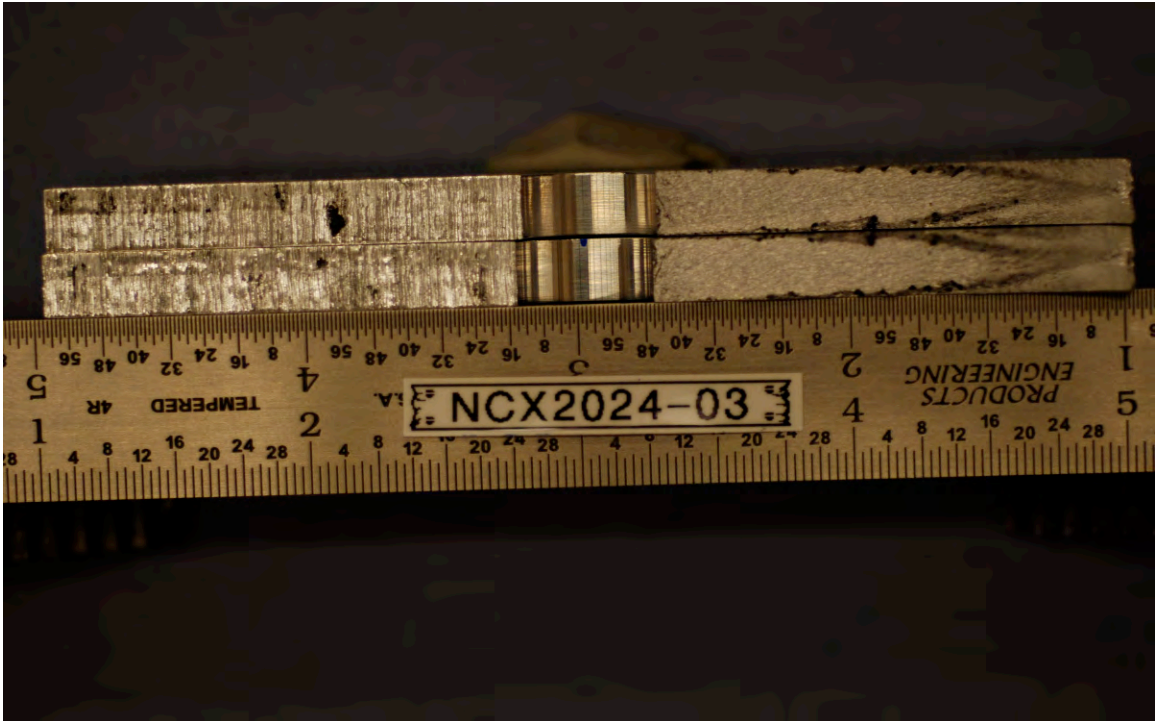
Fig. 99 NON CX 2024-03 specimen. Specimen tested at σ_{max} = 10 ksi, R = 0.1, f = 20, and lab air.

Fig. 100 NON CX 2024-04 specimen. Specimen tested at σ_{max} = 10 ksi, R = 0.1, f = 20, and lab air.

Fig. 101 CX 2024-02 specimen. Specimen tested at σ_{max} = 25 ksi, R = 0.1, f = 20, and lab air.

Fig. 102 CX 2024-04 specimen. Specimen tested at σ_{max} = 25 ksi, R = 0.1, f = 20, and lab air.
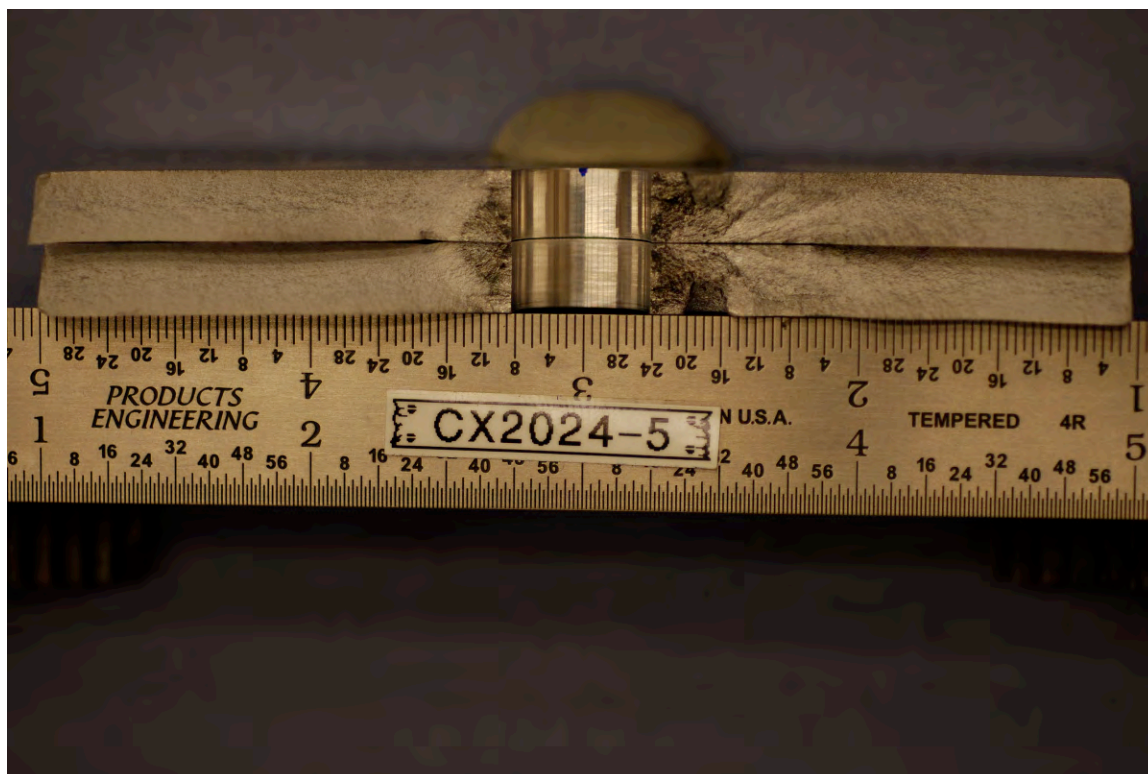
Fig. 103 CX 2024-05 specimen. Specimen tested at σ_{max} = 25 ksi, R = 0.1, f = 20, and lab air.
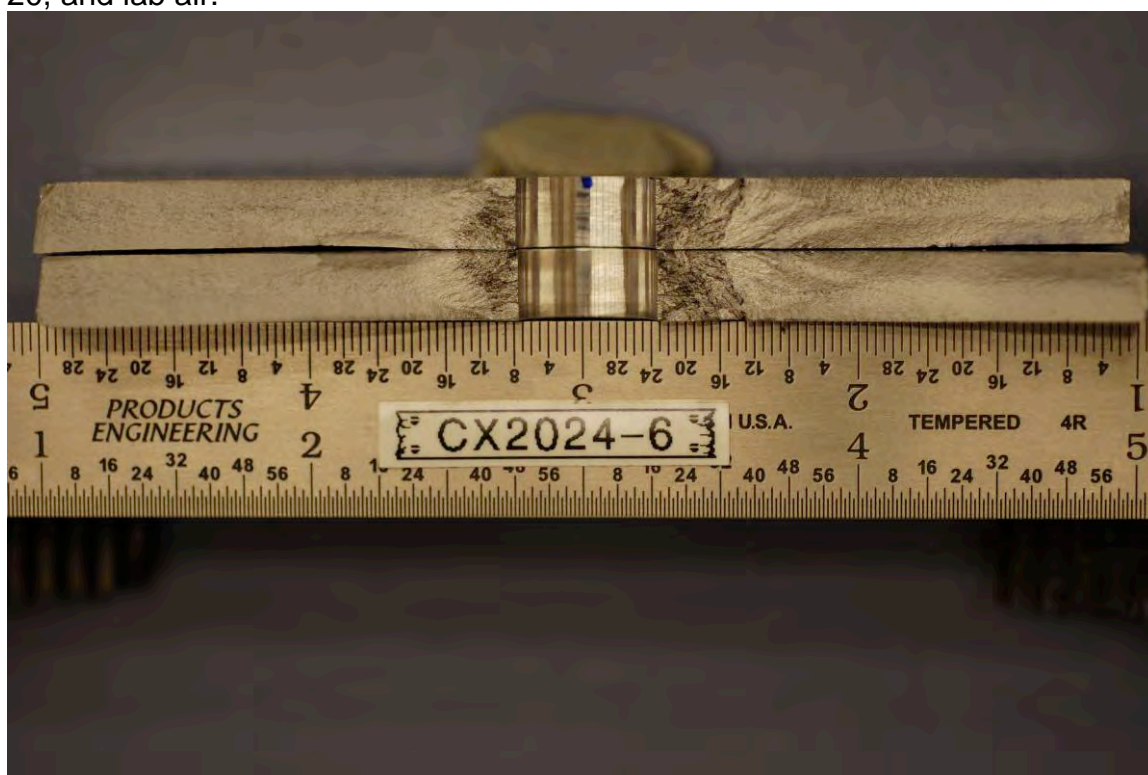
Fig. 104 CX 2024-06 specimen. Specimen tested at σ_{max} = 25 ksi, R = 0.1, f = 20, and lab air.

Fig. 105 CX 2024-12 specimen. Specimen tested at σ_{max} = 25 ksi, R = 0.1, f = 20, and lab air.

Fig. 106 CX 2024-13 specimen. Specimen tested at σ_{max} = 25 ksi, R = 0.1, f = 20, and lab air.
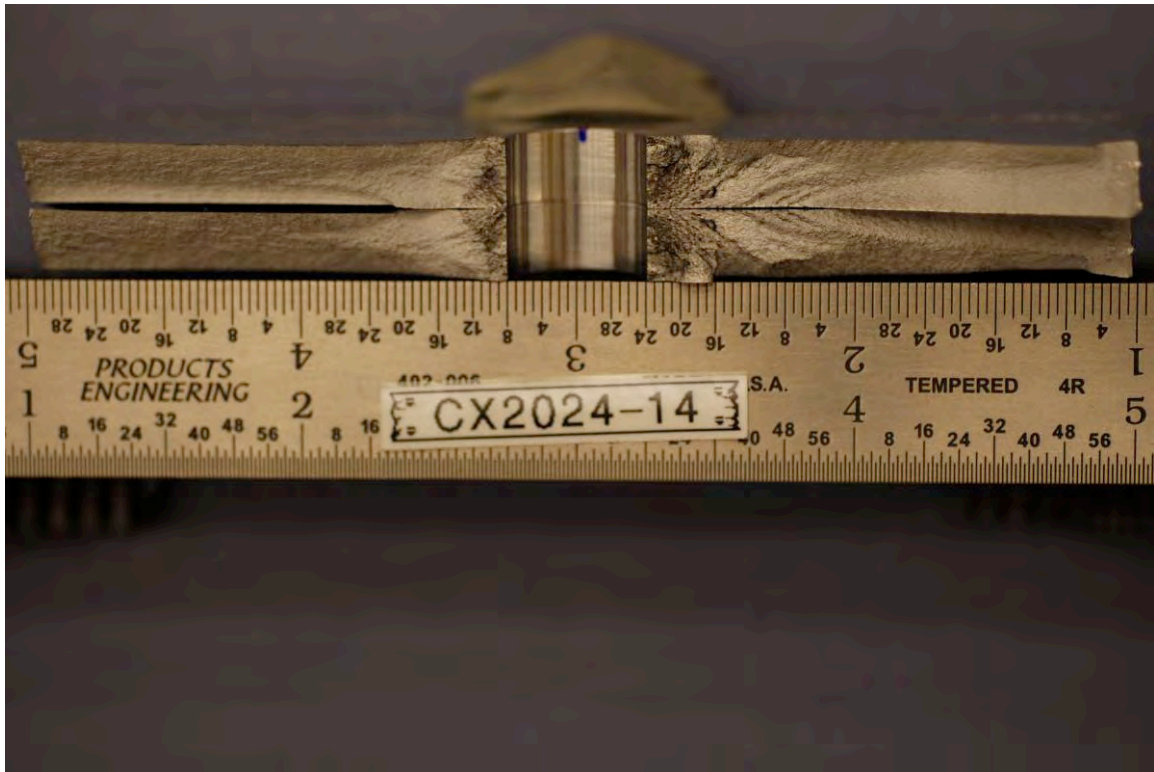
Fig. 107 CX 2024-14 specimen. Specimen tested at σ_{max} = 25 ksi, R = 0.1, f = 20, and lab air.

Fig. 108 CX 2024-15 specimen. Specimen tested at σ_{max} = 25 ksi, R = 0.1, f = 20, and lab air.
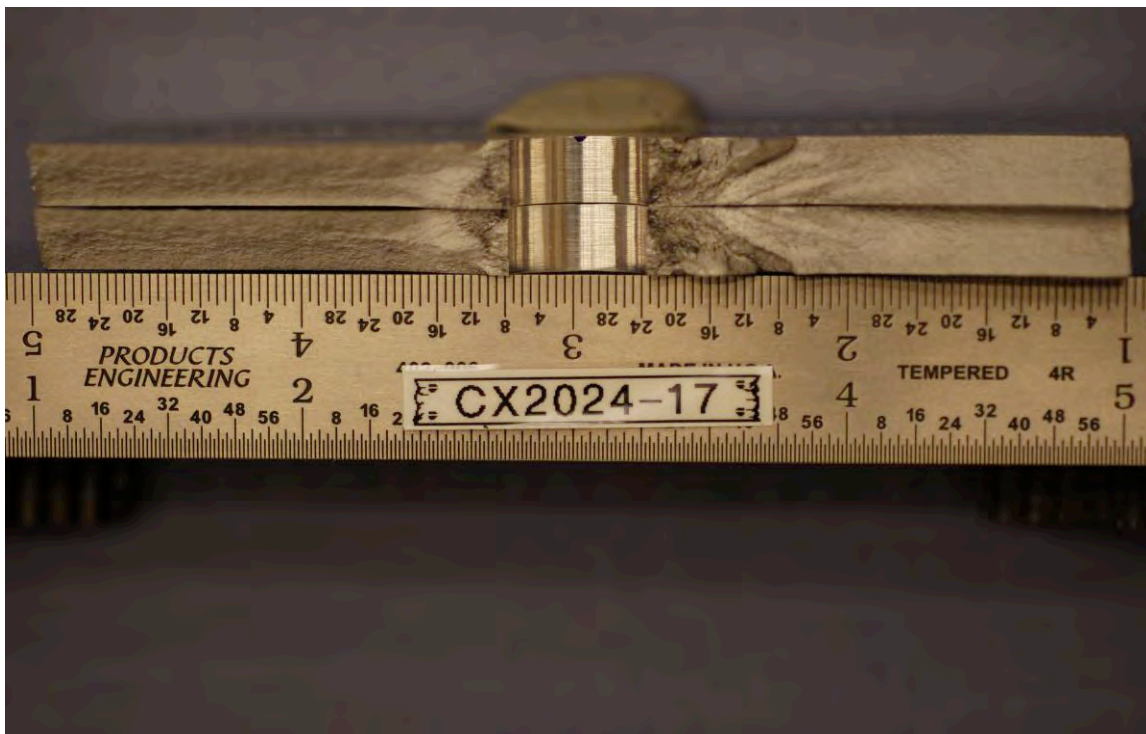
Fig. 109 CX 2024-17 specimen. Specimen tested at σ_{max} = 25 ksi, R = 0.1, f = 20, and lab air.

Fig. 110 CX 2024-01 specimen. Specimen tested at σ_{max} = 25 ksi, R = 0.1, f = 20, and lab air. Specimen failed from surface preparation markings located in the tab bonding region. Represents all tab failures.

APPENDIX E

FATIGUE CRACK GROWTH VERSUS CYCLES PLOTS
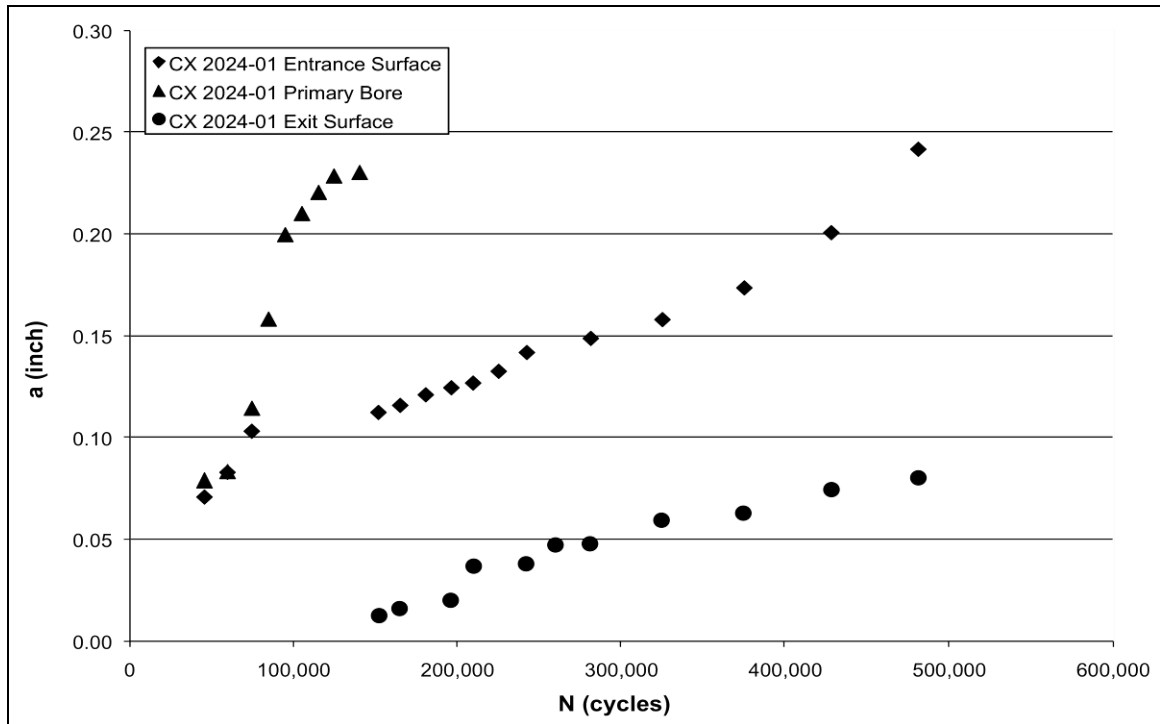
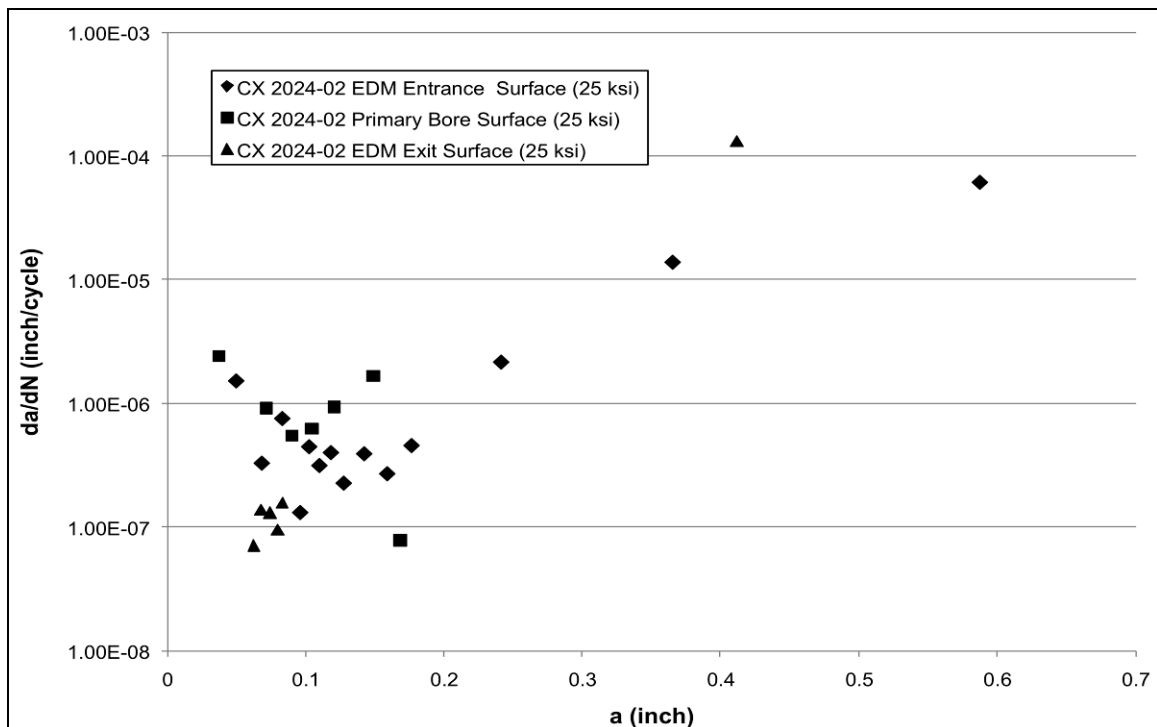Fig. 111 CX 2024-01 crack growth versus cycles. Specimen tested at σ_{max} = 25 ksi, R = 0.1, f = 20, and lab air. Specimen failed at lower grip.
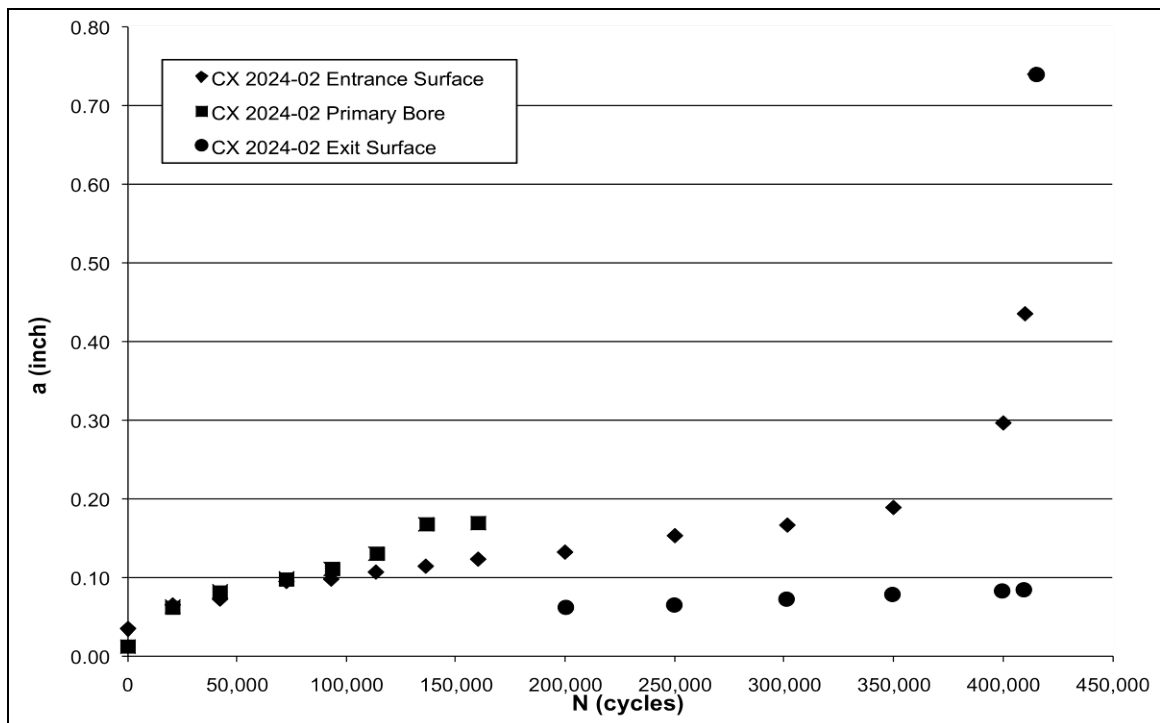
Fig. 112 CX 2024-02 crack growth versus cycles. Specimen tested at σ_{max} = 25 ksi, R = 0.1, f = 20, and lab air.
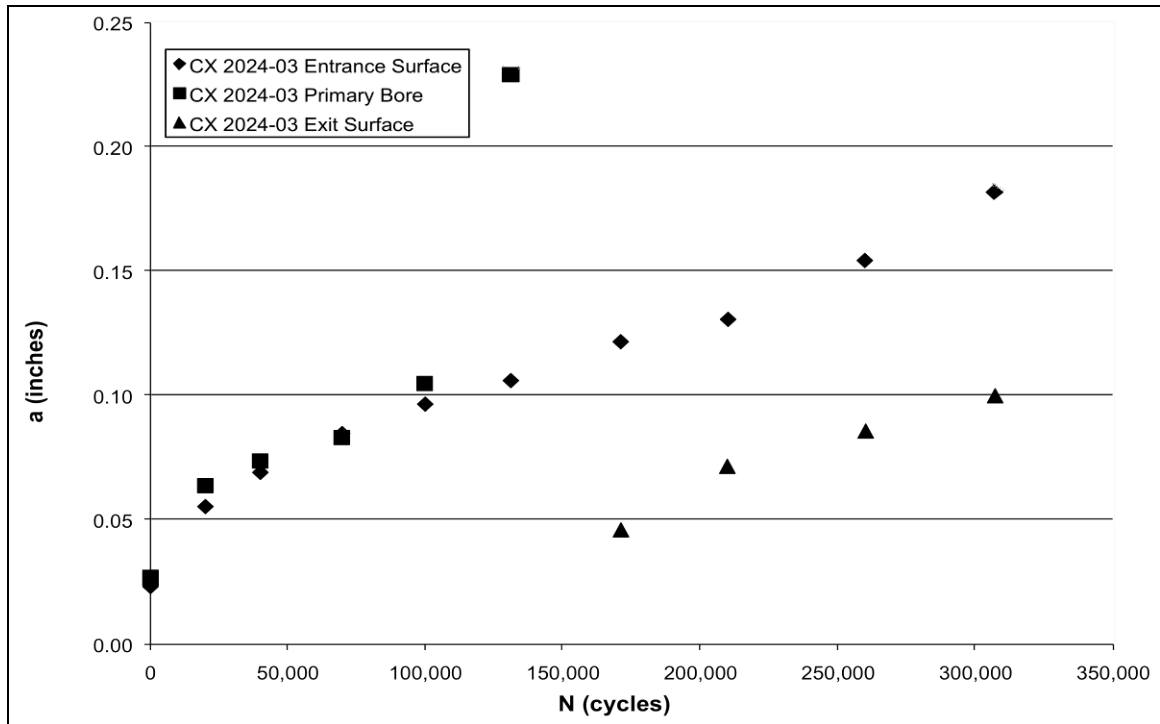
Fig. 113 CX 2024-03 crack growth versus cycles. Specimen tested at σ_{max} = 25 ksi, R = 0.1, f = 20, and lab air. Specimen failed at the top grip.
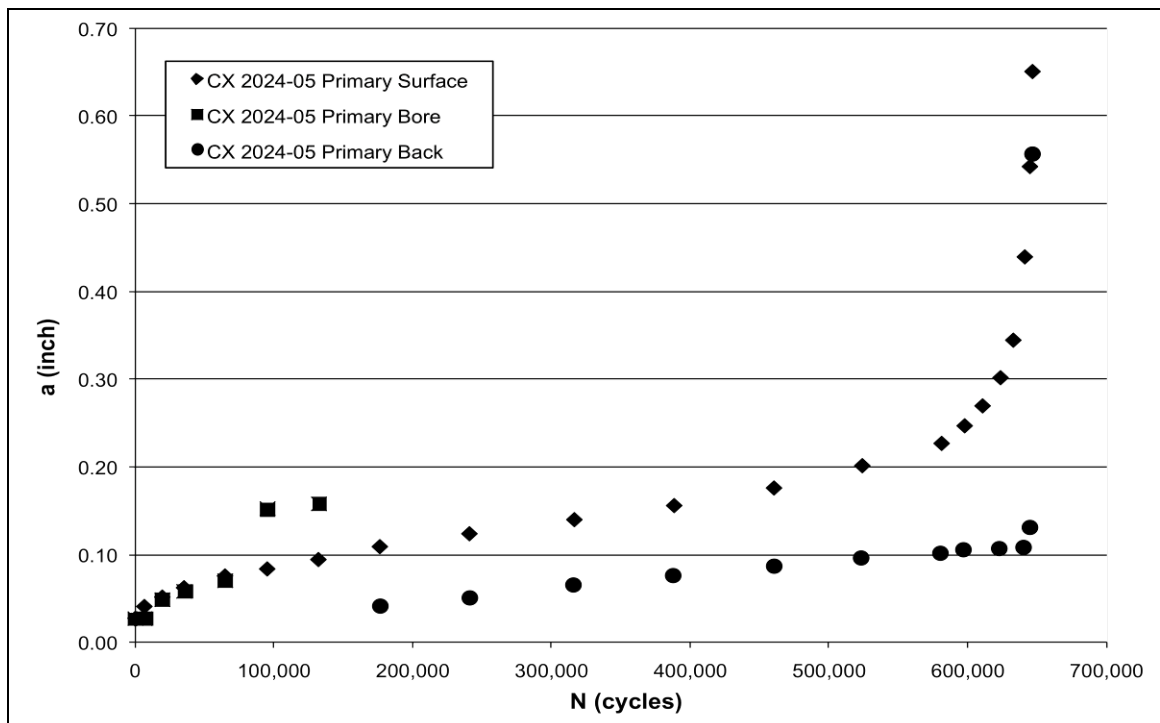
Fig. 114 CX 2024-05 crack growth versus cycles. Specimen tested at σ_{max} = 25 ksi, R = 0.1, f = 20, and lab air.

Fig. 115 CX 2024-06 crack growth versus cycles. Specimen tested at σ_{max} = 25 ksi, R = 0.1, f = 20, and lab air.

Fig. 116 CX 2024-07 crack growth versus cycles. Specimen tested at σ_{max} = 25 ksi, R = 0.1, f = 20, and lab air. Secondary crack was larger than primary crack.
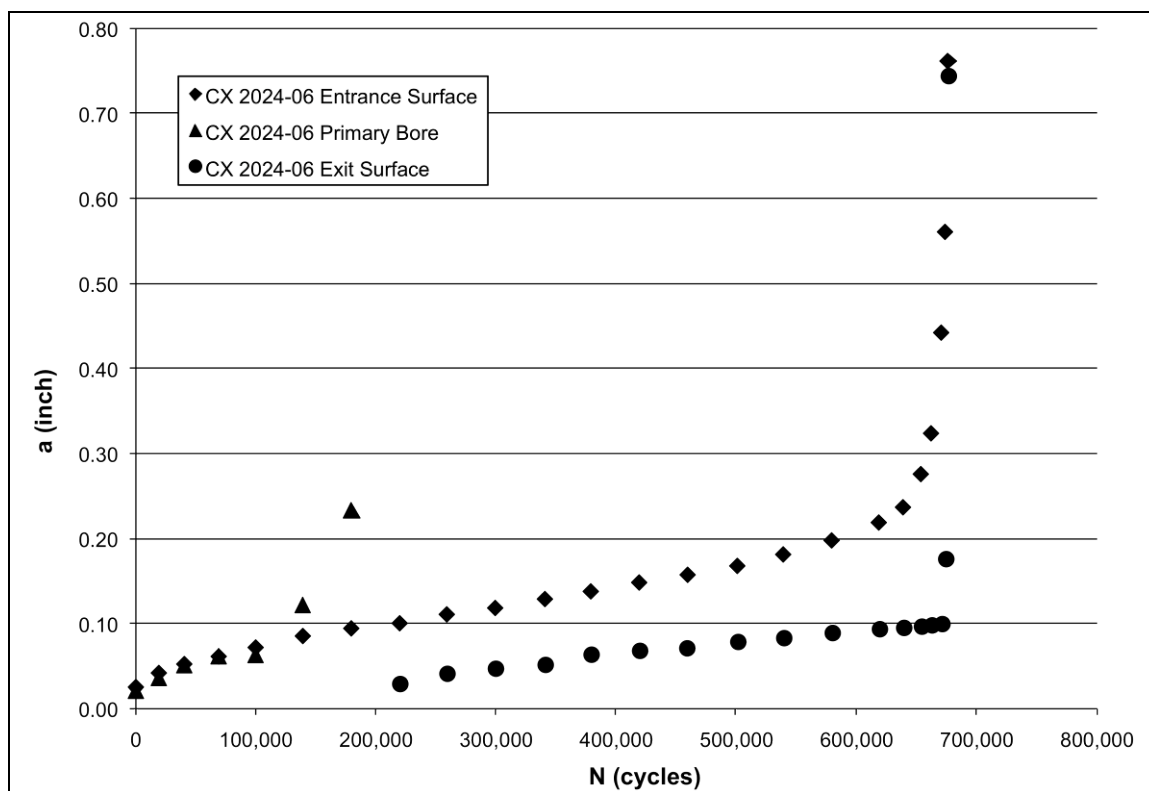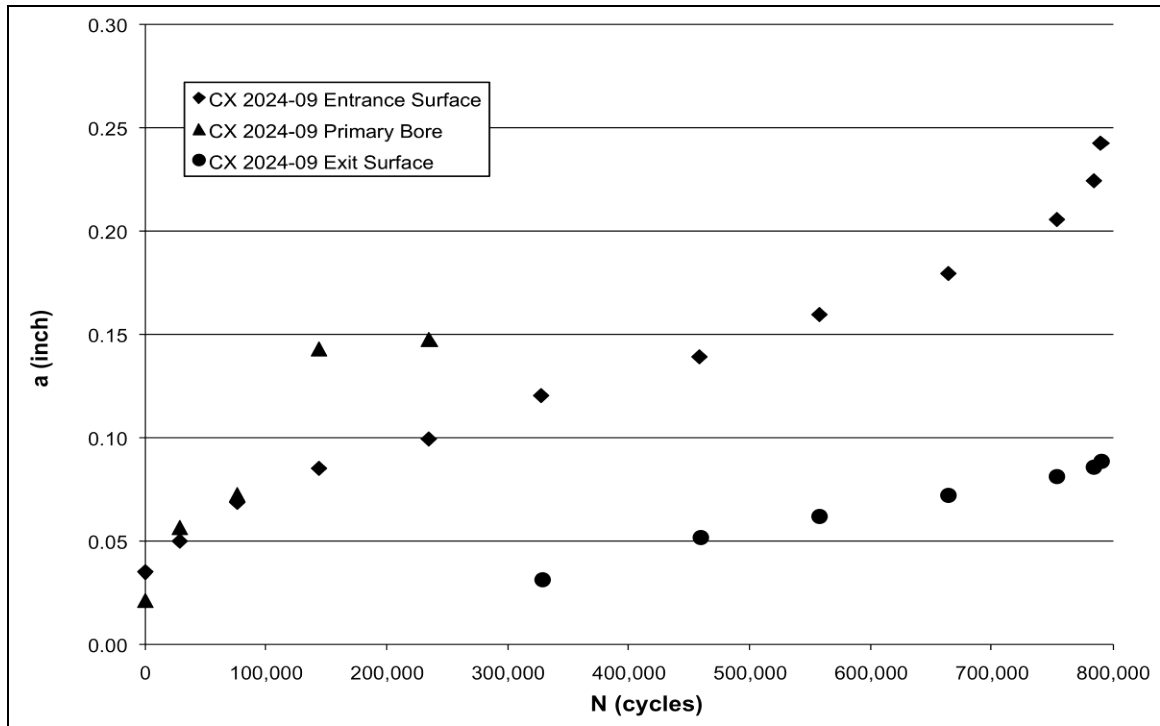
Fig. 117 CX 2024-09 crack growth versus cycles. Specimen tested at σ_{max} = 25 ksi, R = 0.1, f = 20, and lab air. Secondary crack was larger than primary crack.
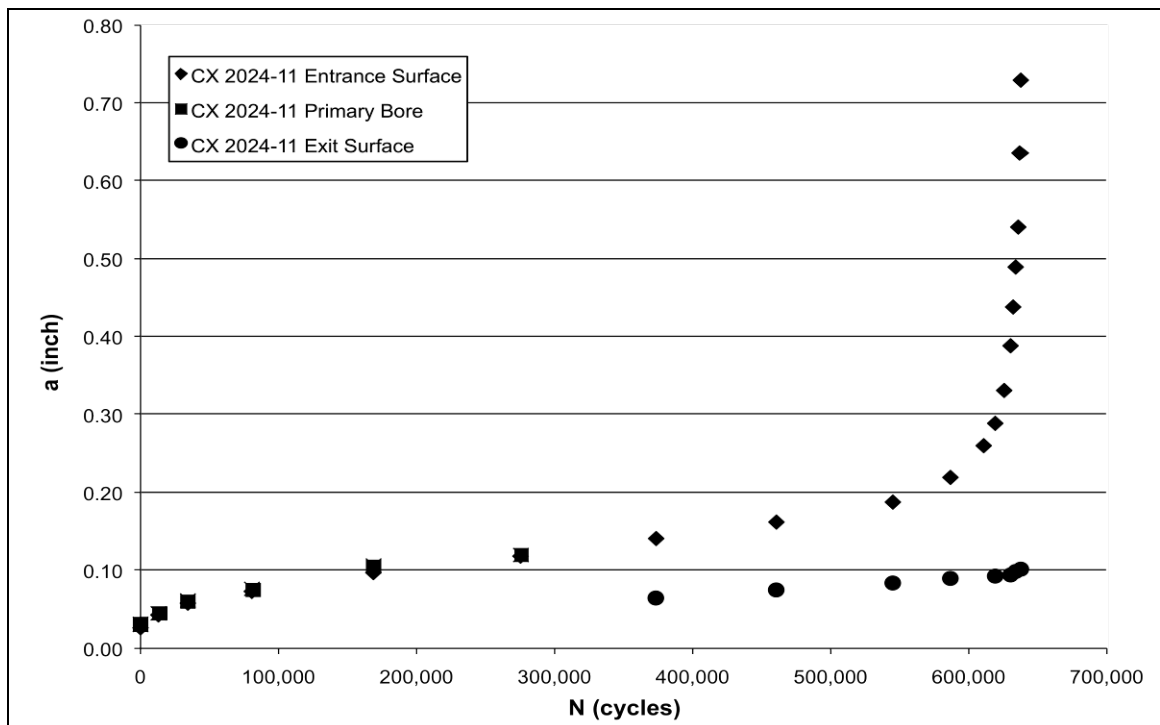
Fig. 118 CX 2024-11 crack growth versus cycles. Specimen tested at σ_{max} = 25 ksi, R = 0.1, f = 20, and lab air.
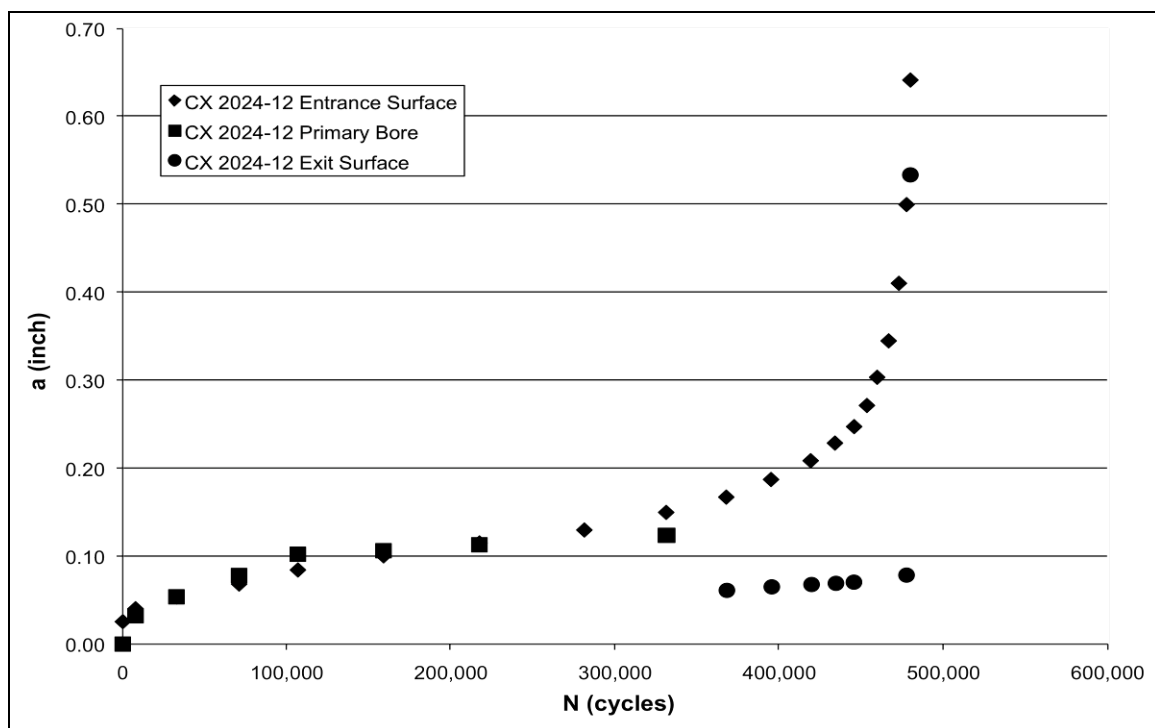
Fig. 119 CX 2024-12 crack growth versus cycles. Specimen tested at σ_{max} = 25 ksi, R = 0.1, f = 20, and lab air.
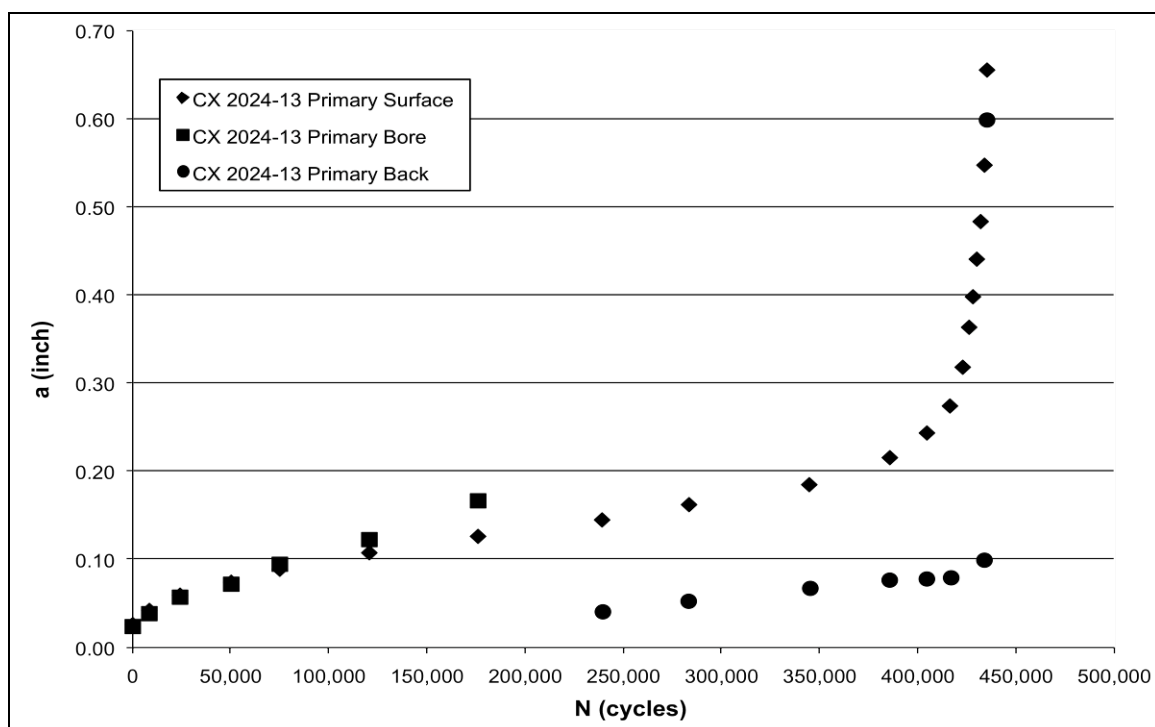
Fig. 120 CX 2024-13 crack growth versus cycles. Specimen tested at σ_{max} = 25 ksi, R = 0.1, f = 20, and lab air.
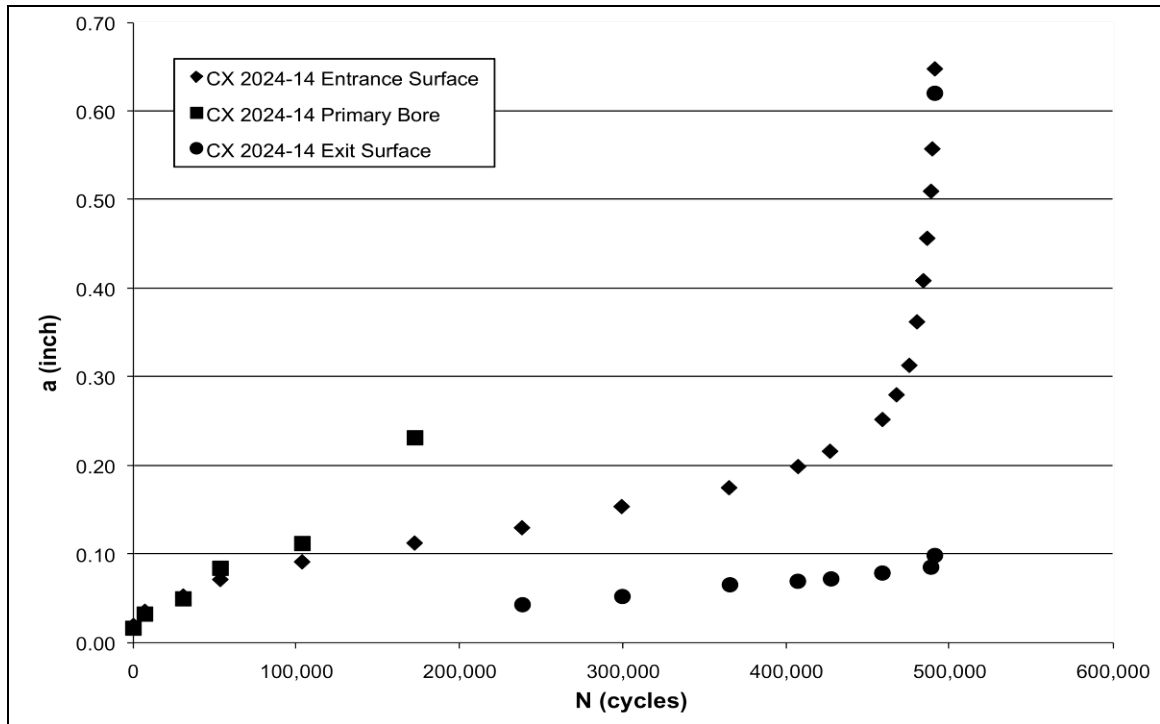
Fig. 121 CX 2024-14 crack growth versus cycles. Specimen tested at σ_{max} = 25 ksi, R = 0.1, f = 20, and lab air.
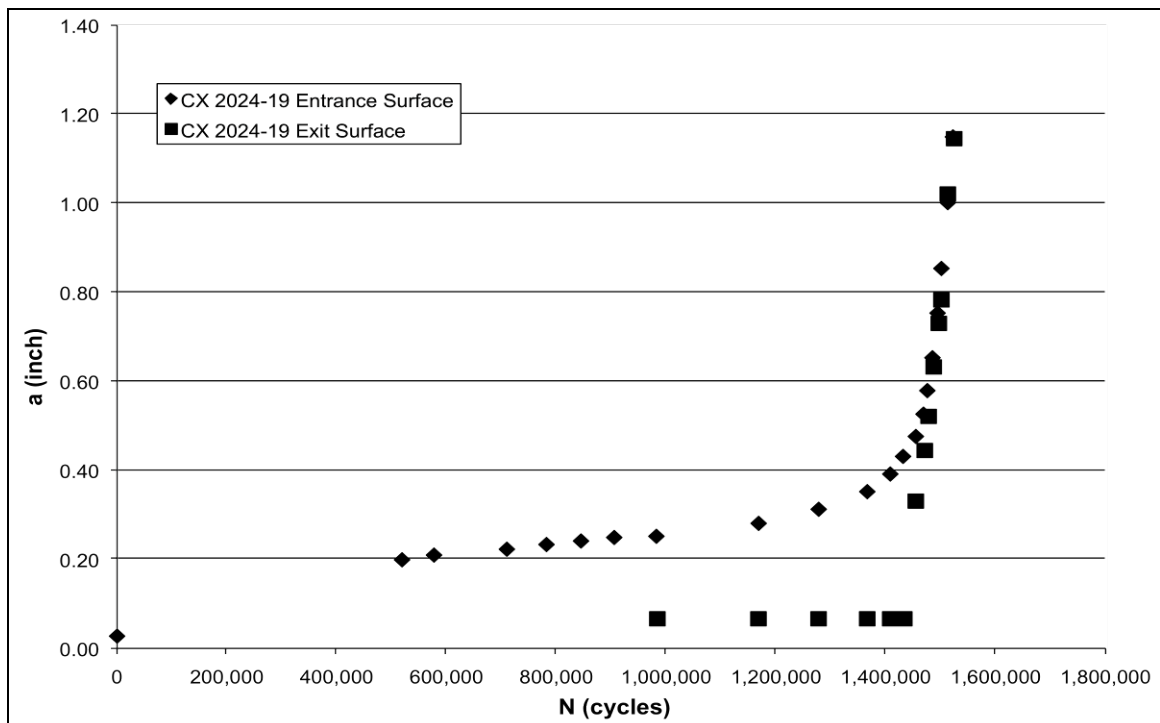
Fig. 122 CX 2024-14 crack growth versus cycles. Specimen tested at σ_{max} = 12 ksi, R = 0.1, f = 20, and lab air. Specimen tested at large crack lengths. Only EDM surface measured.

APPENDIX F

FATIGUE CRACK GROWTH RATE VERSUS CRACK LENGTH PLOTS
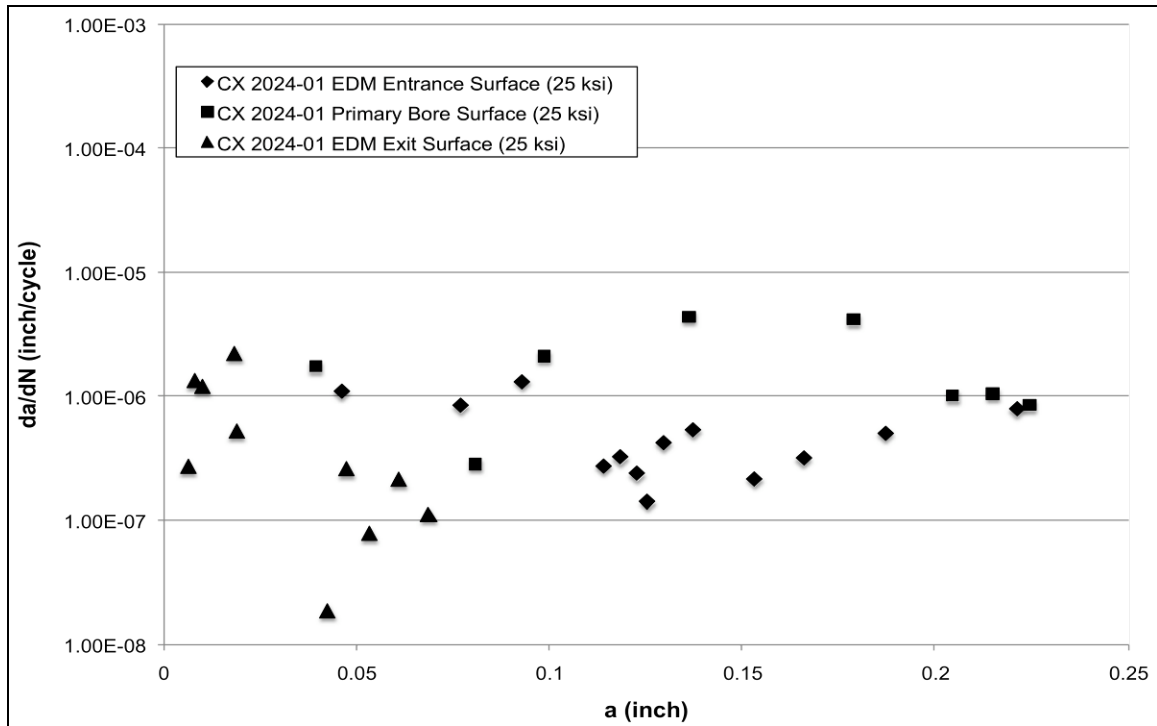
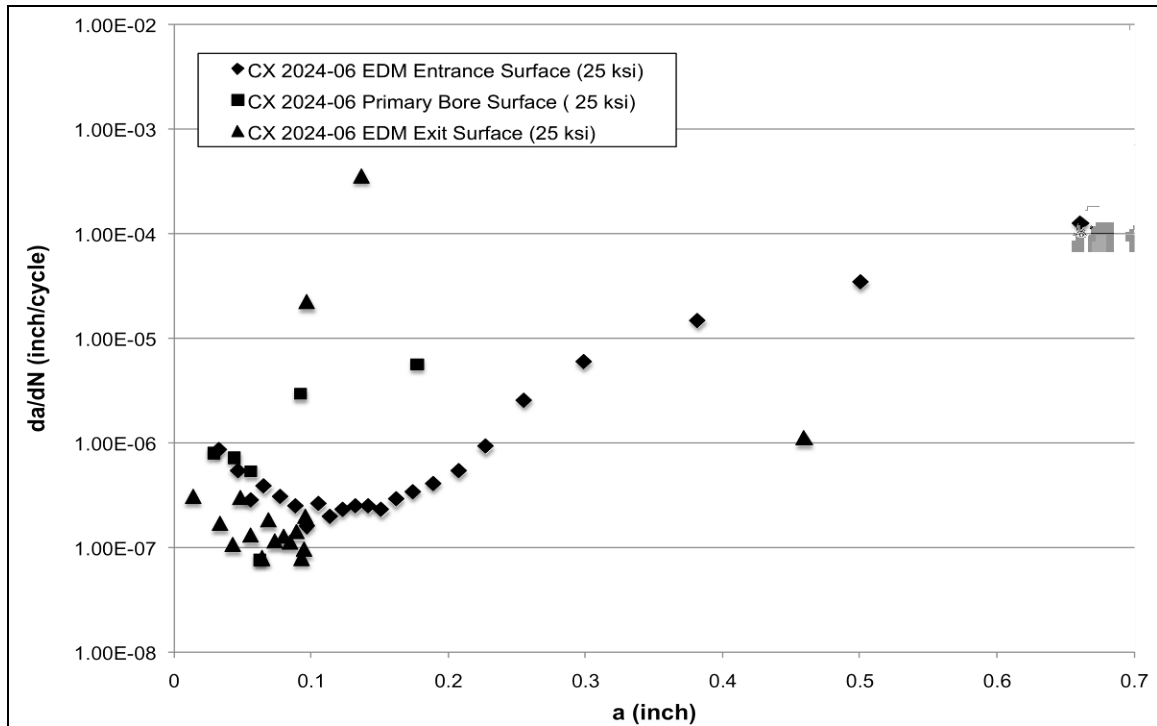Fig. 123 CX 2024-01 crack growth rate versus cycles. Specimen tested at σ_{max} = 25 ksi, R = 0.1, f = 20, and lab air.

Fig. 124 CX 2024-02 crack growth rate versus cycles. Specimen tested at σ_{max} = 25 ksi, R = 0.1, f = 20, and lab air.

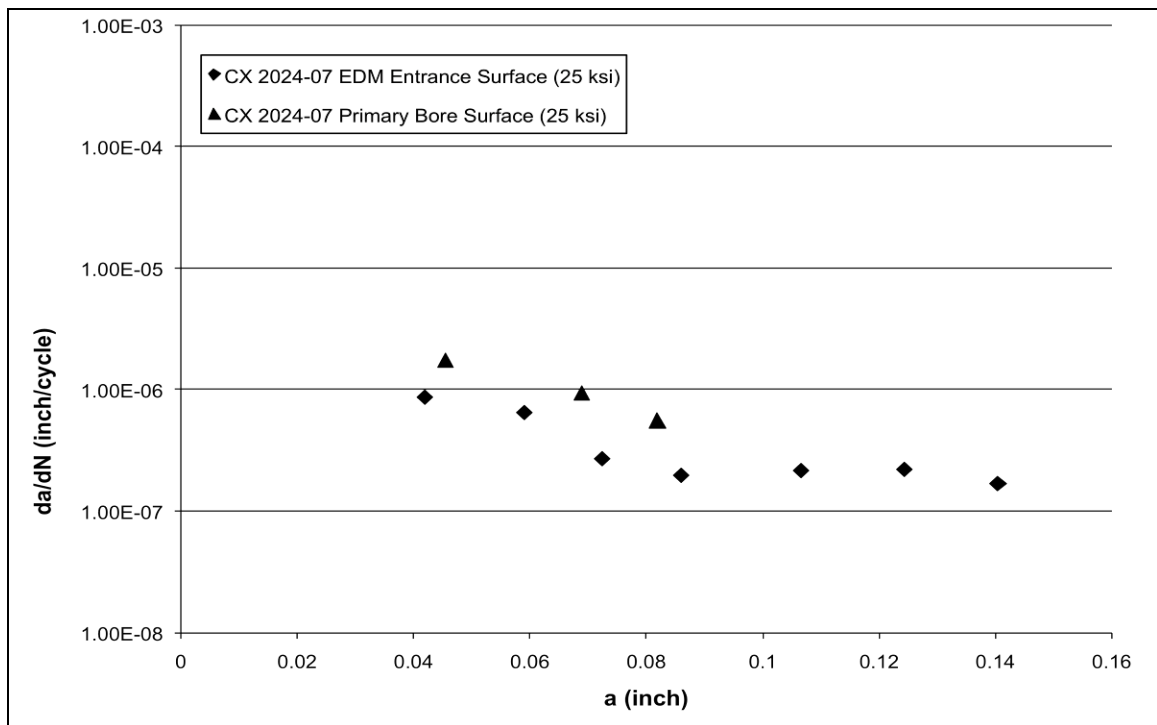Fig. 125 CX 2024-03 crack growth rate versus cycles. Specimen tested at σ_{max} = 25 ksi, R = 0.1, f = 20, and lab air.

Fig. 126 CX 2024-05 crack growth rate versus cycles. Specimen tested at σ_{max} = 25 ksi, R = 0.1, f = 20, and lab air.

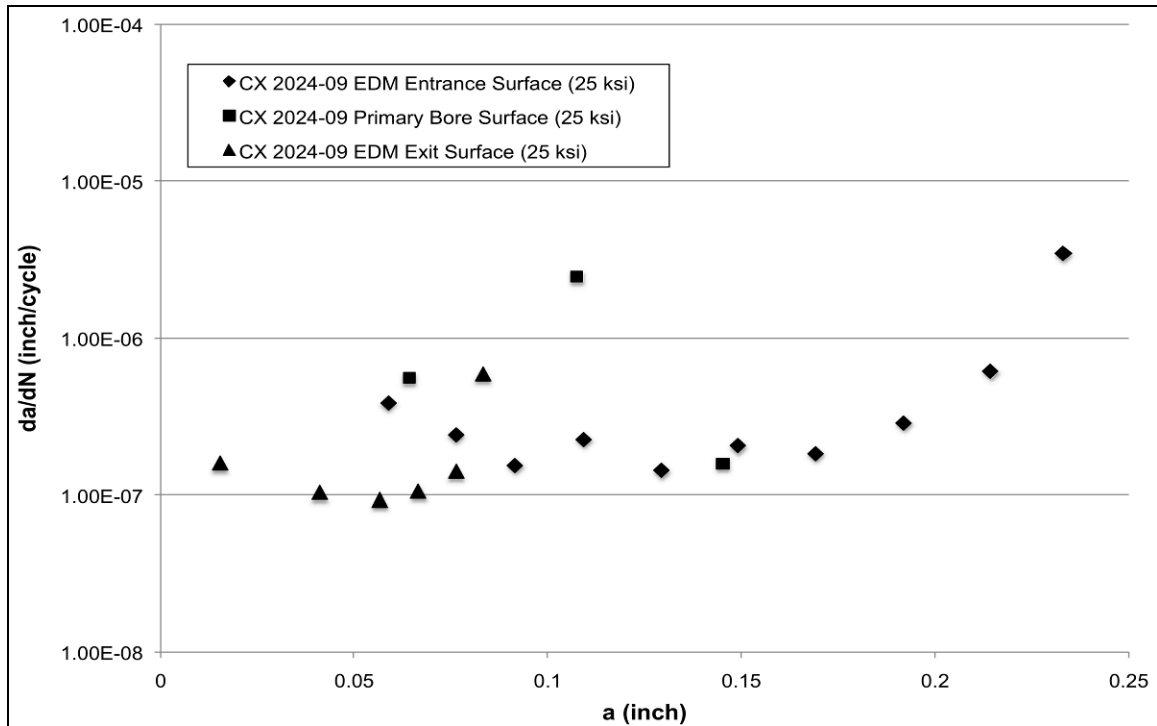Fig. 127 CX 2024-06 crack growth rate versus cycles. Specimen tested at σ_{max} = 25 ksi, R = 0.1, f = 20, and lab air.

Fig. 128 CX 2024-07 crack growth rate versus cycles. Specimen tested at σ_{max} = 25 ksi, R = 0.1, f = 20, and lab air.

Fig. 129 CX 2024-09 crack growth rate versus cycles. Specimen tested at σ_{max} = 25 ksi, R = 0.1, f = 20, and lab air.
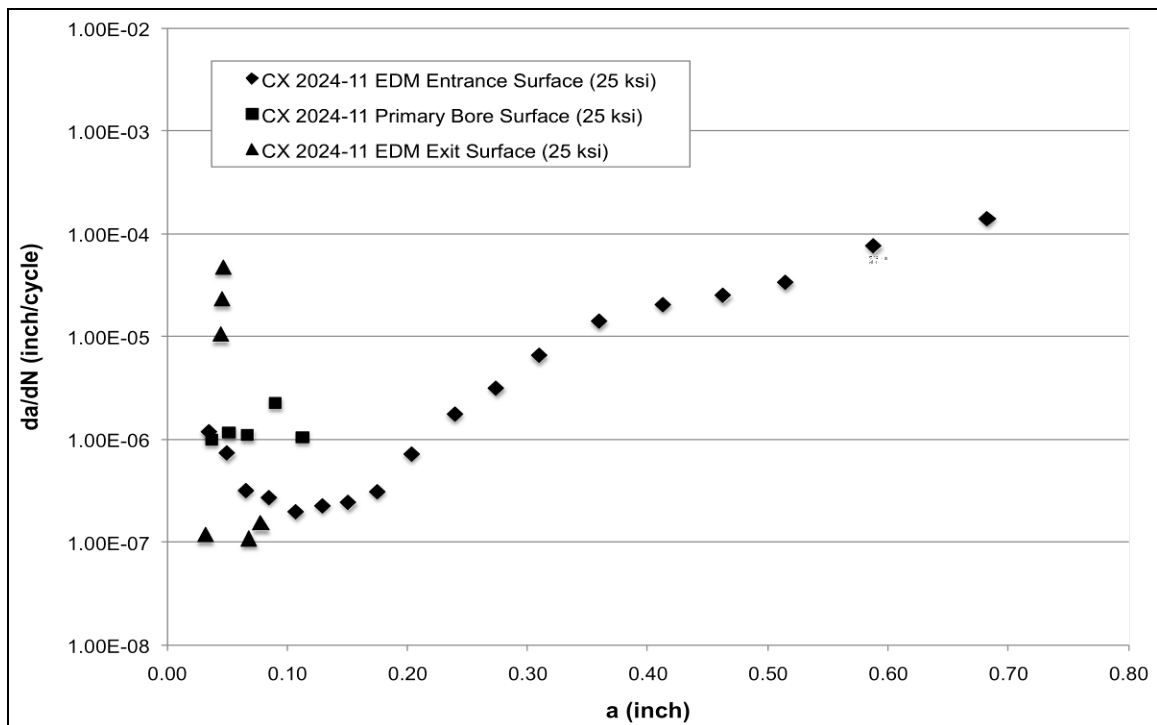

Fig. 130 CX 2024-11 crack growth rate versus cycles. Specimen tested at σ_{max} = 25 ksi, R = 0.1, f = 20, and lab air.
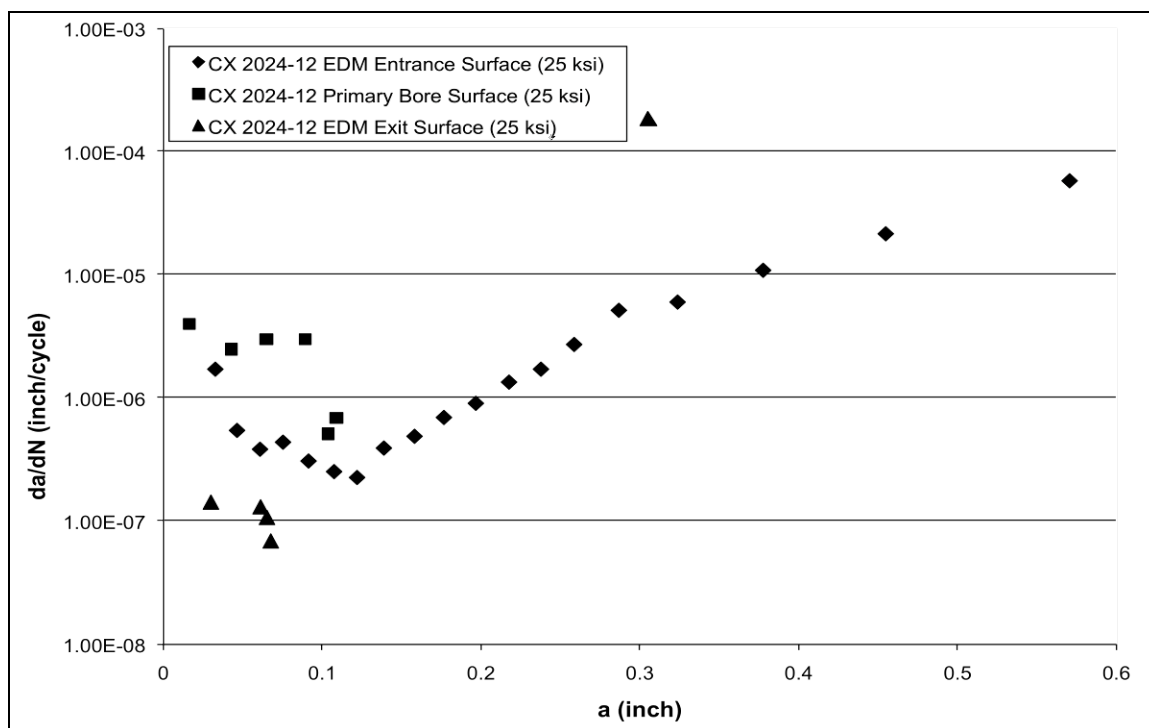
Fig. 131 CX 2024-12 crack growth rate versus cycles. Specimen tested at σ_{max} = 25 ksi, R = 0.1, f = 20, and lab air.
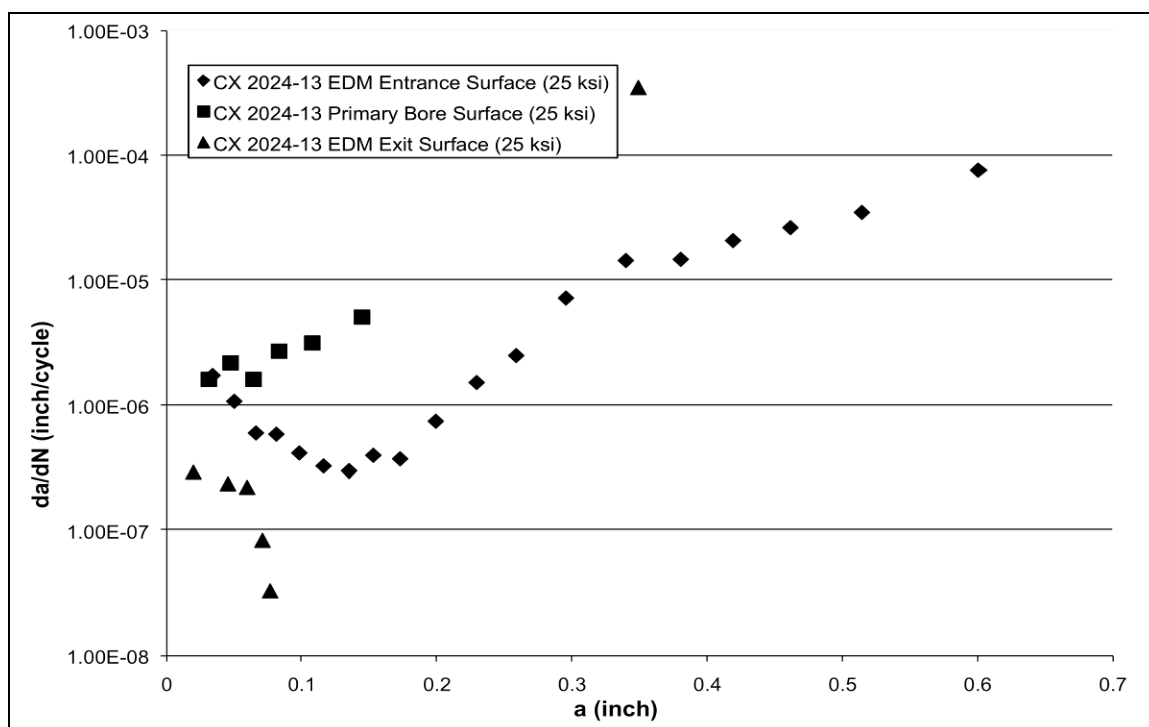

Fig. 132 CX 2024-13 crack growth rate versus cycles. Specimen tested at σ_{max} = 25 ksi, R = 0.1, f = 20, and lab air.
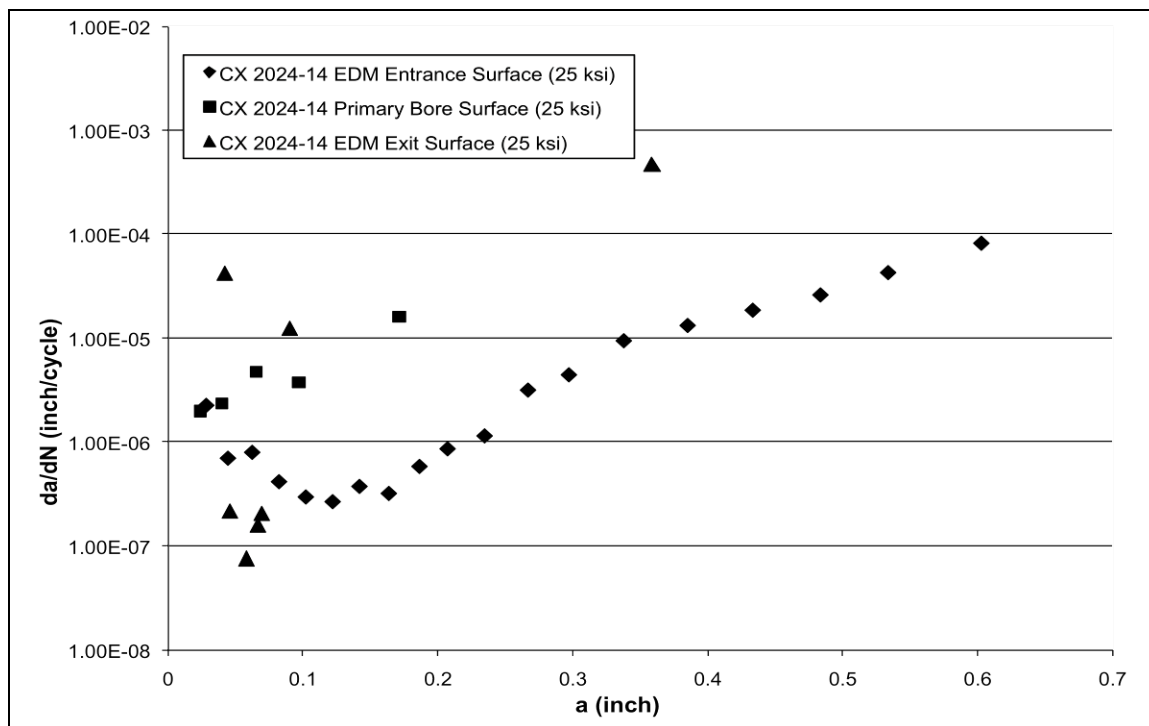
Fig. 133 CX 2024-14 crack growth rate versus cycles. Specimen tested at σ_{max} = 25 ksi, R = 0.1, f = 20, and lab air.

REFERENCES

[1] Anderson, J.D. (1985). *Introduction to Flight.* McGraw-Hill Book Company, New York, NY, USA.

[2] Miner, Milton A. (1945). Cumulative Damage in Fatigue. *Journal of Applied Mechanics,* **12,** 159-164

[3] Buntin, W.D. (1969). *Concept and Conduct of Proof Test of F-111 Production Aircraft*, United States Air Force.

[4] Gallagher, J.P. (2007). A Reiew of Philosophies, Processes, Methods and Approaches that Protect In-Service Aircraft from the Scourge of Fatigue Failures. *ICAF '07 Internation Committee of Aeronautical Fatigue*, Naples, Italy.

[5] Gallagher, J.P; Giessler, F.J.; Berens, A.P. (1984). *USAF Damage Tolerance Design Handbook: Guidelines for the Analysis and Design of Damage Tolerant Aircraft Structures.* USAF Systems Command, Wright-Patterson Air Force Base, OH, USA.

[6] Gran, R.J.; Orazio, F.D.; Paris, P.C.; Irwin, G.R.; Hertzberg, R. (1971). *Investigation and Analysis Development of Early Life Aircraft Structrual Failures,* Report no. AFFDL-TR-75-32. Air Force Flight Dynamics Laboratory, Wright-Patterson Air Force Base, OH, USA.

[7] Fatigue Technologies Inc. (1991). *Extending the Fatigue Life of Metal Structures, Materials Testing*, Seattle, WA, USA.

[8] Pilkey, Walter D. (1997) *Peterson's Stress Concentration Factors*, 2nd edn, John Wiley & Sons, Inc, New York, USA.

[9] Fatigue Technologies Inc. (2002). *FTI Process Specification 8101D Cold Expansion of Holes Using the Standard Split Sleeve System and Countersink Cold Expansion (CsCx™),* Seattle, WA, USA.

[10] Reid, L. and Fatigue Technologies Inc. (2000). Incorporating Hole Cold Expansion to Meet Durability and Damage Tolerance Airworthiness Objectives. Seattle, WA, USA.

[11] Brown, M., Fawaz, S., Arunachalam, S., (2006). *Fatigue Crack Growth Rate Effects on Single – and Mulit-Layered Cold Expanded Aircraft Aluminum*, United States Air Force Academy, Colorado Springs, CO, USA.

[12] Kokaly, M.T., Ransom, J.S., Restis, J.H., Reid, L.F., (2002). Prediction fatigue crack growth in the residual stress field of a cold worked hole. J. Test. Eval. **20**, 1-15.

[13] Cathey, W., Grandt, A., (1980). Fracture mechanics consideration of residual stresses introduced by coldworking fastener holes. *J. Engng Mater. Tech.* **102**, 85-91.

[14] Lacarac, V., Smith, D., Pavier, M., Priest, M, (2000). Fatigue crack growth from plain and cold expanded holes in aluminum alloys. *Int. J. Fatigue* **22**, 189-203.

[15] Priest, M., Smith, D., Pavier, M., (1997). Assessment of fatigue crack growth from cold worked holes. *ICAF '97 International Committee on Aeronautical Fatigue.* Edinburgh, Scotland.

[16] Pavier, M., Poussard, C., Smith, D., (1997). A finite element simulation of the cold working process for fastener holes. *J. Strain. Anal.* **32**, 287-300.

[17] Moreira, P.M.G.P., De Matos, P.F.P., Pinho, S.T., Pastrama, S.D., Camanho, P.P., De Castro, P.M.S.T., (2004). The residual stress intensity factors for cold-worked cracked holes a technical note. *Fatigue Frat. Engng Mater. Struct.* **27**, 879-886.

[18] Janssen, M., Zuidema, J., Wanhill, R.J.H., (2002). *Fracture Mechanics, 2nd edn,* DUP Blue Print, Delft, The Netherlands.

[19] Grant, P.V., Lord, J.D., Whitehead, P.S., (2002). *The measurement of residual stresses by incremental hole drilling technique.* National Physics Laboratory. **53**.

[20] Schajer, G.S., (1981). *Application of finite element calculations to residual stress measurements.* J. Engng Mater. Tech. **157**, 157-163.

[21] Stephens, R.,(2001). *Metal Fatigue in Engineering,* 2nd edn, John Wiley & Sons, Inc., New York, USA.

[22] Chandawanich, N., Sharpe, W., (1979). An experimental study of fatigue crack growth initiation and growth from cold worked holes. *Engng Fract. Mech.* **11**, 609-620.

[23] Ball, D.L., Lowry, D.R., (1998). Experimental Investigation on the effects of cold expansion of fastener holes. *Fatigue Frat. Eng. Mater. Struct.* **21**, 17-34.

[24] Gaerke, J., Zhang, X., Wang, Z., (2000). Life enhancement of fatigue-aged fastener holes using the cold expansion process. In: *Proceedings of the Institute of Mechanical Engineers,* **214**, pp. 281-293.

[25] Kokaly, M.T., Ransom, J.S., Restis, J.H., Reid, L., (2005). *Observations and analysis of fatigue crack growth from cold expanded holes.* Fatigue Technologies Inc., Seattle WA, USA.

[26] Department of Defense, (2006). *DoD Joint Service Specification Guide, Aircraft Structures,* USA

[27] Akins, J.L., (1978). *Damage tolerance analysis for C-5A wing modification, stress gradient factor (β_{Grad}) for web analysis*, Lockheed – Georgia Company, Marietta, GA, USA.

[28] American Society for Testing and Materials (ASTM) Committee E08. (2000). *Standard Test Method for Measurement of Fatigue Crack Growth Rates (E 647)*, ASTM, West Conshohocken, PA, USA.

[29] United States Air Force, (2006). *Damage Tolerance Re-Assessment: Reconfigured Post Desert Storm Severe Spectrum*, Hill Air Force Base, UT, USA.

[30] Alloy 2024 Sheet and Plate (2008). ALCOA Mill Products, Inc. Bettendorf, IA, USA.

[31] Hoeppner, D.W. (2008). Quality Engineering Design Integrity Center (QEDIC), Personal Conversation.

[32] Antolovich, S.D., Saxena, A., (1986). *Fatigue Failures - ASM Handbook Vol. 11 Failure Analysis and Prevention*, ASM International, USA.

[33] AFGROW VASM – Structural Mechanics Branch (2008). AFGROW (Fracture Mechanics and Fatigue Crack Growth Analysis Software), version 4.11.14.0 Air Force Research Laboratories Structural Mechanics Branch, Wright Patterson, Air Force Base, OH, USA.

[34] Prost-Demasky, S., (2008). Analytical Processes and Engineering Solutions (APES), Personal Communication.

[35] Fawaz, S., (2008). United States Air Force Academy CASTLE Group, Personal Communication.

[36] AFGROW VASM – Structural Mechanics Branch (2008). AFGROW (Fracture Mechanics and Fatigue Crack Growth Analysis Software), version 4.11.14.0, Help Files Air Force Research Laboratories Structural Mechanics Branch, Wright Patterson, Air Force Base, OH, USA.